



University  
of Glasgow

<https://theses.gla.ac.uk/>

Theses Digitisation:

<https://www.gla.ac.uk/myglasgow/research/enlighten/theses/digitisation/>

This is a digitised version of the original print thesis.

Copyright and moral rights for this work are retained by the author

A copy can be downloaded for personal non-commercial research or study, without prior permission or charge

This work cannot be reproduced or quoted extensively from without first obtaining permission in writing from the author

The content must not be changed in any way or sold commercially in any format or medium without the formal permission of the author

When referring to this work, full bibliographic details including the author, title, awarding institution and date of the thesis must be given

Enlighten: Theses

<https://theses.gla.ac.uk/>  
[research-enlighten@glasgow.ac.uk](mailto:research-enlighten@glasgow.ac.uk)

The Application of Resonance  
Enhanced Multiphoton Ionisation  
Mass Spectrometry to the Detection  
of Aromatic Molecules.

Alastair Clark  
Department of Physics and Astronomy  
University of Glasgow

**Presented as a thesis for the degree of Doctor of Philosophy  
in the University of Glasgow**

**© Alastair Clark, April 1992.**

ProQuest Number: 11011480

All rights reserved

INFORMATION TO ALL USERS

The quality of this reproduction is dependent upon the quality of the copy submitted.

In the unlikely event that the author did not send a complete manuscript and there are missing pages, these will be noted. Also, if material had to be removed, a note will indicate the deletion.



ProQuest 11011480

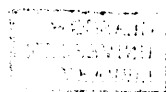
Published by ProQuest LLC (2018). Copyright of the Dissertation is held by the Author.

All rights reserved.

This work is protected against unauthorized copying under Title 17, United States Code  
Microform Edition © ProQuest LLC.

ProQuest LLC.  
789 East Eisenhower Parkway  
P.O. Box 1346  
Ann Arbor, MI 48106 – 1346

***To  
Mum and Dad***





## **Acknowledgements**

I would like to thank the following people:

- my supervisor, Dr. K.W.D. Ledingham for his enthusiasm, advice and encouragement throughout the period of my studies.
- Dr. A. Marshall for inspiration, a constant supply of advice and for keeping me sane in times of despair.
- Drs. R.P. Singhal, R. Jennings, M. Campbell and Wang Li for many helpful discussions on various aspects of my work.
- my fellow research students, Dr. C. J. McLean, Dr. P. T. McCombes, Mr. I. S. Borthwick, Mr. J. Sander and Mr. C. Scott for their friendship.
- Mr. R. Maxwell and Mr. T. McCanny for technical assistance.
- Mr. T. Neil and his staff in the mechanical workshop for construction of instrumental parts.
- Mr. R. Pallester and his colleagues for help and assistance with electronic equipment.
- Mr. A. J. Flavell, Mr. D. J. Martin, Dr. C. Raine, Mr. B. Swann, Mrs. B. Carragher and Mrs. M. Shearer for assistance with computing and data acquisition.
- Miss C. McIntyre for her secretarial assistance.
- The S.E.R.C. for financial support.
- Mum, Dad and Martin for their encouragement, support and considerable financial help.
- and finally, my fiancée Linda Jane for waiting patiently for so long, and for making this all worthwhile.

## **Publications**

### **Resonant Laser Ablation (RLA)**

McLean CJ, Marsh JH, Land AP, Clark A, Jennings R, Ledingham KWD, McCombes PT, Marshall A, Singhal RP and Towrie M

*Int. J. Mass Spectrom. and Ion Proc.* 96 (1990) R1

### **A Spectroscopic study of Aniline Using Resonance Ionisation Mass Spectrometry**

Clark A, Marshall A, Jennings R, Ledingham KWD and Singhal RP  
*Inst. Phys. Conf. Ser. No. 113: Section 5 (1991) 159*

### **Resonant Two-photon Ionisation of Aromatic Molecules: Wavelength Dependences and Fragmentation Data**

Marshall A, Clark A, Jennings R, Ledingham KWD, McLean CJ, and Singhal RP

*Inst. Phys. Conf. Ser. No114: Section 4 (1991) 173*

### **A Laser-based Atmospheric Sensor for Aromatic Molecules**

Marshall A, Clark A, Ledingham KWD, Singhal RP, and Campbell M

*Sensors: Technology, Systems and Applications*, Adam Hilger, Ed KTV Grattan, P151 (1991)

### **Resonant Two-photon Ionisation for Detection of Aromatic Molecules**

Marshall A, Clark A, Ledingham KWD and Singhal RP

*Meas. Sci. and Tech.* 2 (1991) 1078

### **Wavelength-dependent Laser-induced Fragmentation of Nitrobenzene**

Marshall A, Clark A, Jennings R, Ledingham KWD and Singhal RP

*Int. J. Mass Spectrom. and Ion Proc.* 112 (1992) 273

**Resonant Ionisation Spectroscopy of Carbon Atoms Following Fragmentation of Nitro-aromatic Molecules**

Clark A, Ledingham KWD, Marshall A and Singhal RP

*Accepted for publication in Spectrochimica Acta (1992)*

**Laser-induced Dissociation, Ionisation and Fragmentation Processes in Nitroaromatic Molecules**

Marshall A, Clark A, Jennings R, Ledingham KWD, Sander J and Singhal RP

*Submitted for publication to Int. J. Mass Spectrom. and Ion Proc.*

**A Multi-photon Induced Dissociative Pathway from Nitroaromatic Molecules to NO<sup>+</sup> Ions**

Ledingham KWD, Marshall A, Clark A, Jennings R, Sander J and Singhal RP

*Submitted for publication to Chem. Phys. Lett.*

**Detection and Identification of Nitroaromatic Species Using a Laser-based Time of Flight Mass Spectrometer System**

Marshall A, Clark A, Jennings R, Ledingham KWD, Sander J and Singhal RP

*To be submitted for publication to Anal. Chem.*

**Laser Ionisation and Fragmentation Processes in Nitrobenzene**

Marshall A, Clark A, Jennings R, Ledingham KWD, Sander J and Singhal RP

*Submitted for oral presentation at RIS 92, Los Alamos, New Mexico (May 1992)*

**Attenuation characteristics of an all-silica UV fibre**

Campbell M, Javaud S, Zheng R, Ledingham K W D, Singhal R P, Borthwick I S, Clark A, Marshall A and Sander J

*To be presented orally at the 14th Symposium on Photonics Measurements, Sopron, Hungary, 1st-3rd June, 1992*

## Summary

The work presented in this thesis was carried out with the primary objective of developing a sensitive laser based procedure for detecting and identifying aromatic type compounds, in particular nitrobenzene and nitrotoluene. The first chapter discusses the basic underlying principles of Resonance Ionisation Spectroscopy (RIS) as applied to atoms, and of Resonance Enhanced Multiphoton Ionisation Spectroscopy (REMPI) of molecules. Several different laser ionisation schemes are discussed which demonstrate the flexibility of the technique. The purpose of Chapter 2, where the theoretical principles of resonance enhanced multiphoton ionisation spectroscopy are introduced, is to provide the reader with the necessary information required for an understanding of the technique. A semiclassical approach to the interaction of light with atoms and molecules is presented, as well as a discussion of photophysical processes which occur in the excited states of molecules. In addition, a population rate equation model restricted to a three level ionisation scheme (two bound states and the ionisation continuum) allows determination of the necessary laser parameters to efficiently implement the REMPI process.

The experimental apparatus is described in detail in Chapter 3. Chapter 4 deals specifically with a course of preliminary experiments which were performed in a high vacuum chamber with quadrupole filtered ion detection. The results of Resonant 2-Photon Ionisation studies of toluene and aniline vapours are presented. In addition, the experimental results obtained when investigating the possibility of detecting and identifying individual

molecular species in a mixture of molecules (at atmospheric pressure) in a simple home-made ionisation chamber are presented. This work was carried out with Dr. A. Marshall, and the interpretation of the results and analysis was carried out jointly.

Chapter 5 describes the introduction of time-of-flight mass spectrometry to aid the study of REMPI processes in nitroaromatic molecules. The results of a comprehensive series of experiments concerning REMPI of nitrobenzene and mononitrotoluene molecules in the wavelength range 245-250nm are discussed in some detail. One of the most important results of this work was the observation of a characteristic wavelength dependent signature of the  $\text{NO}^+$  ion ( $m/z=30$ ). The author was solely responsible for designing, constructing and commissioning the TOF mass spectrometer system.

The work of Chapter 6 discusses the results of a series of experimental investigations which were conducted in an attempt to identify the dissociation processes which prevail during the interaction between intense ultraviolet laser fields and nitroaromatic vapours. The wavelength dependent ionisation spectra (in the range 233-260nm) of the  $\text{NO}^+$  ion produced from high purity samples of nitric oxide and nitrogen dioxide are compared with the  $\text{NO}^+$  spectra from nitroaromatics (Chapter 5) and several conclusions are made which confirms the manner in which this particular class of molecules break up when irradiated with UV laser light. This work was done in collaboration with Dr. A. Marshall and the results and analysis were carried out jointly.

Chapter 7 discusses the wavelength dependent production of carbon and hydrogen ions from nitroaromatic molecules. Several

sharp transitions in the carbon ion spectrum have been identified as single and multiple photon resonances in neutral atomic carbon. The  $1s \rightarrow 2s$  two-photon resonance in hydrogen has also been observed. In all, six singlet transitions and one triplet transition in carbon have been identified. These have not previously been observed as far as the author is aware. The author was solely responsible for the analysis of the data and the interpretation was shared with Dr. K.W.D. Ledingham.

Finally, Chapter 8 discusses briefly the project as a whole and discusses several experiments which are planned for the future.

# Contents

<i>Frontspiece</i>	(i)
<i>Acknowledgements</i>	(iii)
<i>Publications</i>	(iv)
<i>Summary</i>	(vi)
<i>Contents</i>	(ix)

## **Chapter 1: Introduction.**

§1.1 Introduction	1
§1.2 Resonance Ionisation Spectroscopy	2
§1.3 Laser Ionisation Spectroscopy of Molecules	6
§1.4 Supersonic Jet Cooling	10
§1.5 Ion Mobility Spectrometry	11

## **Chapter 2: Relevant Theoretical Concepts.**

§2.1 Introduction	12
§2.2 Photon-Molecule interactions: A semiclassical approach.	13
§2.2.1 Weak Light Intensities	17
§2.3 Electronic energy levels of molecules	18
§2.4 Electronic transitions in molecules	19
§2.4.1 Born-Oppenheimer approximation	20
§2.4.2 Franck-Condon principle	22
§2.5 The fate of absorbed energy in molecules	22
§2.5.1 Dissociation	22
§2.5.2 Predissociation	23
§2.5.3 Fluorescence and Phosphorescence	23
§2.5.4 Intersystem Crossing and Internal Conversion	24
§2.5.5 Collisional Relaxation and Excitation	24
§2.6 Laser Induced Fragmentation	25

§2.7 Modelling of a REMPI process	26
§2.7.1 Population Rate Equations	27
§2.7.2 High Flux conditions	29
§2.7.3 Low Flux conditions	31
§2.8 Transition Line Broadening mechanisms	31
§2.8.1 Doppler broadening	31
§2.8.2 Radiative broadening	33
§2.8.3 Collisional broadening	34
§2.8.4 Laser induced power broadening	35

### **Chapter 3: Instrumentation.**

§3.1 Introduction	36
§3.2 Excimer laser	38
§3.3 Dye laser	39
§3.4 Wavelength tracking system	41
§3.5 Laser power attenuator	41
§3.6 Pulse energy measurement	42
§3.7 Quadrupole Mass Spectrometer	42
§3.8 Data acquisition timing electronics	45
§3.9 Vacuum chamber	46

### **Chapter 4: R2PI detection of small aromatic molecules in a quadrupole mass spectrometer and a simple ionisation chamber.**

§4.1 Introduction	47
§4.2 Resonant 2-photon ionisation studies of toluene	48
§4.3 Resonant 2-photon ionisation studies of aniline	51
§4.4 Detection and identification of toluene, aniline and phenol vapours in a simple ionisation chamber	53



## **Chapter 5: Development of a linear Time-of-Flight Mass Spectrometer system to study Resonance Enhanced Multiphoton Ionisation (REMPI) processes in nitroaromatic vapours.**

§5.1 Introduction	57
§5.2 Time-of-flight mass spectrometry	57
§5.3 Principle of operation of a TOF mass spectrometer	58
§5.4 REMPI of nitroaromatics in the TOF system	62
§5.4.1 REMPI of nitrobenzene in the wavelength range 245-250nm	63
§5.4.2 REMPI of mono-nitrotoluene isomers in the wavelength range 245-250nm	70
§5.5 Conclusions	73

## **Chapter 6: REMPI studies of NO and NO<sub>2</sub> gases: identifying dissociative and ionisation pathways to NO<sup>+</sup> formation in nitroaromatic molecules.**

§6.1 Introduction	75
§6.2 Classification of electronic states in diatomic molecules	76
§6.3 Vibrational and Rotational substates	78
§6.4 Selection rules in diatomic molecules	78
§6.5 Electronic structure of NO	78
§6.6 Rotational fine structure in electronic transitions	79
§6.7 Selection rules in electronic vibrational transitions in diatomic molecules	80
§6.8 Formation of P,Q and R branches	80
§6.9 REMPI of high purity NO and NO <sub>2</sub> gases	83
§6.9.1 The wavelength range 233-239nm	83
§6.9.2 The wavelength range 245-262nm	88
§6.10 Possible dissociation pathways in the formation of NO <sup>+</sup> during laser interaction with nitroaromatic	

molecules	92
§6.11 Conclusions	95
§6.12 Future experiments	96
 <b>Chapter 7: RIMS of carbon and Hydrogen atoms following laser induced multiphoton dissociation of nitrobenzene and nitrotoluene molecules.</b>	
§7.1 Introduction	97
§7.2 Atomic spectroscopy notation	99
§7.3 Electric dipole selection rules	101
§7.4 RIMS of carbon atoms produced from nitrobenzene and nitrotoluene.	102
§7.5 Power dependence of carbon ion production	107
§7.6 Estimation of the number of carbon atoms liberated per nitroaromatic molecule	110
§7.7 RIMS of hydrogen atoms produced from nitroaromatic molecules	111
§7.8 Conclusions	112
 <b>Chapter 8 Conclusions and Future experiments.</b>	113
 <b>Appendix 1: Second Harmonic Generation</b>	118
<b>Appendix 2: Interaction of a 2-level system with strong laser fields: Power broadening</b>	121
 <b>References</b>	125

*All this, and more, with less than  
half a second of laser light!*

# **Chapter 1**

## **Introduction**

### **§1.1 Introduction**

The requirement for an instrument which can combine high sensitivity and selectivity to detect trace concentrations of environmentally sensitive molecules in the atmosphere has stimulated a large amount of interest in a wide variety of analytical approaches.

Many different types of detector are being investigated and evaluated as possibilities, but the 'ideal' design should possess certain important characteristics. Primarily, the device should be very simple to operate so that essentially unskilled personnel could perform the operation and maintenance tasks. Additionally, in order for the machine to be of more practical use, analysis times should be short to permit real time analysis. The system should be highly reliable, inexpensive to construct and maintain, and, depending on the application, be portable.

The work presented in this thesis was carried out with the aim of assessing the possibility of using the technique of Resonance Enhanced Multiphoton Ionisation Mass Spectrometry for the detection and unambiguous identification of aromatic type vapours, in particular the nitro containing compounds nitrobenzene and mono-nitrotoluene. To date, no definite sensitivity measurements have been made, with most of the work presented being concerned with developing a procedure for the selective detection of these compounds.

The majority of experiments conducted so far have been performed in high vacuum environments using either quadrupole filtered ion detection or by mass separation of ions in a time-of-flight spectrometer. The use of mass spectrometry is necessary at this stage in the development in order to gain as complete an understanding as possible of the photo-molecular processes which occur in the laser/molecule interaction. Should sufficient wavelength discrimination be achieved, the experimental configuration may well include ion mobility separation as opposed to the use of high vacuum mass spectrometry. The main advantages of such a system are obvious, in that analysis would be performed at atmospheric pressure, thus avoiding the need to use high vacuum equipment. Analysis times would remain short compared to existing chromatographic techniques and the possibility of constructing a portable system exists, pending the development of compact, tunable laser sources.

The work of Chapter 7 discusses experiments concerned with resonance ionisation of carbon and hydrogen atoms, which are liberated in the multiphoton interaction of UV light with nitroaromatic molecules. In this chapter, the general aspects of the resonance ionisation technique as applied to atomic detection are considered initially, from where extension is made to multiphoton ionisation of molecules.

## **§1.2 Resonance Ionisation Spectroscopy (RIS).**

Resonance Ionisation Spectroscopy is a technology which was developed in the early seventies, mainly by Letokhov and his co-workers in the USSR Academy of Sciences (Letokhov, 1987) and by Hurst and Payne (1988a, 1988b) at Oak Ridge in the U.S.A. The idea was originally proposed as a separation technique

for Uranium isotopes, but the widespread applicability for atomic identification and detection soon became evident. The nature of the method required very intense light sources, and it was not until the advent of the laser that such sources became available. With very intense pulsed laser sources (typically  $> 10^6 \text{ W/cm}^2$ ) it was possible to induce multiphoton absorption in both atoms and molecules (Ambartsumyan *et al*, 1976; Johnson, 1980; Antonov and Letokhov, 1981; Goodman and Rava, 1981; Hodges *et al*, 1981; Bekov and Letokhov, 1983; Schlag and Neusser, 1983; Whetten *et al*, 1983a; Antonov *et al*, 1984; Letokhov, 1985, 1988; Apel *et al*, 1987), with ionisation being achieved provided the combined photon energies exceeded the first ionisation potential of the system being studied. In the first few years after its development, most interest lay in its possible applications for isotope separation (Ambartsumyan and Letokhov, 1972; Letokhov, 1979; Clark *et al*, 1984). The RIS technique has been put to use in a wide variety of areas, including photochemistry (Letokhov, 1983), high energy physics (Ledingham *et al*, 1986), medicine (Thonnard *et al*, 1989) and depth profiling of semiconductors in the electronics industry (McLean *et al*, 1988).

The principles of RIS are very simple. Each atom in the periodic table has associated with it a unique set of bound energy states. Two distinct types of ionisation, namely resonant and non-resonant, need to be considered, in order to discuss the advantages of the former. In the non-resonant process (Fig. 1.1a)), the multiphoton absorption proceeds through short lived virtual states of the atom, where the absorption cross-section for non-resonant absorption is typically  $10^{-18} \text{ cm}^2$ . The absorption cross-section however, is found to increase dramatically if real bound energy states of the atom are involved in the excitation process. Fig. 1.1b) shows one photon excitation, one photon ionisation of an

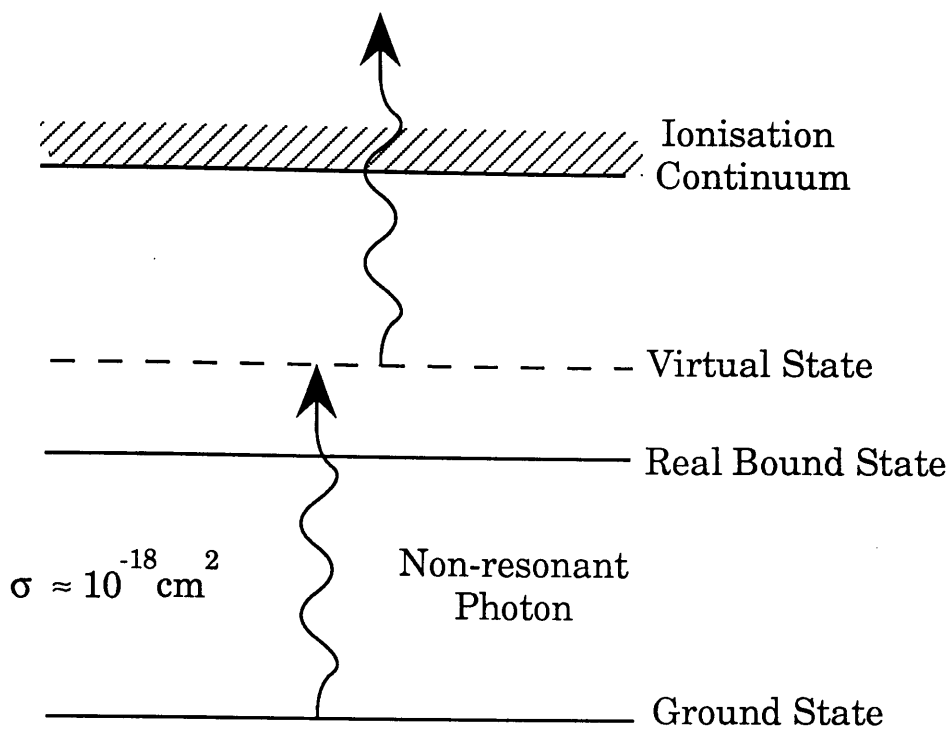


**Fig. 1.1a):** Non-resonant two-photon ionisation.

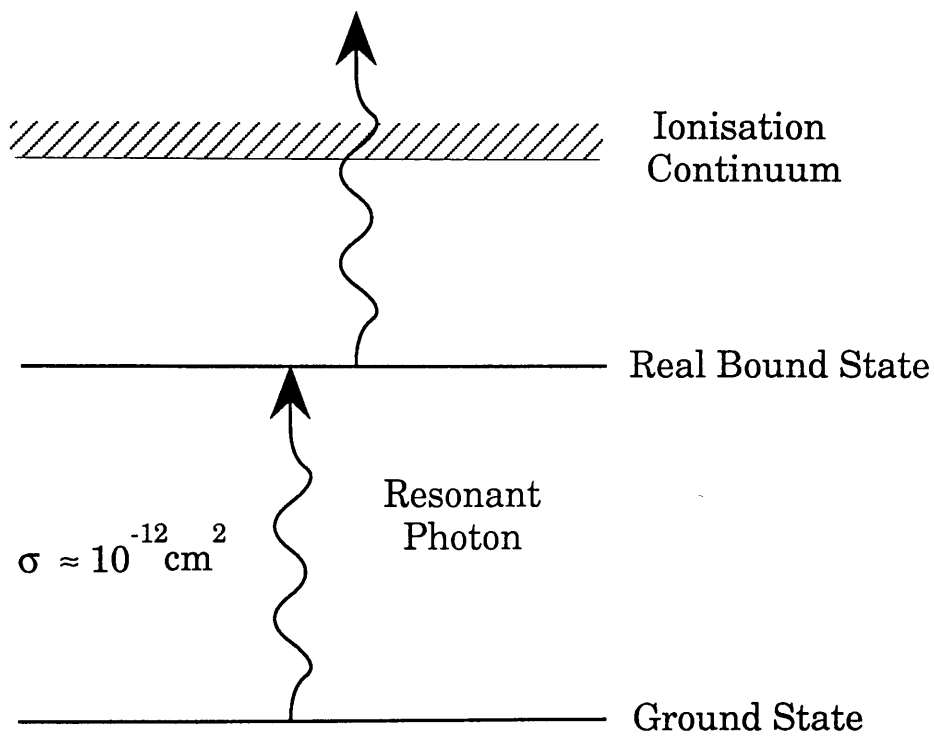


**Fig. 1.1b):** Resonant two-photon ionisation.

atom, with the excitation photon tuned in wavelength such that it is in resonance with a transition in the atom. Resonant transitions in atoms have typical cross sections of  $10^{-12} \text{ cm}^2$ . The atom will continue absorbing photons until eventually, ionisation is effected. Cross-sections for absorption from an intermediate state to the ionisation continuum are typically  $10^{-18} \text{ cm}^2$ . Since each atom has its own unique set of energy levels, different photon energies can be chosen to ionise resonantly different atoms. Elemental selectivity is therefore possible in RIS, which is certainly not possible in non-resonant ionisation.

An added advantage of the RIS process lies in the fact that by using sufficiently high laser fluxes, the ionisation process may be saturated. In this case, an ionisation efficiency of 100% may be achieved in the interaction volume. Due to the small ionisation cross sections in atoms, very large photon fluxes are required in order to optically saturate transitions into the ionisation continuum. To alleviate this difficulty, a sequential multistep process was proposed in which the atom was excited through a series of real states to Rydberg levels lying very close to the ionisation limit. Ionisation of the atom is then achieved by applying an electric field pulse (Bekov *et al*, 1978; Letokhov, 1987). In a similar fashion, the efficiency of ionisation from high lying levels may be enhanced by collisions with buffer gas atoms (Hurst *et al*, 1977; Ledingham *et al*, 1984; Houston *et al*, 1988).

Hurst *et al* (1979, 1980) have listed five basic schemes using at most two lasers to ionise all elements in the periodic table except helium and neon. These particular atoms have very large ionisation potentials and in addition the energy difference between the ground state and the lowest lying excited state is very



large, thereby requiring photons in the deep UV range to excite. The five basic ionisation schemes are shown in Fig. 1.2.

Scheme 1 is the simplest of all, and involves the absorption of two photons from the same laser. This two step process requires the intermediate state to lie more than half way to the continuum if the second photon is to ionise the atom. This scheme is generally restricted to atoms with low ionisation potentials, due to the limitations imposed by available laser dyes to produce photons of the required energy.

The technique of frequency doubling has been employed to extend the range of atoms which can be ionised in a two-step process. In scheme 2, a frequency doubled photon excites the atom to a resonant intermediate state, with ionisation being achieved by absorption of a fundamental photon from the same pulse.

For atoms with higher ionisation potentials, more than two excitation steps can be used. Scheme 3 involves two resonant absorption processes which are effected by photons of different wavelengths from different laser beams. Ionisation is achieved by absorbing a photon of either wavelength. In scheme 4, we have a similar process to scheme 3, but the first absorption is effected by a frequency doubled photon.

Finally, scheme 5 involves a two-photon resonant absorption which proceeds through a short lived virtual state of the atom, with ionisation accomplished by a single photon absorbed from the same laser pulse. The disadvantage of this method is that the absorption cross-section through a virtual state is very small compared to single photon resonant absorption, so in general

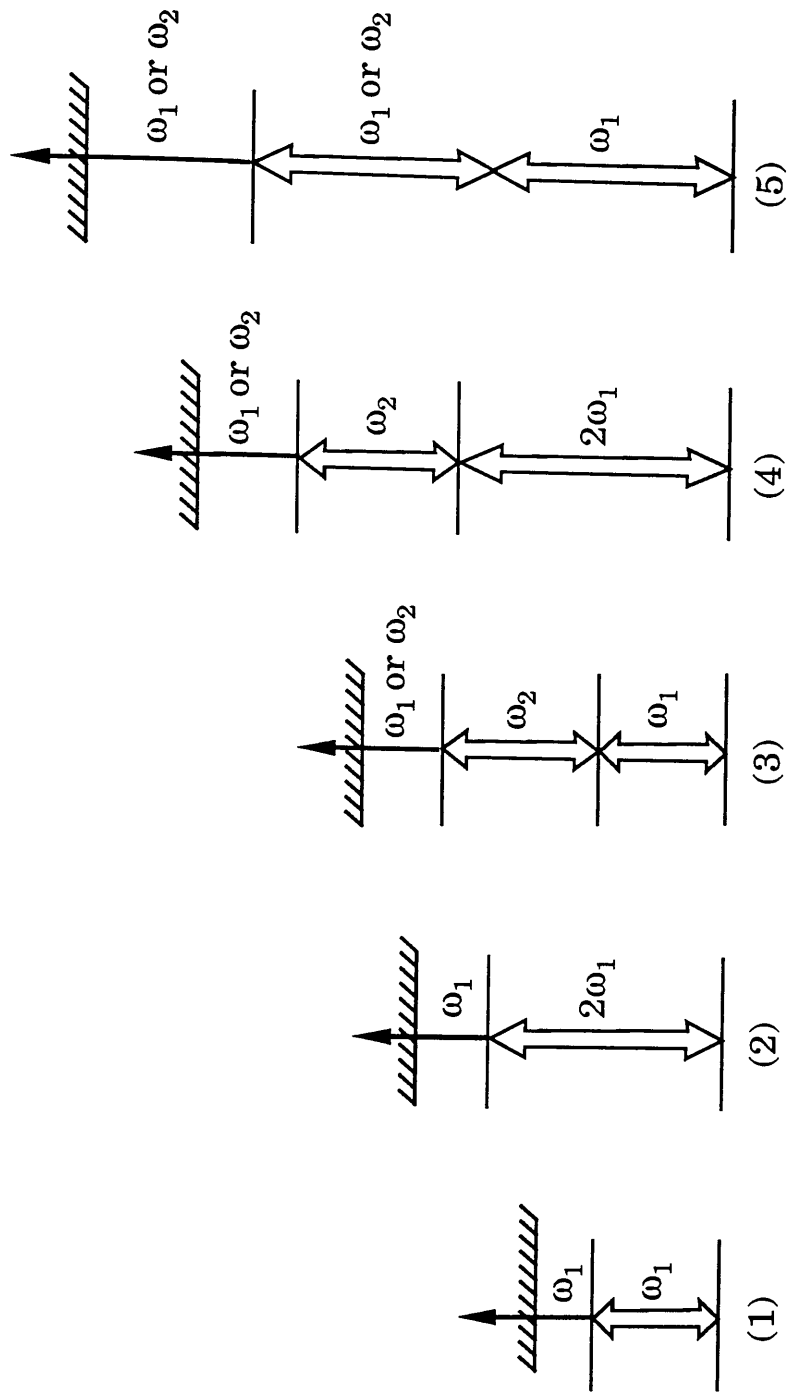


**Fig. 1.2:** The five basic resonance ionisation schemes (Hurst *et al.*, 1979).

schemes of this sort are less efficient than corresponding schemes where resonant absorption is involved. Finally, one distinct advantage of this method lies in the fact that states which are forbidden by electric dipole selection rules for single photon transitions may be studied.

### **§1.3 Laser Ionisation Spectroscopy of molecules.**

The ionisation of polyatomic molecules has been carried out by absorption of a single photon from a vacuum ultraviolet (VUV) light source (Letokhov, 1987). Originally, low flux broadband incoherent sources were used, but lacked both spectral resolution and sensitivity. In addition, all molecules present in the light beam with suitably low ionisation potentials were ionised, so no degree of molecular selectivity was achieved. Such VUV light was also difficult to manipulate since air readily absorbs light in this wavelength range. The sensitivity aspect was improved by using VUV laser sources, such as  $H_2$  lasers, but the practical difficulties mentioned above still exist.

Fig. 1.3 shows five distinct laser ionisation schemes in molecules (Parker, 1983). In Fig. 1.3(i), a single high energy photon (usually in the VUV range) is absorbed by the molecule, and will result in ionisation of the molecule provided the photon energy exceeds the first ionisation potential of the molecule. In the diagram, I.T. represents the ionisation threshold or first ionisation potential of the molecule. Disadvantages associated with this scheme include a lack of molecular spectral selectivity since no characteristic bound molecular states are involved in the ionisation process, as well as the usual difficulties in manipulating VUV radiation.

Fig. 1.3(ii) shows non-resonant  $N$  photon ionisation (e.g  $N=5$ )

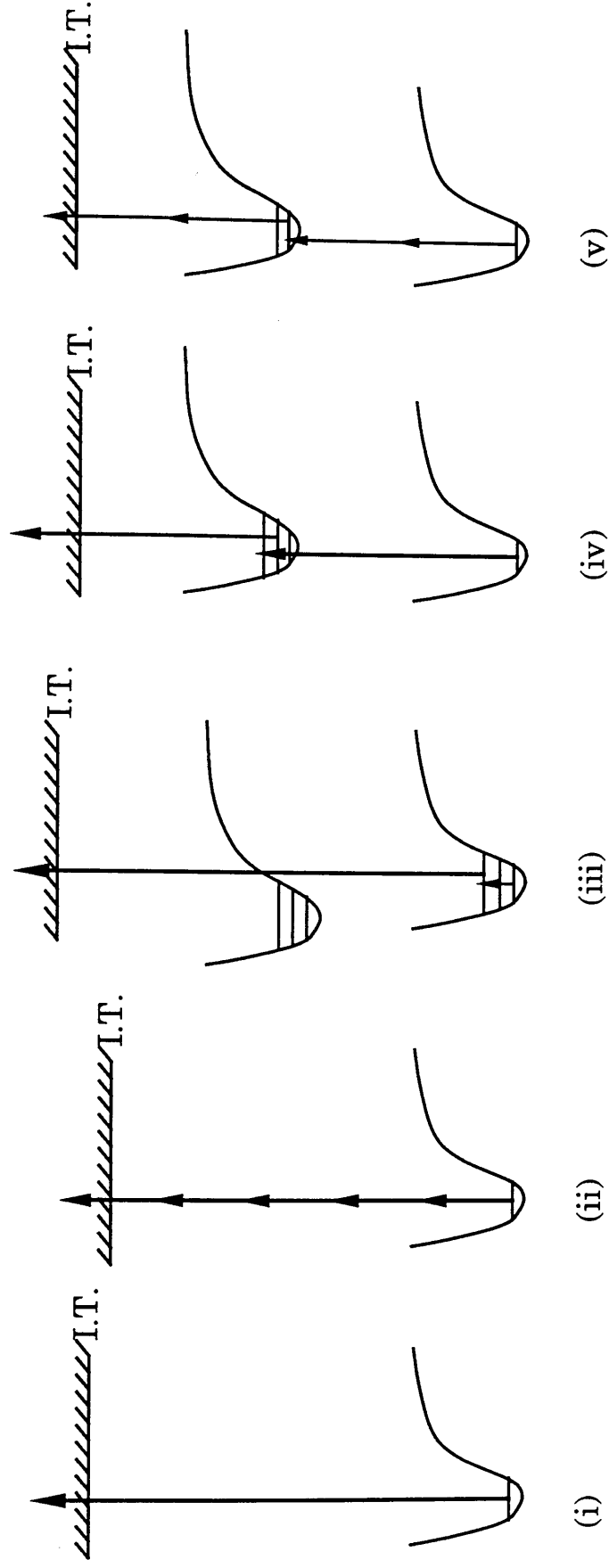


**Fig. 1.3:** Several different molecular ionisation schemes (Parker, 1983). I.T. represents the ionisation threshold of the molecule.

- (i) Single photon ionisation
- (ii) Non-resonant Multiphoton Ionisation (MPI)
- (iii) Resonant two-photon ionisation via ground state rovibrational levels.
- (iv) Resonant two-photon ionisation via excited state rovibrational levels.
- (v) Resonance Enhanced Multiphoton Ionisation (e.g. two photon excitation, two photon ionisation).

of a molecule. The scheme is referred to as being non-resonant since it proceeds through short lived 'virtual' states of the molecule. This multiphoton ionisation (MPI) process provides no molecular selectivity, the overall ionisation cross section is generally small since no resonances are involved, and consequently high photon fluxes are required if this method is to be employed. Background interference from molecules with lower ionisation potentials than that of the sample of interest occurs since they too can be ionised. The ionisation rate of a non-resonant N-photon process is given by,

$$R = \sigma_N \Phi^N \quad \text{-(1.1)}$$

where  $\Phi$  is the laser flux in photons/cm<sup>2</sup>/s and  $\sigma_N$  is the overall N-photon ionisation cross-section (Parker, 1983). Typical cross-sections for 2 and 3-photon non-resonant ionisation in molecules are 10<sup>-50</sup> cm<sup>4</sup> s and 10<sup>-82</sup> cm<sup>6</sup> s<sup>2</sup> respectively (Johnson, 1980).

The scheme shown in Fig. 1.3(iii) involves the stepwise absorption of two photons of different wavelengths. The first photon absorbed (in the IR range) connects the lowest lying ground state vibrational level with a higher lying vibrational level still within the electronic ground state manifold. From this excited state, the molecule is ionised non-resonantly by absorption of a high energy photon, generally in the VUV or UV range. Although molecular selectivity is achieved via the ground state vibrational structure, a major problem lies in the possibility of ionising molecules in the beam which have not absorbed an IR photon. The ionising wavelength requires to be tuned such that it is energetic enough to ionise only those molecules in the excited vibrational level and leave unaffected the unexcited molecules.

Again, ionisation schemes which involve the absorption of VUV light are not really desirable due to the difficulties mentioned above.

In order to make use of the selectivity of characteristic vibrational or rotational structure, but to overcome the drawbacks of scheme (iii), it is more profitable to utilise rovibrational states of an intermediate electronic bound state (Fig. 1.3(iv)). This generally requires light in the visible or near UV range, which is relatively easy to generate. Once excited to the intermediate level the molecule may be ionised by a second photon, either from another laser pulse, or by a photon from the same laser pulse, provided the combined photon energy exceeds the ionisation potential of the molecule. When this is the case, the scheme is termed Resonant Two Photon Ionisation (R2PI) and is the simplest and most efficient of all multiphoton ionisation schemes. The simplicity of this method lies in the facts that only one laser source is required and only two photons are involved in the ionisation process thereby relieving the high flux conditions required in higher order ionisation processes.

In some cases, photons in the deep UV range are required to excite the lowest lying electronic energy states of a molecule. It is often more convenient therefore to utilise two-photon excitation to excite these states. The scheme shown in Fig. 1.3(v) is an example of a 2+2 ionisation process (2 photon excitation followed by 2-photon ionisation) which proceeds through a real bound state of the molecule, situated at the second photon energy. Ionisation schemes of this type are termed resonance enhanced and form the basis of the technique Resonance Enhanced Multiphoton Ionisation Spectroscopy (REMPI). As in the case of

RIS of atoms, the overall cross section for REMPI is generally several orders of magnitude larger than the corresponding non-resonant MPI process, which of course leads to greater ionisation efficiencies. The REMPI technique has been used extensively to study aromatic molecules (Johnson, 1975; Freuholz *et al*, 1980; Lubman *et al*, 1980; Rettner and Brophy, 1981; Sin *et al*, 1984). A common approach involves the use of fixed wavelength laser sources, such as the fourth or fifth harmonic output of a Nd:YAG laser at 266 or 213nm (Kolaitis and Lubman, 1986a, 1986b; Zhu *et al*, 1990).

The advantage of REMPI and R2PI over other laser ionisation schemes and other conventional sources such as chemical ionisation and electron or ion bombardment is that under suitable conditions, an ionisation efficiency of 100% can be achieved within the interaction volume. This saturation of the ionisation process is easier to achieve in schemes where fewer photons are involved in the ionisation process, as can be seen from equation (1.1).

The first MPI experiments were performed in simple gas cells, where ions formed in the interaction were detected by applying a small potential difference between two electrodes and observing a current pulse on one of the electrodes (Johnson, 1975). One of the overwhelming advantages of such an ionisation technique lies in the fact that ions can be detected in simple chambers with efficiencies approaching 100%. Coupled to the inherently high ionisation efficiency of an MPI/REMPI event, this makes the technique highly sensitive. In stark contrast to resonance ionisation in atoms, molecules can be induced to break up or fragment during the laser interaction. This opens the door to a possible identification method using the coupled information

of optical and mass spectral data. In simple ionisation chambers, no information is available on the fragmentation processes occurring in the laser/molecule interaction, so in order to study the laser induced fragmentation patterns of molecules, mass spectrometry has been used extensively in conjunction with laser ionisation techniques. The use of mass spectrometry in conjunction with laser ionisation spectroscopy gives rise to a very powerful two dimensional analytical technique. Lubman (Lubman, 1988a, 1988b) has reviewed the subject of MPI from both an applications viewpoint and the theoretical and instrumentation viewpoints.

#### **§1.4 Supersonic jet cooling.**

Many molecules exhibit wide structureless absorption bands which inevitably reduces the chances of obtaining any degree of selectivity using the REMPI technique. One method which has been used in an attempt to overcome this drawback is supersonic jet cooling, which involves internally cooling sample molecules just prior to the laser interaction in a Joule-Kelvin expansion. This involves seeding the sample molecules of interest in a large amount of inert carrier gas, and expanding the mixture from very high pressure (several atmospheres) to vacuum conditions ( $<10^{-5}$  mbar). In the expanded beam, sample molecules collide with carrier gas atoms, which results in a quenching of the internal rovibrational state populations in the molecules. This cooling process concentrates population into a few low lying internal modes which ultimately leads to a sharpening of the spectral features of the molecule. The technique of supersonic jet cooling has been used by many authors (Smalley *et al*, 1977; Zandee *et al*, 1978; Zandee and Bernstein, 1979a, 1979b; Dietz *et al*, 1980a, 1980b; Mikami *et al*, 1980; Leutwyler and Even, 1981;



Lubman *et al*, 1985; Tembreull *et al*, 1985; Tembreull and Lubman, 1986; Hager and Wallace, 1988; Li and Lubman, 1988). The cooling process may also lead to an increase in detection sensitivity, provided sufficient numbers of sample molecules remain in the laser interaction volume.

### §1.5 Ion Mobility Spectrometry (IMS).

As mentioned earlier, the most practical instrument design is one which operates at atmospheric pressure. One possibility is to employ the technique known as ion mobility spectrometry or plasma chromatography (PC) (Karasek, 1947) in conjunction with REMPI. Ion mobility spectrometry has been in existence for over 20 years, with the first reports on successful operation being made by Cohen and Karasek (1970), in which the PC was used as a detection device in gas chromatography experiments. The first PC's used a 10mCi  $^{63}\text{Ni}$   $\beta$  source to interact with reactant gases, which when ionised, transferred charge to the trace molecules of interest through a series of ion-molecule reactions. Both reactant ions and molecular ions were subsequently removed from the reaction region and injected, by applying a voltage pulse on a wire grid, into an atmospheric pressure drift region. In the drift region, a counter current gas flow opposed the motion of the injected ions through two-body ion-neutral collisions. The ions were attracted to a detector plate by a constant electric field of  $\sim 300\text{V/cm}$ , and were separated according to their characteristic mobilities in the drift gas used. In addition to using a radioactive source to effect ionisation, several other methods have been used including laser induced multiphoton ionisation (Lubman and Kronick, 1982, 1983a, 1983b; Kolaitis and Lubman, 1986b; Zhu *et al*, 1990). The current state of ion mobility spectrometry in analytical science has been reviewed recently by St. Louis and Hill Jr, 1990.

## Chapter 2

### **Relevant theoretical concepts.**

#### **§2.1 Introduction**

This chapter will discuss the basic theoretical concepts required for an understanding of laser ionisation processes in atoms and molecules. Firstly, the theory of the interaction of electromagnetic (e.m.) radiation with atoms or molecules will be described from a semiclassical viewpoint, where the laser field is described classically by a monochromatic plane wave and the atom or molecule treated quantum-mechanically. This approach leads to results concerning resonant absorption of light by a system, which forms the basis of the RIS and REMPI techniques.

Several physical processes act in molecules to compete with further photon absorption from excited electronic states. A brief discussion of the main processes which occur in molecular excited states is given. Ionisation of molecules is often accompanied by laser induced fragmentation especially at very high laser fluxes, so fragmentation processes in molecules are also considered.

The semiclassical approach to photon-molecule interactions is not the most convenient method to use in estimating ion yields, so a population rate equation model is introduced. Factors such as laser fluence, molecular dissociation rates and transition lifetimes can be incorporated in this model with ease. Finally, various transition line broadening mechanisms are discussed.

## §2.2 Photon-Molecule interactions: A semiclassical approach.

A semi-classical treatment of the interaction between e.m. radiation and a non-degenerate two-level quantum mechanical system is presented (Demtrodor, 1982). A diagram of the two-level system being considered is shown in Fig. 2.1, with states **a** and **b** being assumed to be non-degenerate, and having energies  $E_a$  and  $E_b$  respectively. In addition, the excited state **b** is considered as being 'lossless', since no excited state decay mechanisms are included.

The laser field is regarded (rather unrealistically) as a classical monochromatic plane wave of frequency  $\omega$ , which is written as,

$$\underline{E} = \underline{E}_0 e^{-i(\underline{k} \cdot \underline{r} - \omega t)} + \text{complex conjugate.} \quad -(2.1)$$

where  $\underline{E}_0$  is a constant vector, and  $\underline{k}$  is the wavevector of the field. The complex conjugate is included to ensure that the electric field is a real quantity.

In order to simplify the analysis which follows, the interaction Hamiltonian is written in the dipole approximation, where the spatial derivatives of the electric field are neglected, and the amplitude of the electric field is regarded as being constant. This is an excellent approximation in our case since the wavelength of visible/UV light (200-700nm) is very much larger than a molecular dimension (typically 1nm), and therefore the phase of the wave is approximately constant throughout the molecular volume (Demtrodor, 1982). In this approximation, the interaction Hamiltonian,  $V$ , may be written as,

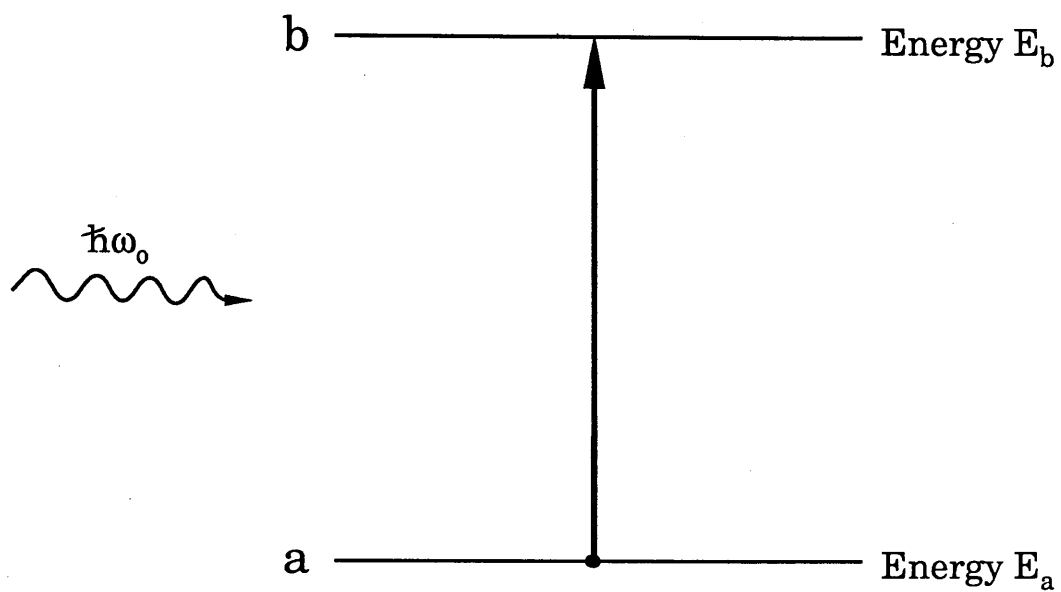


**Fig. 2.1:** Interaction of a monochromatic e.m. wave with a non-degenerate two-level system.

$$V = -e\mathbf{r} \cdot \mathbf{E} = -e\mathbf{r} \cdot [\mathbf{E}_0 e^{i\omega t} + \text{c.c}] \quad -(2.2)$$

where the molecule has been placed at the origin so that  $\mathbf{k} \cdot \mathbf{r} \sim 0$  (for simplicity).

With no external perturbations, the system will behave in a manner which is governed by the time independent Schrodinger equation,

$$H_0 \phi_n = E_n \phi_n \quad (n=1,2,3,\dots) \quad -(2.3)$$

where  $H_0$  is the unperturbed Hamiltonian of the system,  $E_n$  is the total energy of the eigenstate  $\phi_n$ , which may be written in the separated form,

$$\phi_n(\mathbf{r}, t) = u_n(\mathbf{r}) e^{-iE_n t / \hbar} \quad -(2.4)$$

The set  $\{\phi_n\}$  are called the stationary states of the system.

When an external perturbation,  $V$ , is imposed on the system, the interaction Hamiltonian is modified and written as,

$$H = H_0 + V, \quad -(2.5)$$

and the system now behaves in a manner which is described by the time dependent Schrodinger equation,

$$H\psi = i\hbar \frac{\partial \psi}{\partial t} \quad -(2.6)$$

since  $V$  is a time dependent operator. In (2.6),  $\psi$  is the total wavefunction of the system, which, due to the completeness property of the stationary state eigenfunctions, can be written in

the form,

$$\psi(\underline{r},t) = \sum_{n=1}^{\infty} a_n(t)\varphi_n(\underline{r},t) \quad -(2.7)$$

where  $a_n(t)$  are time dependent coefficients.

Therefore, for a two-level system, with energy eigenstates **a** and **b**, the wavefunction for the system is written as a linear combination of the stationary state wavefunctions, thus,

$$\psi(r,t) = a(t)u_a e^{-iE_a t/\hbar} + b(t)u_b e^{-iE_b t/\hbar} \quad -(2.8)$$

where  $a(t)$  and  $b(t)$  are the time dependent probability amplitudes of states **a** and **b** respectively. The terms  $|a(t)|^2$  and  $|b(t)|^2$  therefore represent the probabilities that the system will be in states **a** and **b** respectively, a time  $t$  after the laser pulse is switched on. The ultimate aim of this analysis is therefore to find an expression for  $|b(t)|^2$ .

Upon substitution of (2.8) in (2.6), we obtain,

$$V a(t)u_a e^{-iE_a t/\hbar} + V b(t)u_b e^{-iE_b t/\hbar} = i\hbar \left[ \dot{a}(t)u_a e^{-iE_a t/\hbar} + \dot{b}(t)u_b e^{-iE_b t/\hbar} \right] \quad -(2.9)$$

By multiplying by  $u_a^*$  and integrating (2.9) over the appropriate coordinates,  $\tau$ , we get,

$$i\hbar [\dot{a}(t)e^{-iE_a t/\hbar}] = a(t)e^{-iE_a t/\hbar} \int u_a^* V u_a d\tau + b(t)e^{-iE_b t/\hbar} \int u_a^* V u_b d\tau \quad -(2.10)$$

and eventually,

$$\dot{a}(t) = -\frac{i}{\hbar} [a(t)V_{aa} + b(t)V_{ab}e^{-(E_b-E_a)t/\hbar}] \quad -(2.11)$$

where

$$\begin{aligned} V_{ij} &= \int u_i^* V u_j d\tau = - \int u_i^* (\mathbf{e}_{\mathbf{r}} \cdot \mathbf{E}) u_j d\tau \\ &= -\mathbf{E} \cdot \int u_i^* (\mathbf{e}_{\mathbf{r}}) u_j d\tau \\ &= -\mathbf{E} \cdot \mathbf{R}_{ij} \end{aligned} \quad -(2.12)$$

The quantity  $\mathbf{R}_{ij}$  is called the dipole matrix element for the transition between states  $i$  and  $j$ .

A similar procedure leads to an equation for  $b(t)$  and is written,

$$\dot{b}(t) = -\frac{i}{\hbar} [b(t)V_{bb} + a(t)V_{ba}e^{i(E_b-E_a)t/\hbar}] \quad -(2.13)$$

The terms  $V_{aa}$  and  $V_{bb}$  are both zero, since  $\mathbf{r}$  is an odd function, so after writing  $\hbar\omega_{ba} = E_b - E_a$ , and substituting for  $\mathbf{E}$ , (2.11) and (2.13) simplify to,

$$\dot{a}(t) = i\chi_{ab} [e^{-i(\omega_{ba}+\omega)t} + e^{-i(\omega_{ba}-\omega)t}] b(t) \quad -(2.14)$$

$$\dot{b}(t) = i\chi_{ba} [e^{i(\omega_{ba}+\omega)t} + e^{i(\omega_{ba}-\omega)t}] a(t) \quad -(2.15)$$

$$\text{where} \quad \chi_{jk} = \mathbf{E}_0 \cdot \mathbf{R}_{jk} / \hbar \quad -(2.16)$$

The above equations are coupled and must be solved in order to evaluate  $b(t)$ .

### §2.2.1 Weak light intensities.

In the weak field limit we investigate the solution of (2.14) and (2.15) when the lower state population changes only slightly during the interaction time. In this situation, we can write,

$$a(t) \approx 1 \quad \text{and} \quad |b(t)|^2 \ll 1, \text{ for all times } t. \quad -(2.17)$$

If it is assumed that all molecules occupy their ground states at the instant the radiation field is switched on ( $t=0$ ) then, we may write,

$$a(t)=1 \text{ and } b(t)=0 \text{ when } t=0 \quad -(2.18)$$

In these circumstances, one obtains,

$$b(t) = \chi_{ab} \left[ \frac{e^{i(\omega_{ba}-\omega)t} - 1}{(\omega_{ba} - \omega)} + \frac{e^{i(\omega_{ba}+\omega)t} - 1}{(\omega_{ba} + \omega)} \right] \quad -(2.19)$$

Close to resonance,  $\omega \approx \omega_{ba}$ , the oscillation at frequency  $\omega + \omega_{ab}$  is rapid compared to that at  $\omega_{ba} - \omega$ , and the main contribution to  $b(t)$  is therefore from the term containing  $(\omega_{ba} - \omega)$ . In this case, the  $(\omega_{ba} + \omega)$  term becomes insignificant and may be neglected. This simplification is called the rotating wave approximation (RWA).

In this approximation, the probability of finding the system in state **b** at time  $t$  is given by,

$$|b(t)|^2 = \chi_{ab}^2 \left[ \frac{\sin \left( \frac{\omega_{ba}-\omega}{2} t \right)}{\left( \frac{\omega_{ba}-\omega}{2} \right)} \right]^2 \quad -(2.20)$$

The variation of  $|b(t)|^2$  with frequency is shown in Fig. 2.2. It can be seen that the transition probability is maximum when the



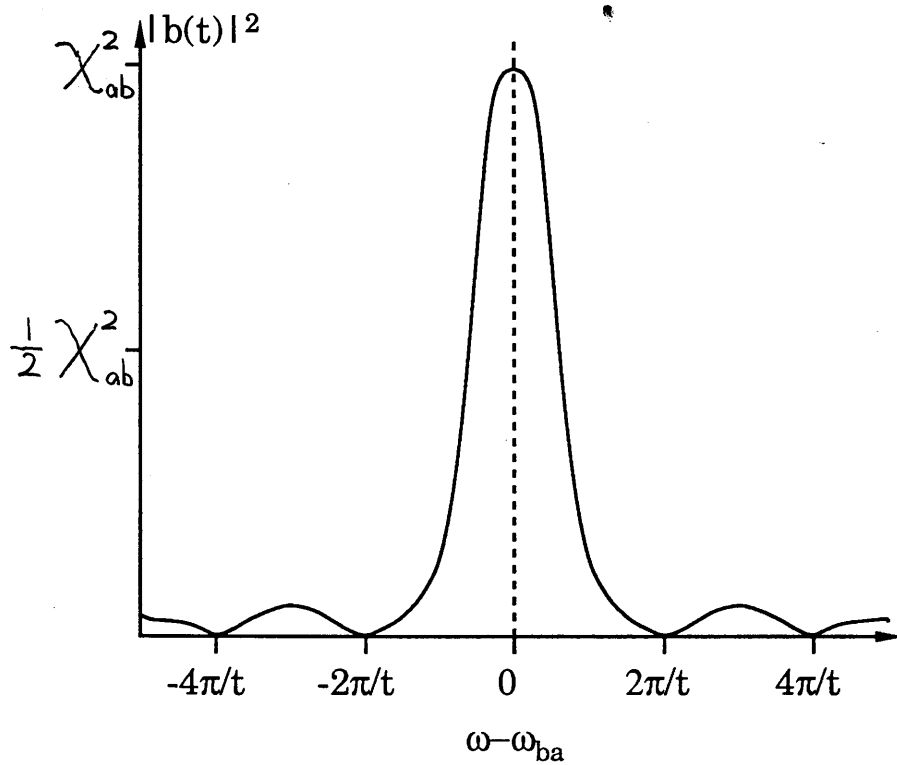


**Fig. 2.2:** Transition probability as a function of detuning.

field frequency is resonant with the molecular transition.

As the laser wavelength is varied, the absorption intensity is maximised therefore when the photon energy matches the energy difference between two bound states of the molecule and of course, it is precisely this fact which forms the basis of the RIS and REMPI techniques.

### §2.3 Electronic energy levels in molecules.

Whereas electronic levels of single and multi-electron atoms are sharply defined, their counterparts in diatomic and polyatomic molecules are found to be broad, structured manifolds, arising because of the additional vibrational and rotational degrees of freedom available to a molecule.

The simplest case to consider is that of a homonuclear diatomic molecule. Such a molecule has electronic levels similar to that shown in Fig. 2.3, where the total electronic energy is drawn as a function of nuclear separation. This so-called Morse potential curve represents a stable state of the molecule since a minimum in the potential energy exists, which arises due to a balancing between the strong *Coulomb* forces and attractive forces between constituent nuclei and 'binding' electrons.

Constraints due to the vibrational and rotational motions are such as to limit the available number of configurations the molecule can assume. These vibrational and rotational sub-levels are quantised and are depicted by the horizontal lines shown. In most molecules, vibrational levels are generally separated by  $\sim 1000\text{cm}^{-1}$  and rotational levels by  $\sim 10\text{-}100\text{cm}^{-1}$ .

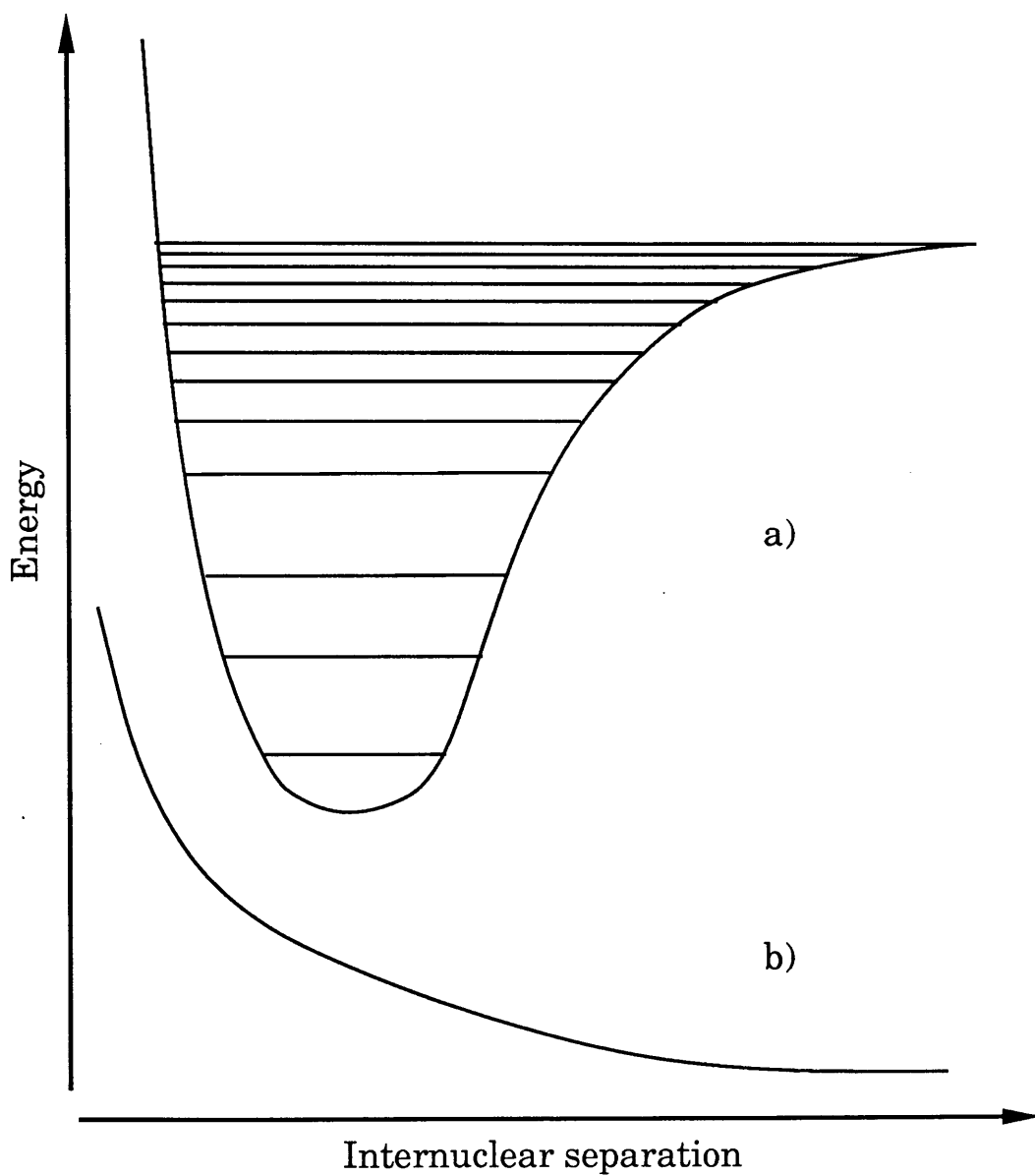


**Fig. 2.3:** **a)** Typical bound electronic energy level of a diatomic molecule, showing discrete rovibrational states.  
**b)** Unbound energy state of a diatomic molecule.

The potential energy curve representing the electronic energy of a state of a polyatomic molecule is generally of the same form as the Morse curve shown in Fig. 2.3a). In this case, the internuclear separation must be replaced by some generalised coordinate, which could be a particular bond length or an angle between two bonds etc. Unstable energy states can also arise when the attractive forces are insufficient to overcome the nuclear repulsive forces. Such a state is included in Fig. 2.3b) and as can be seen, no potential energy minimum is present i.e. the minimum energy of the system corresponds to the constituent atoms (in the diatomic case) or daughter molecular species (in the polyatomic case) being infinitely far apart.

#### §2.4 Electronic transitions in molecules.

A transition between two electronic bands of a molecule not only changes the electronic configuration, it generally incurs a change in the vibrational and rotational motions of the molecule as well. The total Hamiltonian,  $H$ , of the system will in general be dependent on both the nuclear and electronic configurations of the molecule. For a polyatomic molecule, the Hamiltonian is very complicated indeed and can be written in full as (King, 1964),

$$\begin{aligned}
 H = & -\frac{\hbar^2}{2} \sum_{\alpha} \frac{1}{m_{\alpha}} \nabla_{\alpha}^2 - \frac{\hbar^2}{2m} \sum_i \nabla_i^2 + \sum_{\alpha} \sum_{\beta > \alpha} \frac{Z_{\alpha} Z_{\beta} e^2}{4\pi\epsilon_0 r_{\alpha\beta}} - \sum_{\alpha} \sum_i \frac{Z_{\alpha} e^2}{4\pi\epsilon_0 r_{i\alpha}} \\
 & + \sum_j \sum_{i > j} \frac{e^2}{4\pi\epsilon_0 r_{ij}}
 \end{aligned}
 \tag{2.21}$$

where nucleus  $\alpha$  has mass  $m_{\alpha}$  and atomic number  $Z_{\alpha}$ ,  $r_{\alpha\beta}$  is the distance between nuclei  $\alpha$  and  $\beta$ ,  $r_{i\alpha}$  is the distance between electron  $i$  and nucleus  $\alpha$  and finally,  $r_{ij}$  is the distance between

electrons  $i$  and  $j$ . The Schrodinger equation describing the system may be written as,

$$\hat{H}\psi(q_\alpha, q_i) = E\psi(q_\alpha, q_i) \quad -(2.22)$$

where  $q_\alpha$  and  $q_i$  represent the nuclear and electronic coordinates respectively. For the Hamiltonian given by (2.21), the Schrodinger equation (2.22) is extremely difficult or even impossible to solve analytically due to the very large number of interactions that occur within the molecule. Fortunately it can be simplified greatly by making several justifiable approximations.

#### §2.4.1 Born- Oppenheimer approximation.

This approximation is based on the fact that the vibrational motion of the constituent nuclei is very slow compared to the motion of the much less massive electrons. The electronic motion is therefore treated as being completely independent of the nuclear motion, which is not strictly true, but nevertheless represents a first order, and reasonably good, approximation. The total wavefunction of the molecule is then written in separable form as,

$$\psi(q_\alpha, q_i) = \psi_{el}(q_i)\psi_{vib}(q_\alpha) \quad -(2.23)$$

This is known as the Born-Oppenheimer approximation.

The strength of an electronic transition in a molecule can be shown to be proportional to the square of the transition moment,  $M$ , (Harris and Bertolucci, 1978) which is given by,

$$M = \int \psi^* \hat{\mu} \psi d\tau \quad -(2.24)$$

where  $\psi, \psi'$  represent the wavefunctions of the ground and excited states respectively and  $\mu$  is the electric dipole operator. Using the Born-Oppenheimer approximation and writing the electric dipole moment as a sum of nuclear and electronic components,  $\mu_n$  and  $\mu_e$ , the transition moment becomes,

$$M = \int \psi_{e's'}^* \psi_v^* (\mu_n + \mu_e) \psi_{es} \psi_v d\tau \quad -(2.25)$$

$$\begin{aligned} M &= \int \psi_{e's'}^* \psi_v^* \mu_n \psi_{es} \psi_v d\tau + \int \psi_{e's'}^* \psi_v^* \mu_e \psi_{es} \psi_v d\tau \quad -(2.26) \\ &= \int \psi_{e's'}^* \psi_{es} d\tau_{es} \int \psi_v^* \mu_n \psi_v d\tau_n + \int \psi_v^* \psi_v d\tau_n \int \psi_{e's'}^* \mu_e \psi_{es} d\tau_{es} \end{aligned}$$

In the above expressions,  $\psi_{es}$  represents the electronic/spin component of the total wavefunction, and  $\psi_v$  the vibrational component. The integrals have been separated since  $\psi_v$  and  $\psi_{v'}$  are assumed to be independent of the electronic coordinates. The above expression reduces to,

$$M = \int \psi_v^* \psi_v d\tau_n \int \psi_{e's'}^* \mu_e \psi_{es} d\tau_e \int \psi_{s'}^* \psi_s d\tau_s \quad -(2.27)$$

since the electronic wavefunctions,  $\psi_{es}$  and  $\psi_{e's'}$  are orthogonal. In conclusion, provided the various vibrational, electronic and spin matrix elements are known, which requires a knowledge of the appropriate wavefunctions, the total transition probability may in principle be calculated.

### §2.4.2 Franck-Condon principle.

The square of the first term in (2.27) is called the Franck-Condon factor (Herzberg, 1950). This integral represents the overlap between the vibrational wavefunctions of the ground and excited state, which is an important quantity since the overall transition probability depends on the degree of overlap. An electronic transition in a molecule is always depicted by a vertical line connecting the appropriate states involved in the transition, as shown in Fig. 2.4. This is a consequence of the Franck-Condon principle (Herzberg, 1950), which states that electronic transitions in molecules occur on a timescale which is very short relative to the vibrational or rotational periods, and consequently no change in the molecular configuration is incurred during the transition time. The second and third terms in (2.27) respectively give rise to quantum mechanical electronic and spin selection rules.

## §2.5 The fate of absorbed energy in molecules.

As mentioned in Section 2.1, many different processes exist which can depopulate excited states in a REMPI event. Some of the main mechanisms which compete with further photon absorption are considered in the following sections.

### §2.5.1 Dissociation

The process under consideration is that of a transition between electronic vibrational levels as shown in Fig. 2.5. At room temperature, most ground state molecules occupy rotational levels in the lowest lying vibrational state, so only transitions from this vibrational state are considered. As shown in Section 2.4, a bound-bound transition can proceed easily provided the photon energy is correct. However, if the photon energy is sufficiently

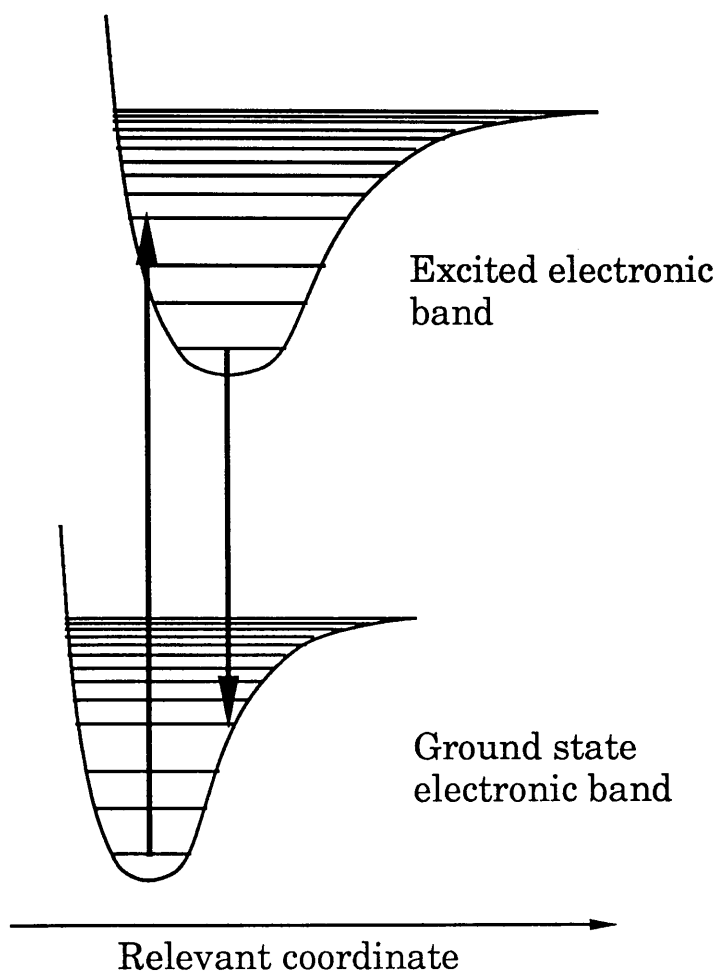


**Figure 2.4:** Basis of the Franck-Condon principle, showing no change in molecular configuration during photon absorption and emission.



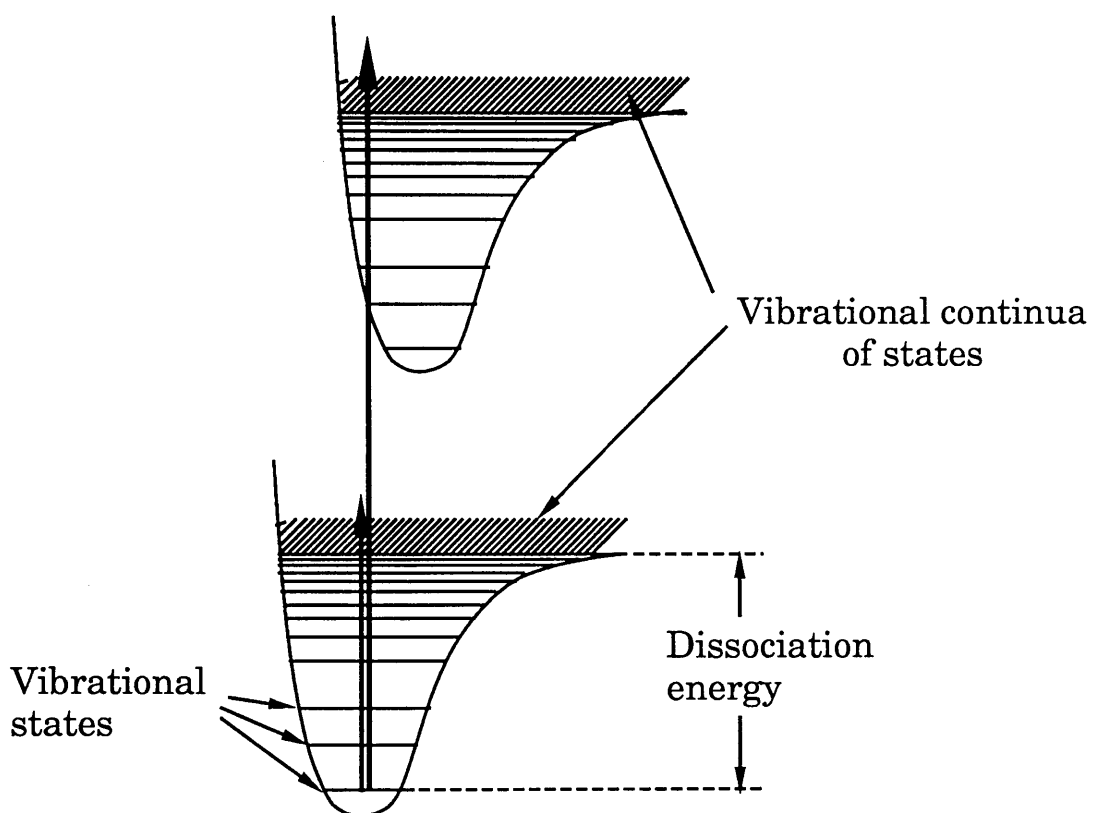


**Fig. 2.5:** Diagram showing excitation into a dissociation continuum of both ground state and excited electronic bands.

large, the molecule can be excited into a continuum of rovibrational states, as shown in the figure, where all levels are unbounded and subsequent break-up of the molecule results. This process is known as dissociation. Dissociation may also occur during a transition between ro-vibrational levels in the same electronic state. This process is also shown in the figure, where the dissociation energy of the ground electronic state is defined.

Dissociation rates of, typically,  $10^{12} \rightarrow 10^{13} \text{ s}^{-1}$  are common, and therefore would represent a large depopulation mechanism in REMPI experiments if ionisation proceeds through such states.

### §2.5.2 Predissociation.

A transition between two bound rovibrational levels in different electronic states as shown in Fig. 2.6, may, under certain circumstances, still result in dissociation of the molecule. If the vibrational state to which the molecule is excited,  $v'$ , lies close in energy to the point of intersection of the potential curves for the bound electronic state and a neighbouring unstable state, then a radiationless transition between these states may occur. This of course results in break-up of the molecule and is known as pre-dissociation.

### §2.5.3 Fluorescence and Phosphorescence.

A molecule in an excited singlet or triplet state, can dissipate excess energy in the form of e.m. radiation, and return to the  $S_0$  ground state. A transition to this ground state from a higher lying singlet state is radiatively allowed, and occurs on a timescale of  $10^{-9} \text{ s}$ , and is called fluorescence. However, if the molecule is excited to a triplet state, it is less likely that a radiative transition to the  $S_0$  state will occur, since triplet-singlet transitions have very

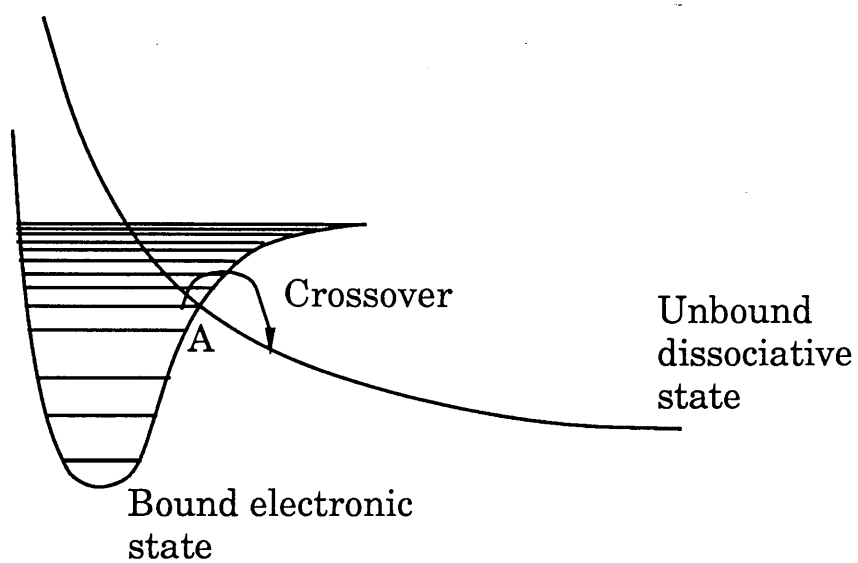


**Figure 2.6:** Isoenergetic crossover from a bound vibrational level to an unbound dissociative state. This process is called predissociation.

small probabilities due to spin selection rules. A transition of this type is called phosphorescence. These transitions can have lifetimes often as long as several seconds. Both processes are shown in Fig. 2.7.

#### **§2.5.4 Intersystem crossing and internal conversion.**

A molecule in a vibrational level of an excited electronic band can, if it lies close to a level in a neighbouring triplet state, make a radiationless transition to the triplet state. This process is called intersystem crossing. When the corresponding process occurs between two states of the same multiplicity, it is known as internal conversion.

#### **§2.5.5 Collisional relaxation or excitation.**

It is possible for a molecule in an excited vibrational level to lose excitation energy by processes which do not involve the emission of a quantum of light. Collisions with other molecules can result in a transfer of energy from the excited molecule into either translational kinetic energy or internal energy of the collision partner. In any case, the excited molecule can relax to a state of lower energy as shown in Fig.2.8. This process is called collisional relaxation or radiationless relaxation, and is dominant at high molecular densities. Collisional processes may also lead to both a shift and a broadening of spectral lines, and will be discussed in the section on transition line broadening. In addition to collisional relaxation, collisional excitation may also occur, in which a molecule gains internal energy via collisions with other molecules. This is also shown in Fig. 2.8.

A generalised energy level diagram of a typical polyatomic molecule, called a Jablonski diagram (Harris and Bertolucci,

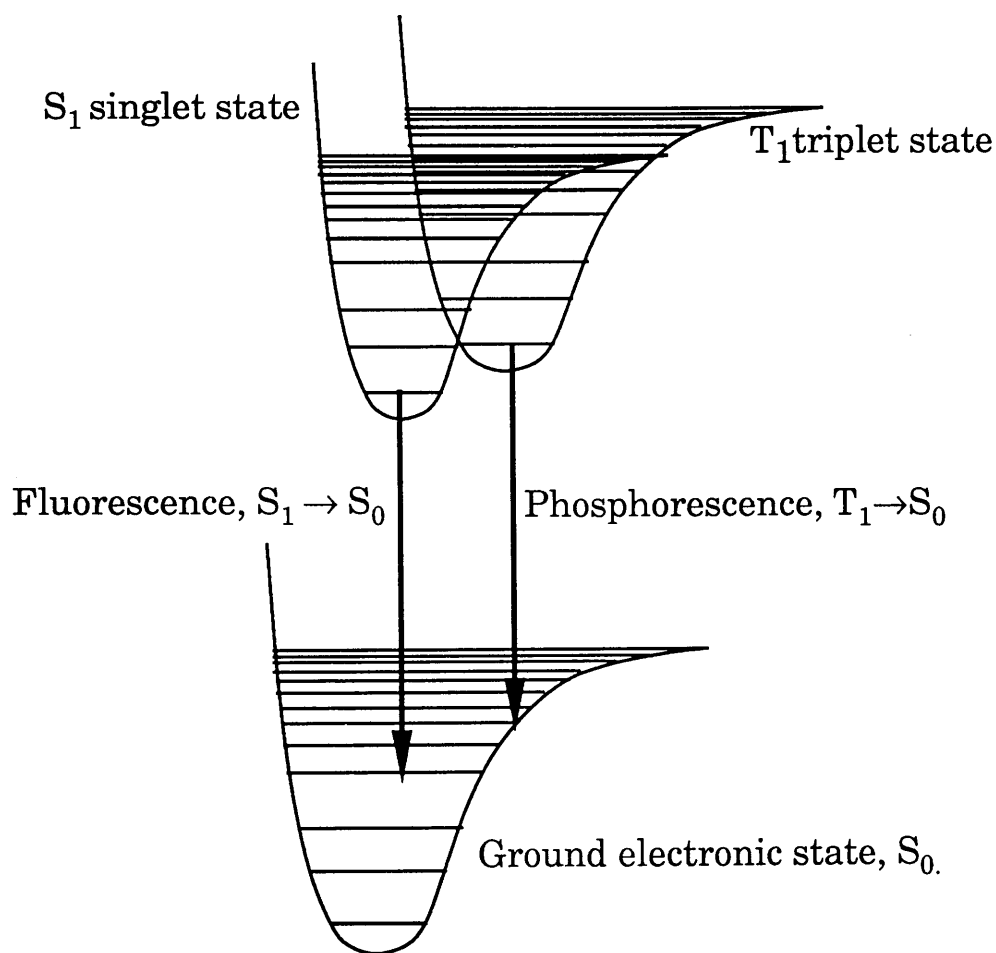


**Fig. 2.7:** Radiative de-excitation to ground state by fluorescence and phosphorescence.

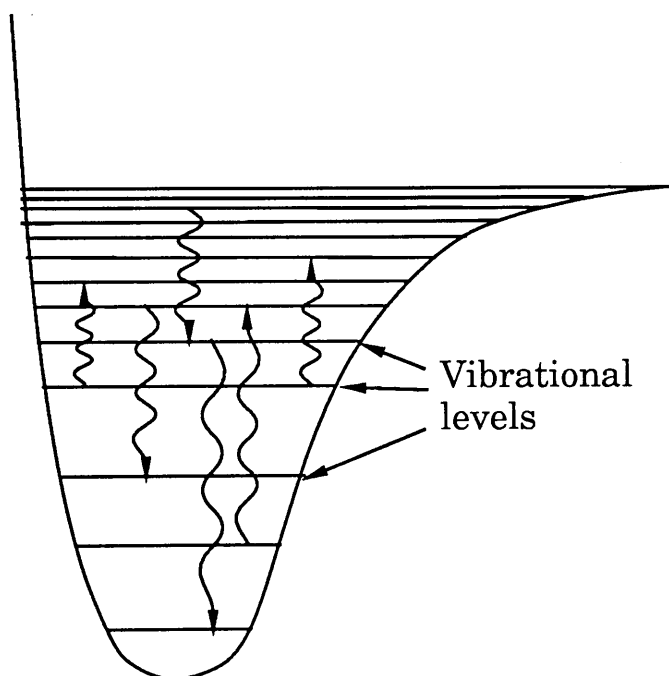


**Figure 2.8:** Vibrational relaxation and excitation processes within a bound electronic band.

1978), is given in Fig. 2.9. It shows in summary all processes discussed previously.

## §2.6 Laser induced fragmentation.

A distinctive feature of molecular systems which have been excited above their ionisation thresholds is that photofragmentation can occur on absorption of additional photons (Bernstein, 1978; Boesl *et al*, 1979, 1981b). This fragmentation process is poorly understood, but in a series of experiments performed by Boesl *et al* (1979), several models were proposed. Statistical models have been developed in an attempt to account for observed fragmentation patterns in polyatomic molecules (Rebentrost *et al*, 1981; Silberstein and Levine, 1980, 1981) and have been tested on a variety of molecules (Lichtin *et al*, 1981; Lubman, 1981). The fragmentation schemes proposed by Boesl *et al* are shown schematically in Fig. 2.10, where a hypothetical ABC molecule is considered.

Scheme (a) is termed parent ion fragmentation. In this scheme, the molecule ABC absorbs a photon from the laser pulse and is excited to the state ABC\*. Upon absorption of another photon, the molecule is excited to an energy which lies above the ionisation threshold, and an ABC<sup>+</sup> ion is formed. The molecular ion, which is still within the laser beam volume, absorbs further photons forming excited states of the ion until enough energy is absorbed such that the appearance potentials of particular fragment ions are exceeded, and the molecule fragments forming smaller daughter ions.

In scheme (b), the ABC molecule continues to absorb photons

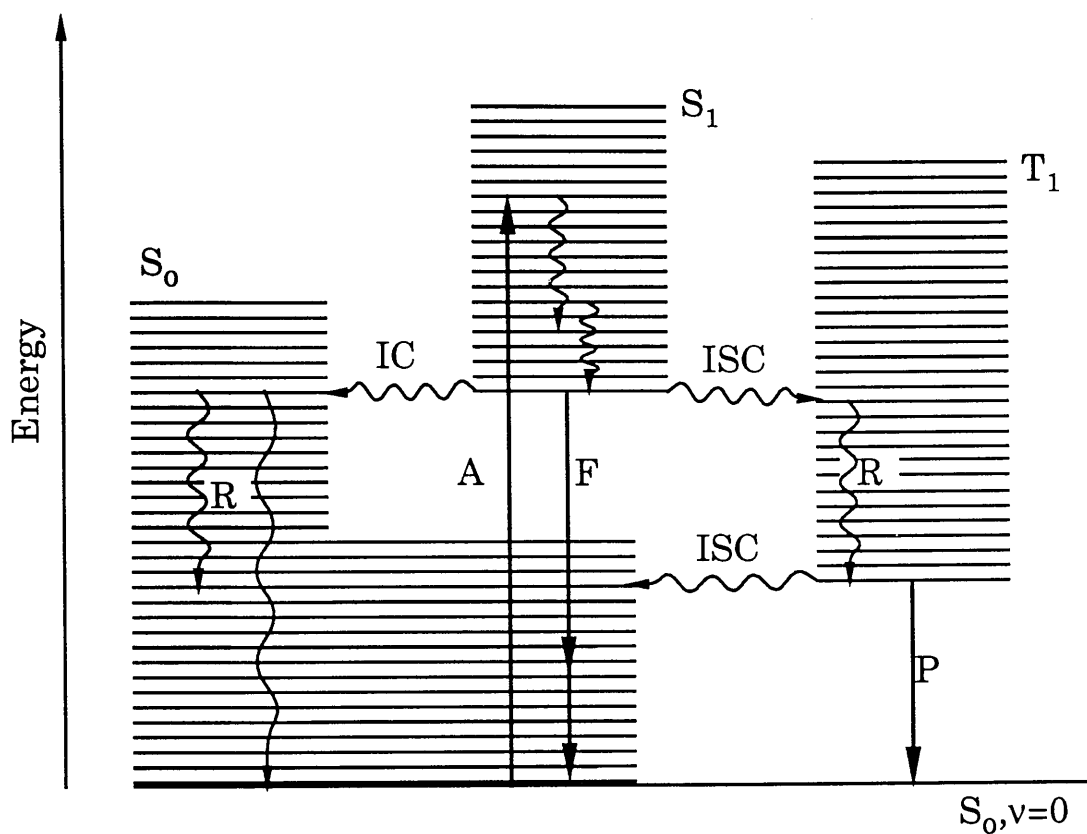


**Fig. 2.9:** Summary of photophysical processes occurring in molecules.

A = absorption

F = fluorescence

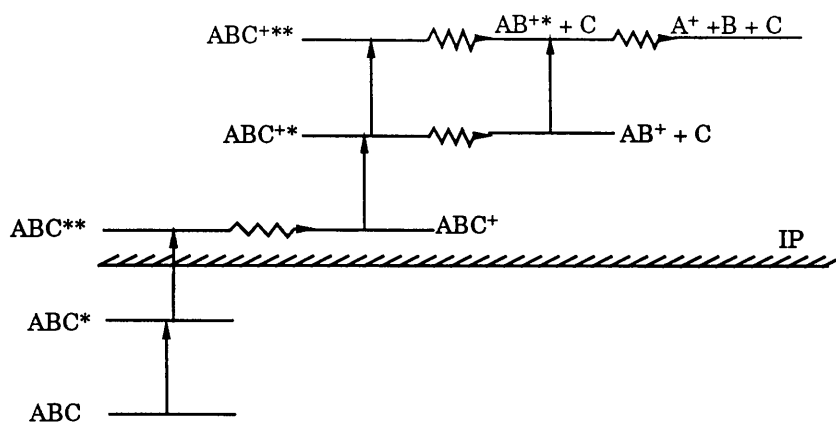
P = phosphorescence

R = relaxation

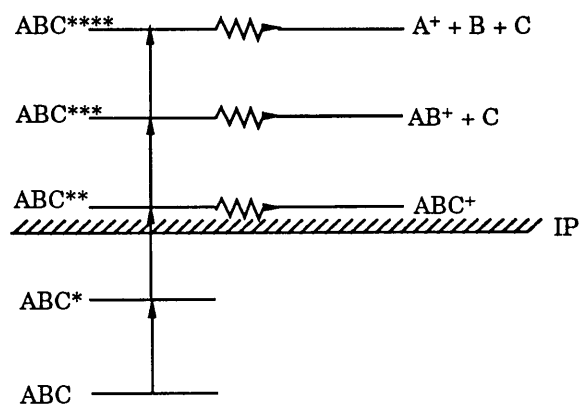
IC = internal conversion

ISC = intersystem crossing

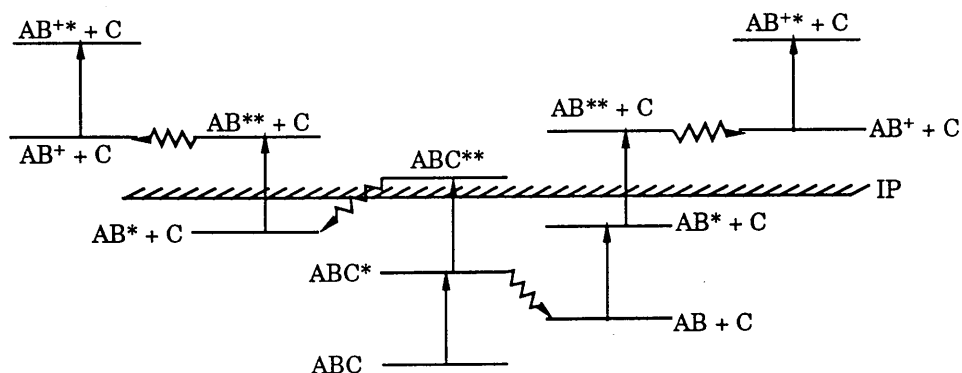




(a): Parent ion fragmentation



(b): Fragmentation proceeding through autoionisation states.



(c): Fragmentation through neutral fragment pathways.

**Fig. 2.10:** Schemes of different fragmentation mechanisms (Boesl *et al*, 1979).

as opposed to directly ionising when excited above the ionisation threshold. This absorption process forms so-called 'superexcited neutral states' of the molecule, which fragment to form a series of smaller ions, provided their appearance potentials are exceeded.

Finally, scheme (c) shows fragmentation occurring through neutral daughter fragment pathways. The ABC molecule, upon absorbing one or more photons from the pulse, can dissociate or predissociate forming neutral daughter molecules, which subsequently absorb energy from the beam and fragment.

## **§2.7 Modelling of a REMPI process.**

The dynamics of the REMPI process are most successfully described by the equations of motion of the density matrix for the particular system being considered (Demtrodor, 1982). In this formulation, irreversible decay processes from a resonant intermediate state, such as intersystem crossing and fluorescence can be easily incorporated. In addition, coherence effects which give rise to Rabi flopping can also be studied using this approach. However, for very complicated systems such as polyatomic molecules, this method becomes very complicated and difficult to solve.

Quantitative predictions of absolute ion yields from a particular ionisation scheme are reliant upon an extensive knowledge of the various wavefunctions of the particular molecule being studied, which are unfortunately not readily available.

It has been shown (Zoller and Lambropoulos, 1980) that a kinetic population rate equation approach may be used to model a REMPI process provided coherence effects are negligible. This is the case if the coherence time of the laser used is very short

compared to the actual length of the pulse (or the interaction time). In our work, a pulsed dye laser with a bandwidth of ~30GHz was used. This gives a coherence time of ~30ps, which is very much less than the 6ns pulse length. A population rate equation approach is therefore justifiable.

### §2.7.1 Population Rate Equations.

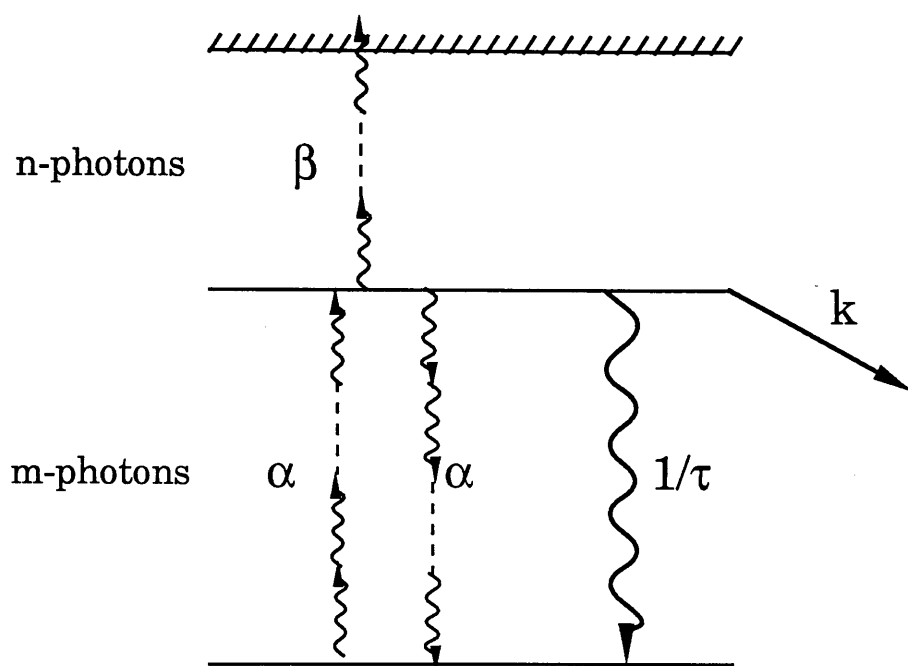
The situation considered here is that of a laser pulse which is tuned to an m-photon resonance of a particular molecule, with subsequent n-photon ionisation from the excited state (Zakheim and Johnson, 1980). Coherence effects are neglected as discussed above. A population rate equation model of a general resonance ionisation scheme in atoms has been written (Singhal *et al*, 1988, 1989). A major drawback of <sup>the</sup> rate equation approach is that the intensity distribution of the laser pulse is not usually known very accurately. A top hat temporal profile of the laser pulse is assumed therefore, in order to simplify the following analysis.

The model under consideration is schematically depicted in Fig. 2.11.

The stimulated absorption and emission rates are assumed to be given by their perturbation theory expressions, as mentioned in Chapter 1. Therefore, the m-photon absorption rate,  $R_m$ , is given by,

$$R_m = \sigma_m \Phi^m \quad \text{-(2.28)}$$

where  $\sigma_m$  is the overall m-photon absorption cross-section, and  $\Phi$  is the laser flux in photons/ cm<sup>2</sup> /second. A similar expression also applies for the n-photon ionisation rate.



$\alpha$  = stimulated m-photon absorption/emission rate  
 $\beta$  = n-photon ionisation rate  
 $k$  = predissociation rate of excited state  
 $\tau$  = lifetime of excited state

**Fig. 2.11:** Population rate equation scheme (m+n photon ionisation)

The rate equations describing the time development of the level populations,  $n_0$ ,  $n_1$  and  $n_I$  are,

$$\frac{dn_0}{dt} = -\alpha n_0 + \alpha n_1 + \frac{n_1}{\tau} \quad -(2.29)$$

$$\frac{dn_1}{dt} = -\alpha n_1 + \alpha n_0 - k n_1 - \frac{n_1}{\tau} - \beta n_1 \quad -(2.30)$$

$$\frac{dn_I}{dt} = \beta n_1 \quad -(2.31)$$

where  $n_0$ ,  $n_1$  are the populations of states 0 and 1 at time  $t$ ,  $n_I$  is the number of ions formed after time  $t$ ,  $k$  is the predissociation rate of the excited state,  $\tau$  is the lifetime of the excited state and  $\alpha = \sigma_m \Phi^m$  and  $\beta = \sigma_n \Phi^n$  are the rate constants for the excitation and ionisation steps respectively. Inspection of (2.31) shows that  $n_I(t)$  must first of all be found if the ionisation yield is to be calculated. Rearranging equations (2.29) and (2.30) gives a second order differential equation for  $n_1(t)$ ,

$$\frac{d^2 n_1}{dt^2} + \left[ 2\alpha + k + \beta + \frac{1}{\tau} \right] \frac{dn_1}{dt} + \alpha(k + \beta)n_1 = 0 \quad -(2.32)$$

which, if all molecules were considered to be in their ground states when the laser pulse was 'switched on' (at  $t=0$ ), gives,

$$n_1(t) = \frac{\alpha N_0}{(\gamma_+ - \gamma_-)} [e^{\gamma_+ t} - e^{\gamma_- t}] \quad -(2.33)$$

where  $N_0$  is the total number of molecules within the laser beam volume and

$$\begin{pmatrix} \gamma_+ \\ \gamma_- \end{pmatrix} = -\lambda \begin{pmatrix} + \\ - \end{pmatrix} [\lambda^2 - \omega^2]^{\frac{1}{2}} \quad -(2.34)$$

where  $2\lambda = 2\alpha + k + \beta + \frac{1}{\tau}$  -(2.35)

and  $\omega^2 = \alpha(k + \beta)$  -(2.36)

Finally, assuming the laser pulse has a flat top temporal profile of pulse length  $T$ , we have from (2.31),

$$n_I(T) = \beta \int_0^T n_I(t) dt \quad -(2.37)$$

which gives, upon integration,

$$n_I(T) = \frac{\alpha\beta N_0}{(\gamma_+ - \gamma_-)\gamma_+} \left[ \frac{1}{\gamma_+} (e^{\gamma_+ T} - 1) - \frac{1}{\gamma_-} (e^{\gamma_- T} - 1) \right] \quad -(2.38)$$

for the number of ions produced after the passing of the laser pulse through  $N_0$  ground state molecules.

The above expression simplifies greatly in the limits of high and low laser fluxes. The two limiting forms are considered below.

### §2.7.2 High flux conditions.

When the stimulated and spontaneous processes occur very rapidly compared to the laser pulse length, i.e. when  $\alpha, \beta, k \gg 1/T$ , the numbers  $\gamma_+ T$  and  $\gamma_- T$  become very large and negative, and the exponential terms in (2.38) tend to zero, giving,

$$n_I(T) = \frac{\alpha\beta}{\gamma_+ \gamma_-} N_0 = \left( \frac{\beta}{\beta + k} \right) N_0 \quad -(2.39)$$

Two separate cases need to be considered.

Case 1. When the ionisation rate,  $\beta \gg$  resonant state decay rate,  $k$ , we have,

$$n_I(T) = N_0 \quad \text{-(2.40)}$$

In this case, every molecule in the laser beam volume is converted into an ion. This is known as saturation of the (m+n) process. Although the sensitivity is maximised under these conditions, the spectral selectivity of the intermediate state is lost, and therefore saturation must be avoided if selectivity is desirable.

Case 2. When the intermediate state decay rate,  $k \gg$  ionisation rate,  $\beta$ , then,

$$n_I(T) = \left(\frac{\beta}{k}\right) N_0 = \left(\frac{\sigma_n \Phi^n}{k}\right) N_0 \quad \text{-(2.41)}$$

It can be shown (Letokhov, 1987) that very high ionisation efficiencies may be attained in the laser beam volume provided the following two conditions on the laser fluence,  $\phi$ , and intensity,  $\Phi$ , holds;

$$\phi \geq \phi_{\text{sat}} = (1/\sigma_{\text{ion}}) \quad \text{-(2.42)}$$

and

$$\Phi \geq \Phi_{\text{sat}} = (1/2\sigma_{\text{exc}}T) \quad \text{-(2.43)}$$

where  $\sigma_{\text{exc}}$  and  $\sigma_{\text{ion}}$  are the excitation and ionisation cross-sections respectively. The quantities  $\Phi_{\text{sat}}$  and  $\phi_{\text{sat}}$  are called the saturation intensity and fluence respectively. For characteristic excitation and ionisation cross-sections of  $10^{-17}$ - $10^{-18} \text{ cm}^2$  and excited state lifetimes of typically  $10^{-8}$ - $10^{-10} \text{ s}$ , the fluence (energy

density) and intensity required to saturate the optical transitions are, respectively,  $0.1\text{-}1\text{ J/cm}^2$  and  $10^7\text{-}10^9\text{ W/cm}^2$ .

### §2.7.3 Low flux conditions.

In the opposite limit when  $\alpha, \beta, k \ll 1/T$ , the exponential terms in (2.38) can be expanded using the binomial theorem, and when taken to the term of 2nd order in  $T$ , we have,

$$n_I(T) = \frac{1}{2}\alpha\beta N_0 T^2 = \frac{1}{2}\sigma_m\sigma_n \Phi^{m+n} N_0 T^2 \quad -(2.44)$$

This equation shows the ionisation yield to be dependent on the  $(m+n)^{\text{th}}$  power of the laser flux, which agrees with the result predicted by perturbation theory.

## §2.8 Transition line broadening.

The frequencies at which a molecule absorbs radiation is defined by the internal electronic structure of the molecule. These transition frequencies are not infinitely sharp but have associated with them a finite width. There are many mechanisms at work which serve to broaden the transition lines of a collection of molecules.

### §2.8.1 Doppler broadening.

The following section shows how the velocity distribution of a collection of molecules leads, via the Doppler effect, to a distribution in the frequencies at which the molecules absorb radiation.

The situation considered here is that of a molecule which has two bound states with energies  $E_2$  and  $E_1$  ( $E_2 > E_1$ ) (Loudon, 1973). At rest, the molecule will readily absorb light of frequency



$\omega_0$ , where,

$$E_2 - E_1 = \hbar\omega_0 \quad -(2.45)$$

We now consider the interaction between a beam of broadband light, with central frequency  $\omega_0$  propagating in the z-direction, with a molecule in energy state  $E_1$  moving at velocity  $\underline{v}_1$ . It is further assumed that the molecule absorbs a photon of frequency  $\omega$  from the beam and is, as a result, excited to energy  $E_2$ . The situation is depicted in Fig. 2.12.

If the molecule recoils with velocity  $\underline{v}_2$  after the absorption takes place, then by applying the laws of energy and linear momentum conservation, we get,

$$\omega_0 = \omega - \underline{v}_1 \cdot \underline{k} - \frac{\hbar k^2}{2mc^2} \quad -(2.46)$$

where  $k$  is the wavenumber of the light beam (at frequency  $\omega$ ),  $m$  is the mass of the molecule and  $c$  is the speed of light in vacuum. Upon inspection of the shift terms in (2.46), and taking  $\omega$  to be in the UV/visible region ( $\omega \sim 10^{15}$ - $10^{16}$  s<sup>-1</sup>), it is reasonable to neglect the last term and write as a first approximation,

$$\omega = \omega_0 + \underline{v}_1 \cdot \underline{k} \quad -(2.47)$$

This equation gives the new absorption frequency of the molecule in terms of the frequency  $\omega_0$  and the velocity of the molecule. A collection of molecules having a thermal velocity distribution will exhibit Doppler broadened lines. If a Maxwellian distribution is assumed, the probability of a molecule in the collection having its z component of velocity,  $v_z$ , in the range ( $v_z$ ,

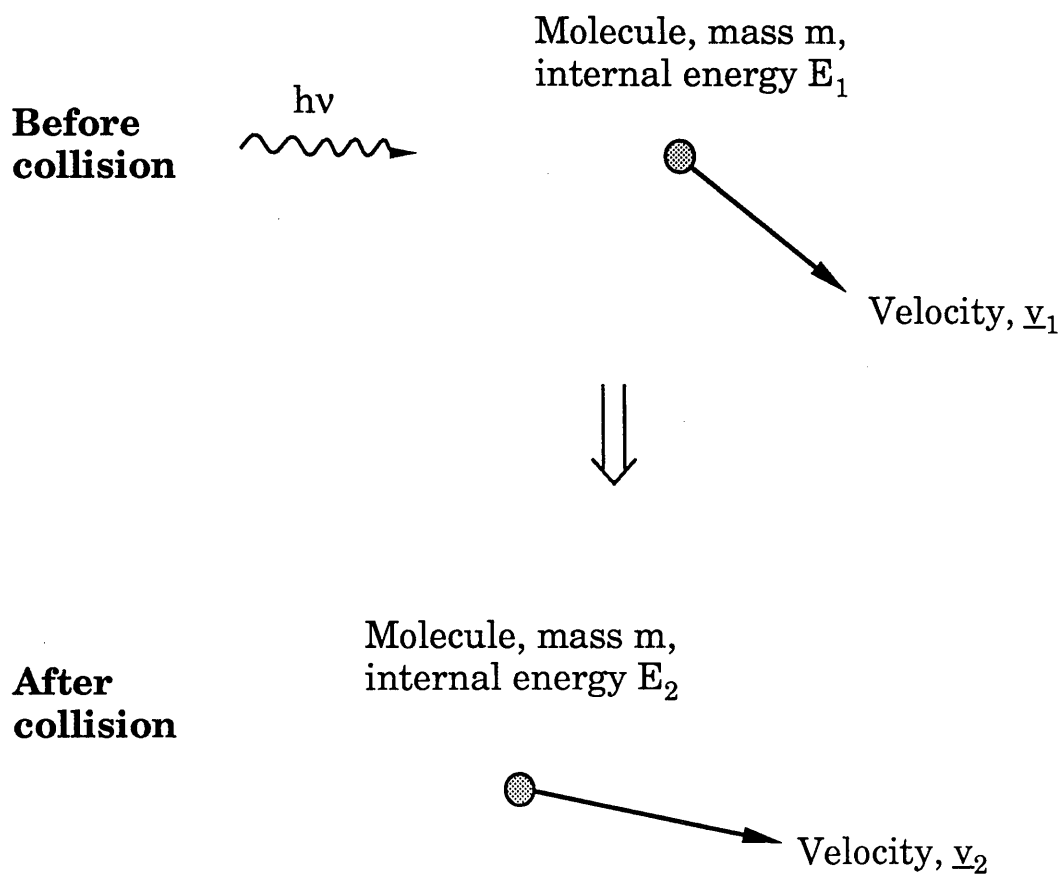


**Fig. 2.12:** Molecule travelling at velocity  $\underline{v}_1$  absorbing radiation at frequency  $\omega$ , and recoiling with velocity  $\underline{v}_2$ .

$v_z + dv_z$ ), is,

$$P(v_z) = \exp\left\{\frac{-mv_z^2}{2kT}\right\} dv_z \quad -(2.48)$$

where  $k$  is the Boltzmann constant and  $T$  the temperature.

Since the beam propagates in the  $z$ -direction,  $\underline{v}_1 \cdot \underline{k}$  may be written in the form  $v_{1z}\omega/c$ , where  $v_{1z}$  is the component of  $v_1$  in the  $z$ -direction, and by substituting for  $v_z$  in (2.48), we obtain,

$$P(\omega) = \exp\left\{\frac{-mc^2(\omega-\omega_0)^2}{2kT}\right\} \left(\frac{c}{\omega_0}\right) d\omega \quad -(2.49)$$

This represents the frequency distribution of the light absorbed from the beam. The width,  $\Delta$ , of such a distribution is given by,

$$\Delta = 2\omega_0 \left[ \frac{2kT \log 2}{mc^2} \right]^{\frac{1}{2}} \quad -(2.50)$$

For light with  $\omega_0 = 10^{15} \text{ s}^{-1}$ ,  $T = 300\text{K}$  and a molecule with mass 100 a.m.u., the Doppler width is approximately 1GHz.

### §2.8.2 Radiative broadening.

Even in the absence of external broadening mechanisms, such as collisional line broadening, electronic transitions in molecules still have finite widths. The reason for this is a manifestation of Heisenberg's uncertainty principle. Consider a radiative transition between two energy levels with energies  $E_2$  and  $E_1$ , ( $E_2 > E_1$ ) and with lifetimes  $T_2$  and  $T_1$  respectively. The uncertainty principle states that the energies of the states have

uncertainties  $\delta E_2$  and  $\delta E_1$  given by,

$$\delta E_i = \frac{h}{\tau_i} \quad (i=1,2) \quad -(2.51)$$

The transition width will therefore be given by,

$$\Delta E = h \left( \frac{1}{\tau_1} + \frac{1}{\tau_2} \right) \quad -(2.52)$$

which reduces to

$$\Delta E = \frac{h}{\tau_2} \quad -(2.53)$$

when the lower state is the ground state, since  $T_1 \rightarrow \infty$ . A state with a lifetime of 10ns, which is typical of polyatomic molecules, therefore has an intrinsic linewidth of 100MHz.

### §2.8.3 Collisional line broadening.

A collection of molecules undergoing random thermal motion results in many collisions between molecules. These collisions can result in a molecule changing state and effectively reduces the lifetime of the states involved. At atmospheric pressure, it can be estimated that there would be approximately  $10^{10}$  collisions per second, giving a reduced state lifetime of  $\sim 10^{-10}$  seconds, which implies a linewidth of  $\sim 10$ GHz. However, most experiments detailed in this thesis were performed at pressures of less than  $10^{-6}$  mbar, so the contribution to the transition width is expected to be negligible in all cases.

As a summary, the contributions of the above mechanisms to the linewidth of a transition are very much less than the 30GHz bandwidth of the laser pulse, and it may be concluded that the

observed linewidths in our experiments will be due mainly to the bandwidth of the laser pulse.

#### **§2.8.4 Laser induced power broadening.**

Under intense radiation fields, the lifetime of a state may be reduced dramatically with respect to the natural state lifetime by stimulated emission and absorption processes. This therefore results in a broadening of the transition and is known as power broadening. A detailed treatment of power broadening is given in Appendix 2.

## **Chapter 3**

### **Instrumentation**

#### **§3.1 Introduction**

The purpose of this chapter is to describe in some detail the apparatus used in performing REMPI experiments which will be discussed in later chapters. A brief overview of the whole experimental system, shown schematically in Fig. 3.1, will be given initially. The discussion will be broken into three distinct areas. Firstly, the generation and manipulation of a source of tunable UV laser light is discussed, followed by a discussion of the operational principles of the mass spectrometer system used, namely a VSW mass analyst quadrupole. Finally, the methods used for data acquisition will be considered.

As mentioned in Chapter 1, REMPI experiments are most conveniently carried out on gas phase samples under high vacuum conditions. The use of high vacuum environments brings several advantages. Firstly, hydrocarbon background which can lead to erroneous results in ultraviolet REMPI studies is minimised, and secondly it allows the use of mass spectrometers to mass analyse any ions produced. The REMPI technique can realise ionisation efficiencies of several percent within the laser beam volume, thereby making it feasible to operate in conditions where there are very small numbers of molecules in the beam i.e. in high vacuum conditions. In addition, the number of collisions between molecules at low pressures is also reduced, which is advantageous since collisionally induced processes including dissociation can greatly complicate mass

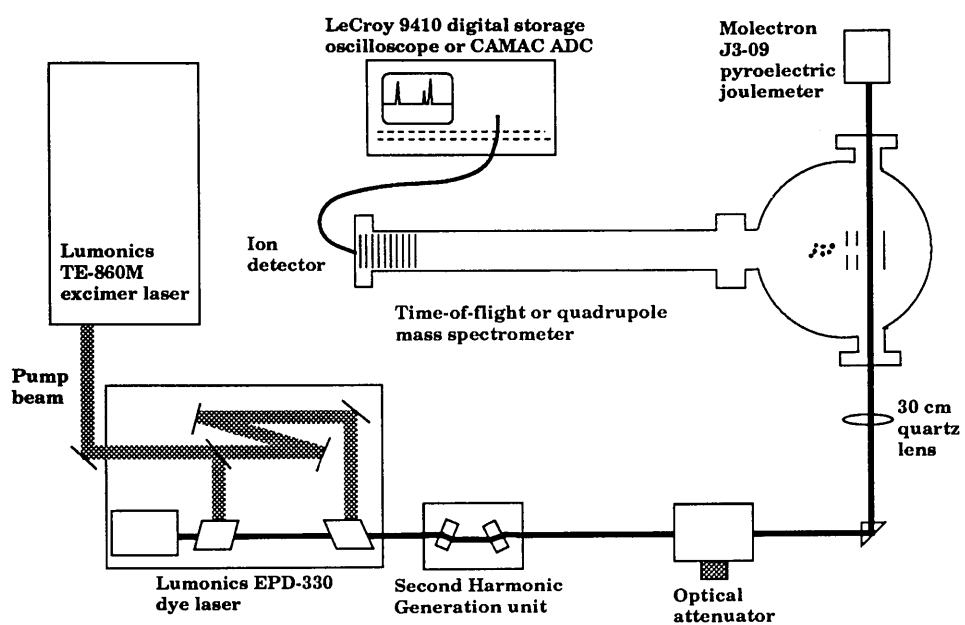


**Fig. 3.1:** Schematic diagram showing experimental set-up.

spectra. However, in real life situations, where samples would be analysed at ambient pressures, the use of high vacuum represents a severe problem since interfacing techniques to introduce the sample to the vacuum chamber would need to be employed. This would inevitably complicate the system and much more importantly lead to increased analysis times.

Molecular samples of interest were placed in a glass phial, and sample vapour was admitted directly into the acceleration region of the quadrupole or TOF mass spectrometer via a leak valve controlled stainless steel hypodermic tube inlet system. Sufficiently high numbers of molecules could be introduced because of the reasonably high saturated vapour pressures (a few Torr) of the samples so far investigated. Some modifications may be required when explosive samples are being studied, since they have in general very small saturated vapour pressures, of typically four orders of magnitude less than the molecules already studied.

A Lumonics excimer pumped dye laser system was used to generate tunable laser radiation in the wavelength range 430-640nm, which could be frequency doubled using appropriate nonlinear crystals to provide laser radiation in the range 217-320nm. This permitted resonant 2-photon ionisation studies of molecules with first ionisation potentials of up to 11.43eV, which includes most nitroaromatic-type molecules. An Inrad autotracking system was used to facilitate continuous UV output while the wavelength of the dye laser was scanned.

Both fundamental and frequency doubled beams were usually focused into the vacuum chamber by a 30cm focal length



quartz lens, where energy densities of up to 20mJ/mm<sup>2</sup> in the UV beam were routinely obtainable. After passing through the chamber, the beams were separated by quartz prisms and the UV pulse energy was measured by a Molectron J3-09 pyroelectric joulemeter. Any ions produced were electrically extracted from the laser/sample interaction region, mass analysed and detected by electron avalanche-type detectors.

In wavelength dependent measurements, signals from both the ion detector and the pulse energy meter were amplified and simultaneously monitored by a CAMAC LSI-11 peak sensing ADC system. Also, once the optimum ionisation wavelength of a particular molecule was found, TOF mass spectra were accumulated by taking the output from the ion detector directly to a LeCroy 9410 digitising oscilloscope, where signals were averaged over typically 1000 laser shots.

### §3.2 Excimer laser

Excimer (excited dimer) lasers are molecular lasers capable of producing high power pulses of ultraviolet / VUV radiation with large beam cross-sections at high repetition rates. They have found widespread use as laser sources for MPI experiments (Apel and Nogar, 1986; Hodges *et al*, 1981; Rossi and Eckstrom 1985), and also as pump sources for tunable organic dye lasers.

The laser pumping cycle of an excimer laser can be understood by considering the dimer molecule as a bound-free system. The electronic ground state of such molecules exhibits a shallow Van der Waal's minimum with a depth less than the thermal energy  $kT$  (see Fig. 3.2.) (Demtroder, 1982). These systems are therefore highly unstable in their ground state and dissociate rapidly on a timescale of ~1-10ps. They do however

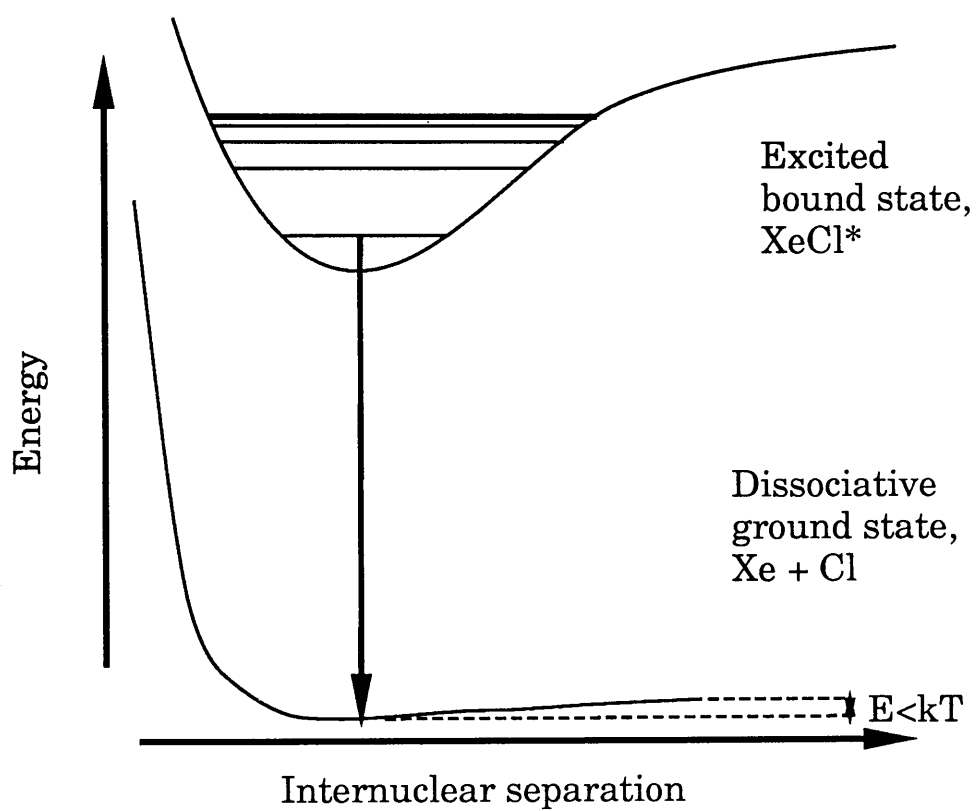


**Fig. 3.2:** Energy levels appropriate to excimer laser operation.

form bound excited states and provided the number density of reactant molecules is sufficiently high, a population inversion is easily achieved, due to the absence of ground state population, and high power pulses of UV radiation are readily available. A transition between the excited bound state and the dissociative ground state results in the emission of radiation which constitutes the laser output. Typical output parameters of the Lumonics TE 860-3 excimer used in this work are displayed in Table 3.1.

### **§3.3 Dye laser**

In the past 20 years pulsed tunable dye lasers have found widespread use in many research laboratories. Qualities such as tunability from 320-950nm using appropriate dyes, narrow bandwidths ( $< 0.01$  nm), high peak powers and ease of use helped revolutionise the fields of atomic and molecular spectroscopy. Most importantly, these attractive characteristics allowed new techniques to be developed such as resonance ionisation spectroscopy and laser induced fluorescence.

Dye lasers rely on the fluorescent properties of organic dye molecules dissolved in suitable solvents for their operation, as shown in Fig. 3.3. Ultraviolet photons from a pump laser, such as an excimer, are absorbed by dye molecules which are excited from low lying vibrational levels of the  $S_0$  ground state into vibrational levels of their  $S_1$  electronic band. Rapid radiationless transitions populate the lowest lying vibrational level ( $v = 0$ ) of the  $S_1$  state, which then serves as the upper lasing level (typical lifetime  $\sim$  several ns). High lying vibrational levels in the  $S_0$  ground state provide a continuous range of possible levels to which the molecule can de-excite. With sufficiently intense pumping a population inversion can be achieved. Radiative

Lumonics TE-860-3 excimer laser

Wavelength	308 nm
Pulse length	8 - 12 ns
Beam size	8 mm x 12 mm
Beam divergence	2.4 x 6 mrad
Max. repetition rate	70 - 80 Hz
Average pulse energy	70 mJ
Pulse to pulse stability	$\pm 5 \%$

**Table 3.1:** Output characteristics of excimer laser.

Lumonics EPD-330 dye laser

Tuning range	320 - 950 nm
Pulse length	6-8 ns
Spectral linewidth	$< 0.02$ nm
Beam size	2 mm x 2 mm
Beam divergence	$< 1$ mrad
Polarisation	$> 95\%$ vertical
Average pulse energy	10 mJ
Pulse to pulse stability	$\pm 5 \%$

**Table 3.2:** Output characteristics of dye laser.

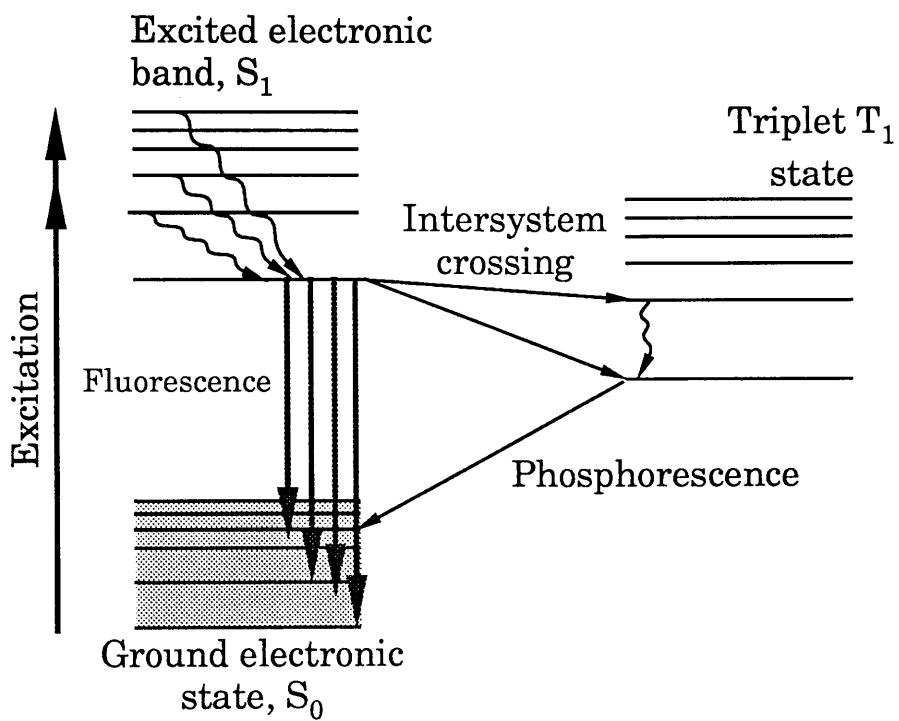


**Fig. 3.3:** Energy levels appropriate to dye laser operation.

transitions (fluorescence) occurring between these levels can experience optical gain and exhibit lasing action. The continuous nature of dye laser radiation is a consequence of the high density of ground state vibrational levels.

However, intersystem crossing from the  $S_1$  level to the nearby triplet  $T_1$  level can occur. This constitutes a loss mechanism, since the  $T_1$  state molecules usually absorb in the UV/visible region. To overcome this problem, the laser dye was circulated through both the oscillator and amplifier cells in order to rapidly remove dye molecules in  $T_1$  states from the lasing volume.

A Lumonics TE-860M excimer laser was used to pump a Lumonics EPD-330 dye (see Fig. 3.4). The excimer pump beam passed through a beamsplitter and  $\sim 10\%$  of the pulse energy was focused into the oscillator dye cell. This initiated laser action, while the remainder of the pump beam was time delayed and focused into an amplifier dye cell, where the oscillator beam caused further stimulated emission from the excited dye and boosted the oscillator power by a factor of  $\sim 15$ . At the peak of the gain curves for most dyes used, output pulse energies of  $\sim 5\text{-}10\text{mJ}$  were easily obtained.

Wavelength tuning throughout the dye gain curve was achieved by using a holographic reflection grating in the oscillator cavity. The beam was incident on the grating at glancing incidence in order to optimise the spectral resolution of the system, and tuning was effected by rotation of the grating according to the equation

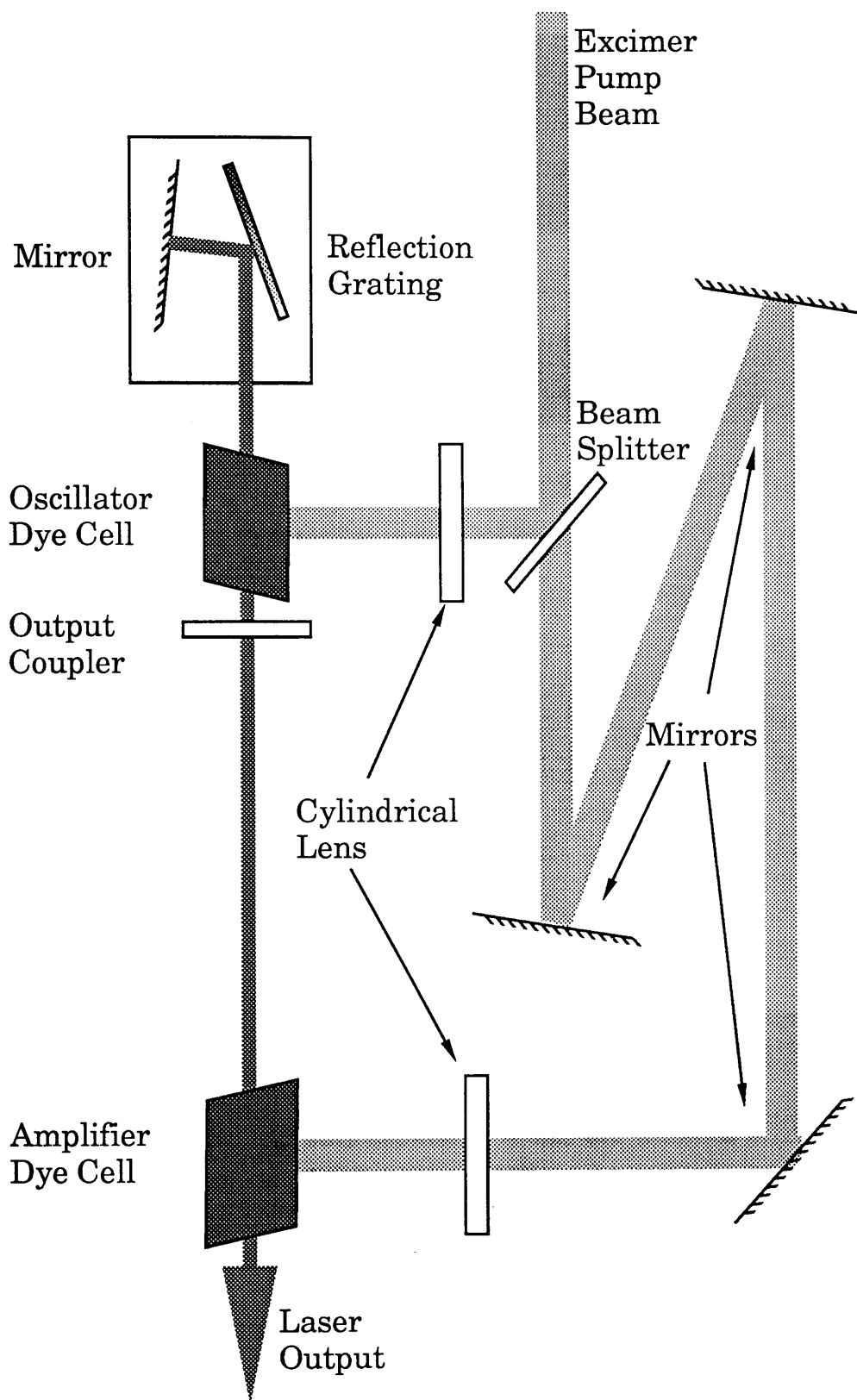


**Fig. 3.4:** Dye laser.

$$2d \sin \theta = \lambda \quad \text{-(3.1)}$$

where  $d$  is the groove separation,  $\theta$  the angle of incidence and  $\lambda$  the laser wavelength.

Typical output beam parameters of the Lumonics EPD-330 dye laser are listed in Table 3.2.

### **§3.4 Wavelength tracking system.**

In order to carry out resonance ionisation studies on a variety of different samples, it is necessary to have available a continuously tunable source of laser radiation. In the case of aromatic molecules, which generally exhibit intense absorption bands between 200 and 300nm, the technique of second harmonic generation must be employed to generate laser radiation in the appropriate wavelength range.

A diagram of the autotracking system is shown in Fig. 3.5. The dye laser output passes through a second harmonic generating crystal and a compensator block which corrects for beam walk-off. After doubling, approximately 1% of both the fundamental and SH beams is diverted by an achromatic beam splitter into the detection arm. Here, a rejection filter cuts out the fundamental beam and the doubled beam is focused between two sensitive fast photodiodes. During scanning, any imbalance in the diode currents is detected and a difference amplifier feedback arrangement drives a stepper motor which in turn rotates the doubling crystal and balances the diode currents. This assures wavelength scanning at maximum UV power output.

### **§3.5 Laser power attenuator.**

In molecular multiphoton ionisation experiments it is often



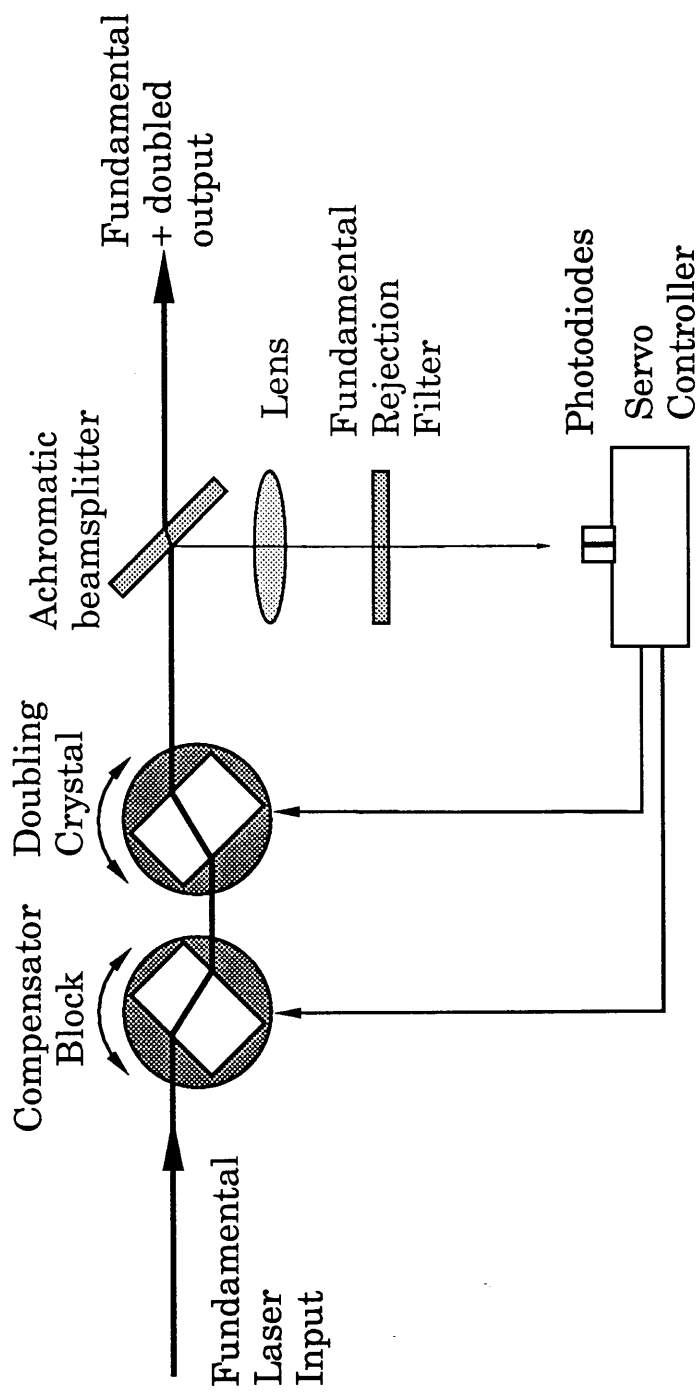


**Fig. 3.5:** Inrad autotracking unit.

desirable to observe various changes in mass spectra at different laser pulse energies. In the work described in this thesis a Newport variable attenuator was used throughout. The unit consists of two pairs of counter-rotating quartz plates arranged in a zero beam deviation configuration. Upon rotation of the plates, the angle of incidence is changed and therefore the degree of attenuation is altered in accordance with the Fresnel relations. When properly aligned the unit covered a dynamic range of 100% - 10%. A schematic of the instrument is shown in Fig. 3.6.

### **§3.6 Pulse energy measurement.**

Absolute measurements of the energy in the UV laser pulses were made using a Molectron J3-09 pyroelectric joulemeter. The operation of the device relies on the absorption of the laser pulse energy by a thin crystal of lithium tantalate. On absorbing laser radiation, the crystal is rapidly heated and becomes electrically polarised. This polarisation produces surface charge which is collected, electrically integrated and observed as a voltage pulse across 50 ohms. The peak height of the signal is then proportional the absolute energy in the pulse, with the calibration of our particular model being 1.21 V/mJ. The instrument is capable of operation at repetition rates up to 4kHz.

### **§3.7 Quadrupole mass spectrometer.**

Preliminary experiments on R2PI of simple aromatic molecules such as Aniline and Toluene were conducted using a VSW quadrupole mass spectrometer for mass analysis of laser produced ions.

A quadrupole mass spectrometer consists of four conducting rods situated at the corners of a square. Diametrically opposite

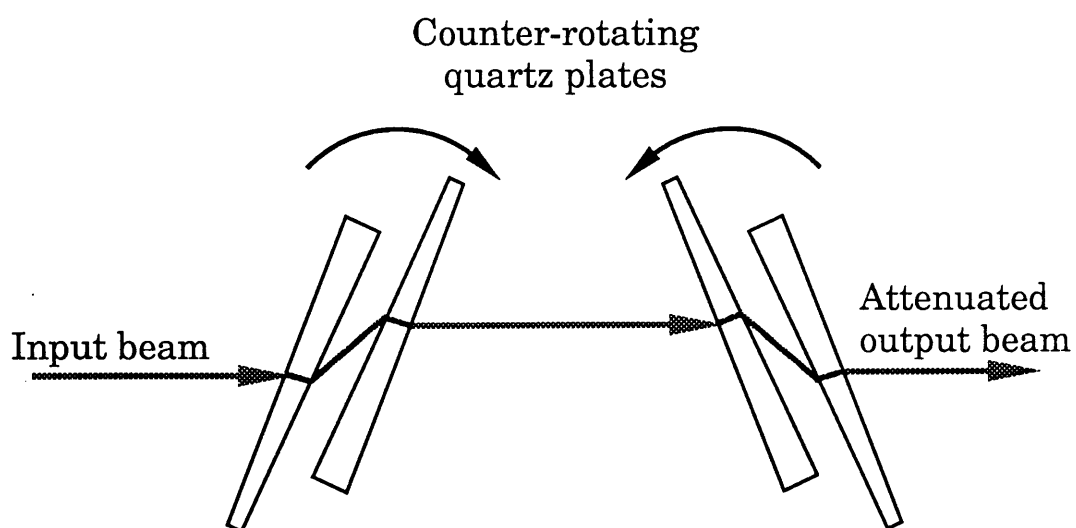


**Fig. 3.6:** Newport power attenuator.

rods have equal DC and RF potentials applied to them as shown in the cross-sectional view in Fig. 3.7. In the diagram  $U$  is the value of the d.c. voltage component,  $V$  is the amplitude of the radio-frequency signal and  $\omega$  is the angular frequency of the r.f. signal. The trajectories of any ions injected into the spectrometer are obtained mathematically by solution of the Mathieu equations (Lawson and Todd, 1972) shown below,

$$\begin{aligned}\frac{d^2x}{d\gamma^2} + (a + 2q\cos 2\gamma)x &= 0 \\ \frac{d^2y}{d\gamma^2} - (a + 2q\cos 2\gamma)y &= 0\end{aligned}$$

where  $a = \frac{8eU}{mr^2\omega^2}$ ,  $q = \frac{4eV}{mr^2\omega^2}$  and  $\gamma = \frac{\omega t}{2}$ .

The solutions to these equations are complicated but fortunately do not concern us here. In order for an ion of a particular mass to be transmitted to the detector, both  $x$  and  $y$  solutions must be bounded by the physical dimensions of the mass filter (i.e  $x, y < r$ ). If either or both solutions are unbounded the ion will be lost on collision with the quadrupole rods. A selective acceptance condition is set up for a particular mass to charge ratio according to the value of the ratio  $U/V$ , provided the r.f. frequency is kept constant.

The instrument used in our work was a VSW mass analyser with a mass range of 0 - 200 a.m.u. Sample vapour was admitted using a stainless steel hypodermic tube as shown in Fig. 3.8. The ionising laser beam intercepted sample vapour in the centre of the cage region shown and laser produced ions were simply forced into the mass filter by a small positive bias applied to a wire grid, also shown in Fig. 3.8. No extract or focusing optics were

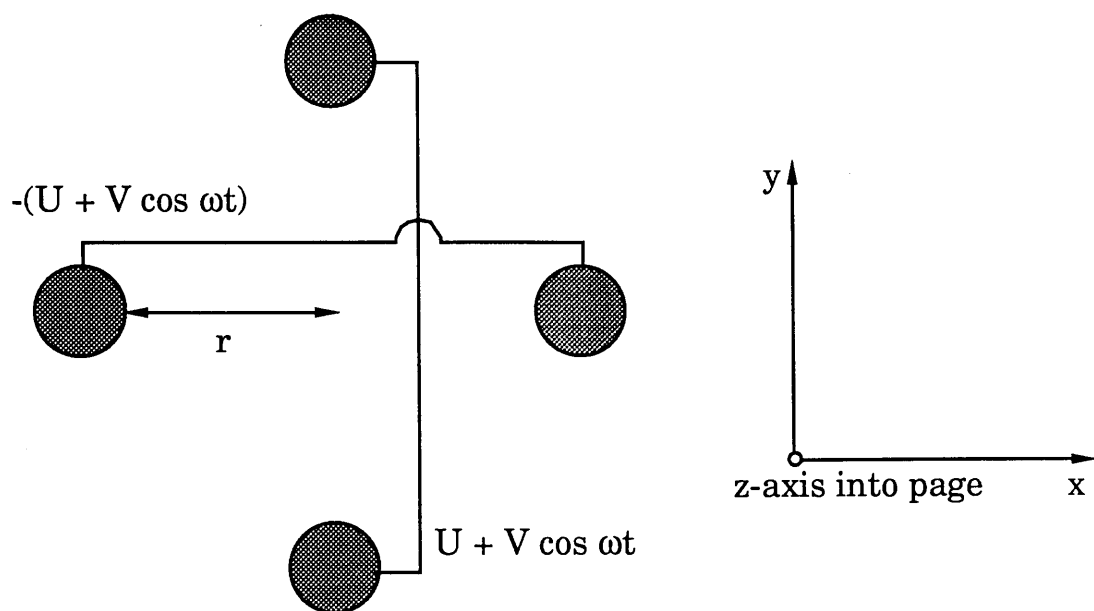


**Fig. 3.7:** Operating conditions of quadrupole mass filter.

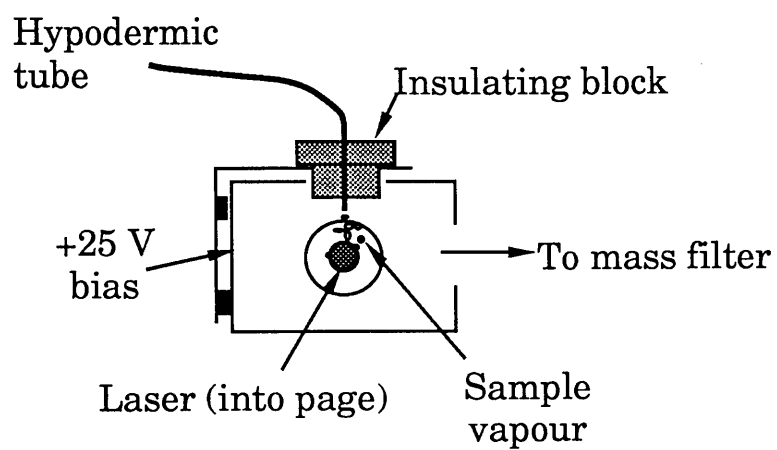


**Fig. 3.8:** Quadrupole laser/sample interaction region.

available at the time of these experiments which unfortunately resulted in very poor ion transmission to the mass filter. As a direct consequence, sample pressures in excess of  $10^{-6}$  mbar (for all samples studied) were required before any reasonable signal-to-noise ratios were obtained. During experiments using the quadrupole the chamber pressure was measured by a standard Edwards CP25 Penning gauge.

Upon entering the mass filter, ions perform complicated trajectories defined by the ion mass/charge ratio and the applied voltages  $U$  and  $V$ . Transmitted ions were detected by a Galileo 4771 Channeltron electron multiplier, which was operated at -3kV. The Channeltron was mounted slightly off spectrometer axis to reduce unwanted noise from neutral particles and stray laser photons. Any ion striking the cone shaped surface of the detector initiates an electron avalanche, which is collected as a charge pulse. A photograph of the Channeltron detector is shown in Fig. 3.9. An EG&G Ortec charge preamplifier converts the charge pulse to a voltage pulse which is further amplified before observation.

Unfortunately the preamp output consisted of both useful signal and unavoidable radio-frequency pick-up from the r.f. generators. To remove this, some r.f. signal was delayed by  $180^\circ$ , amplified and added to the preamp output. This removed the r.f. component after which the signal was further amplified and taken to the ADC for analysis. The electronic arrangement used to process the signal is shown in Fig. 3.10.

The mass resolution of the instrument is most commonly defined as  $R = M/\Delta M$ , where  $\Delta M$  is the width of mass peak  $M$  measured at half-maximum height, and using this definition,

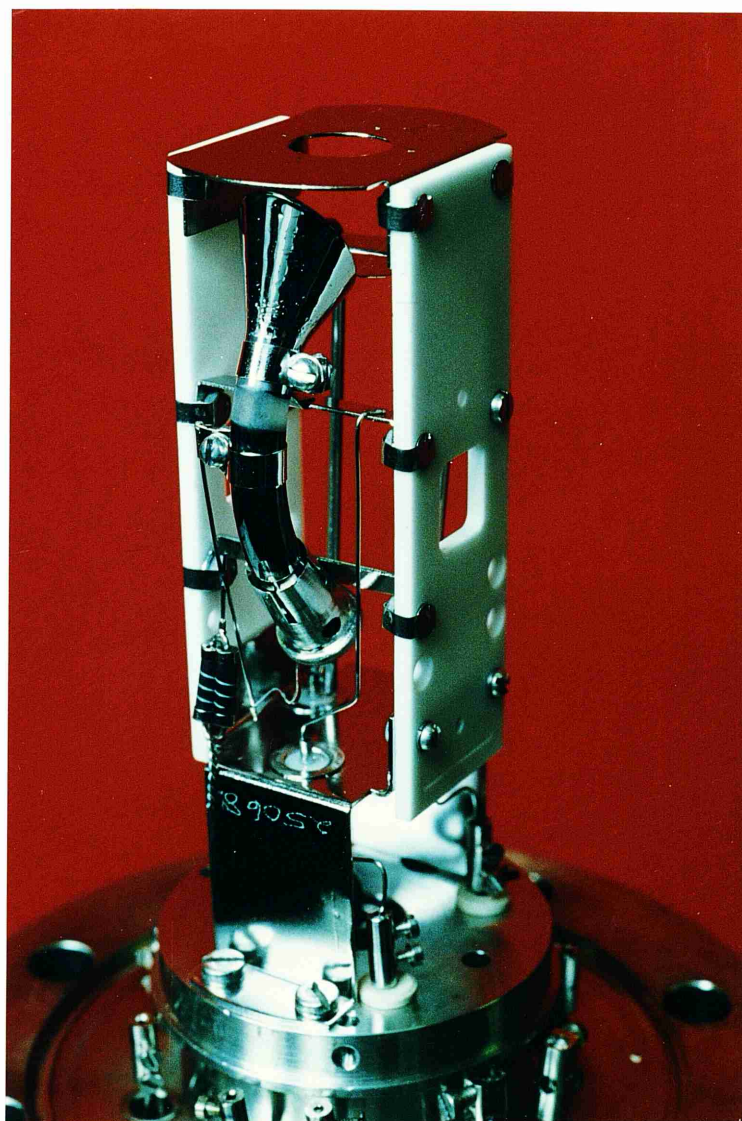


**Fig. 3.9:** Photograph of Channeltron detector.



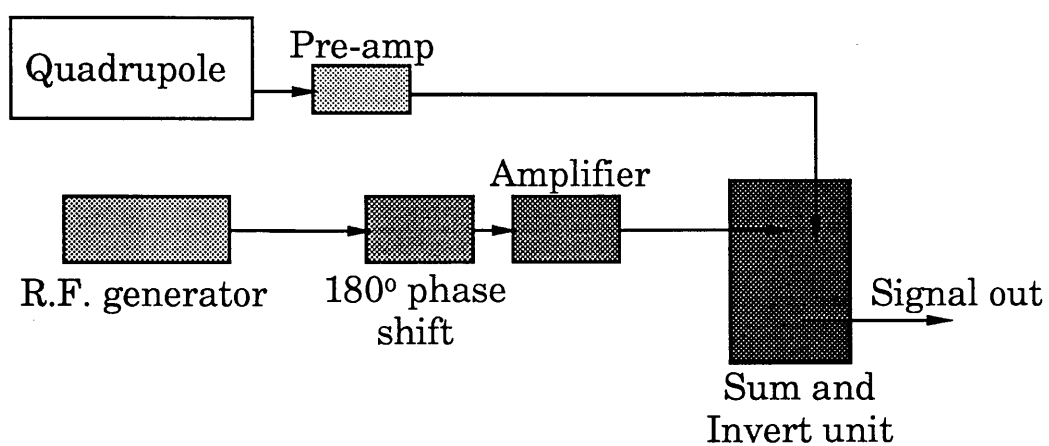


**Fig 3.10:** Electronic arrangement used in quadrupole experiments.

resolutions of greater than 1000 can be realised.

The particular instrument available for this work was unable to fully resolve unit masses in the various spectra recorded. The mass calibration curve for the quadrupole is shown in Fig. 3.11, where a small offset is observed.

### **§3.8 Data acquisition timing electronics.**

In all experiments involving the quadrupole and time-of-flight mass spectrometers, a time delay existed between the laser firing and the detection of the laser produced ions due to the flight times of ions between the ionisation region and the detector. For wavelength dependent measurements where only one ion mass was being investigated at any one time, a 7 channel, 11-bit peak sensing Analogue to Digital Convertor (ADC) was used to record both the ionisation signal and the laser pulse energy, whereas for time of flight spectra, ion signals were digitised and stored on a LeCroy 4910 storage oscilloscope.

A detailed diagram of the electronic arrangement is shown in Fig. 3.12 and shows how a strobe pulse of variable width and delay (with respect to the laser pulse) is generated. The system was capable of recording data at laser repetition rates of up to 50Hz.

The timing sequence in the generation of a strobe pulse at the correct time is as follows. An LSI-11 computer generates a ready signal which is taken to the input of a dual timer, where an infinitely long pulse is produced. This is taken to one input of a 2-fold coincidence unit, where it awaits coincidence with a discriminated photodiode pulse. The output pulse then starts a timer which incurs a delay to ensure that the ADC strobe pulse is

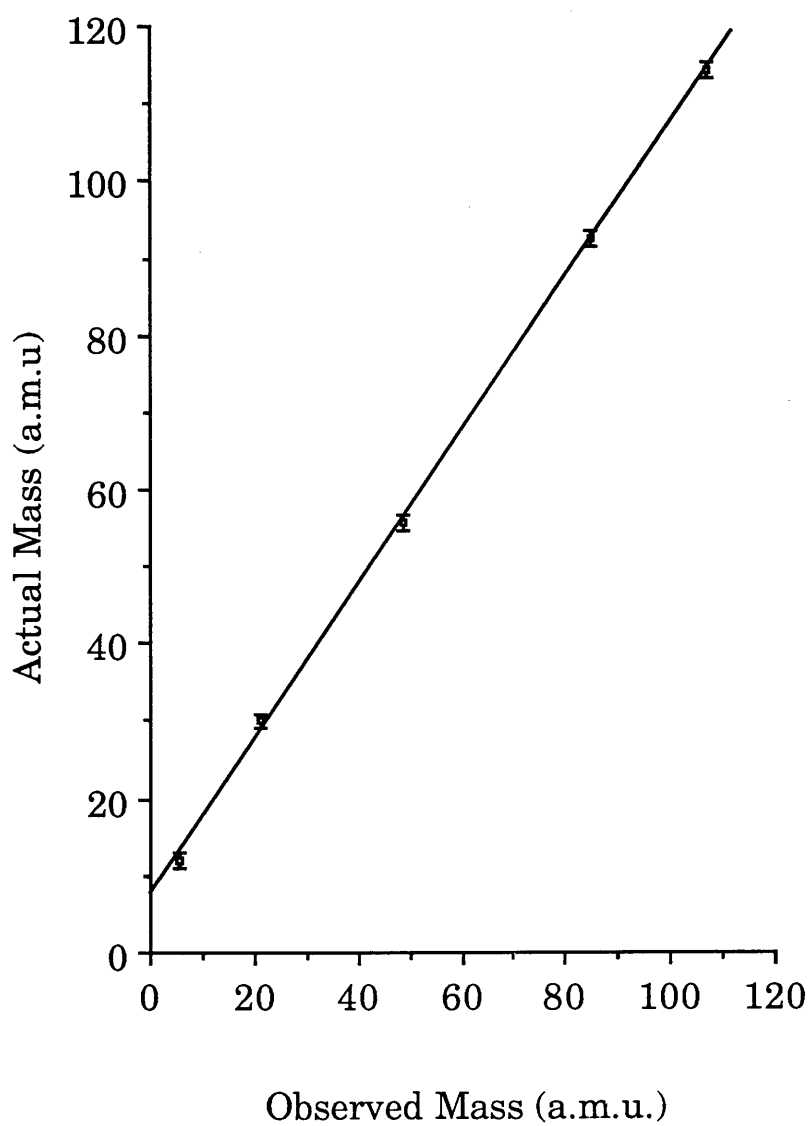


**Fig. 3.11:** Calibration curve for quadrupole mass spectrometer.

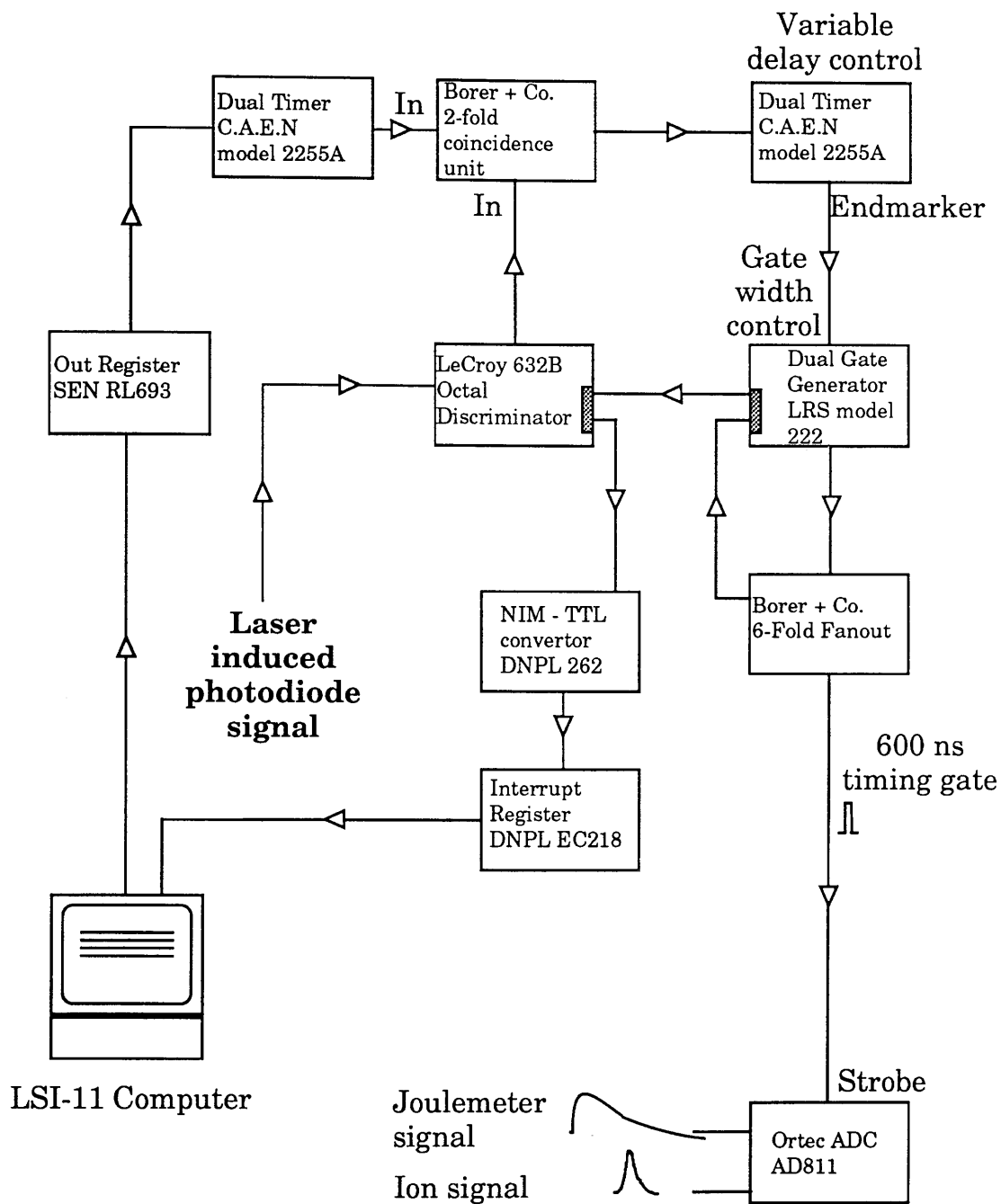


**Fig. 3.12:** Data acquisition electronics.

generated at the correct time to observe the required ion signal.

Time-of-flight mass spectra were recorded on a LeCroy 9410 150MHz oscilloscope. Signals were taken directly from the ion detector and averaged over typically 600-1000 laser pulses.

### **§3.9 Vacuum chamber.**

A schematic overhead view of the high vacuum chamber is shown in Fig. 3.13. The chamber was designed in-house and constructed by VG (Telford Ltd). The main chamber is constructed of stainless steel, and is 28cm in diameter and 30cm in height. Two quartz windows permit the transmission of UV laser light into the chamber. An optional port has been included to allow the use of laser ablation of solid samples, as well as a port symmetrically positioned with this for observation purposes. An additional observation port is situated on the top of the chamber. During all experiments, the chamber was evacuated by a single turbo-molecular pump, backed by a rotary pump, to base pressures of typically  $10^{-8}$  mbar, which was measured by an Ionivac IM210 ion gauge. A cylinder of nitrogen gas was connected directly to a solenoid inlet valve on the turbo pump for purging purposes.

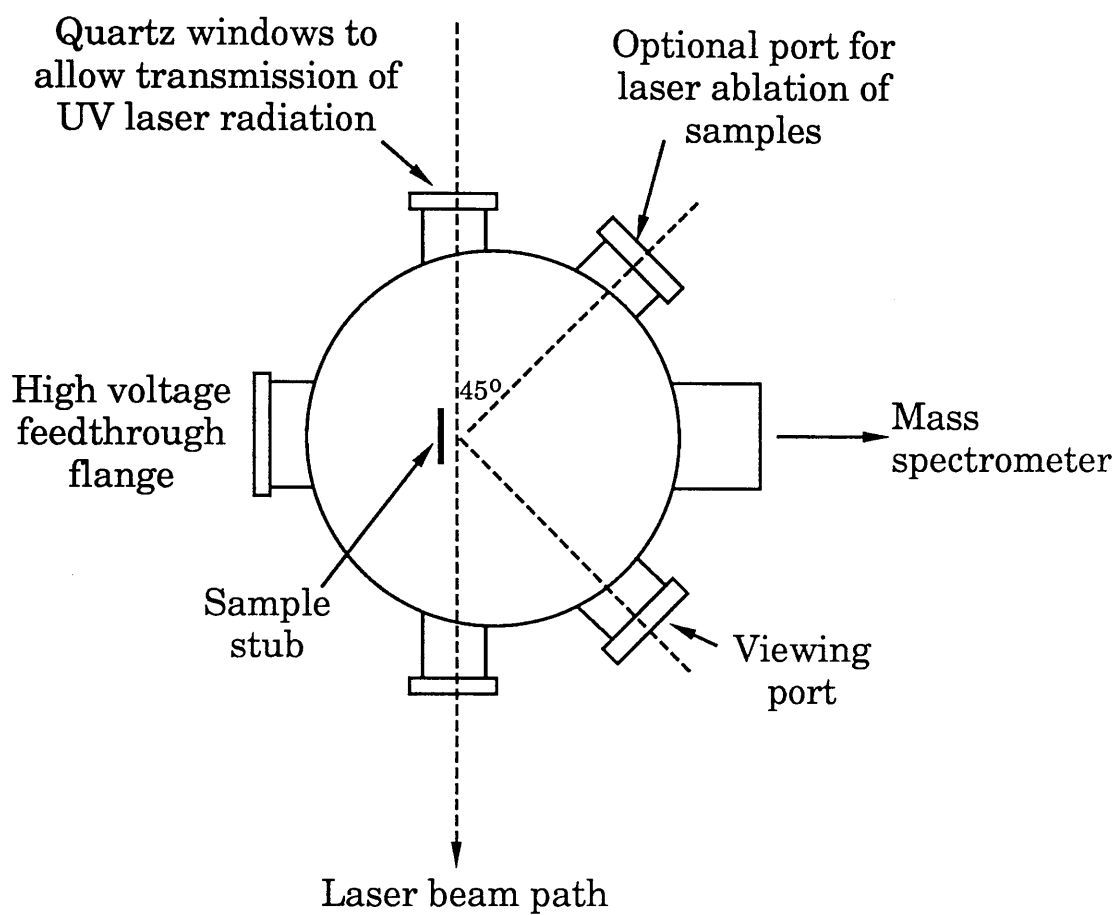


**Fig. 3.13:** Schematic diagram of vacuum chamber.

## Chapter 4

### **R2PI detection of small aromatic molecules in a quadrupole mass spectrometer and a simple ionisation chamber.**

#### **§4.1 Introduction**

In the Glasgow group, early experiments on resonance enhanced multiphoton ionisation involved the detection of photoions in conventional ion chamber and proportional counter systems (Ledingham *et al*, 1984, 1985; Drysdale *et al*, 1986; Towrie *et al*, 1986). In this chapter, the principal reasons for using mass spectrometer systems in conjunction with MPI spectroscopy will be discussed briefly. The development of a high vacuum quadrupole mass spectrometer system, and its use in the experimental work will also be described.

Resonant 2-photon ionisation has been used to study both toluene ( $\text{C}_6\text{H}_5\text{CH}_3$ ) and aniline ( $\text{C}_6\text{H}_5\text{NH}_2$ ) vapours in the wavelength ranges 262.5-269nm and 285.5-297nm respectively. The reasons for choosing toluene and aniline as 'test' samples are essentially three-fold. Firstly, the first ionisation potentials are sufficiently low (7.67eV and 8.62eV (Weast, 1972), respectively) to allow R2PI to be carried out with easily generated laser wavelengths. Secondly, both molecules exhibit very strong absorption bands at energies marginally greater than half their ionisation potentials, and so continuum states just above the ionisation level are connected by the ionising photon. This is desirable since it is in this region that ionisation cross sections are in general larger (Hager and Wallace, 1988). Thirdly, a wealth of spectral knowledge was available for toluene (Drysdale *et al*,

1986; Dietz *et al*, 1982; Boesl *et al*, 1981a) and aniline (Brand *et al*, 1966; Brophy and Rettner, 1979; Chernoff and Rice, 1979; Dietz *et al*, 1980a; Mikami *et al*, 1980; Boesl *et al*, 1981a; Philis and Goodman, 1989), in the above wavelength ranges.

Some preliminary work was also carried out on nitrobenzene detection in a simple ionisation chamber. No signals attributed to nitrobenzene were observed, but aniline was unambiguously identified as an impurity present in the sample.

Finally, the selective detection of toluene and phenol molecules is demonstrated in the ionisation chamber, even although a large structureless background 'contamination' due to aniline is present. Various vapour 'cocktails' of these three compounds were investigated in the ionisation chamber in the wavelength range 264-278nm, and ionisation peaks corresponding to each of the samples could be observed in the composite spectra.

#### **§4.2 Resonant 2-photon ionisation studies of toluene.**

R2PI has been used to study toluene vapour in the wavelength region 262-269nm. This range of UV wavelengths was produced by frequency doubling, in a KDP 'B' crystal, the output of the dye laser operated with Coumarin 153 dye. Typical UV pulse fluences, in the 5-20mJ/mm<sup>2</sup> range, were achieved by focusing the beam into the high vacuum chamber with a 30cm quartz lens. The laser-sample interaction volume was approximately 2mm below the exit point of the sample inlet capillary tube. The maximum pressure of toluene in the chamber was 2x10<sup>-5</sup>mbar, which was carefully monitored on an Edwards CP25K Penning gauge, and manually adjusted by a leak valve



arrangement. The base pressure in the chamber was measured to be  $\sim 2 \times 10^{-6}$  mbar.

The wavelength dependent ionisation yield of the toluene molecular ion ( $\text{C}_6\text{H}_5\text{CH}_3^+$ ;  $m/z=92$ ) was recorded at a laser fluence of  $14 \text{ mJ/mm}^2$  and is shown in Fig. 4.1a). The ionisation spectrum shows three principal resonances at 263.1nm, 263.6nm and 266.7nm. All resonant structure observed is due to single photon electronic transitions between the  $S_0$  ground state and the lowest lying singlet state,  $S_1$  (Murakami *et al*, 1981). The resonance at 266.7nm corresponds to the band origin transition which corresponds to the  $0 \rightarrow 0$  vibrational resonance of the above electronic transition. The structure observed to the red, or longer wavelengths relative to the position of band origin originate from higher lying rotational levels of the zero-vibrational manifold and are called 'hot bands' since they originate from thermally populated rotational states. The potential for selectively detecting toluene vapour in the presence of other compounds is obvious due to the amount of structure present in the ionisation spectrum at these wavelengths.

Fig. 4.1b) shows a UV absorption spectrum which was recorded with toluene present at its saturated vapour pressure. It is clear that strong similarities exist between the spectra of Figs. 4.1a) and 4.1b). Since the R2PI process initially proceeds through the intermediate electronic state which gives rise to the observed absorption spectrum (Fig. 4.1b)), it follows that the ionisation spectrum should mirror the absorption spectrum provided the following points hold;

- 1) the laser fluence is at a level where neither the absorption nor ionisation steps are optically saturated, since this would result in a

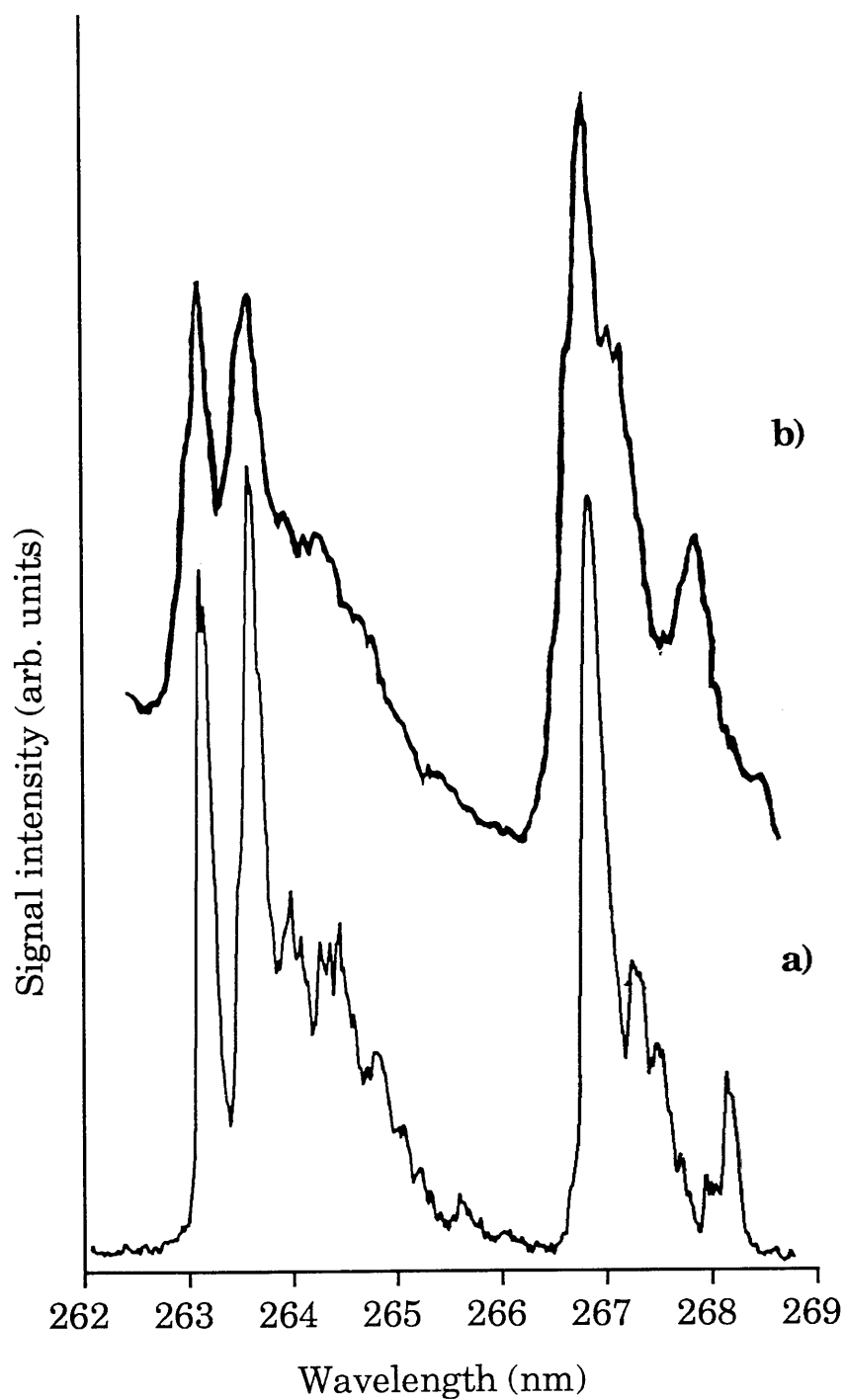


**Fig. 4.1:** a) Resonant two photon ionisation spectrum of toluene  
b) Gas phase ultraviolet absorption spectrum.

general flattening out of the ionisation spectrum.

2) the cross section for ionisation from the excited intermediate level is weakly dependent on the laser wavelength.

Once ions are formed in the laser sample interaction region, they are injected into the quadrupole mass filter by a small positive voltage as described in Chapter 3. Mass analysis of all the injected ions gives rise to the mass spectrum shown in Fig.4.2 which was recorded at a laser fluence of  $12\text{mJ/mm}^2$ . The parent ion observed at  $m/z=92$  is the most abundant in the spectrum, with fragment ion groups observed at  $m/z=27, 39, 52, 65$  and  $75$ . These  $m/z$  values refer to the central point in each of the observed mass peaks. These groups are due to  $C_2, C_3, C_4, C_5$  and  $C_6$  type fragment ions respectively. The resolution of the quadrupole mass filter was such that only fragment groups could be resolved, with individual fragment ion peaks within any of the  $C_n$  type groups being unresolved.

Significant intensities of the fragment ion groups meant that the wavelength dependence of these peaks could be recorded, where the ADC timing gate was positioned at the centre of the particular  $C_n$  group. The wavelength dependence of the fragment ion groups at  $m/z = 39, 52$  and  $65$  are shown in Figs. 4.3b), c) and d) respectively, with the spectrum of the toluene molecular ion shown in Fig. 4.3a) for comparison. Clearly, a high degree of similarity exists between the parent ion spectrum and the fragment ion spectra. Similar observations have also been made in the cases of acetaldehyde (Fisanick *et al*, 1980) and benzene (Zandee *et al*, 1979a). As discussed in Chapter 2, fragmentation often occurs in the MPI of molecules due to the continued absorption of laser radiation by the molecular ion once

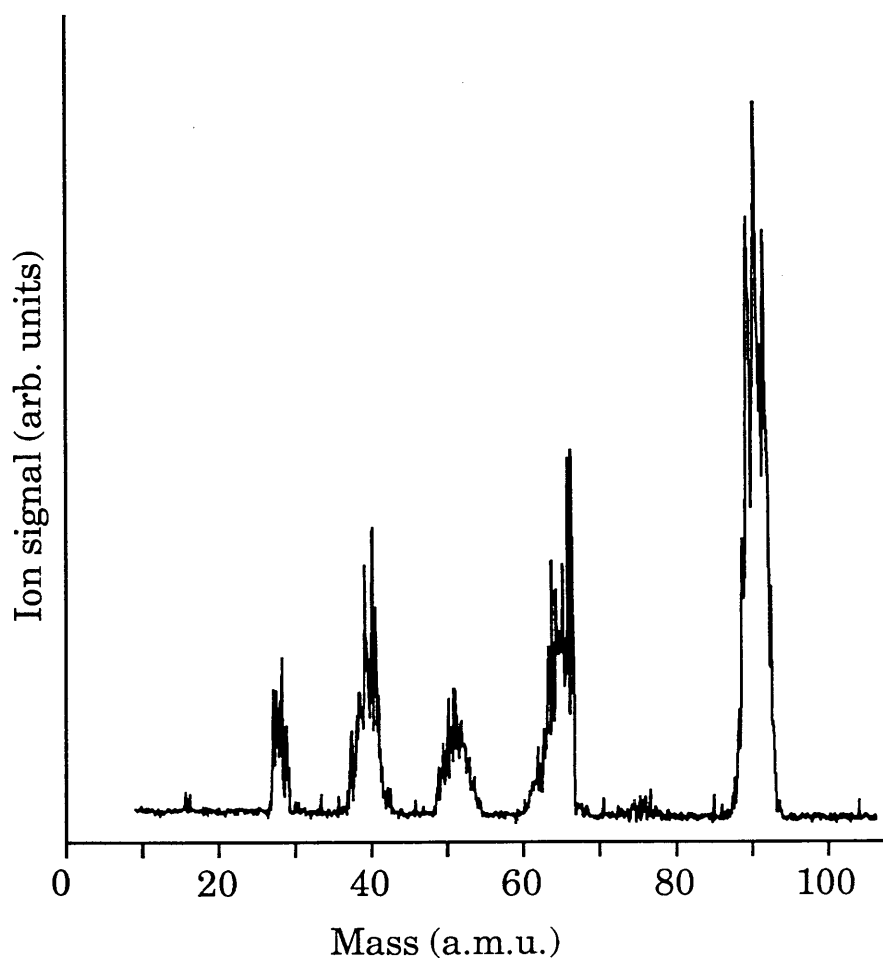


**Fig. 4.2:** Laser induced mass spectrum of toluene vapour.

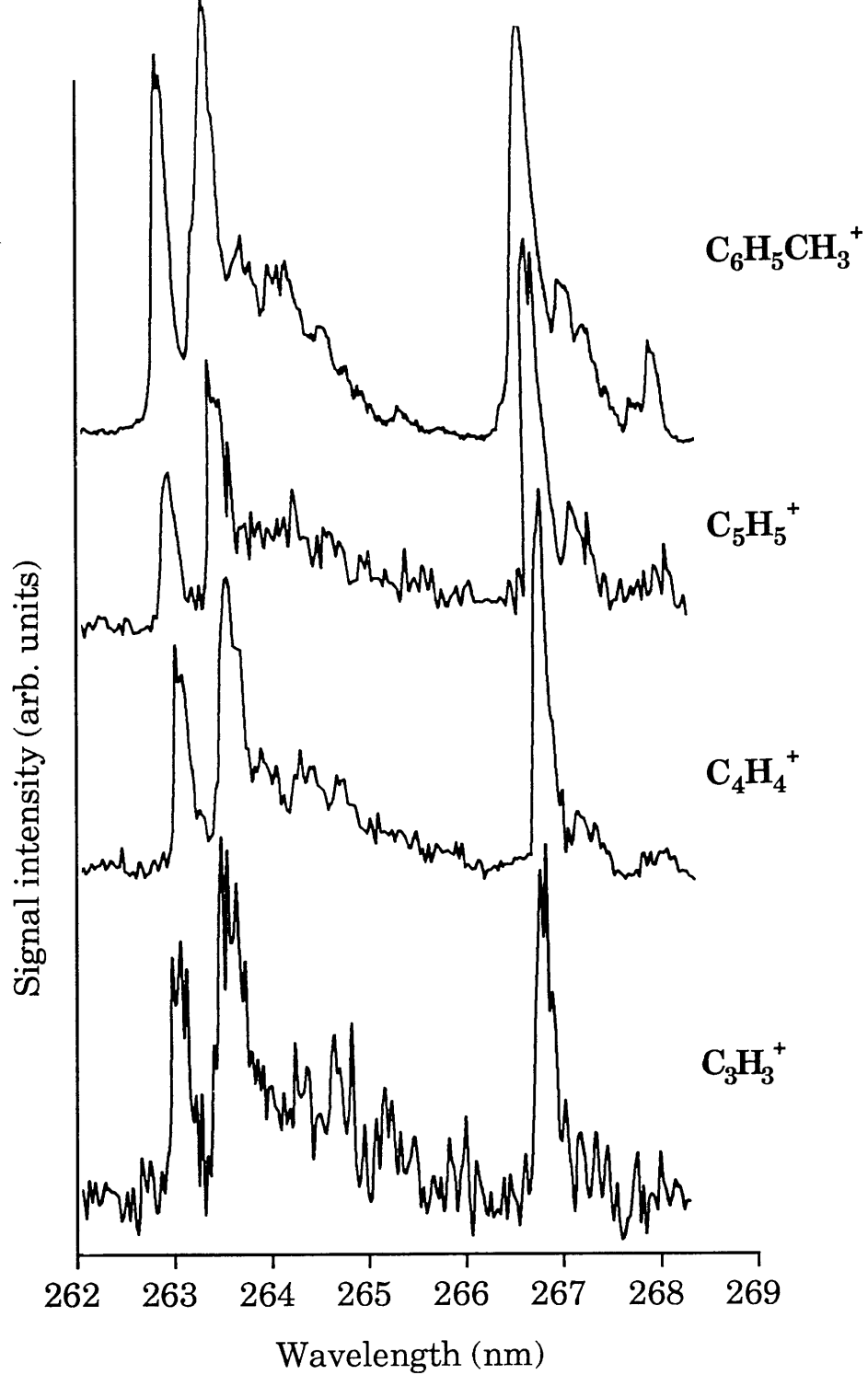


**Fig. 4.3:** Wavelength dependent ionisation spectra of several fragment ions.

it is formed. If this is the case for toluene, the similarities observed are readily explained, provided certain conditions hold. This argument depends on the fact that the wavelength dependent ionisation spectra of the fragment ions should resemble that of the parent molecule provided subsequent photon absorption by the parent ion prior to fragmentation is wavelength independent. In this situation the wavelength dependence of the fragment ions is determined by the wavelength dependence of parent ion production, and in the case of toluene, this is determined by the resonant absorption step in the R2PI process. This observation is extremely important, since it suggests that detection sensitivity of the toluene molecule in MPI could be maximised if the total ion signal is observed without mass selection, and would not result in any loss of spectral detail since all ions follow the same wavelength dependence.

#### **§4.3 Resonant two-photon ionisation studies of aniline.**

A second aromatic molecule, aniline ( $\text{C}_6\text{H}_5\text{NH}_2$ ; mol.wt. = 93), has been studied in the wavelength range 285-297 nm, which was chosen since this particular molecule readily absorbs radiation in this range. The UV laser light was obtained by second harmonic generation, in KDP 'B' crystals, of the output of the dye laser when operated with Rhodamine 590 laser dye.

With the quadrupole mass filter tuned to transmit only ions of  $m/z=93$ , which corresponds to the aniline molecular ion, the laser wavelength was scanned and the variation in the ion signal was monitored as a function of wavelength. The resulting R2PI spectrum is shown in Fig. 4.4a). A UV absorption spectrum recorded by Brand *et al* (1966) is also shown in Fig. 4.4b), and the marked similarities between the spectra are obvious. Four

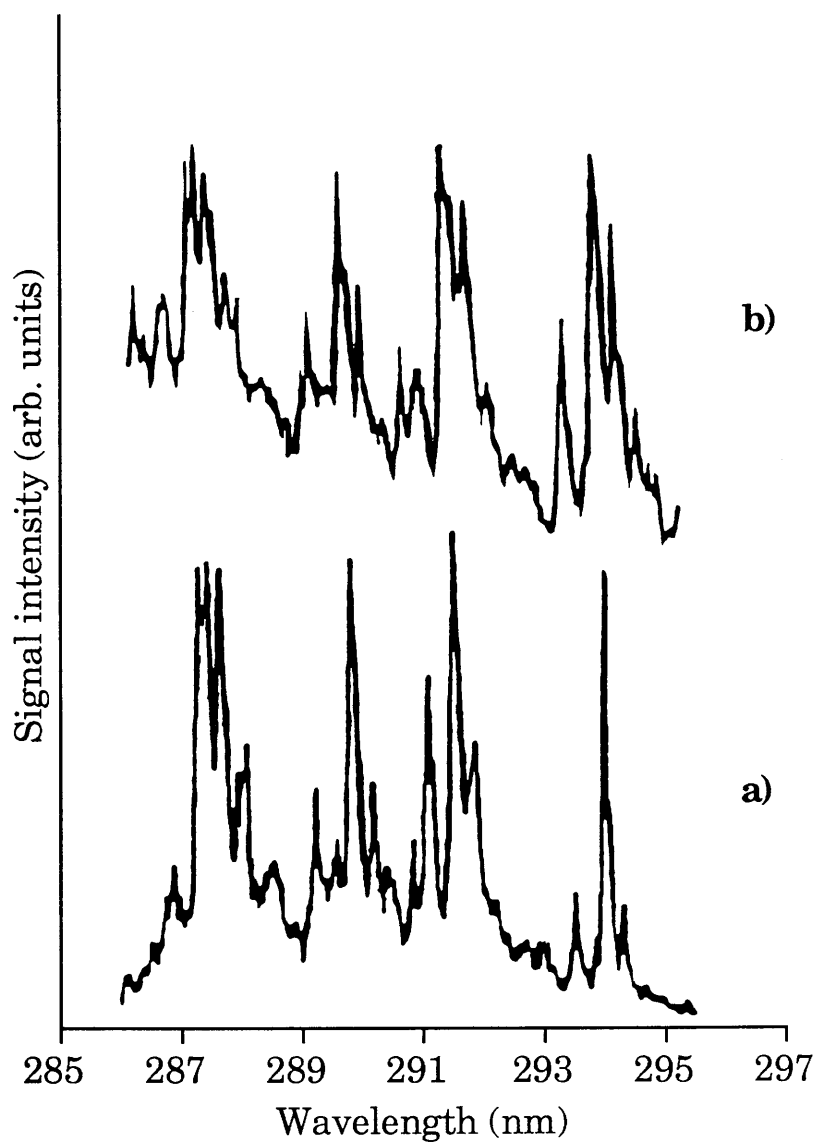


**Fig. 4.4:** a) Resonant two photon ionisation spectrum of aniline vapour.  
b) Gas phase ultraviolet absorption spectrum of aniline.

intense absorption bands are observed in the absorption spectrum, corresponding to different vibrational modes of the molecule. These vibrations have been fully characterised by Chernoff and Rice, (1979). The important point to note is that sharp characteristic structure persists throughout this particular wavelength range and could be used as a means of identifying the molecule.

Again, as discussed in the case of the toluene molecule, the observation that the R2PI spectrum mirrors the absorption spectrum suggests that the non-resonant absorption of the second photon into the ionisation continuum is weakly dependent upon laser wavelength. In addition, neither of the steps in the R2PI process should be near saturation. A typical laser induced mass spectrum of aniline recorded at a fluence of  $12\text{mJ/mm}^2$  is shown in Fig. 4.5 where it is clear that, compared to toluene, the fragmentation is much less severe. Some intensity is observed in the region of the  $\text{C}_5$  type fragment ions but clearly the most dominant ion present in the mass spectrum is the parent molecular ion at  $m/z=93$ . The poor mass resolution of the system unfortunately did not permit exact identification of the particular ions present in the groups observed in the mass spectrum. Also shown in the inset of Fig. 4.5 is a portion of the mass spectrum recorded at much higher detector gain. Ion intensities are observed centered on  $m/z=27, 38, 50, 64$  and  $77$  which are thought to correspond to  $\text{C}_2, \text{C}_3, \text{C}_4, \text{C}_5$  and  $\text{C}_6$  -type fragments respectively.

The wavelength dependent production of the parent ion and various fragment ions associated with aniline have been recorded and are displayed in Figs. 4.6a), b), c) and d) where the particular fragments are identified. Also shown is the ionisation spectrum of



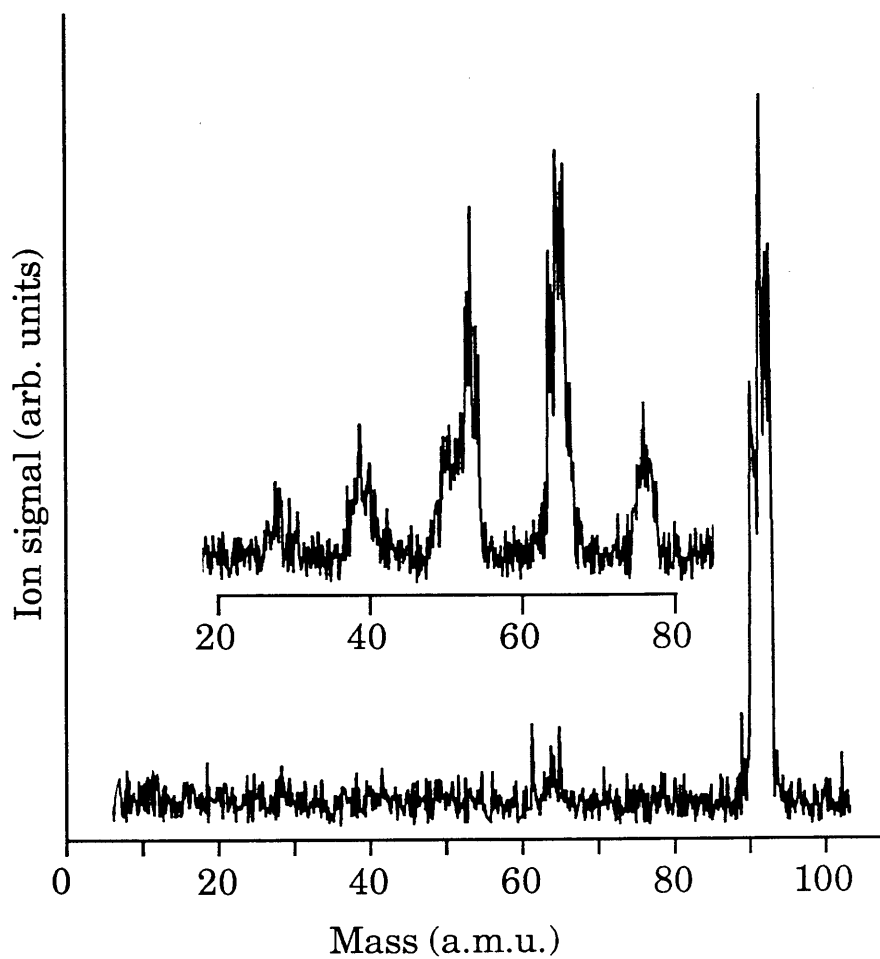


**Fig. 4.5:** Laser induced mass spectrum of aniline. The inset shows a portion of the mass spectrum recorded at higher detector gain, where fragment ions are easily observed.

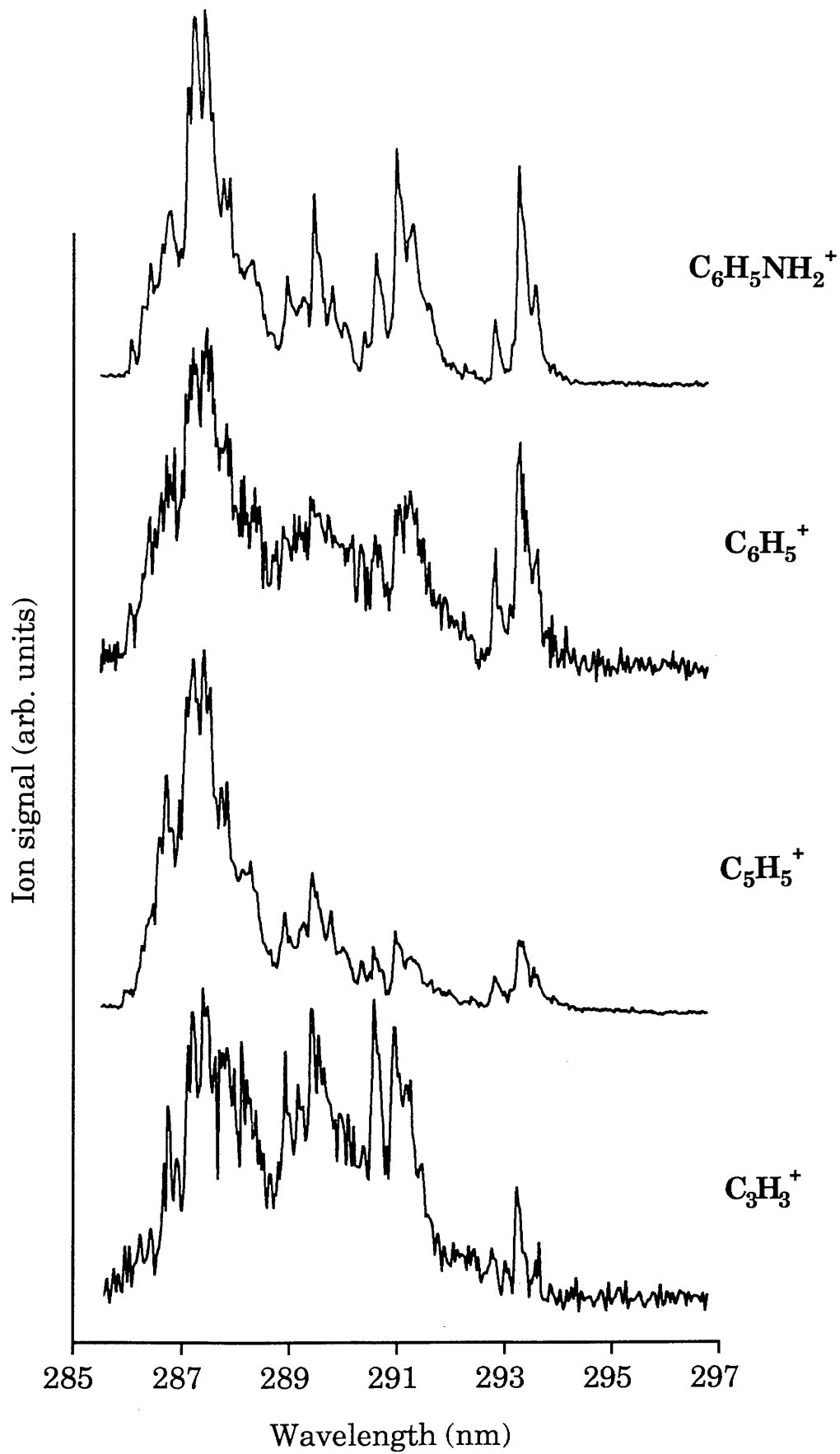


**Fig. 4.6:** Wavelength dependent ionisation spectra of several fragment ions.

the parent molecular ion in order for a detailed comparison to be made. Clearly, in a similar fashion to toluene, the spectra of the fragment ions exhibit similar features to the parent ion. As was mentioned in the case of toluene, this has implications of increased sensitivity if the total laser induced ion signal is measured independent of mass.

#### **§4.4 Detection and identification of toluene, aniline and phenol vapours in a simple ionisation chamber.**

The low resolving power of the quadrupole instrument used would make it impossible to discriminate between aniline and toluene relying solely on the mass analysis data. However, the characteristic wavelength dependent ionisation yields do make it possible to differentiate between the two. For these particular species the wavelength dependence is so powerful that a mass spectrometer system is not necessary for identification purposes.

In order to assess the possibility of discriminating between molecular types using only a simple ionisation chamber, mixtures of toluene, phenol and aniline vapours have been studied in the wavelength range 264-276nm. This particular choice was made because it was known that toluene showed a resonance at 266.7nm as discussed earlier in the chapter, and that phenol showed strong signal enhancement at around 275nm (Towrie *et al*, 1986).

A schematic diagram of the ionisation chamber used is shown in Fig. 4.7. The chamber was constructed in-house from a standard 150mm Edwards vacuum T-piece, and consisted of two parallel stainless steel plates, each 130mm in length, and separated by a distance of 25mm. A potential difference of 700V

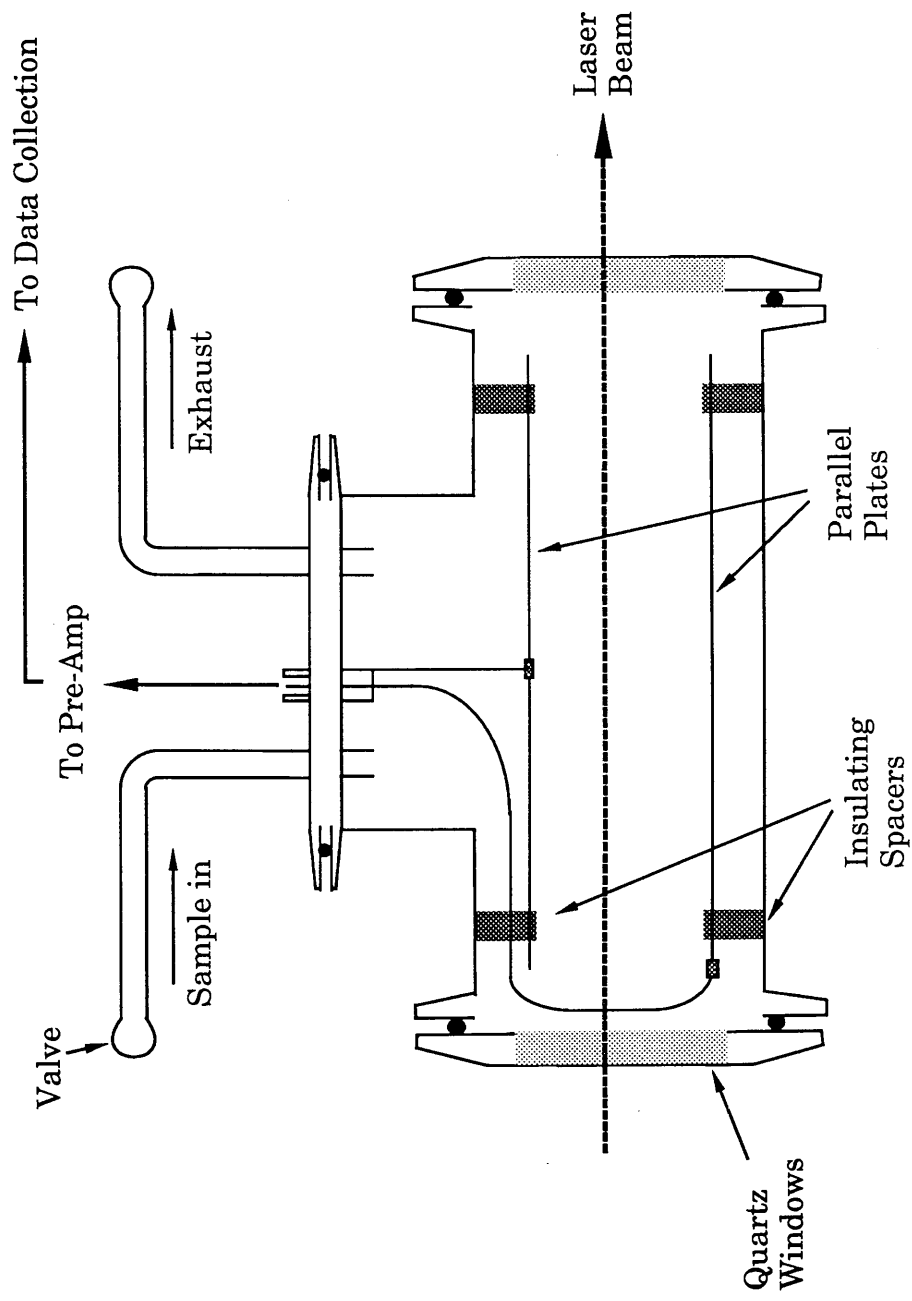


**Fig. 4.7:** Schematic diagram of the ionisation chamber.

was applied between the electrodes, which produced an electric field intensity of  $280\text{Vcm}^{-1}$ . The ionising laser passed through the chamber parallel to the electrodes at a distance of 5mm from the negative electrode. Ions formed in the laser beam volume were attracted to the negative electrode, and detected. A charge sensitive pre-amp was used to generate a voltage pulse which was recorded by the CAMAC system. The positioning of the laser beam was crucial since ion-electron recombination occurred before collection if the ions were produced at larger distances from the collection electrode.

In the following experiments, the laser beam was unfocused and apertured to 0.5mm x 0.5mm square cross section with typical pulse energies being in the 10-50 $\mu\text{J}$  range. To minimise the amount of interference from background contamination, the whole assembly was baked at 150°C in a vacuum oven prior to experiments.

The ionisation spectra of all three molecules were recorded individually in the ionisation chamber at their saturated vapour pressures (Table 4.1) (Weast, 1972), and are shown in Fig. 4.8. The 266.7nm resonance of toluene is observed with several hot bands also apparent. The amount of detail in the spectrum compares well with the mass selected toluene spectrum shown earlier in the chapter. The ionisation spectrum of phenol vapour is very similar to the work of Towrie *et al* (1986) and exhibits strong resonant structure throughout the wavelength range, particularly in the region of 275nm. In contrast to toluene and phenol, the aniline spectrum shows very little characteristic structure in this wavelength range. As discussed earlier, the lowest lying electronic energy band in aniline has a band origin at 293.84nm. At shorter wavelengths, excitation to densely packed

Molecule	Formula	Mass (a.m.u)	SVP at 300K (in Torr)	Ionisation potential	Two-photon ionisation threshold
Toluene	$\text{C}_6\text{H}_5\text{CH}_3$	92	29.53	8.82	280.61
Phenol	$\text{C}_6\text{H}_5\text{OH}$	94	0.71	8.51	290.83
Aniline	$\text{C}_6\text{H}_5\text{NH}_2$	93	0.96	7.67	322.69

**Table 4.1:** Vapour Pressures and Ionisation Potentials of toluene, phenol and aniline.

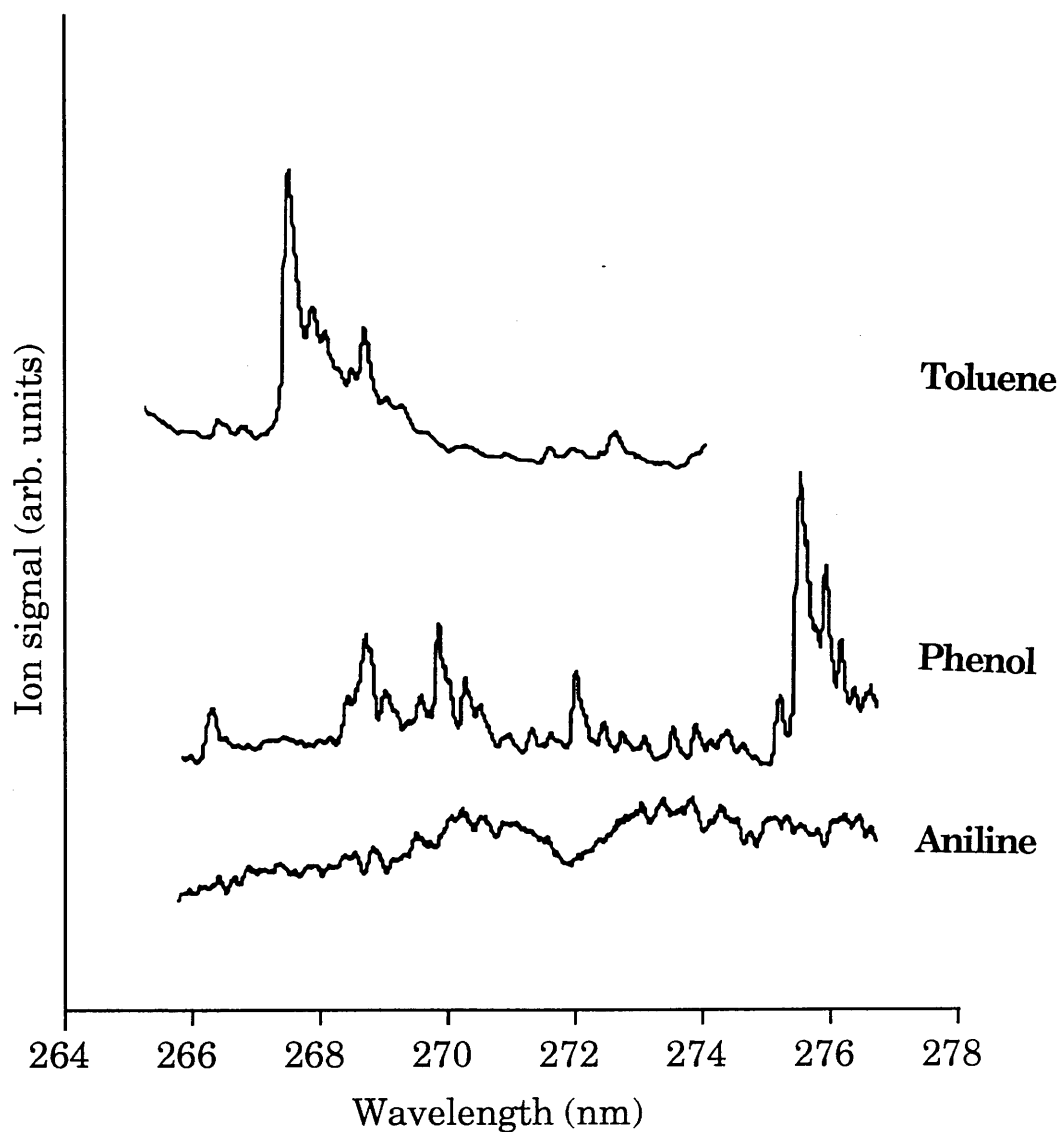


**Fig. 4.8:** Ionisation spectra recorded in the parallel plate ionisation chamber;  
a) Toluene  
b) Phenol  
c) Aniline.

rovibrational states higher up in the band occurs and results in a loss of well defined spectral detail. In order to evaluate the possibility of distinguishing between these three species on the basis of their wavelength dependent ionisation signatures, mixtures of the samples were studied in the same wavelength range.

Figs. 4.9a) shows the composite ionisation spectrum obtained from a mixture of toluene and phenol. In this spectrum, phenol was present in the chamber at saturated vapour pressure (SVP). Due to the relatively high SVP of toluene, a dilution in air of 1:100 was carried out to obtain comparable signal intensities. When toluene was present in the chamber at SVP, detector saturation occurred. The strong resonance at 275nm is clearly visible, as is the 266.7nm transition in toluene. The peaks in the ionisation spectrum corresponding to phenol and toluene are labelled P and T respectively for clarity. This spectrum demonstrates the potential for identifying these particular species in molecular mixtures in air under ambient conditions, provided the wavelength dependent ionisation signatures have been characterised.

Further, both phenol and toluene have been identified in a mixture which contained aniline at its SVP (Fig. 4.9b)). Although aniline exhibits a relatively structureless ionisation spectrum in this wavelength range, the ionisation peaks which are characteristic of phenol and toluene are very clear, and are again labelled P and T for clarity.

Nitrobenzene vapour was also studied in the simple ionisation chamber in the wavelength range 285-297nm. The



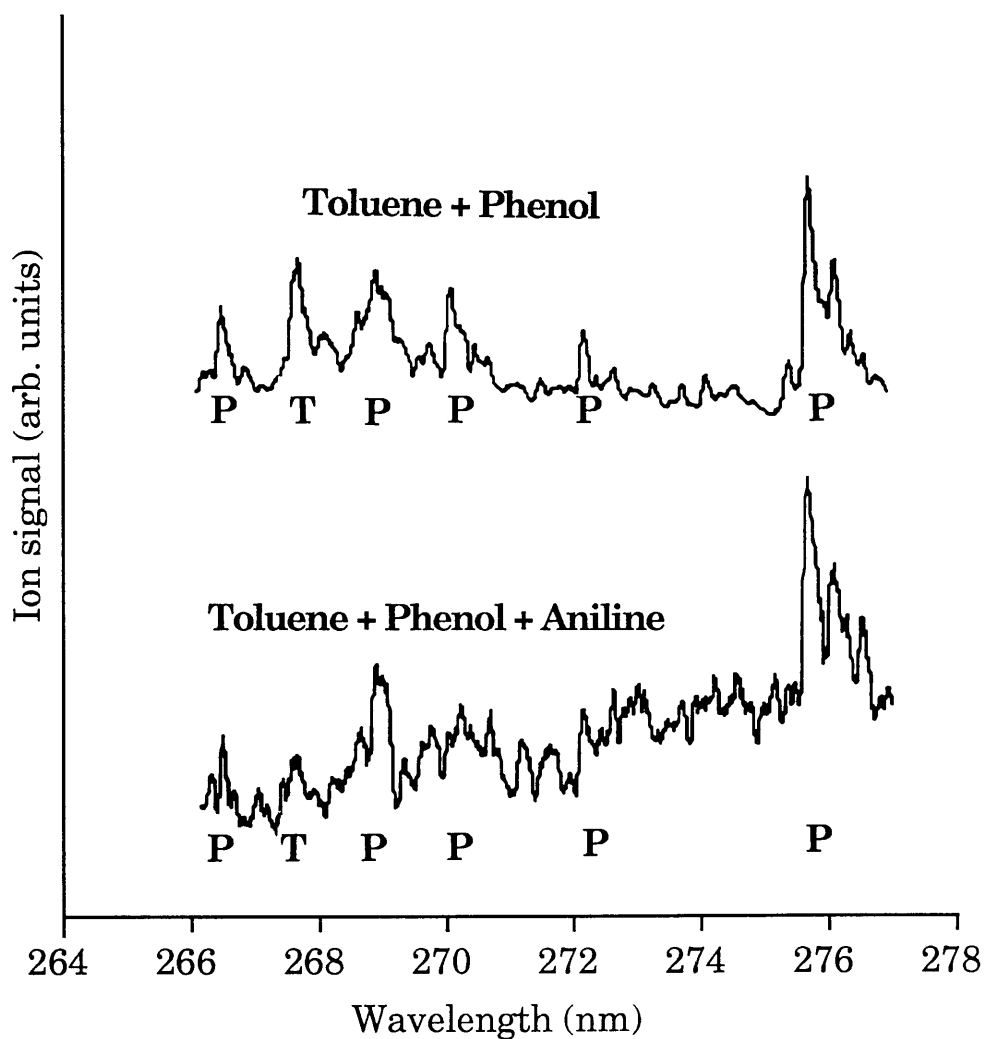


**Fig. 4.9:** a) Ionisation spectrum of a mixture of toluene and phenol vapours.  
b) Ionisation spectrum of a mixture of toluene, phenol and aniline vapours.

first ionisation potential of nitrobenzene is 9.88eV (Matyuk *et al*, 1979) which would require wavelengths shorter than 250.50nm in order for two-photon ionisation to occur. It was thought that a three photon ionisation process might be possible. The ionisation spectrum is shown in Fig. 4.10a), where several intense bands are observed. However, this structure was attributed to aniline on comparison with the mass selected ionisation spectrum shown in Fig. 4.10b).

These experiments show the benefit of building up a library of mass analysed wavelength dependent spectra for important molecular species. Particularly for the samples investigated here, a simple detector system can be used to identify species present by virtue of their characteristic ionisation spectra.

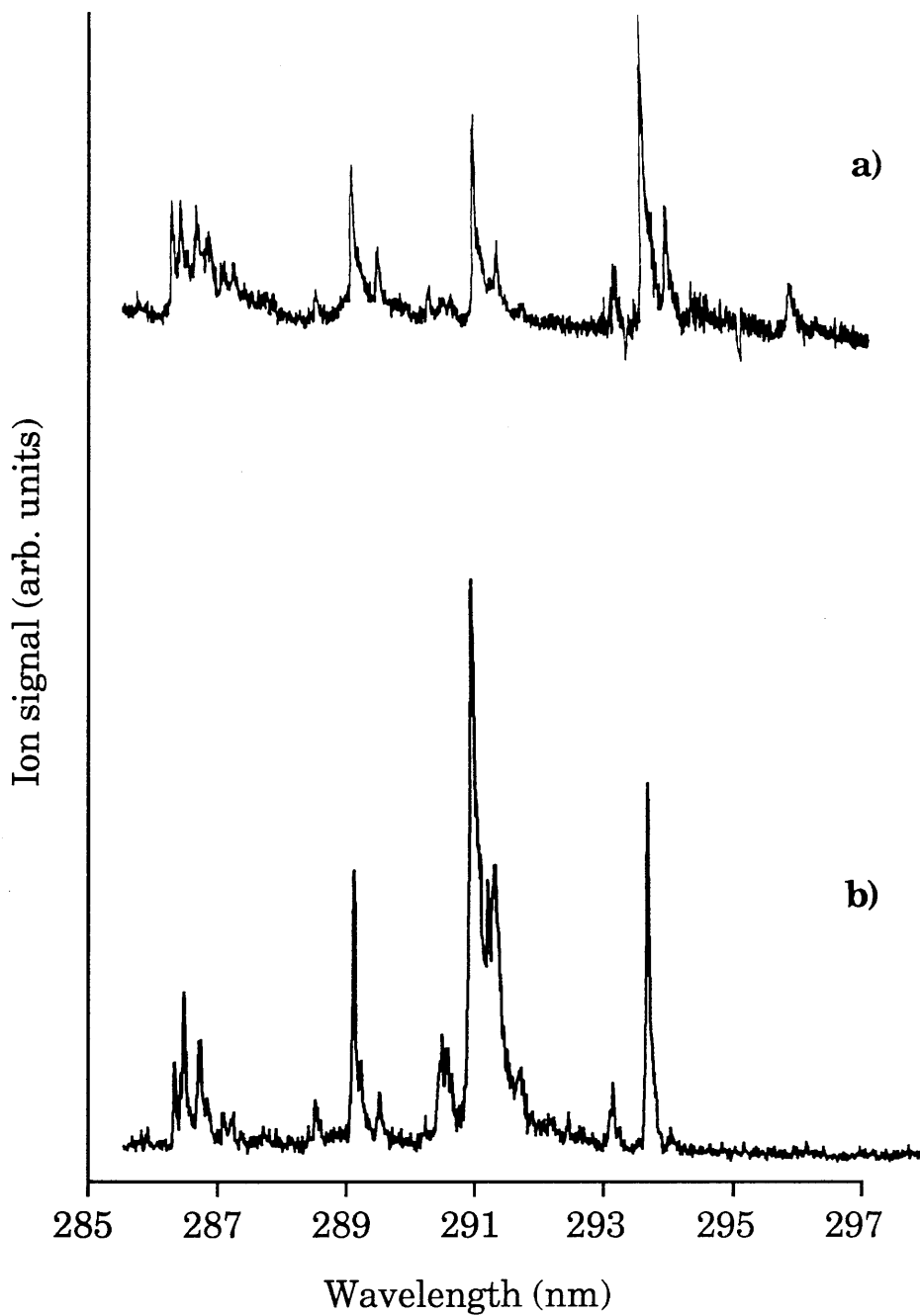


**Fig. 4.10:** a) Ionisation spectrum of aniline contamination in a nitrobenzene sample.  
b) Mass selected ionisation spectrum of aniline.

## **Chapter 5**

### **Development of a linear time-of-flight (TOF) mass spectrometer system to study resonance enhanced multiphoton ionisation (REMPI) processes in nitroaromatic vapours.**

#### **§5.1 Introduction.**

In order to increase the performance of the experimental system, a linear TOF mass spectrometer was designed, constructed and commissioned by the author. A detailed description of the mass spectrometer and a brief summary of the operating principles are given. The benefits of a TOF system compared with a quadrupole are demonstrated by the results of REMPI experiments performed with samples of nitrobenzene and nitrotoluene vapours.

#### **§5.2 Time-of-flight mass spectrometer.**

The decision to change from quadrupole mass spectrometry to time-of-flight mass spectrometry was based on a number of factors. Firstly, the quadrupole system described in Chapter 3 and used in the experiments of Chapter 4 suffered from both very poor mass resolution and poor ion transmission from the interaction region to the mass filter. Secondly, the mass range of the quadrupole was limited to 0-200 a.m.u. which is an obvious disadvantage. Finally, the pulsed nature of the laser ionisation sources used in REMPI experiments is ideally suited to TOF operation, since a complete laser induced mass spectrum of a particular molecule can be recorded for every laser pulse. This is in direct contrast to the quadrupole system where only one mass could be observed at any one time. Added advantages of TOF

systems lie in their simplicity of operation, which obviates the need to employ sophisticated electronic circuitry as is required in the case of quadrupole instruments, and relatively inexpensive construction costs.

The current state of TOF mass spectrometry in analytical science has been the subject of recent reviews (Price, 1990a; Price and Milnes, 1990b).

### **§5.3 Principle of operation of TOF mass spectrometers.**

The principle of operation of a TOF mass spectrometer is very simple. Ions formed at some position in an accelerating electric field gain approximately equal amounts of kinetic energy before being injected into a field free drift space. They are then separated according to their mass to charge ratios,  $(m/q)$  and arrive at the ion detector at different times. The time-of-flight,  $t$ , of an ion of mass  $m$  and charge  $q$  is given by,

$$t = l \sqrt{\frac{m}{2qV}} \quad \text{-(5.1)}$$

where  $l$  is the distance travelled by the ions and  $V$  is the accelerating potential.

The mass resolution,  $R$ , of a TOF spectrometer is defined as,

$$R = \frac{m}{\Delta m} = \frac{t}{2\Delta t} \quad \text{-(5.2)}$$

where  $\Delta t$  is the FWHM of the ion peak at time  $t$ ,  $m$  is the mass corresponding to the peak and  $\Delta m$  is the FWHM of the peak at mass  $m$ .

The earliest reports on successful separation of ions via their times-of-flight in a field free drift space was by Cameron and Eggers (1948). They used a continuous electron beam to ionise a sample of mercury vapour, and the ions formed were injected into a 3.00m field free drift region by applying a voltage pulse to an extract electrode. A mass resolution of  $\sim 4$  at  $m/z = 200$  was achieved.

Five years later, a mass resolution of 20 at  $m/z = 40$  was achieved by Wolff and Stephens (1953), by using a pulsed electron beam to ionise an atmospheric gas sample. After making comparisons between his measured and calculated resolution figures, it was proposed that the main source of the observed resolution degradation was due to the velocity distribution of the ions at the instant of their formation.

In 1955, Wiley and McLaren (Wiley and McLaren, 1955) developed a novel ion optic design which involved accelerating ions through a double field extraction system, as shown in Fig. 5.1. They showed that the overall mass resolution of a particular TOF spectrometer could be optimised by an appropriate choice of operational parameters. Before discussing the operation principles of Wiley-McLaren optics, several effects which serve to reduce the resolution of a TOF spectrometer are considered.

In TOF mass spectrometry, the ideal situation arises when ions of the same  $m/z$  ratio are formed in an infinitesimally thin volume which is perpendicular to the acceleration fields, and with no kinetic energy, as shown schematically in Fig. 5.2. In this situation, all ions of the same ( $m/z$ ) ratio would arrive at the detector at precisely the same time, and the available mass

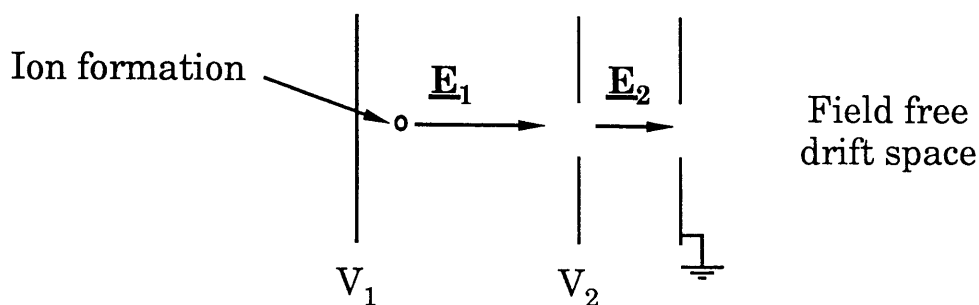


**Fig. 5.1:** Conventional double field extraction system, with singly charged ions created at the sample stub gaining an energy  $eV_1$  before entering the field free drift region.

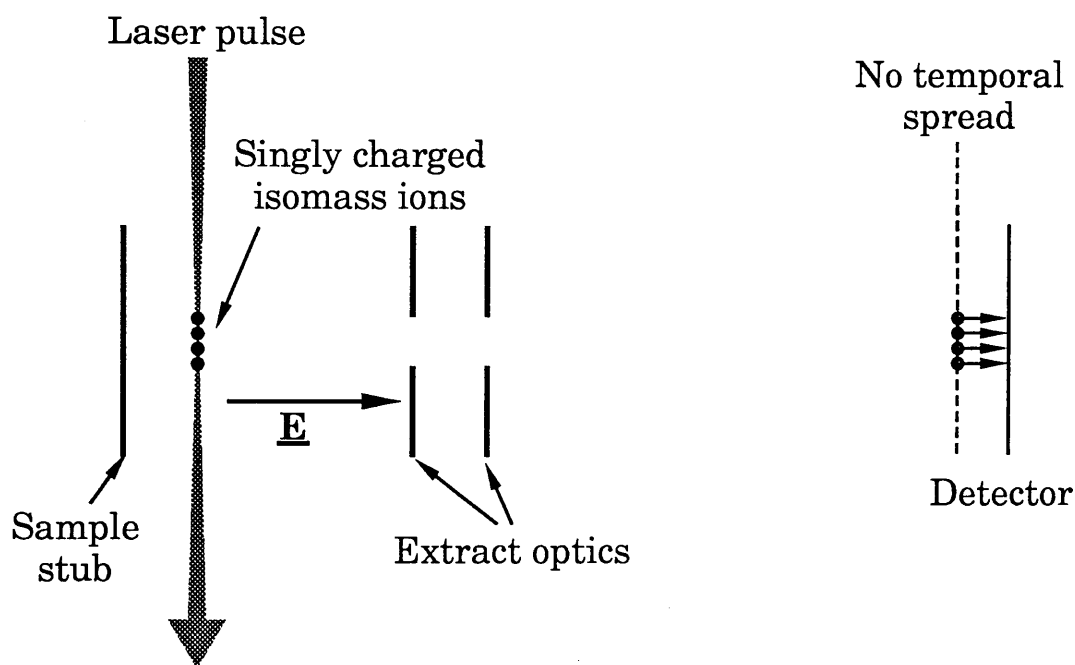


**Fig. 5.2:** Schematic diagram showing the ideal situation in TOF mass spectrometry. Ions of the same ( $m/q$ ) ratio are formed at exactly the same distance from the sample stub with no kinetic energy, and therefore arrive at the detector at the same time.

resolution would be defined entirely by the electrical characteristics of the ion detector.

However, in reality, the initial spatial, temporal and velocity distributions of the laser produced ions limit the resolving power of the instrument, and all three effects will be discussed in the following sections.

The cross-sectional area of the ionising laser beam is the sole cause of an initial ion spatial distribution. This limits the resolution due to the variation in flight time for ions of the same  $m/q$  ratio but which are produced at different points in the laser-sample interaction volume as shown in Fig. 5.3a). This may be reduced if beam focusing is employed, although in doing so the actual number of molecules interrogated by the laser beam is reduced due to the reduction in geometrical overlap.

The initial temporal distribution is due only to the finite length of the ionising laser pulse (laser pulse length  $\sim 8\text{ns}$ , in our case). Each isomass ion packet will therefore have a temporal spread of at least this value at the detector position, and so this represents an upper limit on the available mass resolution.

The mass resolution is also reduced due to the initial velocity distribution of ions formed in the acceleration region. In the very worst case, ions of equal mass having the same speed but initially travelling in opposite directions, as shown in Fig. 5.3b) arrive at the detector with a time difference equal to the turn-around time  $\Delta T$ , of the ion moving away from the detector.

In the Wiley-McLaren design, a compromise is met in



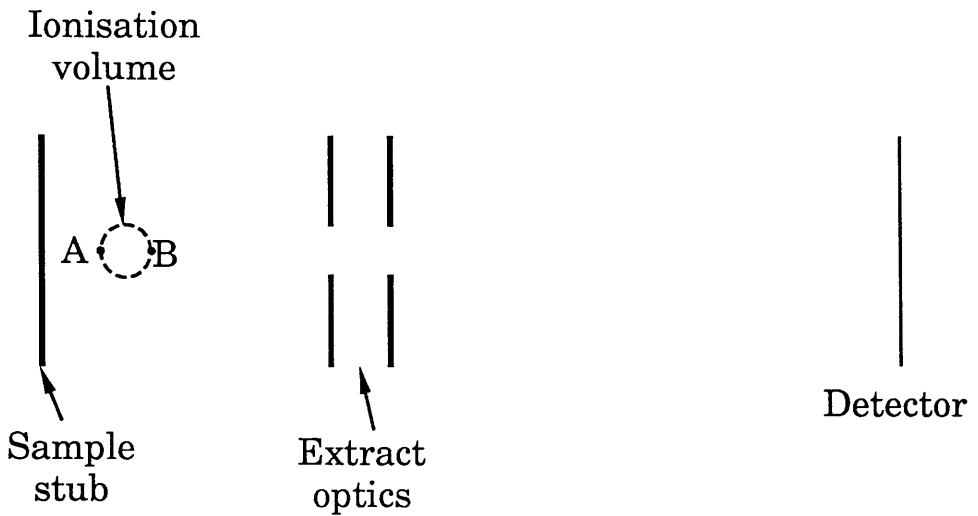


**Fig. 5.3a):** Isomass ions formed with the same velocities but at different positions (e.g. A and B) in the acceleration fields will generally arrive at the detector at different times.

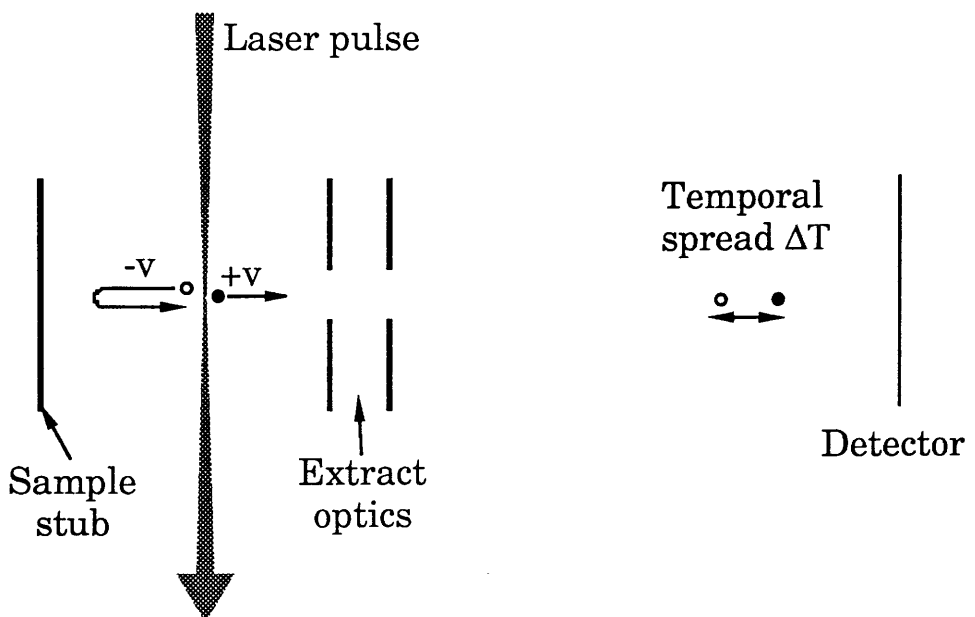


**Fig. 5.3b):** Isomass ions formed at the same distance from the sample stub with equal but oppositely directed speeds arrive at the detector with a time difference equal to the turn-around time,  $\Delta T$ , of the ion initially moving towards the stub.

overcoming the adverse effects of initial spatial and velocity distributions. In the former case, the potential drop across the ionising laser beam width is kept low so that ions gain most of their kinetic energy from the second acceleration region and therefore the fractional difference in their final energies is smaller. In particular, they showed theoretically that a suitable choice of the voltages  $V_1$  and  $V_2$  resulted in isomass ions being spatially focused at the detector position. However, to minimise the effects of an initial non-zero ion velocity distribution, it is desirable to have the electric field in the source region as large as possible in order to reduce the turn-around time  $\Delta T$ . In our experiments, the initial spatial distribution was kept at a minimum by focusing the laser beam, so it is expected that the main source of resolution degradation is from an initial velocity distribution.

The total flight length of the spectrometer used was 1.18m from interaction region to detector. The physical dimensions of the ion optic arrangement are shown in Fig. 5.4. A photograph of the ion optic arrangement is shown in Fig. 5.5. The extract system incorporated x-y deflection plates to correct for off-axis ion extraction, but was rarely used. A standard Thorn EMI 18 dynode electron multiplier was used to record the arrival of laser produced ions. The electrical connections to the detector are shown in Fig. 5.6. Ion signals were observed across 50 ohms, as shown, in order to preserve the resolution of the system.

Under these operating conditions, and with a laser spot size of  $\sim 200\mu\text{m}$  diameter at the interaction site, the mass resolution of the system was approximately 220 measured at  $m/z = 77$ .

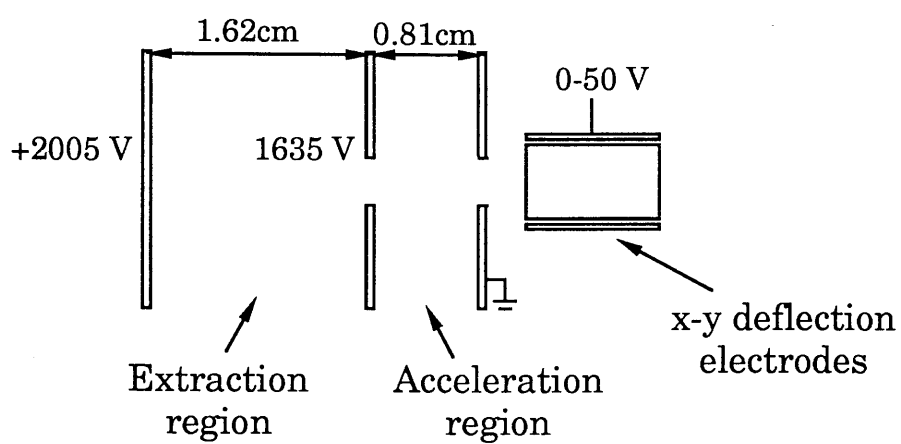


**Fig. 5.4:** Operational parameters of the ion optic arrangement.

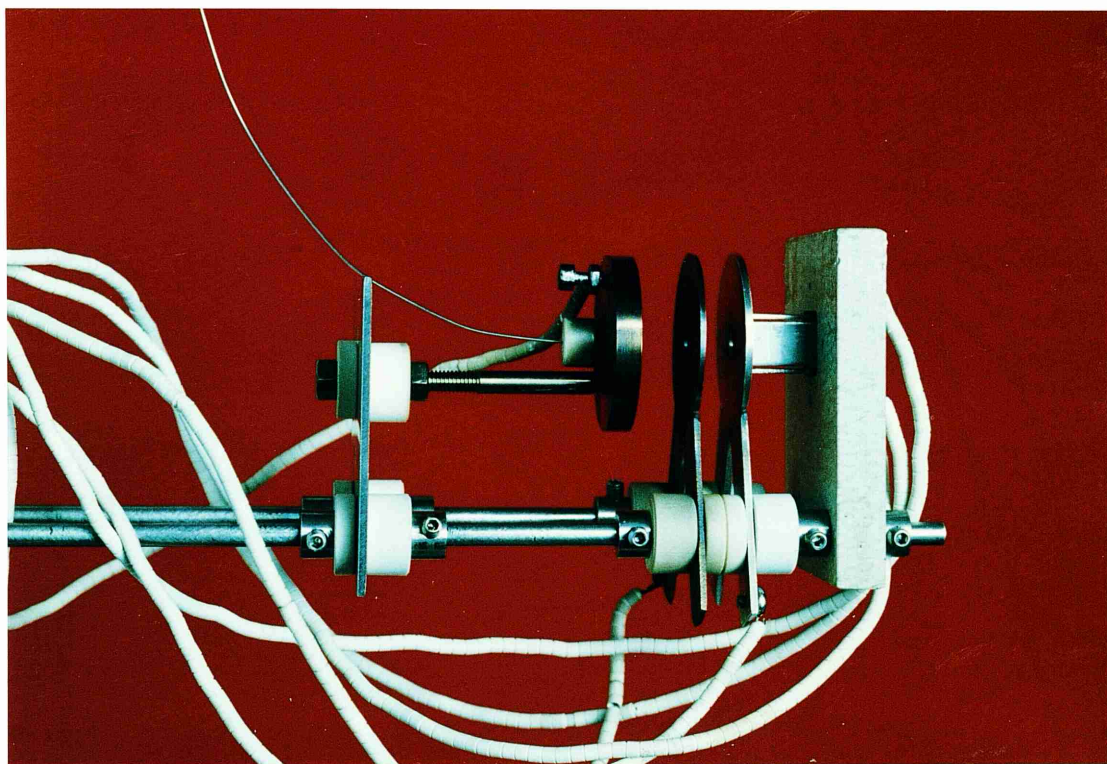


**Fig. 5.5:** Photograph of TOF ion optics.

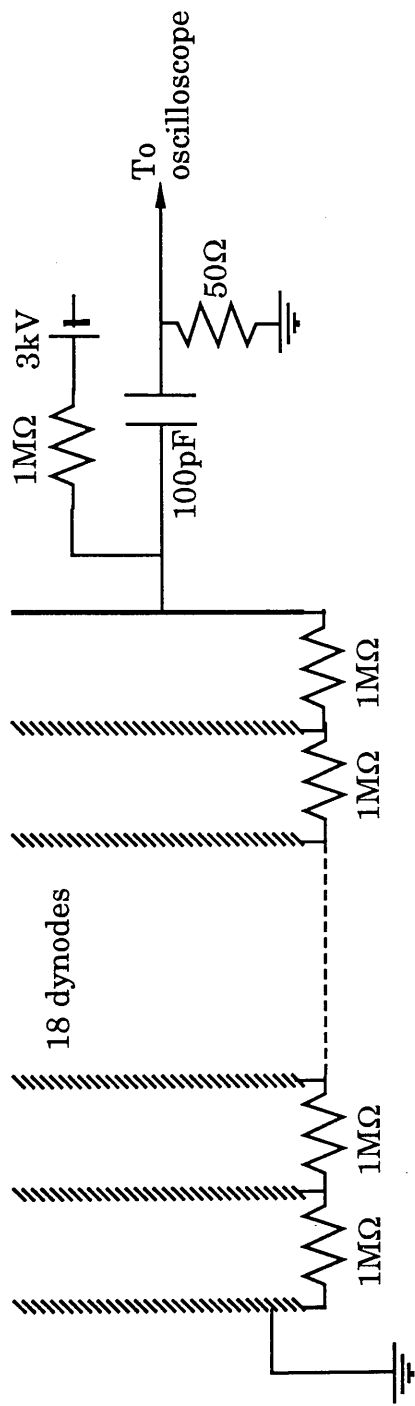


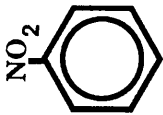
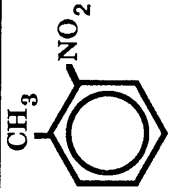
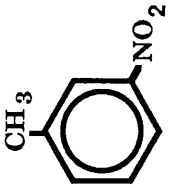
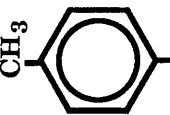
**Fig. 5.6:** Electrical configuration of ion detector.

#### **§5.4 REMPI of nitroaromatic molecules in the TOF system.**

The results obtained while carrying out investigations of REMPI of vapour phase nitroaromatic molecules in the TOF mass spectrometer system will now be discussed. The aim of this series of experiments was to obtain a wavelength dependent 'fingerprint' for these molecules, in order to permit their unambiguous identification in trace quantities in a mixture of molecules.

Nitrobenzene ( $\text{C}_6\text{H}_5\text{NO}_2$ ; mol. wt. = 123) and all three isomers (ortho-, meta- and para-) of nitrotoluene ( $\text{C}_7\text{H}_7\text{NO}_2$ ; mol. wt. = 137) have been studied in the wavelength range 245-250nm. This range which was chosen primarily because it spans the two-photon ionisation edge of nitrobenzene, as can be seen from Table 5.1. The other main reason for this choice was that the absorption cross-section for nitrobenzene was known to peak at ~242nm. Two photons of wavelength 249.7nm provide enough energy to ionise nitrobenzene. All nitrotoluene isomers should also ionise in this wavelength range via a two photon process since they have lower ionisation potentials. Table 5.1 also lists the room temperature saturated vapour pressures of all four molecules (Weast, 1972). The intermediate electronic structures of nitrobenzene and nitrotoluene isomers have been investigated both experimentally (Rabalais, 1972; Kobayashi and Nagakura, 1972) and theoretically (Palmer, 1979).

UV radiation in the range 245-250nm was produced by second harmonic generation of the output from the dye laser which was operated with Coumarin 307 dye. Typical UV laser fluences were in the 5-25mJ/mm<sup>2</sup> range which was achieved by strongly focusing the laser beam. Both fundamental and second

Molecule	Molecular formula	Molecular structure	Vapour pressure at 300K (Torr)	Ionisation Potential (eV)	Two-photon ionisation limit (nm)
Nitrobenzene	$C_6H_5NO_2$		0.358	$9.88 \pm 0.02$	249.7
o-Nitrotoluene	$C_7H_7NO_2$		0.236	$9.69 \pm 0.02$	255.9
m-Nitrotoluene	$C_7H_7NO_2$		0.241	$9.49 \pm 0.02$	261.3
p-Nitrotoluene	$C_7H_7NO_2$		0.194	$9.54 \pm 0.02$	259.9

**Table 5.1:** Vapour pressures and ionisation potentials of nitrobenzene and mono-nitrotoluene isomers (Matyuk *et al*, 1979)

harmonic beams were focused into the vacuum chamber, where they intercepted sample molecules at a distance of 1mm from the sample stub.

Mass spectra have been recorded at a variety of different wavelengths and laser fluences for all four molecules. In all cases, an intense ion signal at  $m/z = 30$  was observed, which corresponds to the  $\text{NO}^+$  ion, as well as a series of  $\text{C}_n\text{H}_m^+$  type fragments. This chapter will be mainly concerned with the hydrocarbon data, while Chapter 6 discusses the significance of the  $\text{NO}^+$  data.

#### **§5.4.1 REMPI of nitrobenzene in the wavelength range 245-250nm.**

Nitrobenzene vapour was introduced into the acceleration region of the TOF mass spectrometer as described in Chapter 3. During experiments the chamber pressure was typically  $5 \times 10^{-7}$  mbar, and was kept constant by careful manipulation of the leak valve. The ion gauge, however, was located at the top of the vacuum chamber and so the value above represents the ambient pressure within the chamber. The actual sample pressure in the laser interaction volume is expected to be somewhat greater, perhaps by a factor of 3 or 4. This factor was estimated by monitoring the decrease in the signal size as the sample inlet line was closed and for the subsequent period when the pressure recorded by the ion gauge remained constant.

Nitrobenzene was the first sample to be studied and was used to provide a mass calibration for the system. The laser was tuned to the peak of the dye gain region ( $\sim 246.5\text{nm}$ ) in order to maximise the laser fluence ( $11.5\text{mJ/mm}^2$ ), and a TOF spectrum of nitrobenzene was recorded (Fig. 5.7). As described earlier, the



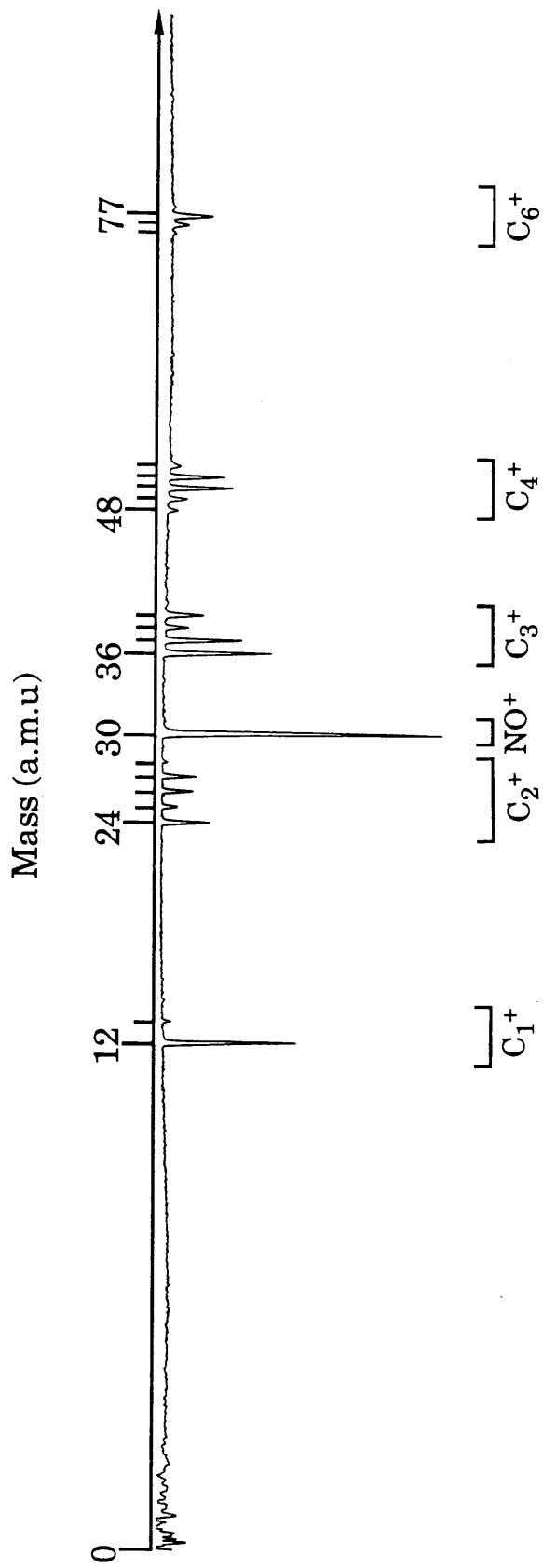
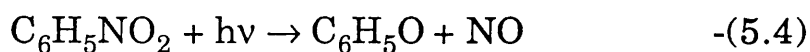
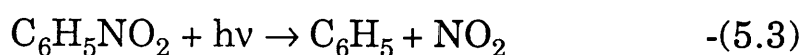


**Fig. 5.7:** TOF mass spectrum of nitrobenzene vapour recorded at 246.5nm and at a laser fluence of 11.5mJ/mm<sup>2</sup> .

flight time of a particular ion through the field free region is proportional to the square root of the ion mass. A calibration curve was drawn of ion mass against (flight time)<sup>2</sup> for the case where ionisation occurs at a distance of 1mm from the sample stub, and is shown in Fig. 5.8. A high degree of linearity is observed with some small offset at  $t=0$ . This is due to an unavoidable delay, relative to the laser firing, in triggering the digital oscilloscope. Clearly, the mass spectrum consists of groups of  $C_nH_m^+$  associated fragments, and a strikingly intense signal at mass 30, which, as already mentioned, corresponds to the  $NO^+$  ion. The highest mass fragment observed was  $C_6H_5^+$  ( $m/z = 77$ ), indicating that no nitrobenzene parent ion,  $C_6H_5NO_2^+$  ( $m/z = 123$ ) was produced in the ionisation process.

The absence of a parent ion in the mass spectrum is not surprising, since it is well known that nitroaromatic compounds have a strong tendency to predissociate when irradiated by UV light (Zhu *et al*, 1990). The two most probable predissociation pathways in the case of nitrobenzene are postulated to be,



In REMPI studies on nitroaromatics, therefore, it is highly unlikely that any parent molecular ion will be produced, since the predissociation lifetimes in excited electronic states are generally in the range  $10^{-9}$  -  $10^{-11}$ s, (King, 1964; Steinfeld, 1974). Only in very intense laser fields where the delivery rate of photons is great enough to compete with the predissociation rate would it be possible to observe a molecular ion in the mass spectrum, but to the authors knowledge no such experiment has been performed.

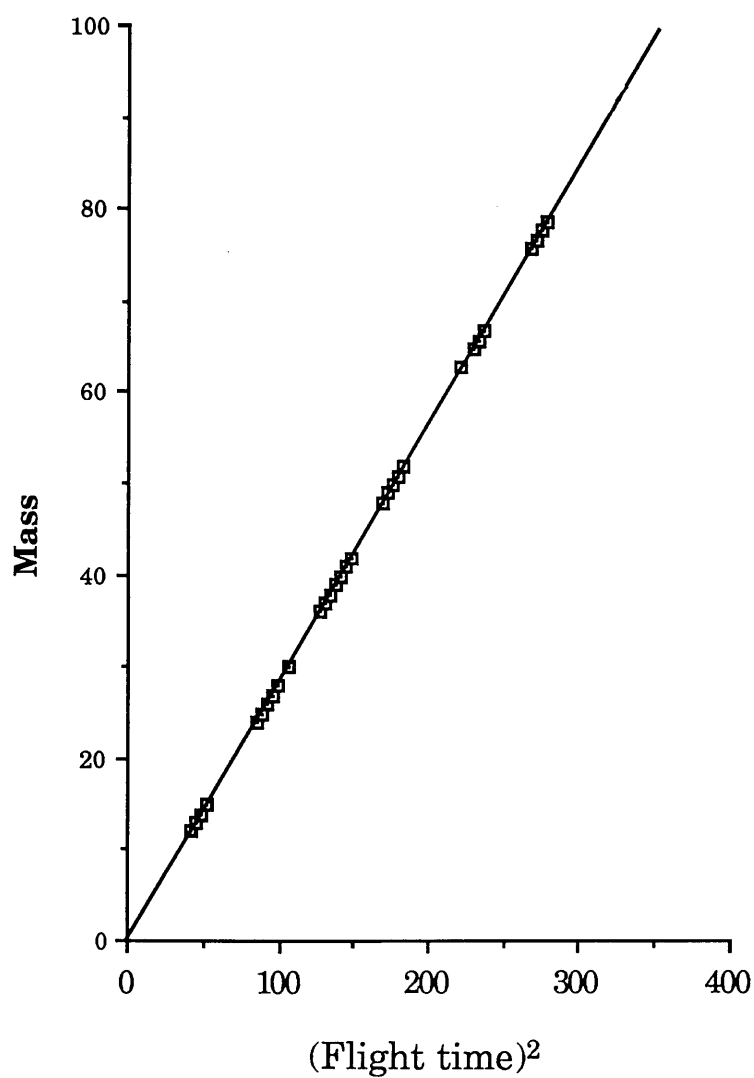


**Fig. 5.8:** TOF mass calibration curve of the TOF mass spectrometer using the data of Fig. 5.7.

The mass spectrum recorded, therefore, is most probably the result of multiphoton ionisation/fragmentation of some intermediate fragment species, possibly  $C_6H_5$  or  $C_6H_5O$ , which are produced in the initial predissociation process.

Fragmentation data recorded by Apel and Nogar (1986) is shown in Fig. 5.9. Their spectrum was recorded at 248nm and at a laser fluence of between 1 and 10mJ/pulse, using a KrF excimer laser source. Unfortunately, it bears very little resemblance to the spectrum shown in Fig. 5.7. The highest ion mass observed was 93, which they assigned to the  $C_6H_5O^+$  ion, and would correspond to the loss of NO from the parent ion. The omission of a strong  $NO^+$  ion, which we now believe is characteristic of  $NO_2$  containing compounds, suggests that Apel and Nogar were observing some impurity in the nitrobenzene sample, possibly aniline, since aniline had been previously identified as an impurity in nitrobenzene samples (Marshall *et al*, 1990) in the wavelength range 285-300nm.

It was emphasised in Chapter 4 that the R2PI spectrum obtained for a particular sample should appear, under certain conditions, very similar to the gas phase absorption spectrum for that molecule. The UV absorption spectrum of nitrobenzene vapour, recorded on a Beckman UV spectrophotometer, was measured. Fig. 5.10 shows the spectrum obtained when the resolution of the instrument was 0.1nm. A rather broad structureless absorption band in the range 210 - 330nm is observed with a maximum absorption at ~242nm, and with absorption falling off monotonically with increasing wavelength. The general appearance of this spectrum is very similar to a number of nitroaromatics and is characteristic of predissociation

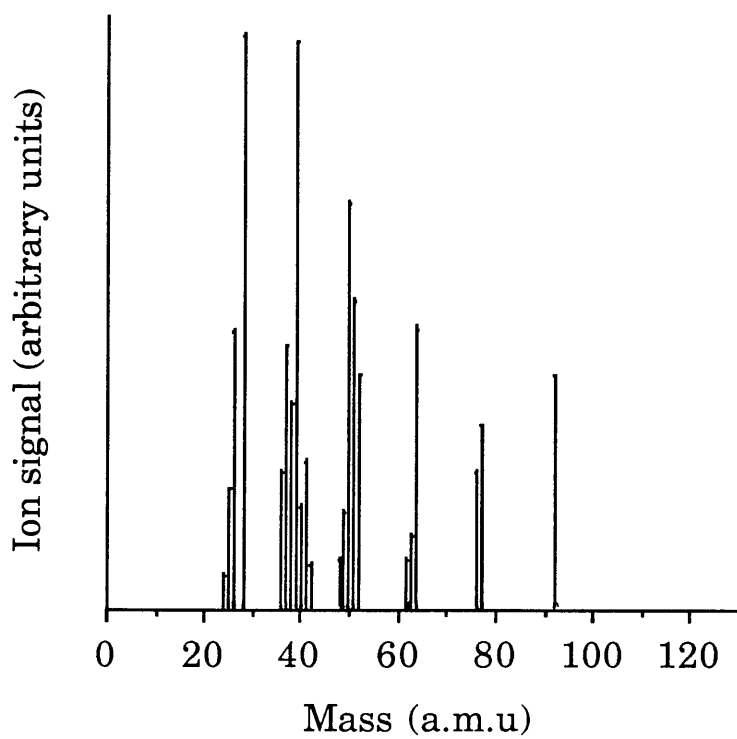


**Fig. 5.9:** TOF mass spectrum of nitrobenzene vapour recorded at 248nm by Apel and Nogar, (1986).

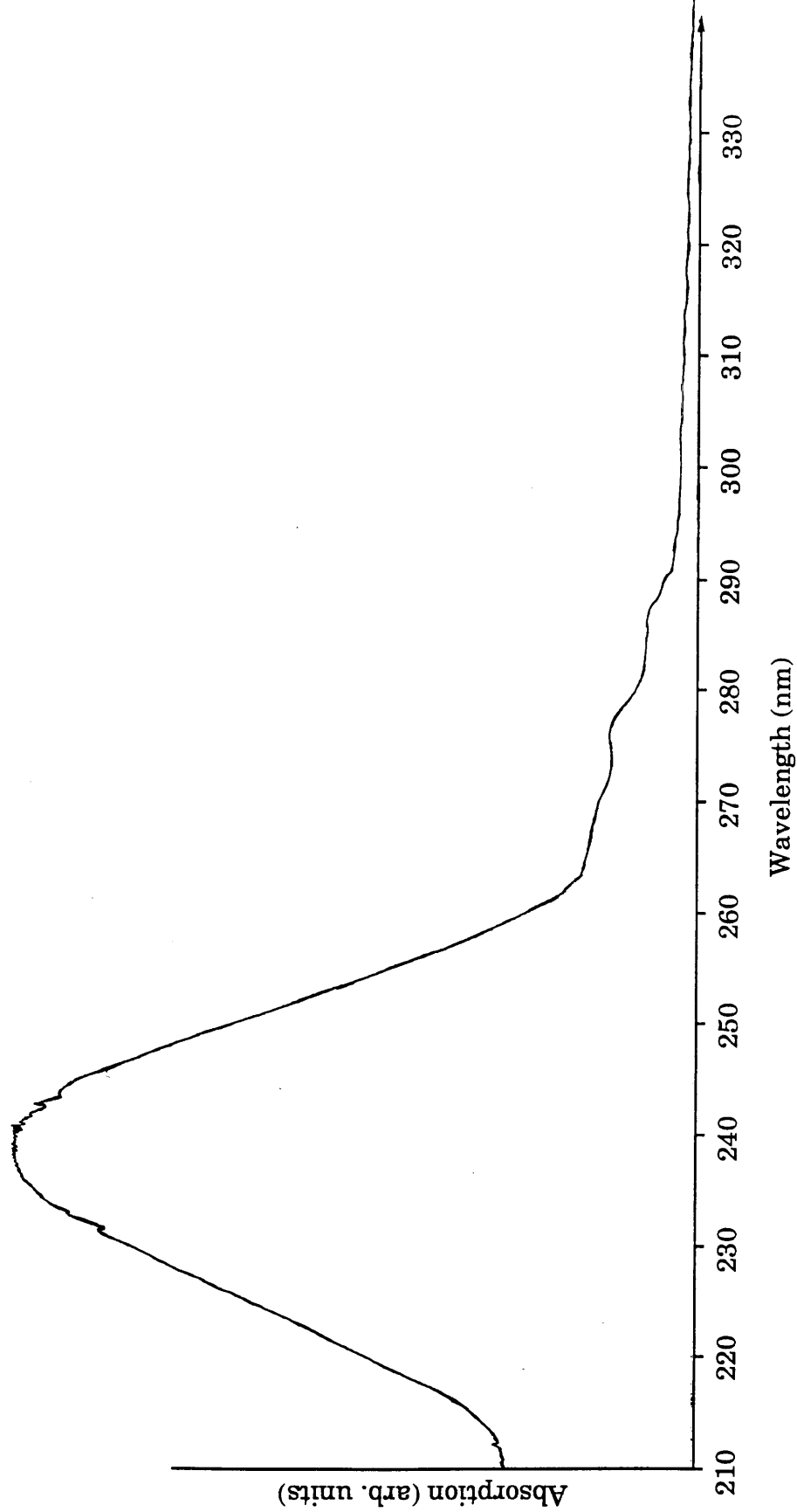


**Fig. 5.10:** Ultraviolet absorption spectrum of nitrobenzene vapour.

(Steinfeld, 1974). The use of such a spectrum to identify unambiguously nitrobenzene vapour would therefore be minimal due to the lack of any well defined structure. Nitrobenzene vapour was present at its saturated vapour pressure when this absorption spectrum was recorded.

Since it was believed that there might be intermediate absorbing fragments deriving from the parent molecule, the wavelength dependence of some of the fragment ions appearing in the mass spectrum was measured and they are displayed in Fig. 5.11. The most obvious features in all spectra are the peaks at 245.7 and 249.1nm and the broad peak at 247.2nm. Sharp structure is observed in all spectra at 246.6nm in the spectra of the  $\text{C}_6\text{H}_5^+$ ,  $\text{C}_4\text{H}_2^+$  and  $\text{C}_3\text{H}_3^+$  fragments. In the spectra of  $\text{C}_3^+$ ,  $\text{C}_2^+$  and  $\text{C}^+$  ions, an increase in ion intensity is observed in the range 245-246nm, but this is a result of higher fluences in this localised region for these particular fragments. A typical laser fluence profile is shown in Fig. 5.12. In addition, the spectrum of the  $\text{C}^+$  ion shows some sharp resonant structure at 247.9nm. This was investigated in more detail by taking several carbon spectra in the range 245-250nm at several different fluences. As can be seen in Fig. 5.13, numerous sharp resonance features are clearly visible at the highest fluence. These have been identified as multiphoton ionisation processes in atomic carbon which have been produced by dissociation of nitrobenzene molecules. Transitions originating from both ground and excited states of carbon have been identified and are discussed in detail in Chapter 7.

Obviously, the wavelength dependent spectra shown here bear no resemblance to the single UV absorption spectrum of Fig. 5.10. In the wavelength range studied the absorption intensity falls steadily from 245-250nm with no obvious structure. This

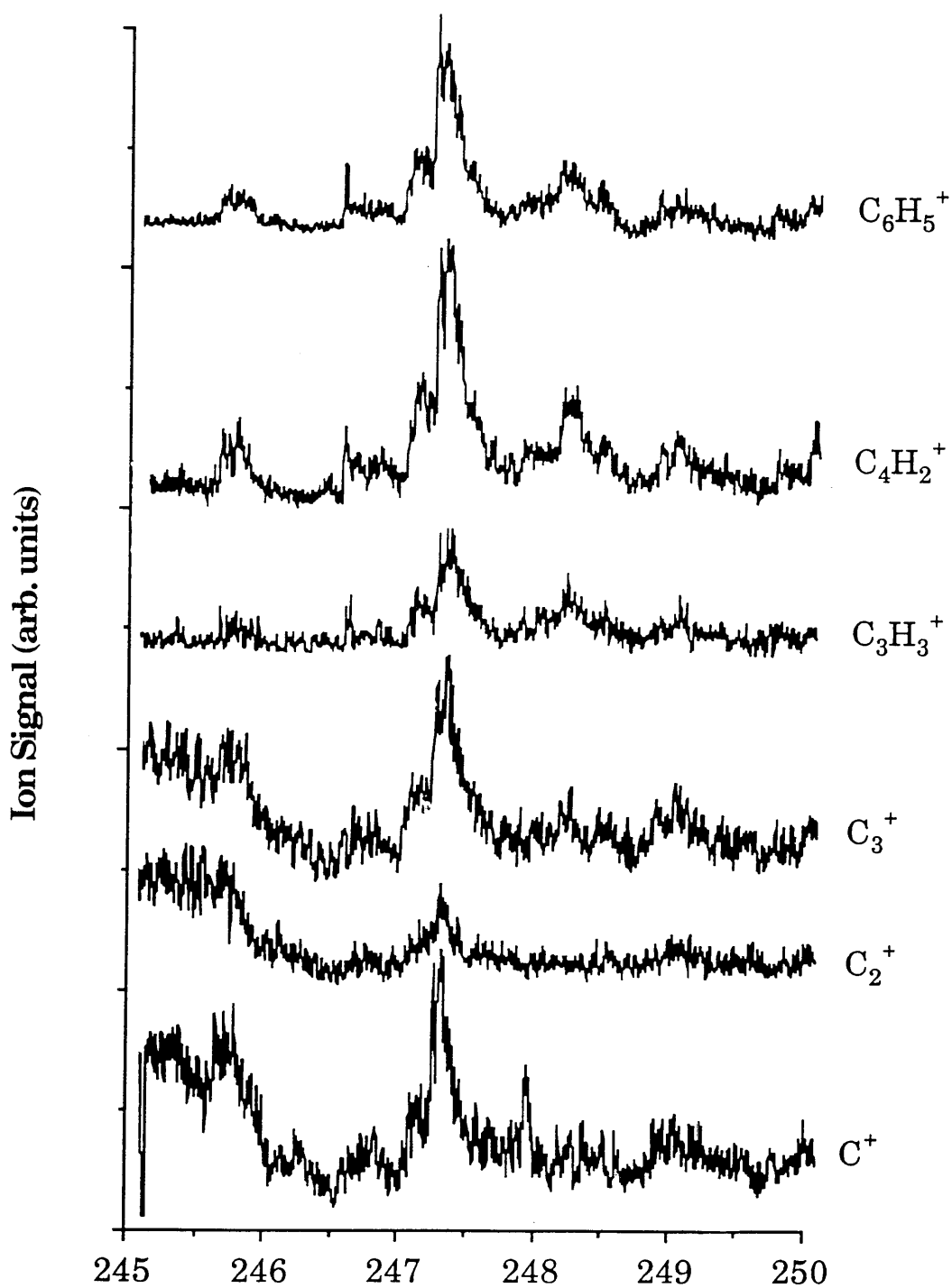


**Fig. 5.11:**Wavelength dependence of fragment ion production from nitrobenzene sample.



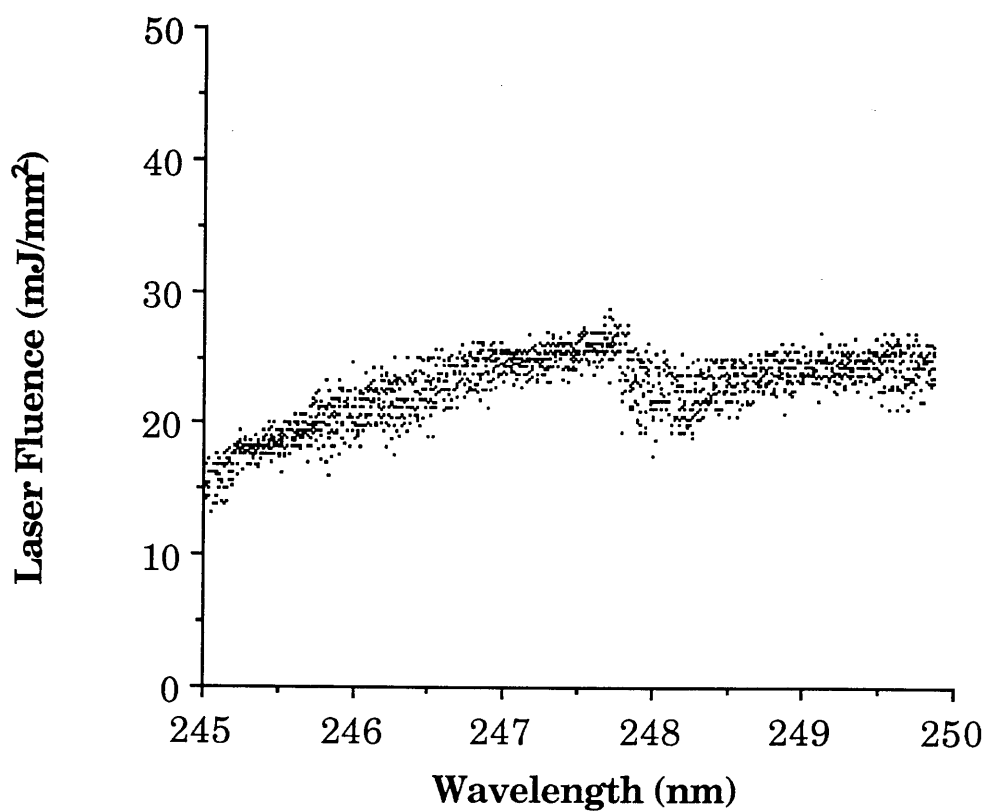


**Fig. 5.12:** Laser fluence profile recorded simultaneously with the ionisation data shown in Fig. 5.11.

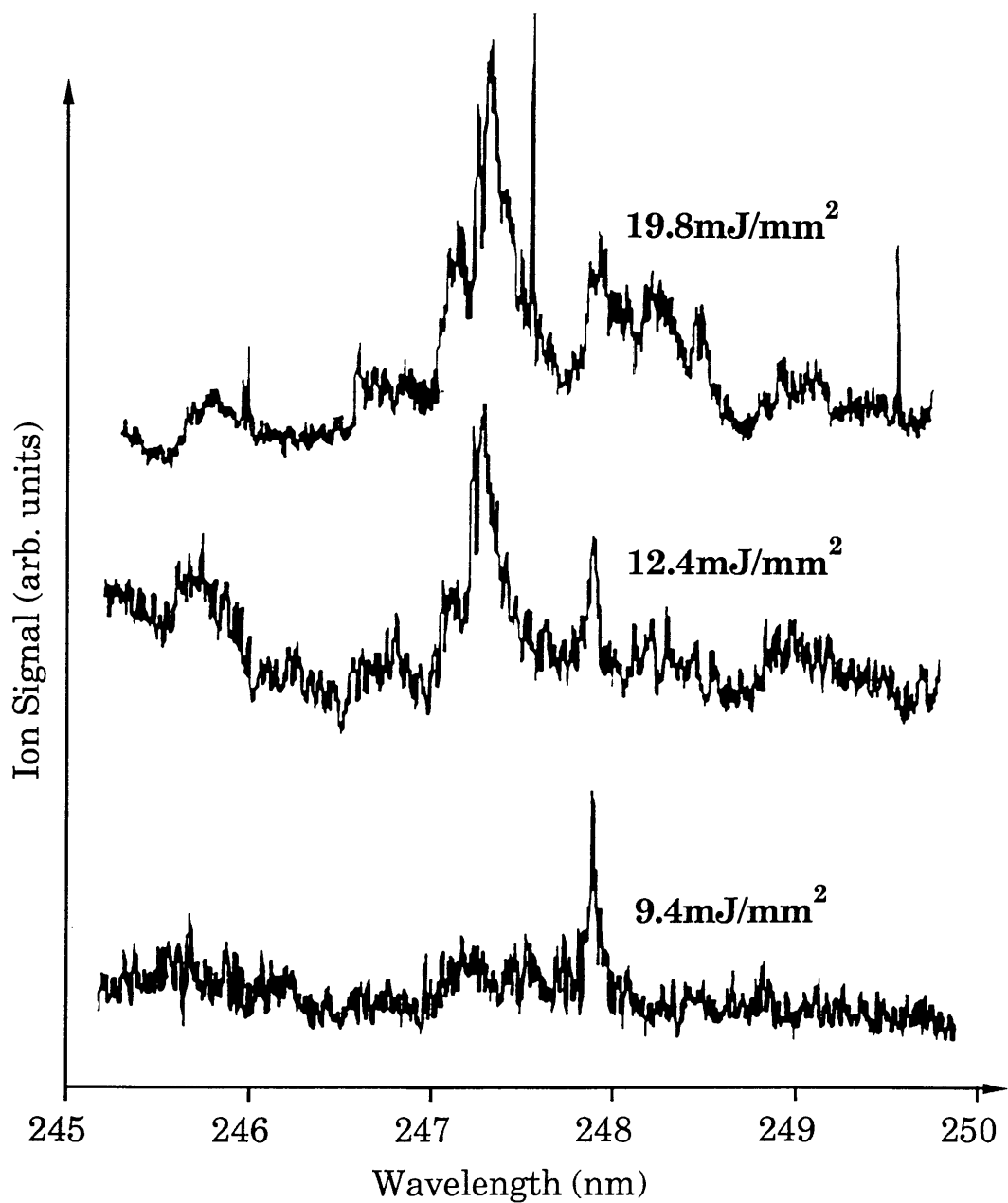


**Fig. 5.13:** Wavelength dependence of carbon ion production from nitrobenzene, showing sharp atomic-like transitions.

information coupled with the fact that no parent ion is observed in the mass spectrum further strengthens the view that there is a predissociation process occurring after the parent molecule absorbs one or more UV photons from the laser pulse. The spectral features observed in Fig. 5.11 must therefore be characteristic of some intermediate neutral species or fragment ion. A strong candidate is  $\text{C}_6\text{H}_5$  or possibly  $\text{C}_6\text{H}_5^+$ , since the mass 77 ion was the highest mass fragment observed in any mass spectrum recorded for nitrobenzene.

Very strongly wavelength dependent ionisation was also observed in this wavelength range for the  $\text{NO}^+$  ion. A typical spectrum is shown in Fig. 5.14 which also shows the laser fluence profile. The two most striking features of this spectrum are the edges observed at 247.07nm and 247.81nm. The spectrum is characteristic of the rotational features of small di- or tri-atomic molecules and the transitions have been identified as the  $\text{A } ^2\Sigma_{1/2} (\nu'=0, J') \leftarrow \text{X } ^2\Pi_{1/2, 3/2} (\nu''=1, J'')$  transition in nitric oxide (NO). The two edges observed have been identified as band head transitions from the first vibrational manifolds of the two members of the electronic ground state. This spectrum therefore carries a vast amount of information regarding the dissociation pathways which are followed while nitrobenzene molecules interact with UV radiation. As mentioned previously, the two most probable pathways are given by (5.3) and (5.4), with the former being the most likely in view of the fact that  $\text{C}_6\text{H}_5^+$  was the highest mass fragment ion observed in the mass spectrum at any wavelengths used. In order to investigate the dissociation pathways, high purity NO, and nitrogen dioxide ( $\text{NO}_2$ ) have been studied in a wider wavelength range, 232 - 260nm, and will be the subject of the following Chapter.

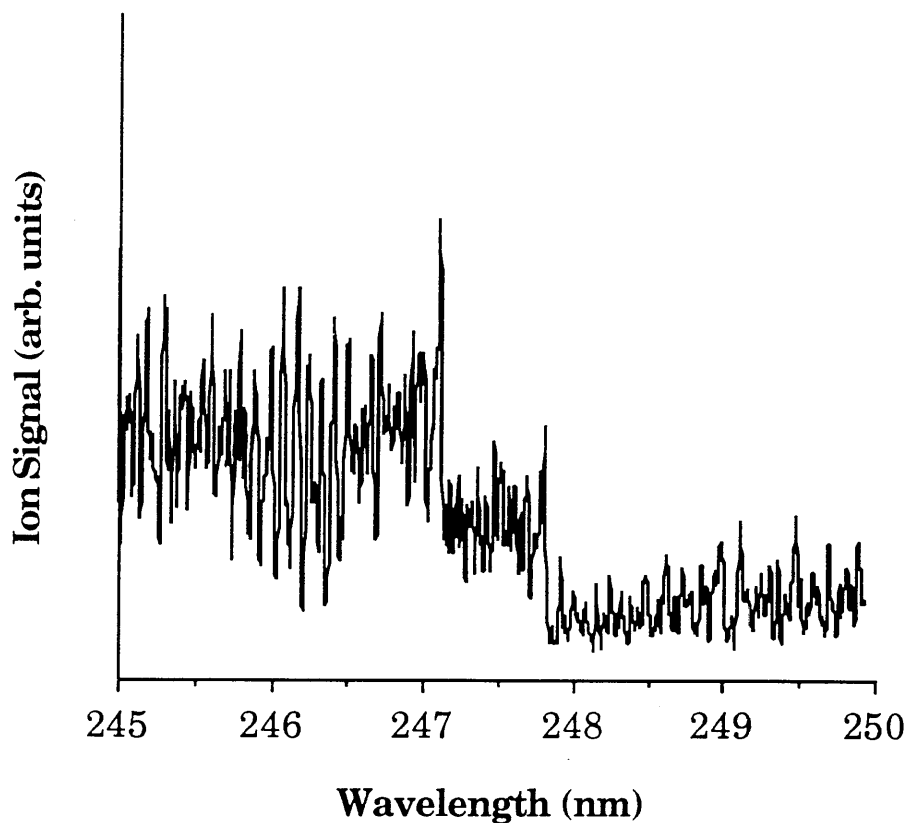
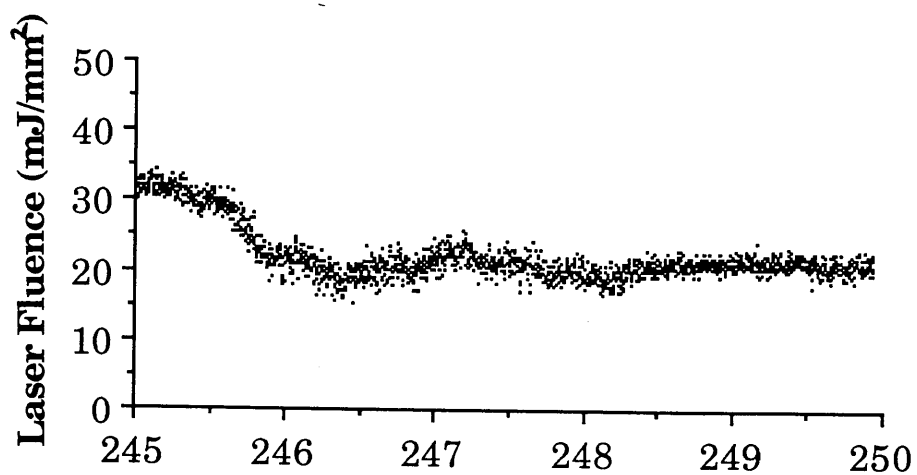


**Fig. 5.14:** Wavelength dependence of  $\text{NO}^+$  ion production from nitrobenzene. Also shown is the laser fluence profile which was recorded simultaneously with the ionisation signal.

Once the wavelength dependence of ionisation was known, mass spectra were recorded at specific wavelengths where certain fragment ion intensities exhibited resonance structure. Firstly, several mass spectra were recorded at 247.2nm, where the  $\text{C}_6\text{H}_5^+$  fragment ion was prominent in the mass spectrum, at a variety of laser fluences. These spectra are shown in Fig. 5.15, where the laser fluences are also given. Even at the lowest fluence level the  $\text{C}_6\text{H}_5^+$  fragment intensity is observed at a level well above the noise, whereas the only other fragments observed (some  $\text{C}_5$  type fragments and the  $\text{NO}^+$  ion) are barely visible. Some interesting features were noted, however, when the laser fluence was increased. Between  $0.5 \text{ mJ/mm}^2$  and  $5.0 \text{ mJ/mm}^2$  the group of fragments around mass 77 increase in intensity only very slightly (by  $\sim 20\%$ ), whereas all other fragment ion intensities show a much greater rate of increase. The rate of increase of these other fragment ions then slows down somewhat at laser fluences greater than  $5.0 \text{ mJ/mm}^2$ . The power dependence of the  $\text{C}_6\text{H}_5^+$  ion is shown in Fig. 5.16 where it is apparent that the intensity of this particular ion increases until the fluence level reaches  $\sim 4.5 \text{ mJ/mm}^2$ , above which it then begins to decrease. At the highest fluences available, the  $\text{NO}^+$  ion dominated the mass spectrum at this particular wavelength.

Two different models are proposed to explain the decrease in intensity of the  $\text{C}_6\text{H}_5^+$  ion intensity. Firstly, a model in which the initial dissociation of the nitrobenzene molecule liberates a wide range of mostly neutral species is considered. In this case, the resulting increase in the fragment ion intensities could be the result of further multiphoton ionisation/fragmentation of the many neutral species in the laser beam. However, this cannot account for the decrease in the  $\text{C}_6\text{H}_5^+$  ion intensity.

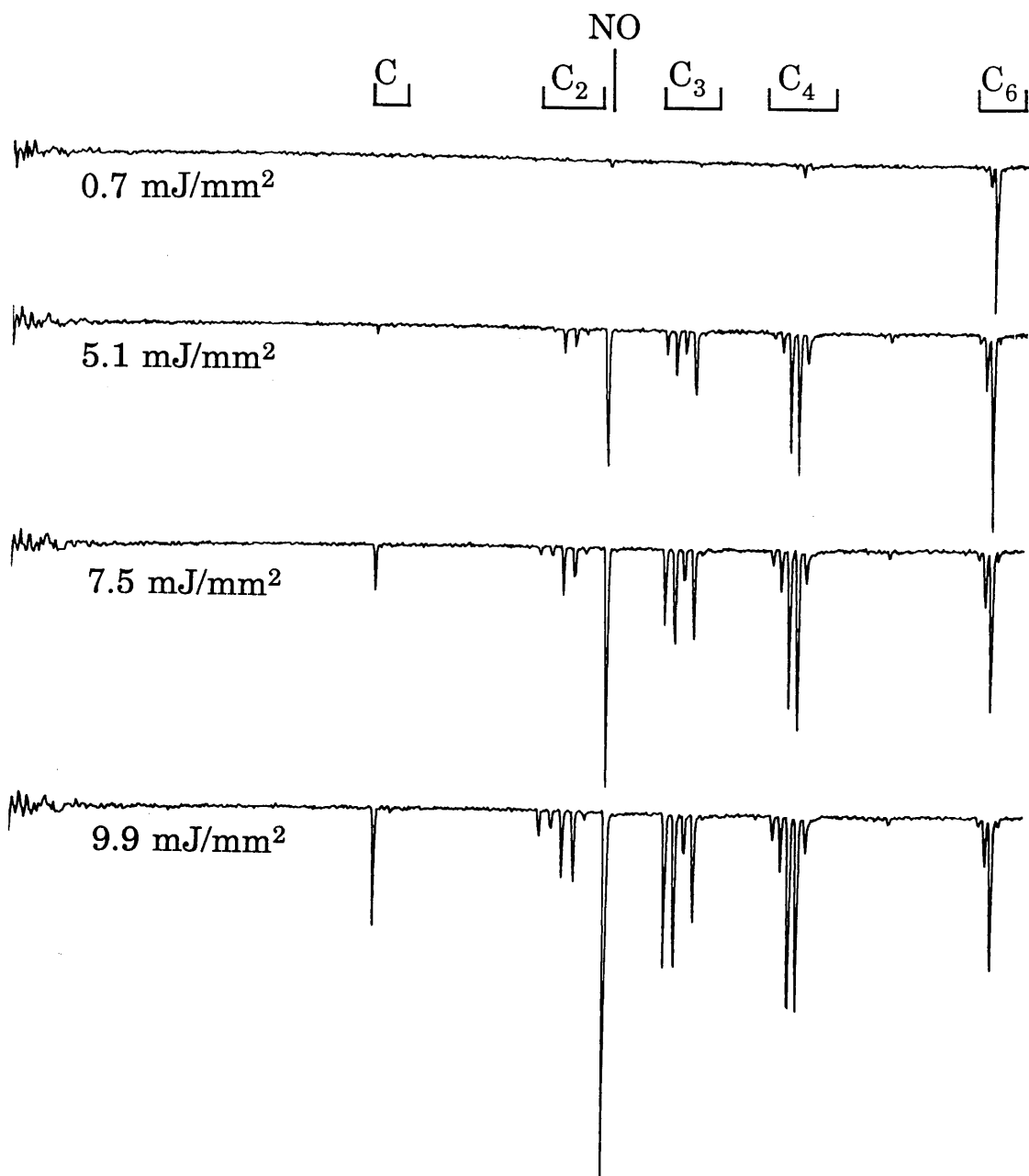


**Fig. 5.15:** TOF mass spectra of nitrobenzene recorded at 247.2nm, at various laser fluences.

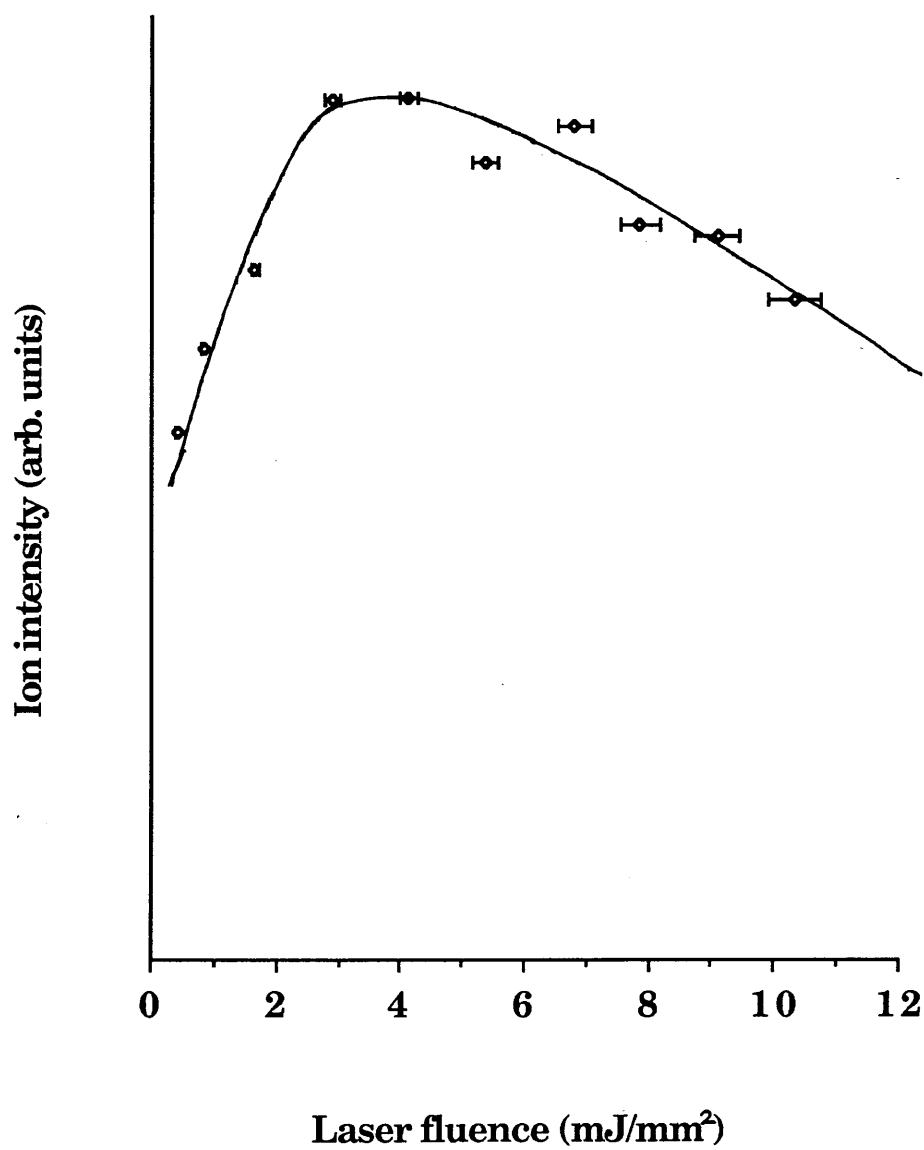


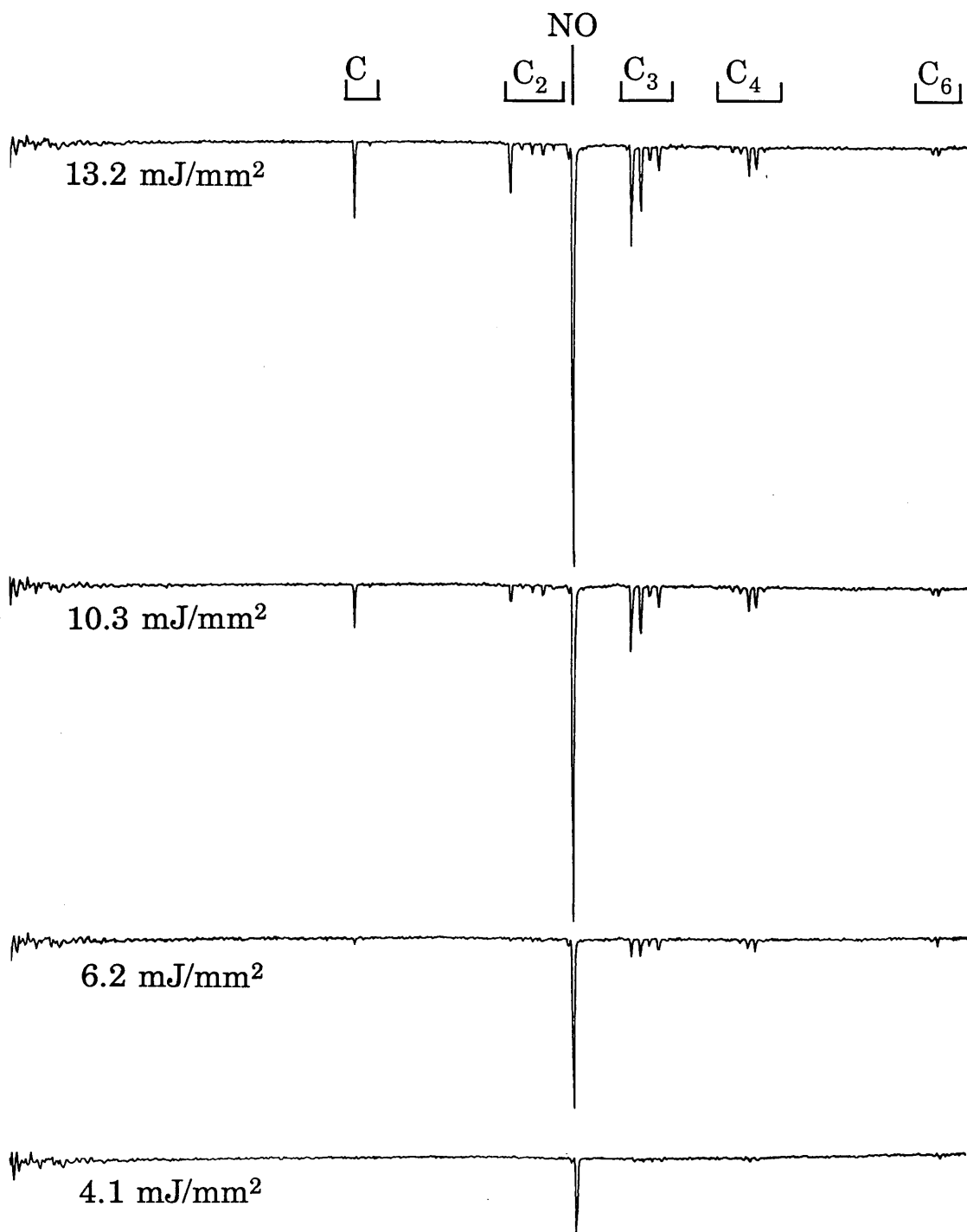
**Fig. 5.16:** Variation of  $\text{C}_6\text{H}_5^+$  ion intensity with laser fluence at 247.2nm.

A second model which considers the increase in spatial overlap of the laser beam and the sample molecules as the fluence is increased is postulated to account for both the decrease in the  $\text{C}_6\text{H}_5^+$  ion intensity and the increase in the intensities of all other ions in the mass spectrum. As the fluence in the central part of the laser beam increases from zero, the intensity of the  $\text{C}_6\text{H}_5^+$  ion increases until a point is reached where fragmentation begins to dominate and consequently the ion intensity decreases. Simultaneously, the intensity in the wings of the laser pulse becomes greater and contributes to the  $\text{C}_6\text{H}_5^+$  signal until it too becomes great enough to fragment the species. This could also be happening in the first model and it is possible that a combination of the above models is required to explain the changes in the mass spectrum as the laser fluence is altered. Both further fragmentation of the  $\text{C}_6\text{H}_5^+$  ion in the central parts of the laser pulse could account for the decrease in  $\text{C}_6\text{H}_5^+$  intensity, whereas the increase in all other fragment ion intensities could be due to a combination of either multiphoton ionisation of any neutral species produced in the dissociation process or as a result of an increase of the effective ionisation volume.

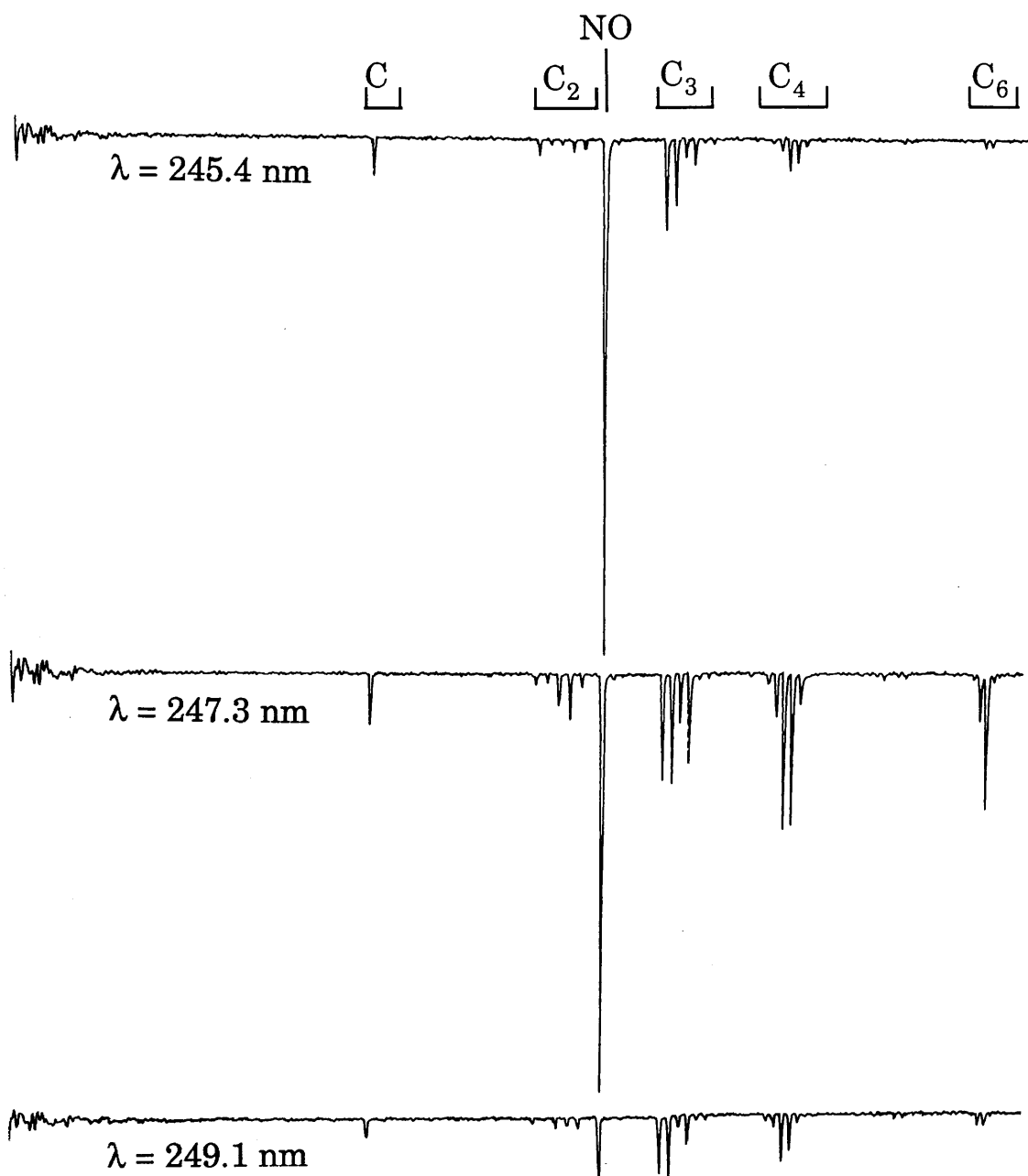
At 245.1nm, which corresponds to a resonance of the  $\text{NO}^+$  ion, only very small  $\text{C}_6\text{H}_5^+$  ion intensities were observed at any fluence level. Several mass spectra recorded at this wavelength at various laser fluences are shown in Fig. 5.17. At a fluence of  $4.1\text{mJ/mm}^2$ , the  $\text{NO}^+$  ion is clearly the most intense in the spectrum. This is true at all laser fluences at this wavelength. At the highest fluence of  $13.2\text{mJ/mm}^2$  carbon ions were observed in the mass spectrum, which is indicative of rather severe fragmentation.

Fig. 5.18 shows the ease with which particular fragment ion





**Fig. 5.17:** Mass spectra of nitrobenzene recorded at 245.1 nm, which corresponds to a resonance of the NO<sup>+</sup> ion, at various laser fluences.



**Fig. 5.18:** Mass spectra of nitrobenzene recorded at 245.4nm, 247.3nm and 249.1nm, all at the same laser fluence.

intensities may be enhanced in the mass spectrum by simply choosing the appropriate wavelength. All three spectra were recorded at a laser fluence of  $8.7 \text{ mJ/mm}^2$ . The wavelengths chosen correspond to resonance features in  $\text{NO}^+$ ,  $\text{C}_6\text{H}_5^+$  and where the ionisation spectra for all fragments show no obvious structure.

#### **§5.4.2 REMPI of mono-nitrotoluene isomers in the wavelength range 245-250nm.**

All three isomers of mono-nitrotoluene have also been investigated in the wavelength range 245-250nm. A gas phase UV absorption spectrum of o-nitrotoluene was recorded and is shown in Fig. 5.19. Sample vapour was present at the saturated vapour pressure when this spectrum was recorded. It appears very similar to the UV absorption spectrum of nitrobenzene vapour which was shown in Fig. 5.10, in that no apparent sharply defined structure is present. It should be noted that the spectra are drawn with arbitrary intensities on the absorption axes, so no information on the relative magnitudes of the cross-sections is known. It is obvious that the cross section for absorption decreases fairly rapidly in the wavelength range 245-250nm.

To allow a comparison of the laser induced mass spectrum of o-nitrotoluene with those of nitrobenzene, mass spectra were recorded at wavelengths corresponding to a resonance in the  $\text{C}^+$  ion signal, a resonance in the  $\text{NO}^+$  ion signal and at 249nm. The spectra obtained are displayed in Fig. 5.20 and correspond to a laser fluence of  $24 \text{ mJ/mm}^2$ . All amplifier and detector gains were the same.

The highest mass fragment appears at  $m/z=51$ , which

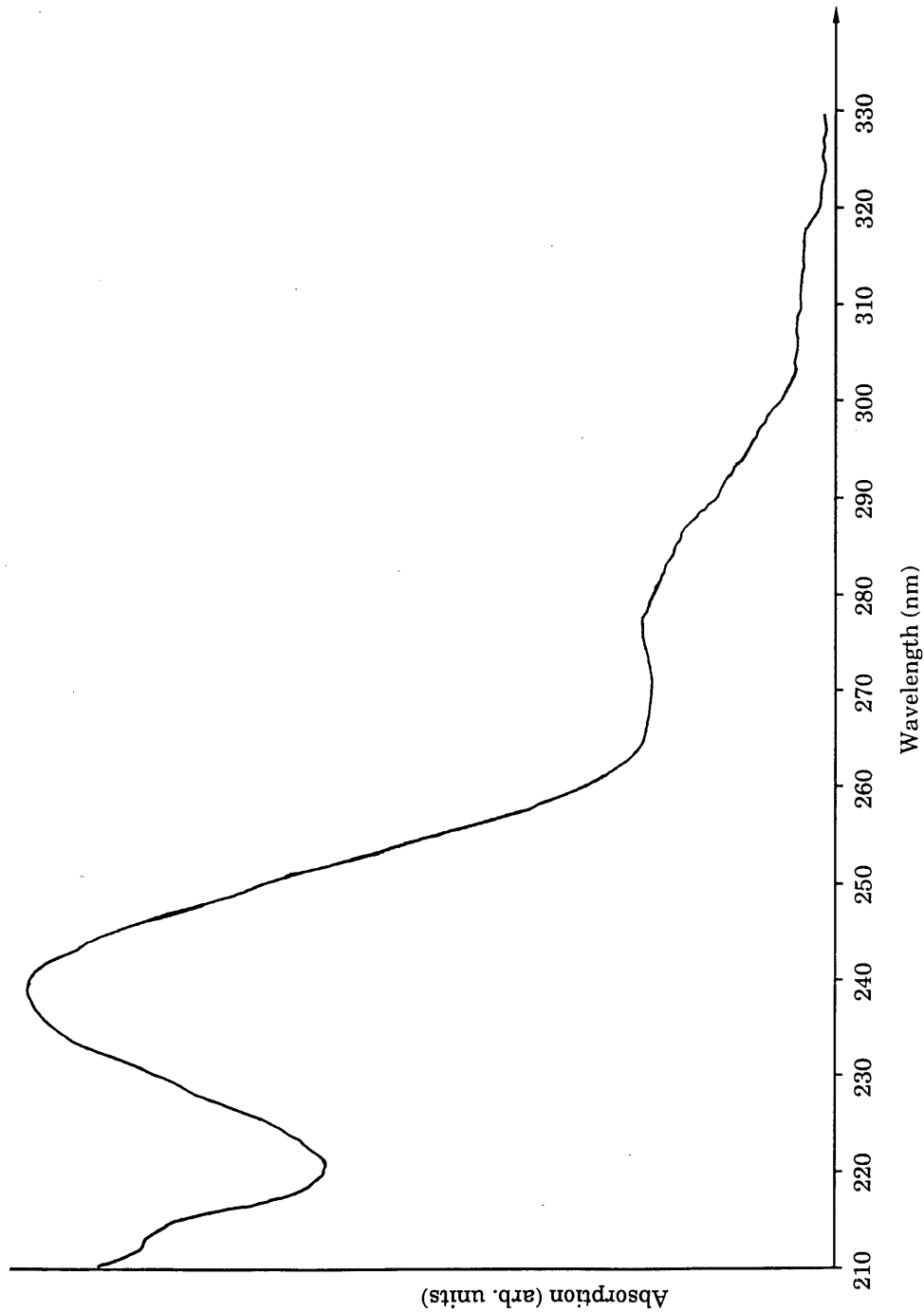


**Fig. 5.19:** Ultraviolet absorption spectrum of o-nitrotoluene vapour.

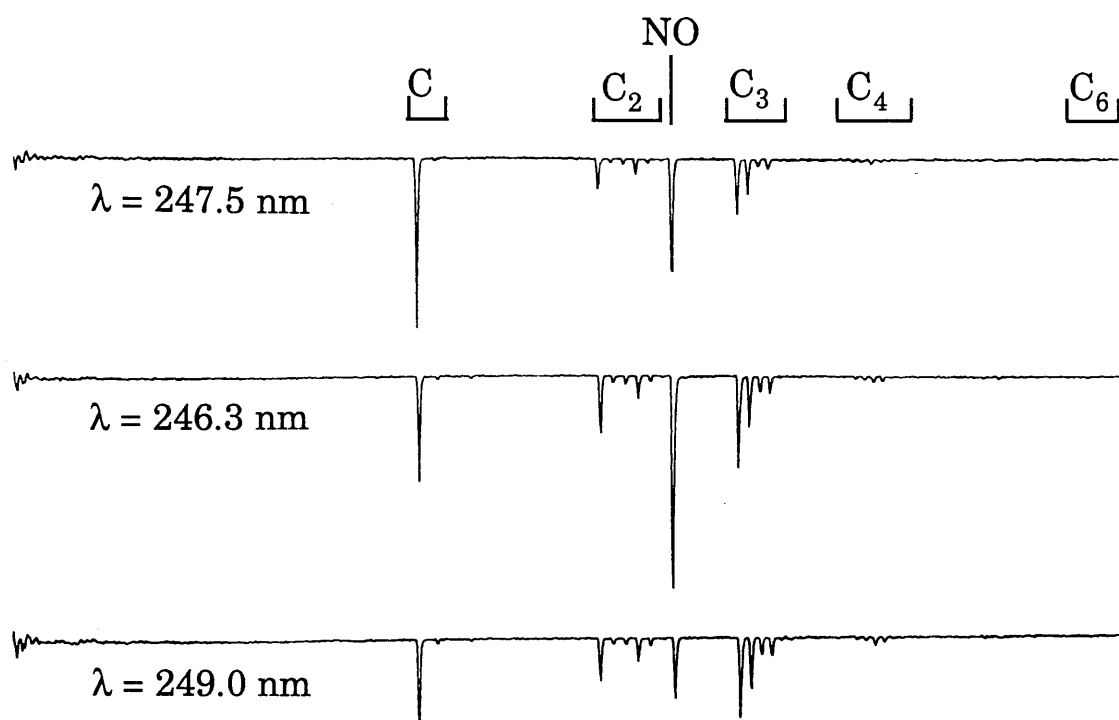


**Fig. 5.20:** TOF mass spectra of o-nitrotoluene recorded at 247.5nm, 246.3nm and 249.0 nm, all at the same laser fluence.

corresponds to the  $\text{C}_4\text{H}_3^+$  ion, whereas the highest mass fragment observed in the case of nitrobenzene was at  $m/z=77$ . As mentioned when discussing the nitrobenzene spectra, it is well known that the  $\text{NO}_2$  group rapidly predissociates from nitroaromatic molecules during irradiation by UV light. It is likely, therefore, that the  $\text{C}_7\text{H}_7$  species, which remains in the laser interaction volume after the  $\text{NO}_2$  group predissociates from the parent molecule, rapidly dissociates. This could either happen spontaneously or upon absorption of more UV photons from the laser pulse to produce smaller fragment ions with  $m/z < 51$ .

The spectra again demonstrate the ease with which the intensity of the  $\text{C}^+$  or  $\text{NO}^+$  fragments can be enhanced in the mass spectrum by simply varying the laser wavelength. It should also be noted that the intensities of the  $\text{C}_n\text{H}_m^+$  type fragments appear to remain relatively constant at all three wavelengths. This observation is verified by the wavelength dependent spectra shown in Fig. 5.21, where it is clear that the fragment ions  $\text{C}_2^+$ ,  $\text{C}_2\text{H}_3^+$ ,  $\text{C}_3^+$  and  $\text{C}_3\text{H}_1^+$  exhibit no obvious structure in this wavelength range. This observation suggests that identifying this particular molecule by virtue of some wavelength dependent hydrocarbon signature is highly unlikely, at least in this wavelength range. The laser fluence profile is also shown in Fig. 5.21 and was recorded simultaneously with the ion signals.

A very strong wavelength dependent  $\text{NO}^+$  ion signal was observed and is shown in Fig. 5.22 along with the laser fluence profile. Similar structure to that observed in nitrobenzene is seen with two very clear cut features at 246 and 246.7nm. Detection of a characteristic  $\text{NO}^+$  signal in nitrobenzene and nitrotoluene spectra that is both strongly wavelength dependent and very

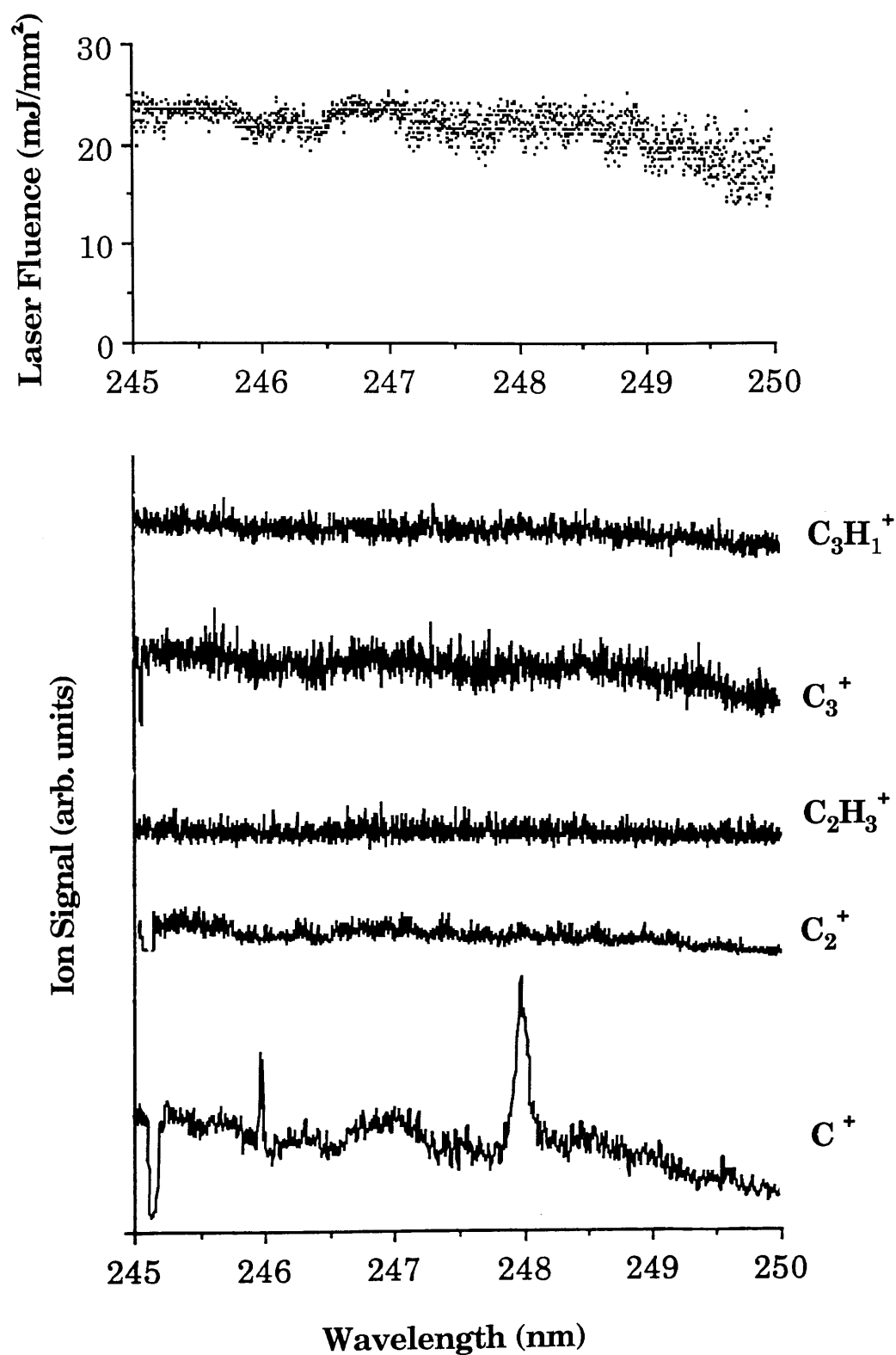


**Fig. 5.21:** Wavelength dependence of fragment ion production from o-nitrotoluene, with laser fluence profile.

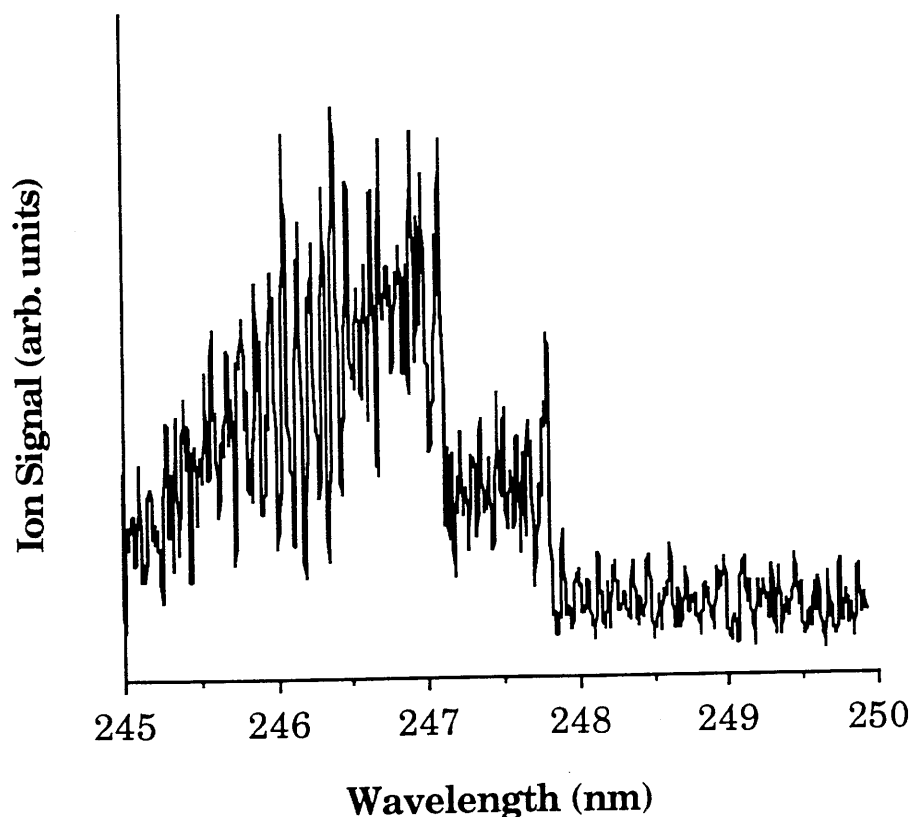
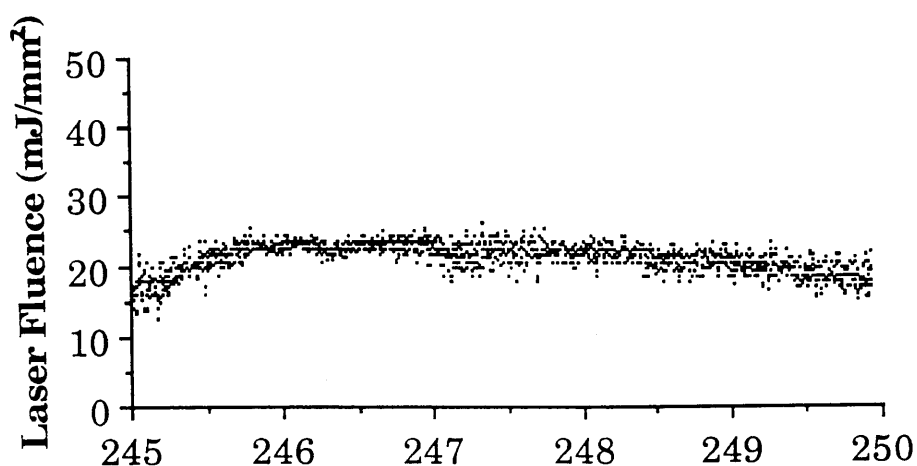


**Fig. 5.22:** Wavelength dependence of  $\text{NO}^+$  ion production from o-nitrotoluene. Also shown is the laser fluence profile which was recorded simultaneously with the ionisation signal.



intense, raises the possibility of using this as a fingerprint for the detection of NO<sub>2</sub> containing compounds. In addition, the C<sup>+</sup> spectrum again shows sharp atomic-like structure at 246 and 247.9 nm, similar to that in nitrobenzene.

Several mass spectra were recorded at a carbon resonance wavelength (247.5nm), and at several laser fluences (Fig. 5.23). At the lowest fluence of 8.3mJ/mm<sup>2</sup>, the NO<sup>+</sup> fragment at m/z = 30 is observed to be dominant. However, as the laser fluence increases the carbon fragment groups increase in magnitude, relative to the NO<sup>+</sup> ion. The most rapid increase is observed in the C<sup>+</sup> ion intensity. As in the case of nitrobenzene, this resonance has been identified as a transition in atomic carbon which has been liberated from the molecule during the interaction time.

By simply changing the laser wavelength to 246.3nm, which corresponds to a resonance in the NO<sup>+</sup> spectrum, it is noted that it is the intensity of the NO<sup>+</sup> signal which increases rapidly with laser fluence. Throughout the fluence range, NO<sup>+</sup> is always the most intense ion signal in the mass spectrum, as shown in Fig. 5.24. The difference in the behaviour of the mass spectra at the carbon and NO resonances shows that there is a higher fluence threshold for C<sup>+</sup> production even on resonance, than for NO<sup>+</sup> production.

The meta- and para- isomers were studied briefly in the same wavelength range. The wavelength dependent fragment spectra for these two isomers are shown in Fig. 5.25 and 5.26 respectively, along with the shot-to-shot laser fluence profiles. Again, no obvious structure is present in the spectra of any of the C<sub>n</sub>H<sub>m</sub><sup>+</sup> type fragments, but the usual sharp structure associated with the carbon ion is again noted in the case of the m-

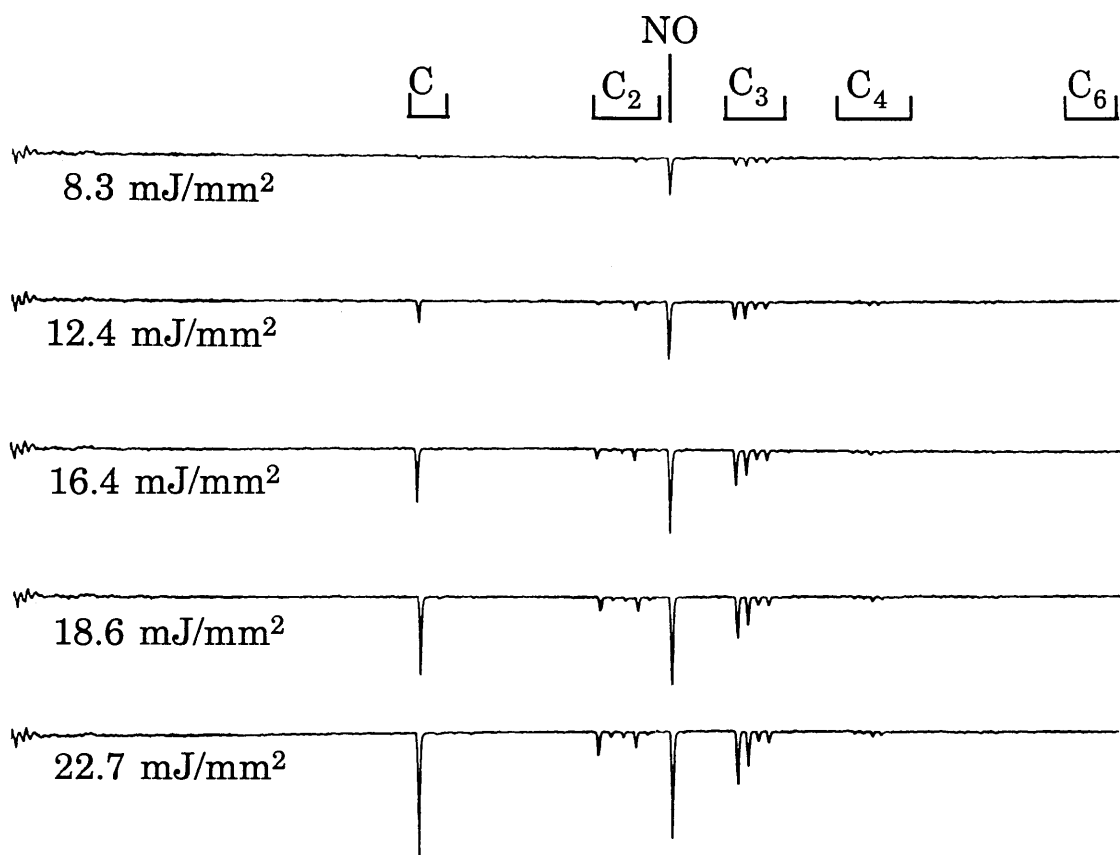


**Fig. 5.23:** TOF mass spectra of o-nitrotoluene recorded at 247.5nm, which corresponds to a resonance in the carbon ion signal, at various laser fluences.

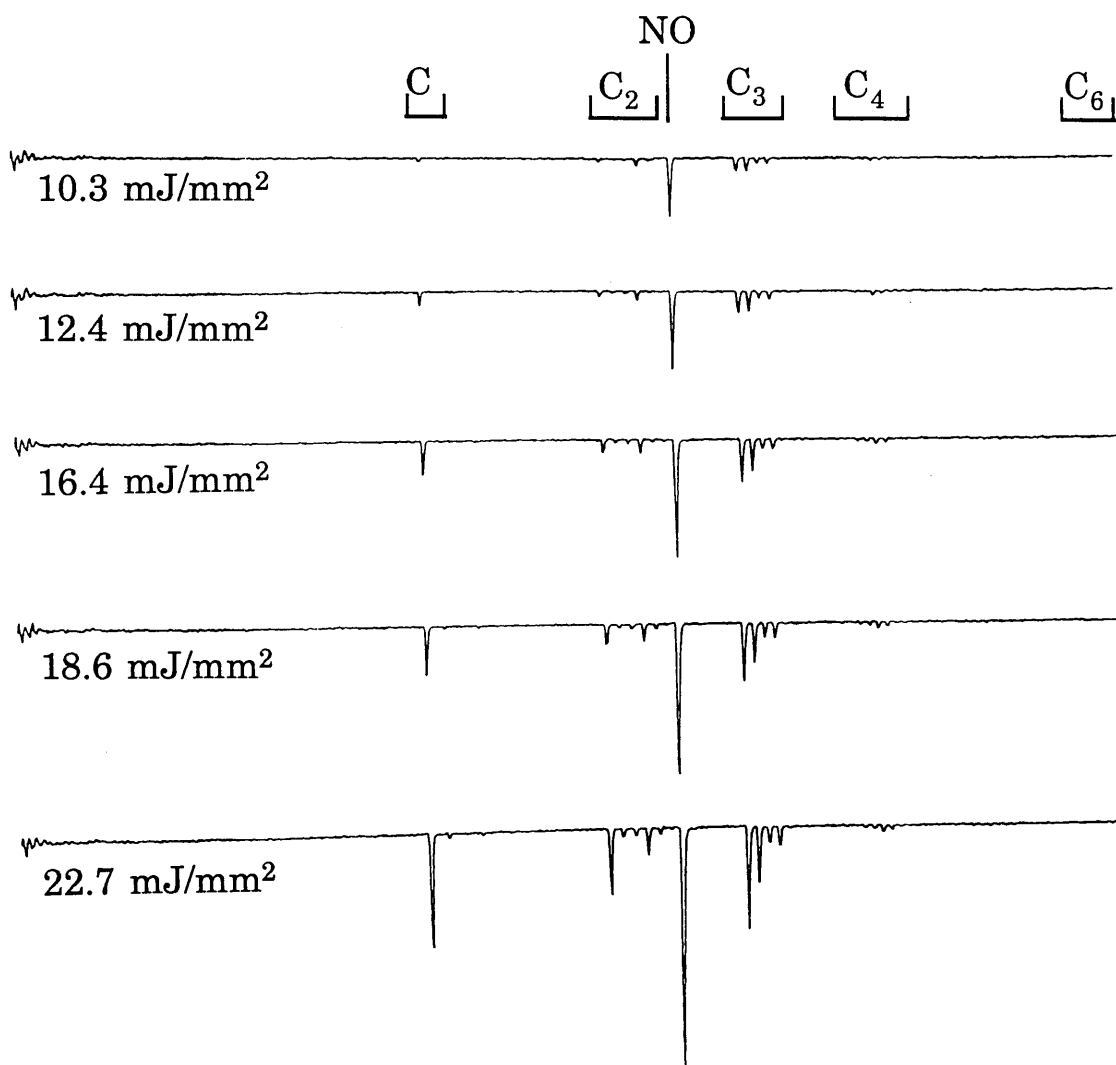


**Fig. 5.24:** TOF mass spectra of o-nitrotoluene recorded at 246.3nm, which corresponds to a resonance in the NO<sup>+</sup> ion signal, at various laser fluences.

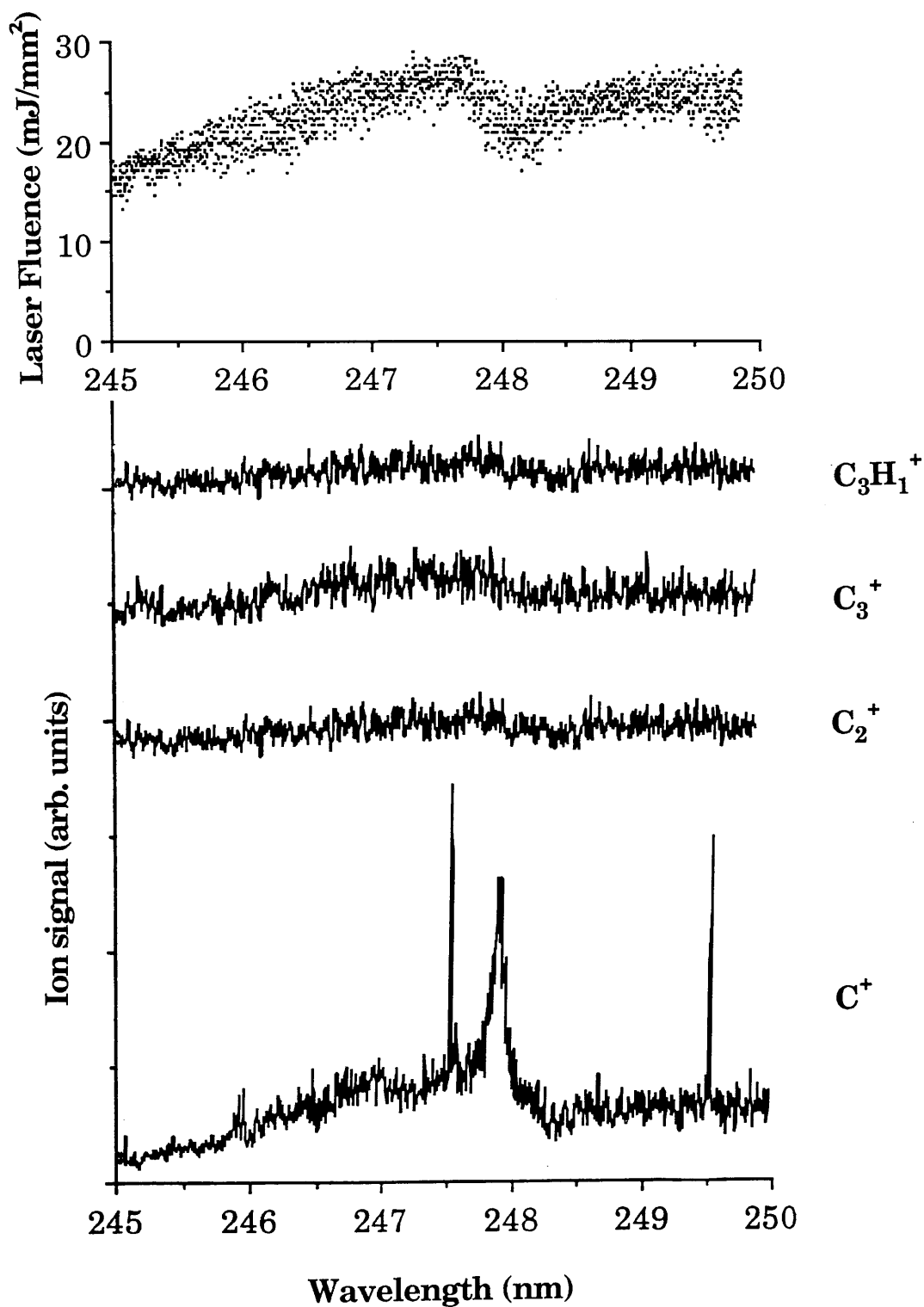


**Fig. 5.25:** Wavelength dependence of fragment ion production from m-nitrotoluene. Also shown is the laser fluence profile which was recorded simultaneously with the ionisation signal.

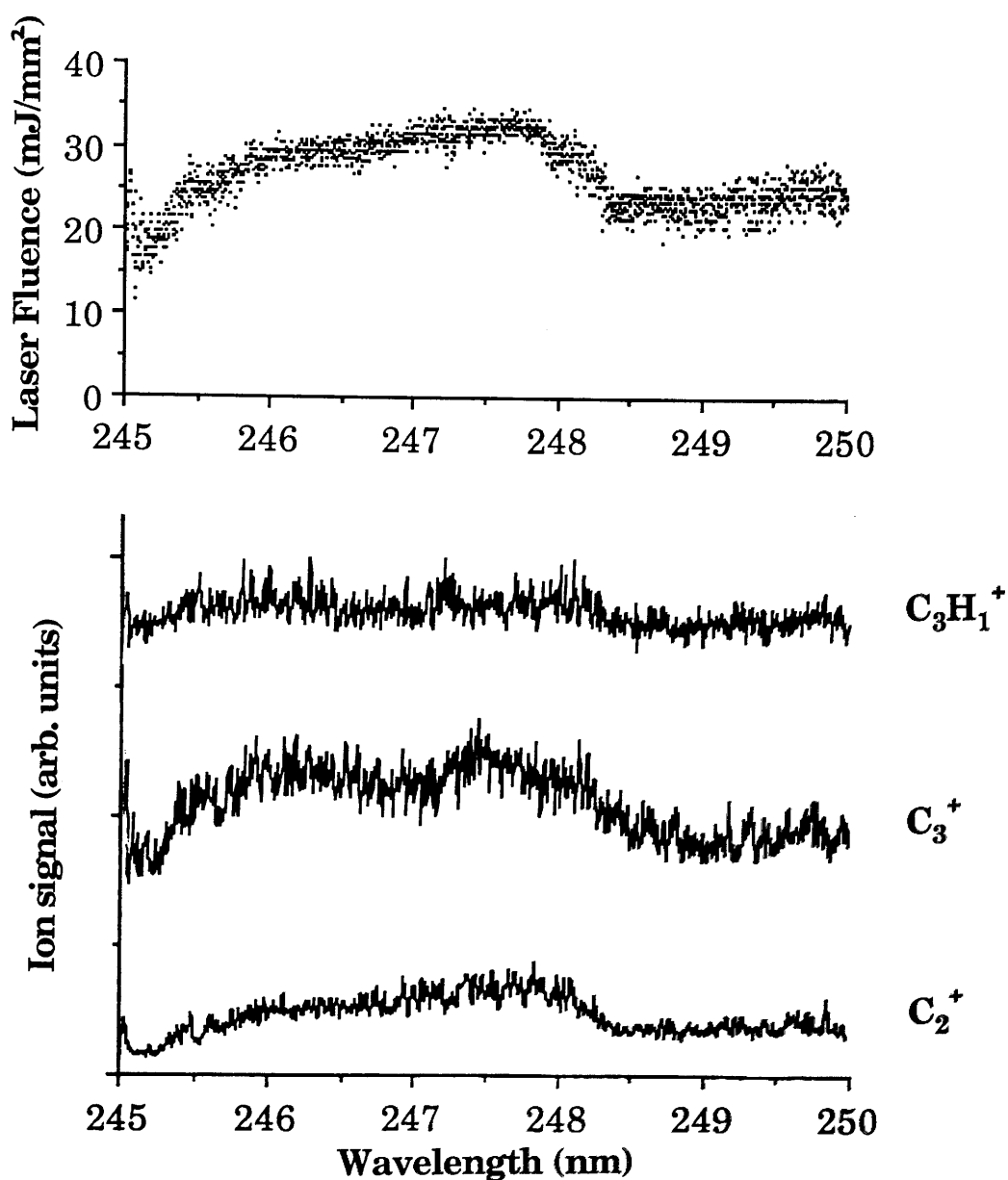


**Fig. 5.26:** Wavelength dependence of fragment ion production from p-nitrotoluene. Also shown is the laser fluence profile which was recorded simultaneously with the ionisation signal.

nitrotoluene isomer. In both cases, a strong  $\text{NO}^+$  ion signal was observed, and the wavelength dependences of this ion are shown in Fig. 5.27 and 5.28 respectively. The spectra again exhibit the characteristic features at 246 and 246.7nm.

Typical mass spectra for the m- and p- isomers which were recorded at 247.5nm and at a laser fluence of  $12.4\text{mJ/mm}^2$  are shown in Fig. 5.29a) and 5.29b) respectively. Both show similar patterns to the ortho isomer in that the highest mass observed was at  $m/z = 51$ .

### **§5.5 Conclusions.**

The study of REMPI processes in nitrobenzene and nitrotoluene isomers has yielded valuable mass spectral information which may serve to differentiate between these compounds in a highly sensitive manner. In the case of nitrobenzene, fragmentation of the molecule was noticeable even at the lowest laser fluences used, with no parent ion ( $m/z=123$ ) being observed. It should be mentioned that intense ion signals with good signal to noise statistics were obtained at pressures as low as  $10^{-7}$  mbar, which corresponds to  $\sim 3 \times 10^9$  molecules/ $\text{cm}^3$ . At this pressure, the signal to noise ratio of the  $\text{NO}^+$  ion signal recorded at a resonant wavelength of 245.4nm was  $\sim 20$  (see Fig. 5.18), so a further improvement in the sensitivity by a factor of 10 to give S/N ratios of  $\sim 2/1$  is expected to be achievable. This would correspond to minimum detectable pressures of around  $10^{-8}$  mbar, giving a detection sensitivity of approximately 10 picomoles. The hydrocarbon fragment ions produced from a sample of nitrobenzene all exhibit similar resonant structure in the wavelength range studied, a fact which could be used to unambiguously detect the molecule. This was in contrast to the

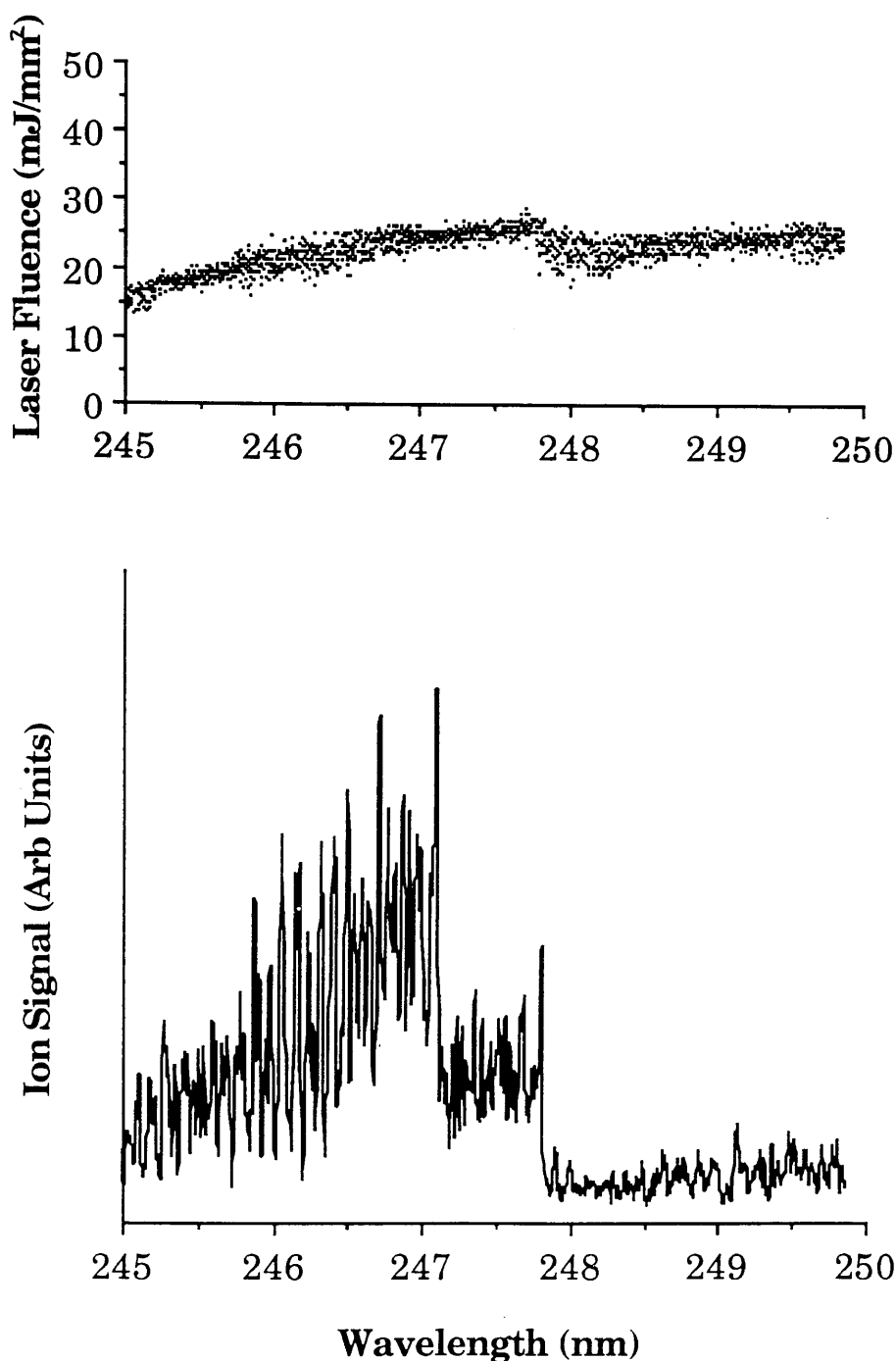


**Fig. 5.27:** Wavelength dependence of  $\text{NO}^+$  ion production from m-nitrotoluene sample. Also shown is the laser fluence profile which was recorded simultaneously with the ionisation signal.

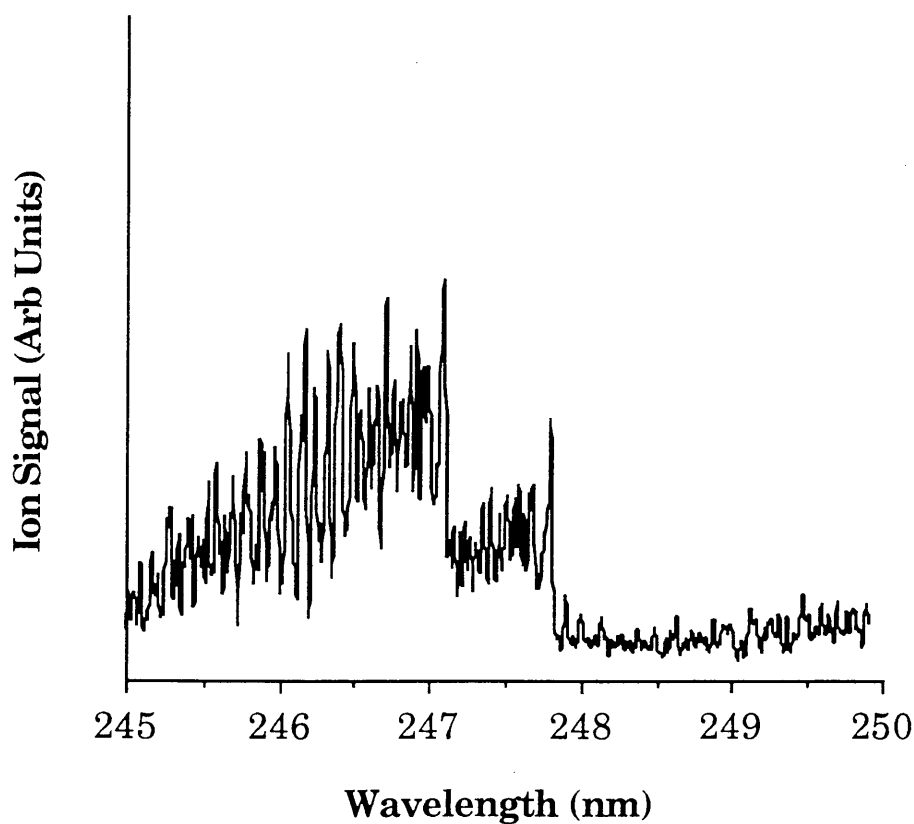
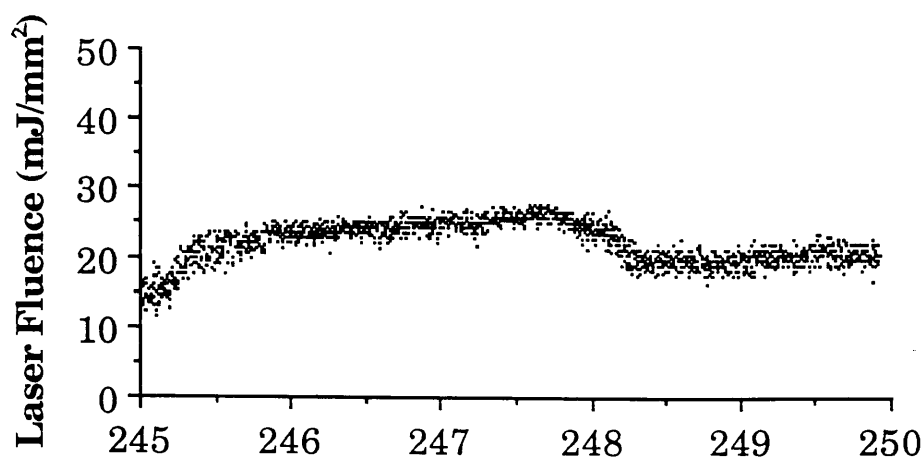


**Fig. 5.28:** Wavelength dependence of  $\text{NO}^+$  ion production from p-nitrotoluene sample. Also shown is the laser fluence profile which was recorded simultaneously with the ionisation signal.



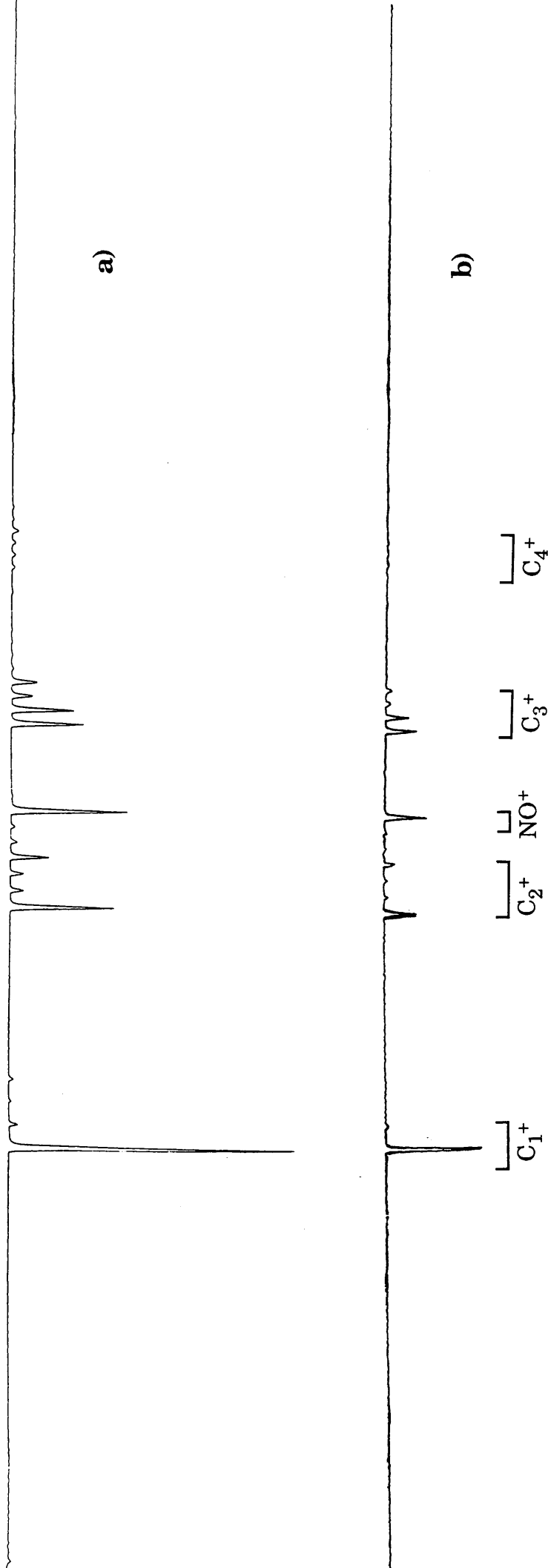


**Fig. 5.29a):** TOF mass spectrum of m-nitrotoluene recorded at 247.5nm, and at a laser fluence of 12.4mJ/mm<sup>2</sup> .

**b):** TOF mass spectrum of p-nitrotoluene recorded at 247.5nm, and at a laser fluence of 12.4mJ/mm<sup>2</sup> .

nitrotoluene isomers which showed no apparent structure in this range. It was also stressed that both compounds exhibited very distinct wavelength dependent fragmentation patterns with the highest mass fragments observed in the cases of nitrobenzene and nitrotoluene being 77 and 51 respectively.

For both samples, very strong wavelength dependent  $\text{NO}^+$  ion signals were observed, which may be used as a sensitive tag by which to identify this particular class of molecule. The resonant structure of the  $\text{NO}^+$  signal has been studied in great detail, and will be discussed in Chapter 6, where comparisons of  $\text{NO}^+$  spectra obtained from samples of  $\text{NO}$ ,  $\text{NO}_2$  and nitroaromatic molecules allow the actual physical processes occurring in the interaction to be determined.

It is also noted that it was generally more difficult to produce the same quality of data for nitrotoluene as it was for nitrobenzene, since much higher laser fluences were required to obtain the same signal to noise ratios. In addition, it was necessary to operate at higher pressures to achieve similar S/N statistics when studying nitrotoluene. This could be due to a number of factors. Firstly, it is possible that the cross section for absorption in nitrotoluene is smaller than that of nitrobenzene, which would result in smaller ion intensities at similar laser fluences. Secondly, the experiments on nitrotoluene were performed at a later date when the detector gain may have been degraded enough to significantly reduce signal sizes.

## Chapter 6

**REMPI studies of NO and NO<sub>2</sub> gases: identifying dissociative and ionisation pathways to NO<sup>+</sup> formation in nitroaromatic molecules.**

### §6.1 Introduction

The spectroscopy of nitric oxide (NO) relating to the rovibrational populations within the electronic ground state has been studied extensively using a variety of techniques (Bray *et al*, 1974; Esherick and Anderson, 1980; Kosanetzky *et al*, 1980; Sirkin *et al*, 1982; Esherick and Owyong, 1983; Goldstein *et al*, 1983; Slanger *et al*, 1983; Lahmani *et al*, 1985; Jacobs *et al*, 1986; Winkler *et al*, 1986; Feigerle and Miller, 1989)

The experiments described in this chapter were undertaken in an attempt to reveal information on the dissociation and ionisation pathways followed when vapour phase nitroaromatic molecules are irradiated by intense ultraviolet light. Chapter 5 discussed the UV multiphoton dissociation/ionisation of several nitroaromatic vapours in the TOF system, focusing particularly on the C<sub>n</sub>H<sub>m</sub><sup>+</sup> type fragments in the wavelength range 245-250nm. The strong wavelength dependent signature of the NO<sup>+</sup> ion was also noted. It is the purpose of this chapter to describe experiments concerning the NO<sup>+</sup> ion in much more detail, and in particular to look at REMPI of both nitric oxide (NO) and nitrogen dioxide (NO<sub>2</sub>) gases. REMPI in the wavelength range 233-260nm has been used to study the formation of NO<sup>+</sup> ions from both samples. The first ionisation potentials of these molecules are 9.25eV and 9.79eV (Weast, 1972) respectively, and

therefore both can, in principle, be ionised by two photons in this wavelength range (2 photons of wavelength 250nm  $\equiv$  ~10eV). From the results of these experiments some important conclusions regarding the most probable dissociation pathways followed in the nitroaromatic species can be drawn. All spectra presented in this chapter were recorded with both UV and fundamental radiation interrogating the molecular samples. Several investigations were made with only the UV beam entering the chamber, but no differences were observed in the spectra.

As discussed in chapter 5, the strong spectral features observed in the NO<sup>+</sup> ion spectrum are typical of the rovibrational spectra of small diatomic molecules. The spectral features observed have been identified as transitions between rovibrational levels in the ground state and rovibrational levels of a particular excited state in NO. In order to discuss these features at length, it is necessary to invoke certain spectroscopic terms, and therefore, a simple discussion of the electronic spectroscopy of diatomic molecules is given, where appropriate terms are introduced.

## §6.2 Classification of electronic states in diatomic molecules.

In a typical diatomic molecule which is not rotating, the total angular momentum of the molecule is due entirely to the orbital and spin motions of the valence electrons. For diatomic molecules in which the constituent nuclei have low atomic numbers, L-S coupling is the most appropriate model to use in describing the electronic structure. In this model, the electrons couple in such a way as to produce a total orbital angular momentum,  $\mathbf{L}$ , and a total spin angular momentum  $\mathbf{S}$ . These vectors have magnitudes  $[L(L+1)]^{1/2}\hbar$  and  $[S(S+1)]^{1/2}\hbar$ , where L and S are the orbital and spin quantum numbers respectively. In diatomic molecules, the

electron cloud exhibits axial symmetry, and as a consequence,  $L$  is not a good quantum number since it is not fixed in magnitude or direction. However, the projection of  $\mathbf{L}$  along the internuclear axis remains constant, and is written as  $\Lambda h$  where  $\Lambda$  can take any of the values  $-L, -L+1, \dots, L-1, L$ . Also, the total electronic energy of the molecule is the same whether the projection of  $L$  is in the positive or negative directions, so making each  $\Lambda \neq 0$  state doubly degenerate. In analogy with atomic notation, the different  $\Lambda$  values are assigned code letters.

Value of $\Lambda$	0	1	2	3 .....
Code letter	$\Sigma$	$\Pi$	$\Delta$	$\Phi$ .....

Similarly, the total spin angular momentum,  $\mathbf{S}$ , is coupled to the internuclear axis due to the magnetic interaction between the spin of the electrons and the orbital motion of the electrons. The projection of  $\mathbf{S}$  along the bond axis is written as  $\Sigma h$ , where  $\Sigma$  can take the values  $S, S-1, \dots, -S+1, -S$ . The vectors  $\mathbf{L}$  and  $\mathbf{S}$  couple to form a resultant component along the internuclear axis,  $\Omega = |\Lambda + \Sigma|$ , and is called the total electronic angular momentum of the molecule. The coupling of  $\mathbf{L}$  and  $\mathbf{S}$  to the internuclear axis is shown in Fig. 6.1.

The multiplicity of an electronic state is  $2S+1$ , since for each value of  $\Lambda \neq 0$ , there are a total of  $2S+1$  possible orientations of  $\mathbf{S}$ . In conclusion, an electronic state of a diatomic molecule is written in the notation,

$$^{2S+1}(\text{Code letter})_{\Omega}$$

For example, the state with  $\Lambda=1$  and  $S=1/2$  can have  $\Omega=1/2$  or  $3/2$

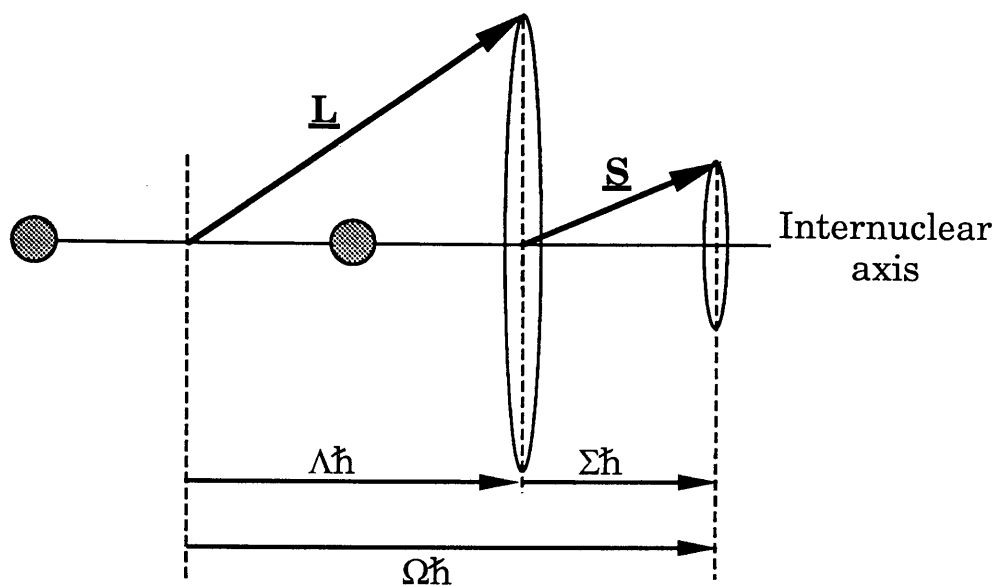


**Fig. 6.1:** Coupling of  $\underline{L}$  and  $\underline{S}$  vectors to the internuclear axis of a diatomic molecule.

and is written as  ${}^2\Pi_{1/2,3/2}$ .

### §6.3 Vibrational and rotational substates.

For a particular electronic configuration of a diatomic molecule, a number of vibrational and rotational configurations may be assumed. However, only the rotational motion contributes to the angular momentum of the molecule. Both vibrational and rotational motions are quantised, and are identified by quantum numbers  $v$  and  $J$  respectively. These values are written in brackets after the electronic state classification. As an example, the molecular state with  $S=1/2$ ,  $\Lambda=1$ ,  $\Omega=3/2$ ,  $v=2$  and  $J=5$  is written in the notation  ${}^2\Pi_{3/2}$  ( $v=2$ ;  $J=5$ ). In addition, it is conventional to use the superscripts " and ' to signify rovibrational states in the ground and excited electronic states respectively.

### §6.4 Selection rules in diatomic molecules.

Several quantum mechanical selection rules act to decide the probability of single photon transitions in diatomic molecules. It is stressed that transitions referred to as being forbidden are not strictly so, but certainly have very small transition probabilities. For single photon absorption or emission the rules which apply are (Hollas, 1987);

- 1)  $\Delta\Lambda = 0, \pm 1$
- 2)  $\Delta S = 0$
- 3)  $\Delta\Sigma = 0$
- 4)  $\Delta\Omega = 0, \pm 1$

### §6.5 Electronic structure of NO.

The ground state configuration of NO is designated as  ${}^2\Pi_{1/2,3/2}$ , where the splitting results from spin orbit interactions.

The  $^2\Pi_{1/2}$  electronic level is of lowest energy, with the gap between the potential well minima of the  $^2\Pi_{1/2}$  and  $^2\Pi_{3/2}$  states being  $\sim 124.2 \text{ cm}^{-1}$  (Morrison *et al*, 1981). The vibrational level spacing in the  $^2\Pi_{1/2}$  and  $^2\Pi_{3/2}$  states are  $1904 \text{ cm}^{-1}$  and  $1903.6 \text{ cm}^{-1}$  respectively (Herzberg, 1950), but due to the anharmonic nature of these potential wells, the vibrational spacing tends to decrease as the vibrational quantum number  $v''$  increases. In both ground state manifolds, the rotational level splitting is  $1.705 \text{ cm}^{-1}$  (Herzberg, 1950).

The lowest lying excited electronic level is designated as  $A^2\Sigma_{1/2}$ , with the  $^2\Sigma_{1/2}(v'=0;J'=0)$  state having an energy of  $44140.8 \text{ cm}^{-1}$  relative to the  $^2\Pi_{1/2}(v''=0;J''=0)$  state, as shown in Fig. 6.2. Fig. 6.2 also shows several vibrational state energies in both the  $^2\Pi_{1/2}$  and  $^2\Sigma_{1/2}$  states.

### §6.6 Rotational fine structure in electronic transitions.

In this section, a transition between rotational levels in the  $v'', v'$  manifolds of different electronic bands is considered. In a given vibrational manifold, the energies of the rotational states are given to a good approximation by,

$$E_{\text{rot}} = (\hbar^2/8\pi^2 I_c) \cdot J(J+1) = BJ(J+1) \quad \text{where } J=0,1,2,3,\dots$$

where  $I$  is the moment of inertia of the molecule about the rotation centre,  $J$  is the rotational angular momentum quantum number and  $B$  is the rotational constant for the molecule (Hollas, 1987). The energy change in a transition between the  $(v'';J''=0)$  and  $(v';J'=0)$  levels is written as  $E(v'',v')$ . The change in the total energy,  $\Delta E$ , of a transition  $(v'';J'') \leftarrow (v';J')$  may then be written as,



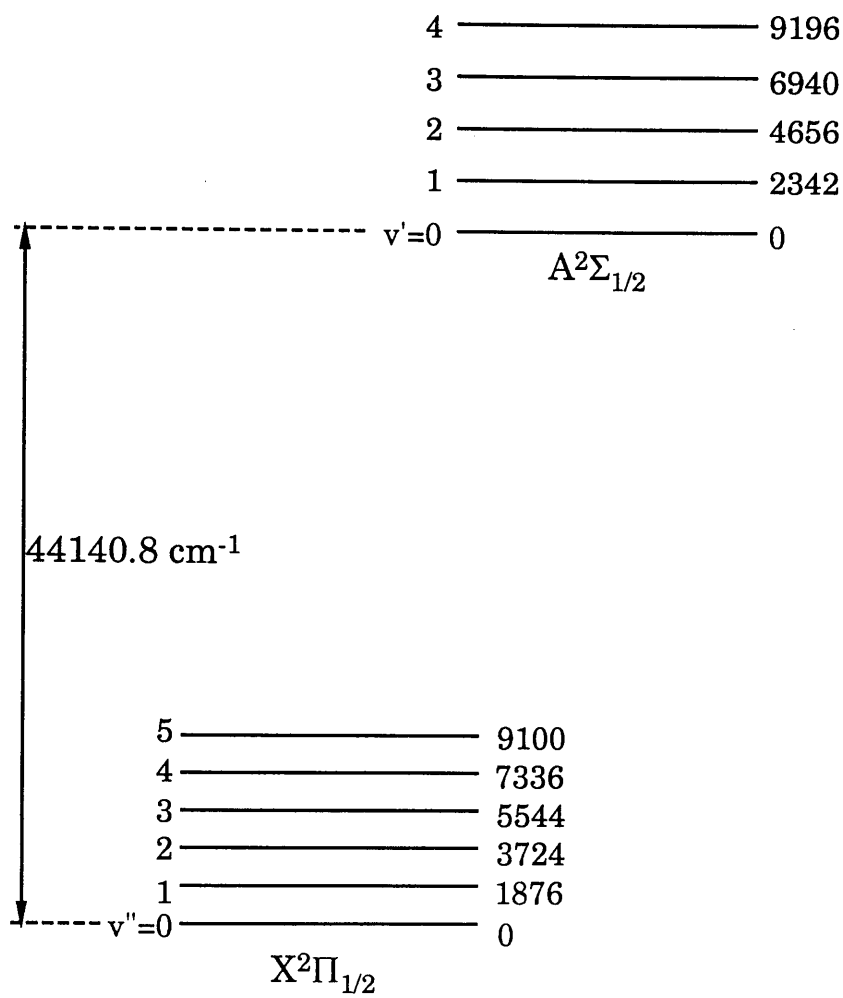


**Fig. 6.2:** Diagram showing the relevant energy levels of the  $^2\Pi$  and  $^2\Sigma$  electronic states.

$$\Delta E = E(v'', v') + \Delta[B'J'(J'+1) - B''J''(J''+1)]$$

where the final term is the change in the rotational energy which occurs during the transition. In general, the rotational constant varies between electronic bands (due to the different moments of inertia of different states), and so must be written as B'', B' for the values in the ground and excited states respectively. The total energy change,  $\Delta E$ , may finally be written as,

$$\Delta E = E(v'', v') + B'J'(J'+1) - B''J''(J''+1).$$

### §6.7 Selection rules in electronic vibrational transitions in diatomic molecules.

The probability of single photon transitions occurring in diatomic molecules is defined entirely by the transition moment as explained in Chapter 2. The electronic selection rules governing single photon absorptions in diatomic molecules were stated in Section 6.4, but changes in the rotational and vibrational quantum numbers are restricted also, in accordance with the following rules (Herzberg, 1950);

- 1)  $\Delta v$  is unrestricted.
- 2)  $\Delta J = 0, \pm 1$
- 3)  $J'' = 0 \leftrightarrow J' = 0$  is forbidden.

Transitions with  $\Delta J = 0$  form what are called Q-branch lines, and  $\Delta J = -1, +1$  form P- and R- branch lines respectively. The next section will discuss the formation of P, Q and R -branch spectra in some detail.

### §6.8 Formation of P, Q and R branches.

Firstly, the formation of the Q-branch spectrum in the

situation where  $B' > B''$  is considered, i.e where the spacing of rotational levels in the excited state is greater than that of the ground state (as is the case of nitric oxide). The energies of the Q-branch lines, are given by,

$$E_Q = E(v'', v') + (B' - B'')J'' + (B' - B'')J''^2 \quad \text{where } J'' = 1, 2, 3, \dots$$

$J'' = 0$  has been omitted due to selection rule 3. Also, since  $B' > B''$ , all of the Q-branch lines lie to the high energy side of  $E(v'', v')$ , and their spacing increases with increasing  $J''$ . Such a branch is shown diagrammatically in Fig. 6.3b). The density of lines decreases as the transition energy increases (in this case) and this is termed "shading to the violet", since the band intensity decreases to the blue or short wavelength side of  $E(v'', v')$ . The transition corresponding to energy  $E(v'', v')$  is called the band origin transition, which due to selection rule 3, is never observed in single photon transitions.

In considering the formation of R-branch spectra, again in the situation where  $B' > B''$ , the energies of the R-branch lines may be written in the form,

$$E_R = E(v'', v') + (B' + B'')(J'' + 1) + (B' - B'')(J'' + 1)^2, \quad (6.1)$$

or

$$E_R = E(v'', v') + \alpha(J'' + 1) + \beta(J'' + 1)^2, \quad \text{where } J'' = 0, 1, 2, \dots$$

and transitions are from  $J'' \rightarrow J'' + 1$  only.

Since  $\alpha$  and  $\beta$  are positive numbers, it is evident that the R-branch spectrum again shades to the violet, since the line energy and line spacings both increase with  $J''$ . The R-branch lines are

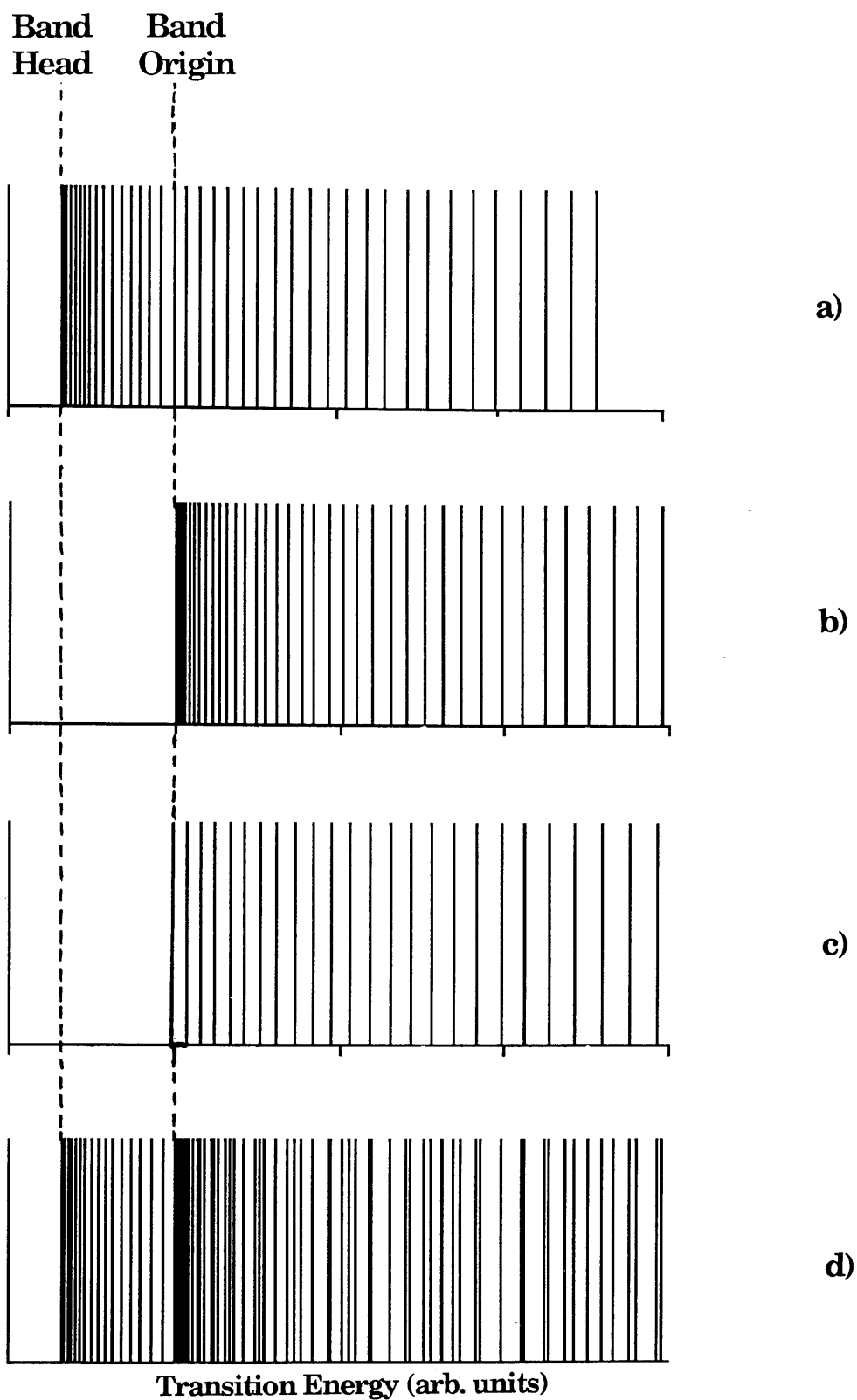


**Fig. 6.3:** Rotational lines of a typical electronic vibrational transition in a diatomic molecule showing;

- a) P-branch spectrum
- b) Q-branch spectrum
- c) R-branch spectrum
- d) Composite spectrum

shown in Fig. 6.3c).

The formation of the P-branch spectrum is slightly more complicated. In a similar fashion to above, the energies of the P-branch lines may be written as,

$$E_P = E(v'',v') - (B'+B'')(J'+1) + (B'-B'')(J'+1)^2 \quad (6.2)$$

or

$$E_P = E(v'',v') - \alpha(J'+1) + \beta(J'+1)^2, \quad \text{where } J' = 0,1,2,\dots$$

and transitions are from  $J''=J'+1 \rightarrow J'$  only.

Upon inspection of (6.2) it is clear that, depending on the relative magnitudes of  $\alpha$  and  $\beta$ , the P-branch lines decrease in energy with line spacing increasing as  $J'$  increases until a turning point in the energy  $E_P$  is reached. At this point, they then begin to increase in energy with spacing decreasing as the  $\beta(J''+1)^2$  term becomes dominant at high  $J''$  values. The overall effect is that the spectrum shades to the violet, similar to the Q and R-branches, but many of the lines lie on the low energy side of the band origin  $E(v'',v')$ . The position in the spectrum at which  $E_P$  has a turning value is called the band head. The P-branch spectrum is shown in Fig. 6.3a). The composite spectrum is shown in Fig. 6.3d), and shows the respective positions of the band origin and the band head. The example spectra shown were calculated for the case where  $B''=0.95B'$  and values were calculated up to  $J=30$  in each branch.

In the opposite case where  $B'<B''$ , the band head is formed in the R-branch and all bands shade to the red in an analogous manner to the violet shading discussed above.

## **§6.9 REMPI studies of high purity NO and NO<sub>2</sub> gases.**

The observation of strong wavelength dependent NO<sup>+</sup> ion signals in the mass spectra of all nitroaromatic molecules so far studied has prompted extensive investigations of REMPI processes in NO ( $m/z=30$ ) and NO<sub>2</sub> ( $m/z=46$ ) gases. NO, with a purity of >99%, and NO<sub>2</sub>, with a purity of >99.5% were admitted to the vacuum chamber in the usual fashion via a needle valve, and were investigated in the wavelength range 233-250nm. In addition to the work on nitroaromatic molecules presented in the preceding chapter, nitrobenzene has been studied in the range 233-250nm, and o-nitrotoluene in the range 246-262nm. The main features in the above wavelength range were observed in the ranges 233-239nm and 245-250nm, and therefore only spectra in these subranges will be presented. In the cases of both NO and NO<sub>2</sub> gases, the minimum chamber pressure at which signals were observed was  $\sim 10^{-5}$  mbar.

### **§6.9.1 REMPI of NO and NO<sub>2</sub> gases in the range 233-239nm.**

R2PI in the wavelength range 233-239nm has been employed to study the spectral features of NO gas, and to detect the presence of NO molecules which are produced in the UV laser induced predissociation of NO<sub>2</sub> gas, nitrobenzene and o-nitrotoluene in the TOF mass spectrometer. In order to cover this range, the dye laser was operated with Coumarin 102 laser dye, the output of which was frequency doubled in a BBO ( $\beta$ - barium borate) second harmonic generation crystal. Gases and vapours were, in turn, admitted into the acceleration region of the spectrometer where laser/sample interaction occurred at a distance of  $\sim 1$ mm from the sample stub.

Typical ionisation spectra of the NO<sup>+</sup> ion which has been

produced from NO, NO<sub>2</sub>, nitrobenzene and o-nitrotoluene in the wavelength range 233-239nm are shown in Fig. 6.4 a), b), c) and d) respectively. All spectra consist of a series of closely spaced peaks which persist throughout the range, and all are, in general, very similar in appearance. The most striking features observed in all spectra are the sharp edges at 236.0nm and 236.7nm, which have been identified as the  $^2\Sigma_{1/2}(v'=0;J') \leftarrow ^2\Pi_{1/2}(v''=1;J'')$  and  $^2\Sigma_{1/2}(v'=0;J') \leftarrow ^2\Pi_{3/2}(v''=1;J'')$  band head transitions in NO. Two distinct bands of lines are clearly visible to the short wavelength side of both band head positions, which are assigned to transitions in the above electronic-vibrational transitions, but which originate from higher lying rotational levels of the ground state members. The separation of the two band heads is measured to be  $(0.74 \pm 0.02)\text{nm}$ , corresponding to an energy difference of  $(132 \pm 4)\text{cm}^{-1}$ , which is in close agreement with the accepted ground state splitting.

This marked band head similarity between the NO<sup>+</sup> fragments and the NO<sup>+</sup> ion signal from NO gas suggests that neutral NO is being formed at some stage during the break up of the larger nitroaromatic molecules. As mentioned in Section 6.5, the rotational level spacing in the ground state is less than that of the A<sup>2</sup>Σ excited state so line shading to the violet is expected, and this effect is in fact very clear in the spectra shown. The transitions observed on the blue or short wavelength side of the band head positions originate from higher lying J'' levels in the v''=1 vibrational manifold of the ground states, which connect to rotational levels in the v'=0 vibrational level of the A<sup>2</sup>Σ state. The UV laser fluence profiles which were measured during the accumulation of the ionisation spectra are also shown in Fig. 6.4 a), b) and c). A very important point to note is the shape of the

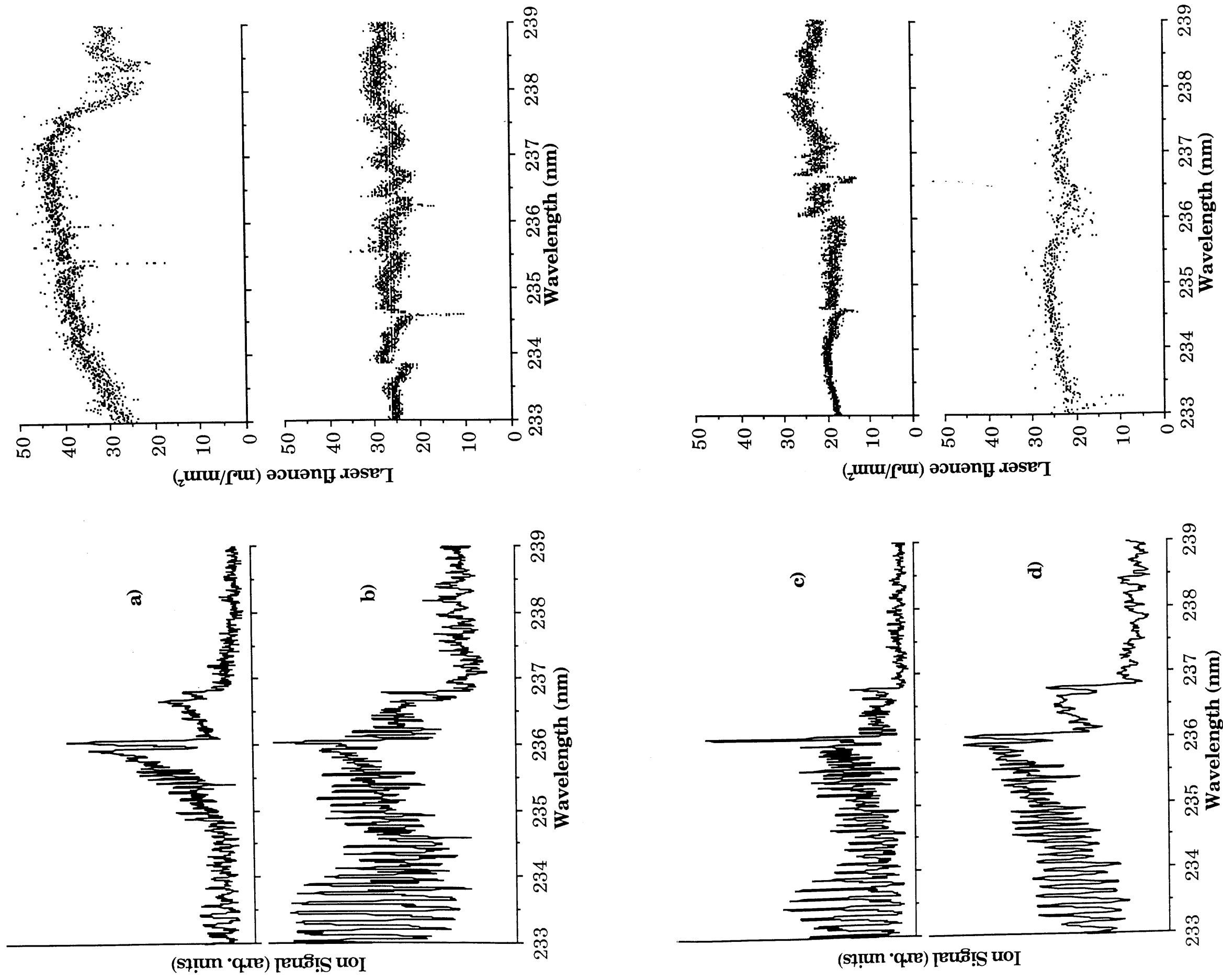


**Fig. 6.4:** Ionisation spectra of the  $\text{NO}^+$  ion produced from;

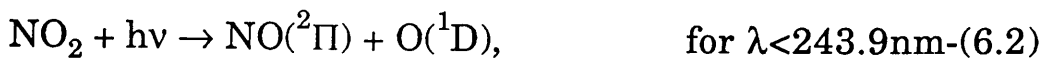
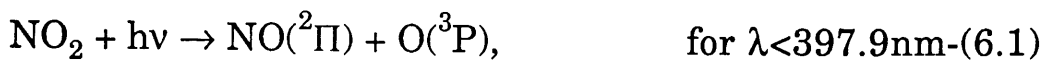
a) NO gas, b)  $\text{NO}_2$  gas, c) Nitrobenzene, d) o-nitrotoluene



spectra just to the blue side of both band head positions. In pure NO, the ion intensity is observed to decrease rapidly with decreasing wavelength, whereas in the spectra of NO<sub>2</sub> and nitroaromatics, the ionisation intensity remains high throughout the range. This suggests that neutral NO molecules produced in the predissociation of NO<sub>2</sub> and the nitroaromatic molecules are prepared in a variety of rotationally excited states. The similarity of the NO<sub>2</sub> and nitroaromatic spectra suggests that NO is produced from neutral NO<sub>2</sub> molecules in the dissociation of nitroaromatic molecules, rather than via the (M-NO) + NO channel. This is further supported by the fact that no (M-NO)<sup>+</sup> ion is observed in the mass spectra of either of the nitroaromatic species, as mentioned in the previous chapter. As will be discussed shortly, several higher lying vibrational levels in NO are also populated more densely when produced from nitrobenzene and nitrotoluene.

Several authors have studied the spectroscopy of NO<sub>2</sub> using a variety of multiphoton absorption procedures (Uselman and Lee, 1976; Zacharias *et al*, 1981; Morrison *et al*, 1981; McKendrick *et al*, 1982; Morrison and Grant, 1982; Slanger *et al*, 1983; Bigio and Grant, 1985). It is well known that at UV wavelengths below 397nm, NO<sub>2</sub> is excited into electronic states which rapidly predissociate to form both vibrationally and rotationally excited NO molecules, and oxygen atoms which evolve in a variety of atomic states. Two distinct dissociation channels prevail in NO<sub>2</sub> depending on the irradiation wavelength (Morrison and Grant, 1982). The threshold energy for production of NO and O fragments in their respective ground states is 25,132cm<sup>-1</sup> (Busch and Wilson, 1972) which corresponds to 397.9nm. In the wavelength range 233-260nm, the maximum amount of fragment internal energy available is 17,879cm<sup>-1</sup>. This is

insufficient to populate the lowest lying electronic band in NO, but is enough to produce oxygen atoms in the <sup>1</sup>D electronic state. The <sup>1</sup>D state in oxygen lies at an energy of 15,868cm<sup>-1</sup> above the <sup>3</sup>P ground state. The threshold energy for production of ground state NO fragments and oxygen atoms in their <sup>1</sup>D states is therefore 41,000cm<sup>-1</sup>, which corresponds to wavelength less than 243.9nm. These two distinct dissociation channels in NO<sub>2</sub> are summarised in (6.1) and (6.2) below;



A schematic diagram showing these processes is given in Fig. 6.5.

Zacharias *et al* (1981) obtained a similar spectrum to Fig. 6.4a) for NO using the technique of laser induced fluorescence (LIF). Here, the absorption spectrum of bulk NO in a gas cell is observed by recording the total fluorescence intensity emitted (into a certain solid angle) from the cell after irradiating the sample with a tunable laser source. Experiments involving both NO gas, and NO produced by dissociation from NO<sub>2</sub> were carried out and similar spectra to those shown in Fig. 6.4a) and b) were observed. The main conclusion from the work of Zacharias *et al* was that ~70% of the excess energy available after predissociation of NO<sub>2</sub> was channelled into internal energy of the dissociation products, of which ~51% was transferred into vibrational modes of NO and ~16% into rotational modes of NO. The remainder of the energy was converted into recoil energy of the dissociation products.

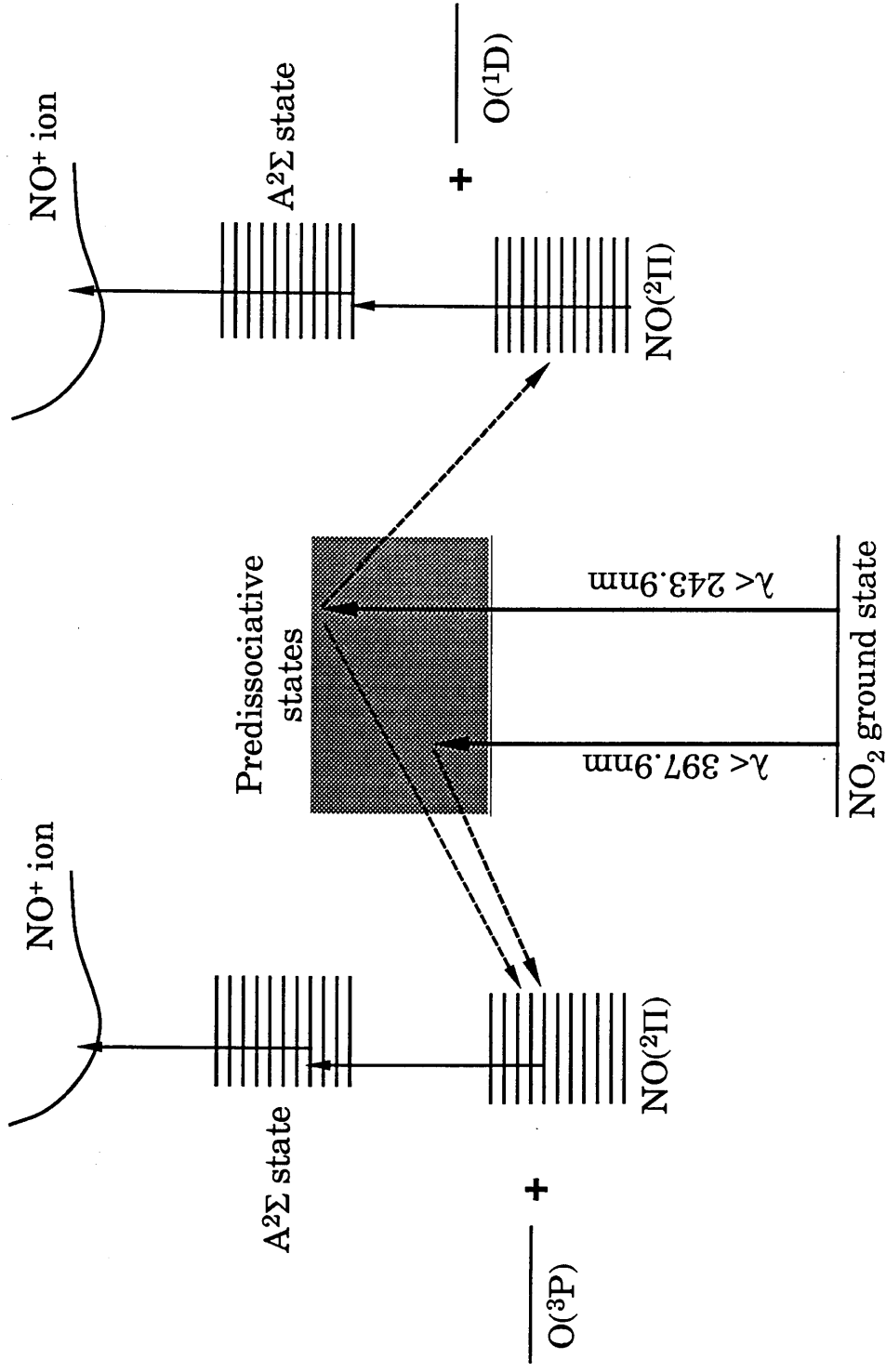


**Fig. 6.5:** Possible wavelength dependent dissociation pathways in  $\text{NO}_2$ .

In our experiments, the internal energy available for NO fragments after predissociation of NO<sub>2</sub> is at most 17,879cm<sup>-1</sup>, depending upon which dissociation channel is followed. If the figures above are taken to be representative of the partitioning fractions, then they predict that ~5800cm<sup>-1</sup> of energy is channelled into vibrational modes of the NO fragment. This of course assumes that the NO<sub>2</sub> molecules formed by predissociation from nitroaromatics are produced in their ground states. It is energetically possible therefore, that, on using the vibrational state energies given in Fig. 6.2. NO vibrational states up to v''=3 in the electronic ground state could be populated.

NO<sub>2</sub> gas was admitted into the chamber to a pressure of 1x10<sup>-5</sup> mbar, and a mass spectrum was recorded at 245.85nm, corresponding to a resonance in NO. The spectrum is shown in Fig. 6.6 where a very small ion peak is observed at m/z=46. This corresponds to the position of the NO<sub>2</sub><sup>+</sup> ion. The laser fluence was 10mJ/mm<sup>2</sup> when this spectrum was recorded. A relatively large NO<sup>+</sup> ion signal is observed at m/z = 30, which confirms that the NO<sub>2</sub> molecule breaks up readily in this wavelength range, either via predissociation of NO<sub>2</sub> followed by R2PI of neutral NO or by above threshold fragmentation of either NO<sub>2</sub> or NO<sub>2</sub><sup>+</sup>. The measured ratio of NO<sup>+</sup>/NO<sub>2</sub><sup>+</sup> is approximately 1:100. The fact that the wavelength dependent ionisation spectra shown in Fig. 6.4a) and b) are very similar suggests that the predissociation channel is preferred, since fragmentation would exhibit the wavelength dependence of the NO<sub>2</sub> molecule and not of NO. Therefore, once a photon is absorbed by an NO<sub>2</sub> molecule, ionisation from the intermediate state is in direct competition with rapid predissociation to form NO and O. At the laser fluxes used in these experiments, the predissociation rate is apparently

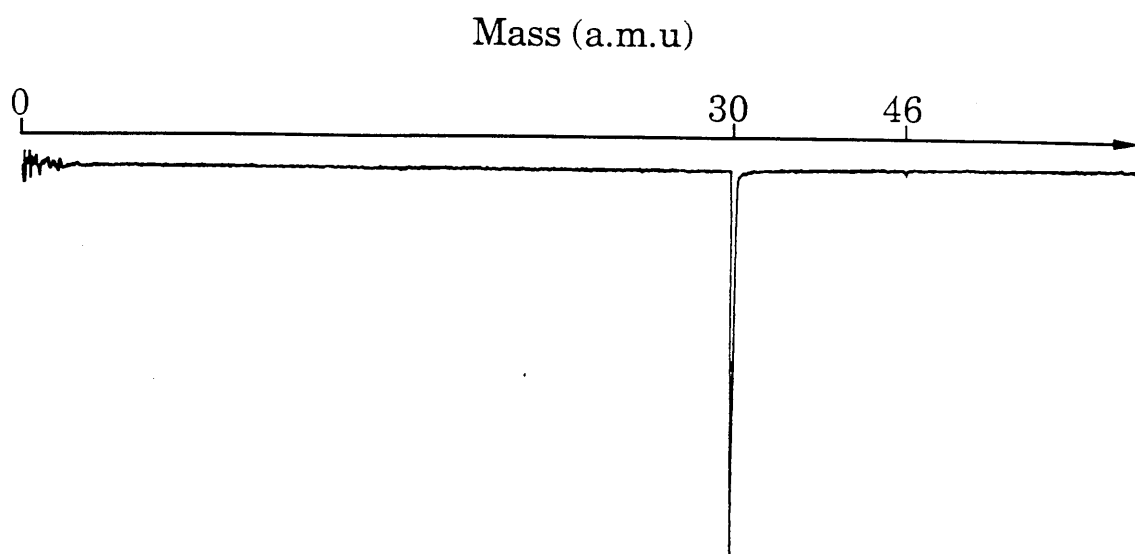


**Fig. 6.6:** TOF mass spectrum of NO<sub>2</sub> gas recorded at 245.8nm and at 10mJ/mm<sup>2</sup>.

much larger than the ionisation rate since only very small NO<sub>2</sub><sup>+</sup> ion intensities are observed. Mass spectra at both high and low detector gain were recorded for nitrobenzene at 245.86nm and at a laser fluence of 11.5 mJ/mm<sup>2</sup>, and are shown in Fig. 6.7. A small ion peak is observed at m/z = 46, whereas the intensity of the NO<sup>+</sup> ion peak is larger by a factor of ~100. The relative intensities of the peaks in ionisation spectra of nitrobenzene and NO<sub>2</sub> are comparable, which supports the idea that, in nitrobenzene at least, the NO<sup>+</sup> ion is created from NO which is produced from a neutral NO<sub>2</sub> molecule.

Also shown in Fig. 6.8 is a mass spectrum which was recorded from pure NO gas showing the NO<sup>+</sup> ion to be the only species formed. The spectrum was recorded at 249.30nm and at a fluence of 8.5 mJ/mm<sup>2</sup>.

### §6.9.2 REMPI of NO and NO<sub>2</sub> gases in the range 245-262nm.

To investigate the possibility of creating NO molecules in either the v" = 2 or v" = 3 levels of the ground state, the laser wavelength was tuned to the region 245-262nm, where the electronic-rovibrational transitions  ${}^2\Sigma_{1/2}(v'=0;J') \leftarrow {}^2\Pi(v''=2;J'')$  and  ${}^2\Sigma_{1/2}(v'=0;J') \leftarrow {}^2\Pi(v''=3;J'')$  were expected to occur. The wavelength dependence of ionisation of NO from NO gas, and by dissociation from NO<sub>2</sub>, nitrobenzene and o-nitrotoluene were recorded. The spectra obtained in the wavelength range 245-250nm from NO and NO<sub>2</sub> gases are shown, along with the laser fluence profiles, in Fig. 6.9a) and b) respectively. The ionisation spectrum shown in Fig. 6.9b) shows enhancement in the ion intensity in the region 245.6-247nm and a sharp edged transition at 249.1nm. The transition at 249.1nm exhibits fine rotational structure which appears to shade to the red, so an electronic transition into the A<sup>2</sup>Σ state is not possible. The transition has been

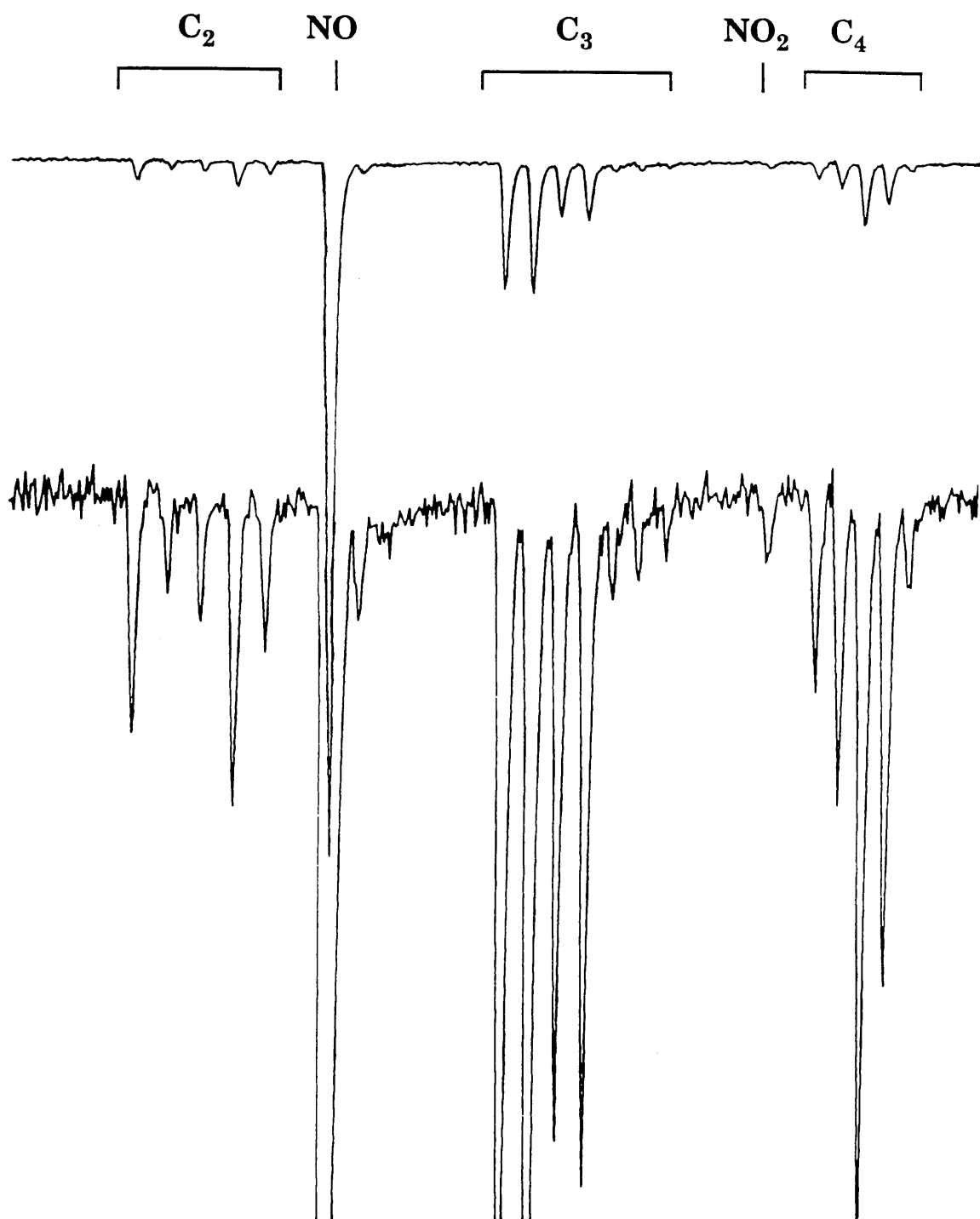


**Fig. 6.7:** TOF mass spectra of nitrobenzene recorded at 245.86nm and a laser fluence of  $11.5\text{mJ/mm}^2$ , recorded at low (upper trace) and high gain (lower trace).

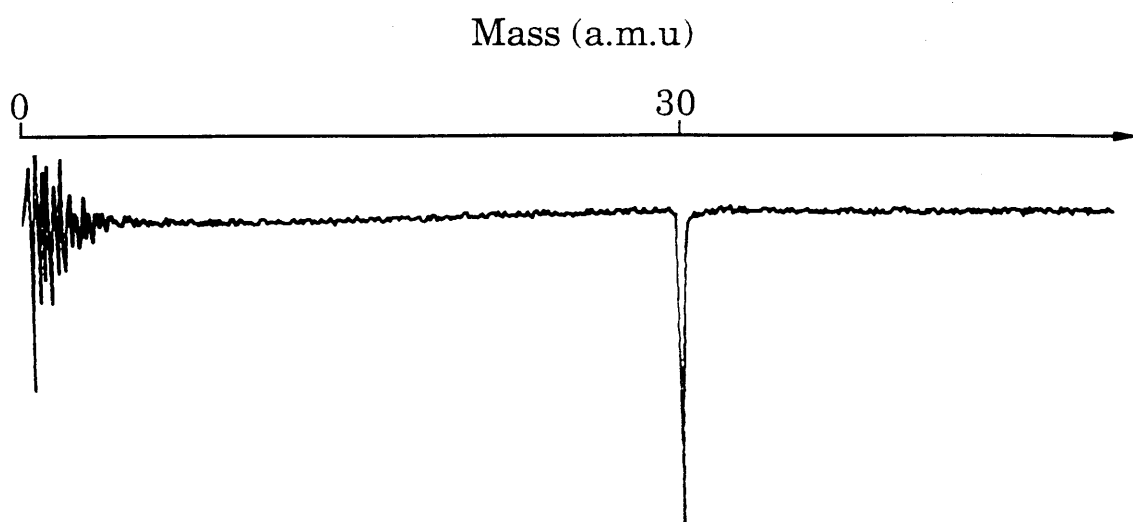


**Fig. 6.8:** TOF mass spectrum of NO gas recorded at 249.30nm and at  $8.5\text{mJ/mm}^2$ .



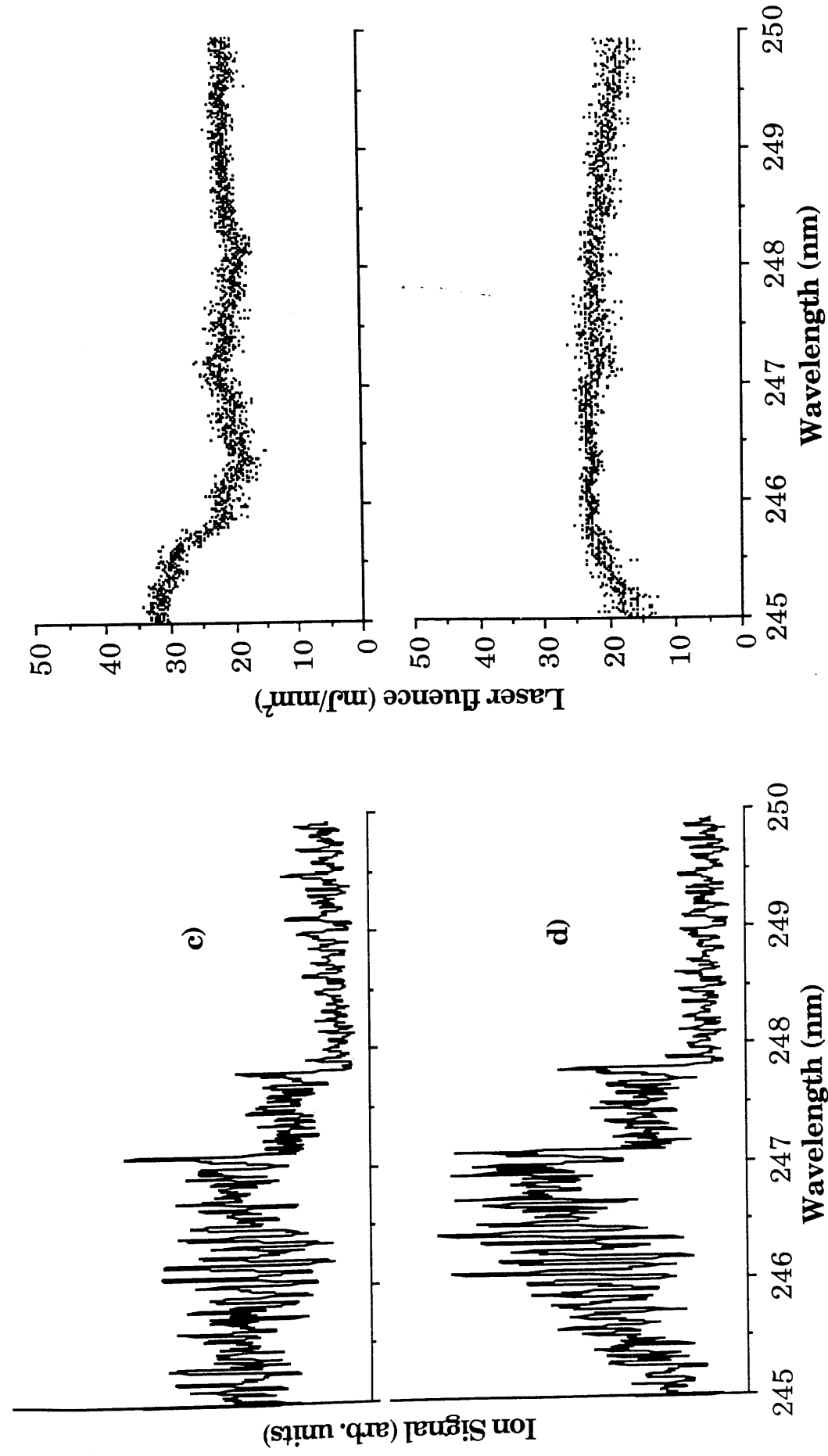
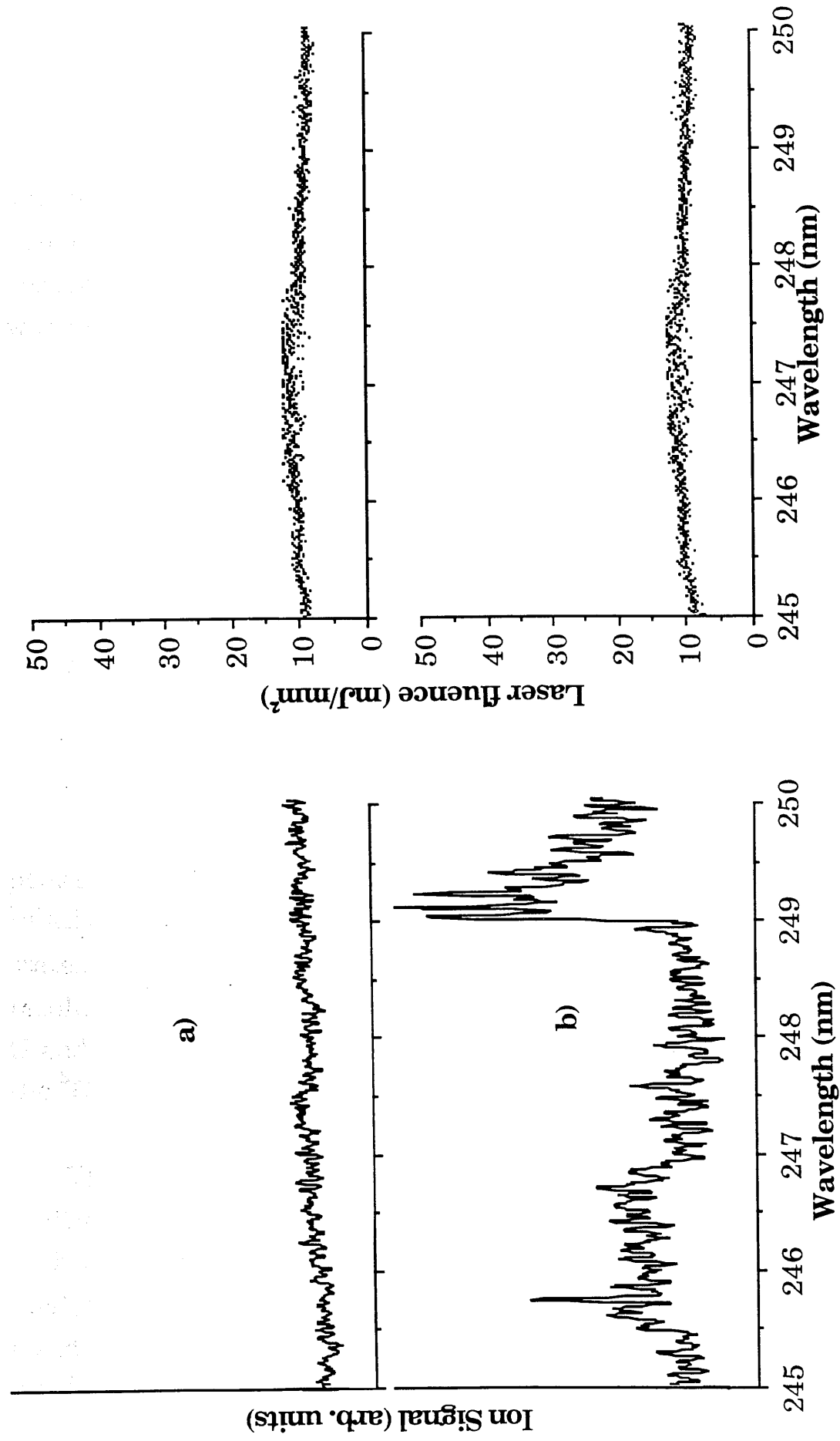


**Fig. 6.9:** Ionisation spectra of the  $\text{NO}^+$  ion produced from;

**a)** NO gas, **b)**  $\text{NO}_2$  gas, **c)** Nitrobenzene, **d)** o-nitrotoluene

identified as the  $B^2\Pi(v'=2) \leftarrow X^2\Pi(v''=4)$  transition in NO (Slanger *et al*, 1983). In contrast, the spectrum of pure NO shown in Fig. 6.9a) shows no characteristic wavelength dependent structure in this range. In order to explain this observation, an ultraviolet absorption spectrum of pure NO gas was recorded and is shown in Figs. 6.10a) and b).

Fig. 6.10a) was recorded at a resolution of 0.10nm, and the transitions corresponding to the absorption peaks observed are shown in the figure. Of particular note is the fact that the relative intensities of the  $A^2\Sigma(v'=0) \leftarrow X^2\Pi(v''=1)$  (236nm) and  $A^2\Sigma(v'=0) \leftarrow X^2\Pi(v''=0)$  (226nm) transitions are approximately 1:600, suggesting that at room temperature, most NO molecules occupy the  $v''=0$  state in the  $X^2\Pi$  state. No absorption intensity was measured at wavelengths which correspond to transitions from the  $v''=2$  level of the  $X^2\Pi$  state. It is clear from Fig. 6.10a) that the peaks labelled C, F and H are shading to the violet as expected for transitions into the  $A^2\Sigma$  electronic state, whereas the peaks labelled A, B, D and E are shading to the red due to the relative rotational level spacings of the  $X^2\Pi$  and  $B^2\Pi$  electronic states. The spectrum shown in Fig. 6.10b) was recorded at higher resolution (0.05nm) and shows each of the labelled peaks (except G and I) to be split which corresponds to the spin orbit splitting of the  $^2\Pi$  electronic ground state.

The spectra obtained from samples of nitrobenzene and o-nitrotoluene were presented in Chapter 5, but are shown again in Fig. 6.9c) and d) with the laser fluence so that a detailed analysis of the spectral features can be made. Again, two strong band heads are observed at 247.07nm and 247.81nm, corresponding to the transitions  $^2\Sigma_{1/2}(v'=0;J') \leftarrow ^2\Pi_{1/2}(v''=2;J'')$  and

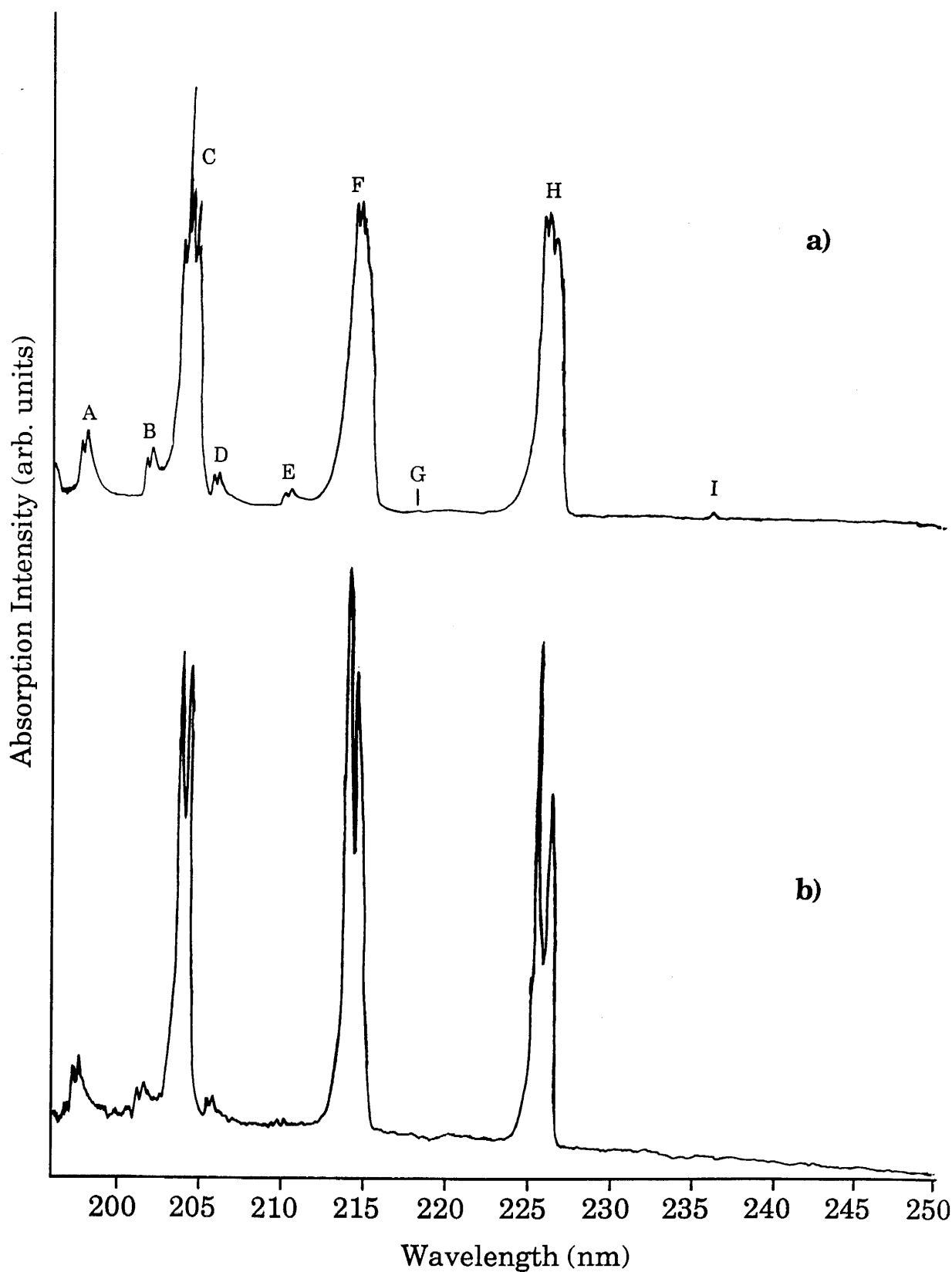


**Fig. 6.10:** Ultraviolet absorption spectrum of pure NO gas recorded at;  
a) High pressure  
b) Lower pressure

$^2\Sigma_{1/2}(v'=0;J') \leftarrow ^2\Pi_{3/2}(v''=2;J'')$  respectively. The appearance of these spectra are very similar to the spectra shown in Figs. 6.4c) and d) respectively. To the short wavelength side of the band head positions, the ion intensities remain high, and correspond to transitions from higher lying rotational levels of the  $v''=2$  state. The fact that these band head transitions are observed in the spectra obtained from nitroaromatics shows that neutral NO molecules are created in the  $v''=2$  vibrationally excited manifold of the ground electronic states. As mentioned above, no absorption intensity was measured at around 247nm in pure NO gas, and this observation is confirmed by the ionisation spectrum shown in Fig. 6.9a). In this wavelength range, photons are not energetic enough to connect to states in the A or B bands from either the  $v''=0$  or 1 vibrational states of the ground state. The spectrum arises due to non-resonant transitions from the  $v''=0$  and 1 states. It is also concluded that transitions to high lying vibrational levels within the ground state manifold do not occur with any significant intensity. The nitrobenzene spectrum in Fig. 6.9c) shows slightly different behaviour in the range 245-246nm, in that the ion intensity remains high in this range. However, on examining the laser fluence profile for this spectrum, one sees immediately that the laser power in this range was somewhat higher in the case of nitrobenzene than for the nitrotoluene isomers.

In the NO<sub>2</sub> spectrum shown in Fig. 6.9b), very little resonant structure is observed at wavelengths corresponding to transitions from the  $v''=2$  manifold, suggesting that in the predissociation of NO<sub>2</sub>, only vibrational levels  $v''=0,1$  are extensively populated. The band edges corresponding to the  $^2\Sigma_{1/2}(v'=0;J') \leftarrow ^2\Pi_{1/2}(v''=2;J'')$  and  $^2\Sigma_{1/2}(v'=0;J') \leftarrow ^2\Pi_{3/2}(v''=2;J'')$  transitions are observed, but are of

very small intensity compared to the 249.1nm resonance. This is in agreement with Slanger *et al* (1983) who claimed that at these wavelengths, a population inversion in the vibrational states of the NO ground state occurred, with the  $v''=7$  level being most highly populated. McFarlane *et al* (1991) also reported similar findings with the  $v''=5$  being most highly populated. One possible explanation is that the intermediate NO<sub>2</sub> molecules have more internal energy as a result of their predissociation from the parent molecule, thus allowing population of higher vibrational levels in the NO molecules which are produced from it. However, no evidence of a vibrational population inversion is present in the spectra of nitroaromatics in the range 245-250nm. This may be due to dissociation channel (6.2) operating within the NO<sub>2</sub> molecules, which are themselves dissociated from the nitroaromatic species, even although the irradiating wavelength suggests channel (6.1) should be followed. The additional energy required to reach the 243.9nm dissociation threshold could be found from internal energy which the NO<sub>2</sub> molecules possess as a result of their predissociation from the nitroaromatic species.

As mentioned earlier, using Zacharias' figures for the partitioning of energy into internal modes, it should be feasible to populate up to  $v''=3$  in the ground state with the wavelength range available. Fig. 6.11 shows the NO<sup>+</sup> ion yield from o-nitrotoluene in the range 246-262nm. Band heads of the vibrational transitions  ${}^2\Sigma_{1/2}(v'=0;J') \leftarrow {}^2\Pi_{1/2}(v''=2;J'')$  and  ${}^2\Sigma_{1/2}(v'=0;J') \leftarrow {}^2\Pi_{3/2}(v''=2;J'')$  and  ${}^2\Sigma_{1/2}(v'=0;J') \leftarrow {}^2\Pi_{1/2}(v''=3;J'')$  and  ${}^2\Sigma_{1/2}(v'=0;J') \leftarrow {}^2\Pi_{3/2}(v''=3;J'')$  can be seen at 258.7nm and 259.60nm respectively. The inset shows the structure associated with the  $v''=3$  transition in much more detail. The intensity of the  $v''=3$  band head transitions are approximately one third the intensity of the  $v''=2$  transitions, whereas the laser fluence at both

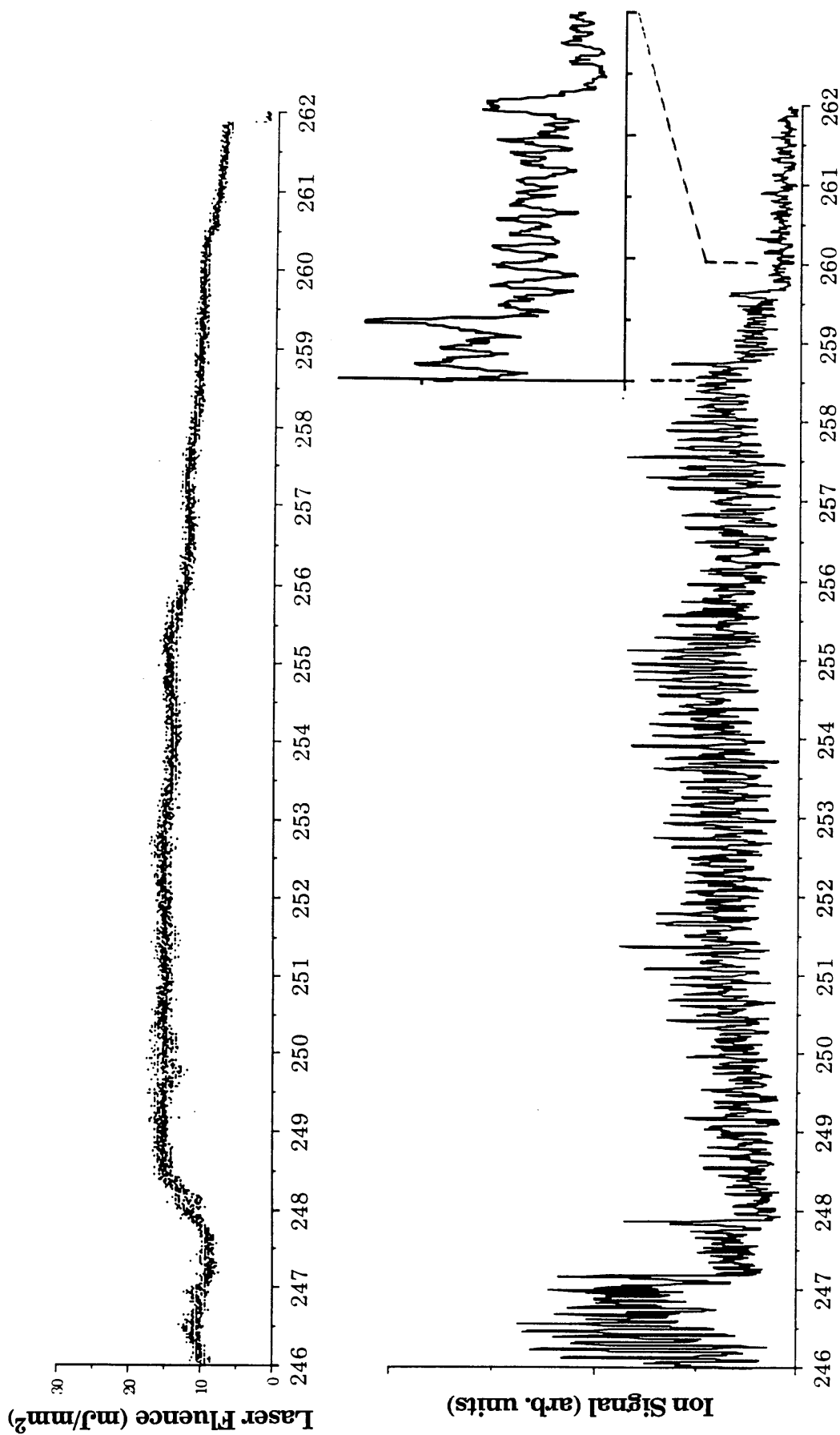


**Fig. 6.1.1:** Ionisation spectrum of the  $\text{NO}^+$  ion produced from o-nitrotoluene in the extended wavelength range 246-262nm, showing the  $0\leftarrow 2$  and  $0\leftarrow 3$  transitions.

bands is roughly the same. This suggests lower populations in the  $v''=3$  level, as would be expected, assuming Franck-Condon factors for both transitions are not appreciably different.

In the case of NO and NO<sub>2</sub>, no comparable resonant structure is observed in the region of the  $v''=2$  or 3 transitions. This suggests that the NO molecules produced by predissociation of NO<sub>2</sub> molecules, which are themselves produced by predissociation of nitroaromatics, are formed with a different internal energy distribution. NO<sub>2</sub> molecules which are produced by predissociation from nitroaromatics seem to access different energy states en route to NO<sup>+</sup> formation. When predissociating to form NO molecules, the excess internal allows channel (6.2) to be followed even although the wavelength is too long.

### **§6.10 Possible dissociation pathways in the formation of NO<sup>+</sup> during laser interaction with nitroaromatic molecules.**

The problem addressed here was to find out how nitroaromatic molecules, labelled M, actually break up when irradiated by intense UV light. It is known that nitroaromatic species readily predissociate when they absorb UV radiation (Zhu *et al*, 1990). The order of the actual steps taken in the dissociation process had not been previously confirmed. In our experiments, we have isolated one of the many possible pathways as being the most likely. A number of possible pathways are postulated and summarised below;

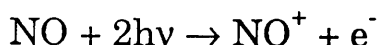
#### **Pathway 1.**



The appearance potential for NO<sup>+</sup> ion production from

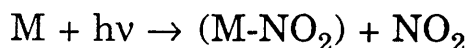
nitrobenzene is 11.93eV (Brown, 1970), and would therefore require multiphoton absorption of at least three photons by the parent molecule in this wavelength range.

### Pathway 2.



This scheme involves excitation of the parent molecule, M, to a predissociative state by one photon absorption, which results in (M-NO) and NO formation, followed by two-photon ionisation of NO to form NO<sup>+</sup> + e<sup>-</sup>.

### Pathway 3.



- (i)  $\text{NO}_2 + 2h\nu \rightarrow \text{NO}_2^+ + e^-$
- (ii)  $\text{NO}_2 + 3h\nu \rightarrow \text{NO}^+ + \text{O} + e^-$
- (iii)  $\text{NO}_2 + h\nu \rightarrow \text{NO} + \text{O}$
- $\text{NO} + 2h\nu \rightarrow \text{NO}^+ + e^-$

This scheme involves predissociation of the parent molecule, M, by single photon absorption to produce (M-NO<sub>2</sub>) and NO<sub>2</sub> species, followed by;

- (i) Two photon ionisation of the NO<sub>2</sub> molecule, which requires two photons with wavelength less than 248nm.

OR (ii) Three photon fragmentation of an NO<sub>2</sub> molecule to produce an NO<sup>+</sup> ion and an oxygen atom. The appearance potential of this process is 12.5eV (Nakayama *et al*, 1959).

OR (iii) Single photon predissociation of NO<sub>2</sub> to form NO + O neutrals, with subsequent two photon ionisation of NO to



produce NO<sup>+</sup> ions.

In pathway 1 the nitroaromatic molecule, M, absorbs  $n$  UV photons ( $n \geq 3$ ) from the laser pulse in a stepwise fashion until the total absorbed energy exceeds the appearance potential for NO<sup>+</sup> production from M. M then fragments to produce an NO<sup>+</sup> ion, an (M-NO) neutral fragment and an electron. The (M-NO) fragment could continue to absorb photons from the same laser pulse and further dissociation/fragmentation could occur which would account for the remainder of the mass spectrum. In this model, however, the NO<sup>+</sup> ion would exhibit the spectral features of the dissociation process in the parent molecule since it does not proceed through energy levels of the neutral NO molecule. As already observed, the NO<sup>+</sup> ion exhibits the structure associated with NO, and so it seems highly unlikely that this pathway is followed. Additionally, no (M-NO)<sup>+</sup> ion is observed in any of the mass spectra, a fact which further strengthens the notion that this model is incorrect.

In pathway 2, the nitroaromatic molecule, M, predissociates on absorption of a single photon to produce (M-NO) and NO. Subsequent absorption of more photons by the (M-NO) molecule can result in either ionisation or fragmentation. The NO molecule can absorb photons resonantly to produce the observed spectral features. Again, the fact that no (M-NO)<sup>+</sup> ion is observed in the mass spectra of any of the nitroaromatic samples discourages this particular model.

In pathway 3, the nitroaromatic molecule, M predissociates after absorbing a single photon to produce (M-NO<sub>2</sub>) and NO<sub>2</sub> molecules. The (M-NO<sub>2</sub>) daughter species may then absorb more

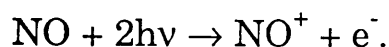
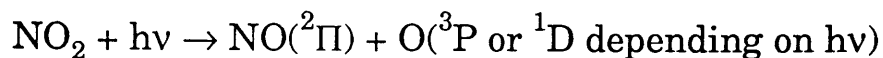
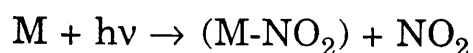
photons from the same pulse, which could result in either direct ionisation to produce  $(\text{M-NO}_2)^+$ , or in fragmentation to produce smaller mass fragments. The  $\text{NO}_2$  molecule could then absorb 2 photons in this wavelength range and directly ionise to produce  $\text{NO}_2^+$  (i). Alternatively, the  $\text{NO}_2$  molecule could absorb three photons from the beam and fragment, producing  $\text{NO}^+$  ions (ii). In addition, the  $\text{NO}_2$  molecule could predissociate upon absorbing a single photon which would result in the formation of NO and an oxygen atom. Within the same laser pulse, the NO molecule could absorb 2 photons and be ionised to produce the  $\text{NO}^+$  ion signal with the correct spectral features (iii).

Pathway 3 is favourite in the author's opinion since NO and  $\text{NO}_2$  wavelength spectra are very similar in areas and secondly, no  $(\text{M-NO})^+$  ion is seen in any mass spectrum. This latter point that no  $(\text{M-NO})^+$  ion is observed may be a result of the  $(\text{M-NO})$  species being highly unstable, so might in fact not represent a strong argument. In addition, a small  $\text{NO}_2^+$  ion peak was observed in the mass spectrum of NB in approximately the same relative intensity as in  $\text{NO}_2$  gas. This observation strongly suggests that the  $\text{NO}_2$  dissociation channel is dominant in the interaction of nitroaromatics with intense ultraviolet light.

### **§6.11 Conclusions and future experiments.**

The similarity of wavelength dependent ionisation spectra of NO molecules, created directly by R2PI of nitric oxide, and by R2PI of NO molecules formed by predissociation of  $\text{NO}_2$  and nitroaromatic molecules in the wavelength range 233-260nm strongly suggests that during UV laser interaction with nitroaromatic molecules, the strong  $\text{NO}^+$  ion signal is produced via neutral  $\text{NO}_2$  dissociation pathways. The mass spectra

obtained from NO<sub>2</sub> and nitrobenzene vapour show both NO and NO<sub>2</sub> ion signals in approximately the same relative intensities, a fact which further suggests the above dissociation pathway is most probably correct. In the above wavelength range, a dissociation threshold exists which influences the vibrational levels populated in the dissociation of NO<sub>2</sub>. The dissociation/ionisation mechanisms which are thought to prevail in the multiphoton interaction of UV light with nitroaromatic molecules, M, are summarised as follows;



### §6.12 Future experiments.

In order to obtain further information on the various dissociation processes which occur within nitroaromatic species, the wavelength range will be extended down to 220nm, where the  ${}^2\Sigma_{1/2}(v'=0;J') \leftarrow {}^2\Pi_{1/2}(v''=0;J'')$  and  ${}^2\Sigma_{1/2}(v'=0;J') \leftarrow {}^2\Pi_{3/2}(v''=0;J'')$  transitions occur (~226nm). It is hoped that signal intensities obtained in this wavelength regime will be of much greater intensity than the transitions discussed in this chapter. The UV absorption spectrum shown in Fig. 6.11 shows that the absorption intensity is much very much larger at 226nm than at 236nm (~600:1), but this does not necessarily apply in the case of nitroaromatic molecules. A series of experiments are currently underway at Glasgow to investigate the possibility of increasing sensitivity by using shorter UV wavelengths.

## **Chapter 7.**

### **RIMS of carbon and hydrogen atoms following laser induced multiphoton dissociation of nitrobenzene and nitrotoluene molecules.**

#### **§7.1 Introduction.**

During investigations into the UV multiphoton ionisation/dissociation of several nitroaromatic molecules in a TOF mass spectrometer, a number of interesting features have been observed in the spectra of both the carbon ( $m/z=12$ ) and hydrogen ( $m/z=1$ ) ions. Laser radiation in the wavelength range 240-260nm was generated by frequency doubling the output of the dye laser operating with Coumarin 500 dye which covered the range 480-520nm. Both fundamental ( $\omega$ ) and second harmonic ( $2\omega$ ) beams irradiated nitroaromatic sample vapour in the acceleration region of the TOF mass spectrometer. In most experiments, both laser beams were strongly focused to spot sizes of  $\sim 200\mu\text{m}$  diameter, as estimated from specified divergence values and from spot size measurements on light sensitive 'burn paper'. As a result, pulse fluences of at most  $30\text{mJ/mm}^2$  in the  $2\omega$  beam and  $100\text{mJ/mm}^2$  in the fundamental beam could be attained, with fluence levels being controlled by a Newport attenuator. The beams were spatially separated by a prism arrangement so that the pulse energy of the  $2\omega$  beam could be measured using a Molectron J3-09 joulemeter, after the pulse had passed through the chamber.

While monitoring the intensity of the carbon ion as the laser wavelength was scanned, broad molecular structure evident in

the spectra of all other hydrocarbon fragment ions was observed. However, as the fluence was increased to above  $\sim 5.0 \text{ mJ/mm}^2$ , a number of very sharp resonances became clearly visible in the spectrum. These have been identified as single and multiple photon resonances in neutral atomic carbon by matching combinations of  $2\omega$  and  $\omega$  photon energies with transition energies given in Table 7.1 (Moore, 1971). Also shown in Table 7.1 is the ionising photon required, which has been decided on both laser fluence and energetic considerations. The dissociation process appears to produce atomic carbon in both ground state ( $^3\text{P}$ ) and excited state ( $^1\text{S}$  and  $^1\text{D}$ ) configurations, since transitions originating from these states have been observed. In total, six singlet transitions and one triplet transition in atomic carbon have been identified in this wavelength range. In addition, the  $1\text{s} \rightarrow 2\text{s}$  two photon transition at  $243.13 \text{ nm}$  in neutral atomic hydrogen has also been recorded.

The production of bare metal atoms by photodissociation of  $\text{Fe}(\text{CO})_5$  has been reported (Whetten *et al*, 1983b). Similar features in the case of carbon have been observed previously, in the wavelength range  $286.7\text{--}287.4 \text{ nm}$  by Pratt *et al* (1985), while studying the UV multiphoton dissociation of carbon tetrachloride ( $\text{CCl}_4$ ), and by Das *et al* (1983) while studying UV multiphoton dissociation of carbon suboxide ( $\text{C}_3\text{O}_2$ ), in the wavelength range  $284\text{--}287 \text{ nm}$ . This latter case used laser induced two-photon fluorescence detection. Whetten *et al* (1983c) observed 16 atomic carbon resonances in the wavelength range  $279.4\text{--}320.4 \text{ nm}$  following UV multiphoton dissociation of several aromatic molecules in a pulsed jet/quadrupole mass spectrometer system. However, no hydrogen ion signal was observed, which was thought to be due to the low efficiency of a 4-

Peak Number	2 $\omega$ Wavelength (nm)	State		J value		State energy (cm <sup>-1</sup> )		Excitation photons	Ionisation photon	Parity change
		Initial	Final	Initial	Final	Initial	Final			
1	245.867 245.918 245.968 245.972 246.000 246.054 246.100	2p <sup>2</sup> <sup>3</sup> P	2p4p <sup>3</sup> P	0	2	0	81344.48	2 $\omega$ + 2 $\omega$	1 $\omega$	No
		"	"	1	2	16.4	81344.48	2 $\omega$ + 2 $\omega$	1 $\omega$	"
		"	"	0	0	0	81311.52	2 $\omega$ + 2 $\omega$	1 $\omega$	"
		"	"	1	1	16.4	81326.33	2 $\omega$ + 2 $\omega$	1 $\omega$	"
		"	"	2	2	43.5	81344.48	2 $\omega$ + 2 $\omega$	1 $\omega$	"
		"	"	2	1	43.5	81326.33	2 $\omega$ + 2 $\omega$	1 $\omega$	"
		"	"	2	0	43.5	81311.52	2 $\omega$ + 2 $\omega$	1 $\omega$	"
2	247.51	2p <sup>2</sup> <sup>1</sup> S	4p <sup>1</sup> S	0	0	21648.4	82252.31	2 $\omega$ + $\omega$	$\omega$	No
3	247.93	2p <sup>2</sup> <sup>1</sup> S	3s <sup>1</sup> P <sup>o</sup>	0	1	21648.4	61982.2	2 $\omega$	2 $\omega$	Yes
4	249.49	2p <sup>2</sup> <sup>1</sup> S	4p <sup>1</sup> D	0	2	21648.4	81770.36	2 $\omega$ + $\omega$	$\omega$	No
5	254.60	2p <sup>2</sup> <sup>1</sup> S	4p <sup>1</sup> P	0	1	21648.4	80563.57	2 $\omega$ + $\omega$	$\omega$	No
6	255.69	2p <sup>2</sup> <sup>1</sup> D	3p <sup>1</sup> P	2	1	10193.7	68858.0	2 $\omega$ + $\omega$	$\omega$	No
7	258.27	2p <sup>2</sup> <sup>1</sup> D	6d <sup>1</sup> D <sup>o</sup>	2	2	10193.7	87632.0	2 $\omega$ + $\omega$ + $\omega$	$\omega$	Yes

**Table 7.1:** Carbon resonance wavelengths with initial and final atomic states identified.

photon non-resonant ionisation process at the laser fluences available. To the author's knowledge, no multiphoton processes in hydrogen atoms have been observed during dissociation of organic molecules.

## **§7.2 Atomic spectroscopy notation.**

The ground state configuration of atomic carbon is  $1s^2 2s^2 2p^2$ . It therefore has two valence electrons, which may couple in a number of ways to form a variety of ground state electronic configurations. Closed electron shells contribute zero angular momentum to the atom in accordance with the Pauli exclusion principle, so only valence electrons need be considered provided only these valence electrons are excited in photoabsorption processes. The total spin angular momentum,  $\underline{S}$ , of the atom is found by vector summation of the individual spin angular momenta,  $\underline{s}_i$  ( $i=1,2$ ) of the valence electrons,

$$\underline{S} = \sum \underline{s}_i$$

The magnitude of the spin angular momentum is given by  $[S(S+1)]^{1/2}\hbar$ , where  $S$  is called the total spin quantum number.  $S_z$  can have any of the values  $-S, -S+1, \dots, S-1, S$ , and it follows that in atoms with odd/even numbers of valence electrons will have  $S$  values which are half integral/integral respectively.

Similarly, the total orbital angular momentum,  $\underline{L}$ , of the atom is given by the vector sum of the individual orbital angular momenta,  $\underline{l}_i$  ( $i=1,2$ ) of the valence electrons,

$$\underline{L} = \sum \underline{l}_i$$

and has magnitude  $[L(L+1)]^{1/2}\hbar$ , where  $L$  is the total orbital

angular momentum quantum number.  $L_z$  can take any value between  $-L, -L+1, \dots, L-1, L$ .

In conventional spectroscopic notation, total orbital angular momenta values of  $L=0, 1, 2, 3, 4, \dots$  are represented by the letters S, P, D, F, G, ...etc.

In the case of carbon, a relatively light element, LS coupling dominates (since spin-orbit interactions are weak in carbon) and the total angular momentum of the atom,  $\mathbf{J}$ , is simply given by the vector sum,

$$\mathbf{J} = \mathbf{L} + \mathbf{S}.$$

In an analogous manner to  $\mathbf{L}$  and  $\mathbf{S}$ , the magnitude of  $\mathbf{J}$  is given by  $[J(J+1)]^{1/2}\hbar$ , where  $J$  is the total angular momentum quantum number. The projection of  $\mathbf{J}$  along the magnetic axis is written as  $M_J$ .

For each electronic state with  $\mathbf{L} \neq 0$ , there are  $2S+1$  possible orientations of the vector  $\mathbf{S}$ , and this number is called the multiplicity of the state. The total spin angular momentum of the carbon atom is either 0 or 1 depending on the way in which the individual spin angular momenta couple. States with  $S=0$  are called singlets (since  $2S+1=1$ ) whereas those with  $S=1$  are triplets since there are three possible orientations of the vector  $\mathbf{S}$  with respect to the total orbital angular momentum vector (i.e.  $2S+1=3$ ). In what follows, the electronic states of carbon will be written in the form,

$$^{2S+1}(\text{L-letter})_{J\text{-value}}$$



So, for example, the  $^3D_2$  state of carbon has  $S=1$ ,  $L=2$  and  $J=2$ . The ground state configuration of carbon is a triplet of states designated as  $^3P_{2,1,0}$ .

### **§7.3 Electric dipole selection rules.**

Many electronic transitions are predicted by quantum mechanics to have vanishingly small probabilities, and are called forbidden transitions. This gives rise to a set of selection rules which decide the allowedness of single and multiple photon transitions in atoms and molecules. The rules governing one-photon (Corney, 1977) and two-photon (Bonin and McIlrath, 1984; Melikechi and Allen, 1985) transitions in atoms are summarised in the following sections.

#### One-photon selection rules.

- 1)  $\Delta J = 0, \pm 1$ , but  $J=0 \leftrightarrow J'=0$  forbidden.
- 2)  $\Delta M_J = 0, \pm 1$ .
- 3) There must be a parity change. i.e.  $\Delta l = \pm 1$ .
- 4)  $\Delta S = 0$ .
- 5)  $\Delta L = 0, \pm 1$ , but  $L=0 \leftrightarrow L'=0$  is forbidden.

#### Two-photon selection rules.

- 1)  $\Delta J = 0, \pm 1, \pm 2$ .
- 2)  $\Delta l = 0, \pm 2$ .
- 3)  $\Delta S = 0$ .
- 4)  $\Delta L = 0, \pm 1, \pm 2$ .

In two-photon excitation, there can be no parity change since the  $l$ -value changes either by zero or two. Also, in the special case when two equal frequency photons are absorbed, two additional

rules apply;

5)  $J=0 \leftrightarrow J'=1$  are strictly forbidden.

6)  $\Delta M_J \neq 0$ .

In the case of  $2\omega+\omega$  transitions, where the photons are cross-polarised, the additional selection rule applies;

7)  $J=0 \leftrightarrow J'=0$  is strictly forbidden.

#### **§7.4 RIMS of carbon atoms produced from samples of nitrobenzene and nitrotoluene.**

While carrying out REMPI studies of nitrobenzene in the TOF mass spectrometer system, the wavelength dependent ionisation spectrum of the carbon ion has yielded a large amount of information not present in the spectra of the other fragment ions. As observed in Chapter 5,  $C_nH_m^+$  fragment ions produced by dissociation from nitrobenzene all yield some resonant structure at 247.2nm. Using nitrobenzene as our sample, and with the laser wavelength set at 247.2nm, several mass spectra were accumulated at different UV fluences. The fundamental laser beam was also focused into the vacuum chamber and overlapped both temporally and spatially with the UV beam.

TOF mass spectra recorded at various UV laser fluences are shown in Fig. 7.1. In all the spectra shown, the amplifier and detector gains were the same and the partial pressure of sample in the vacuum chamber was held constant at  $2.2 \times 10^{-7}$  mbar. As mentioned in previous chapters, the sample pressure at the interaction site is expected to be somewhat greater than the measured value, perhaps by a factor of approximately 3 or 4. From the spectra shown, it is clear that the intensity of the carbon

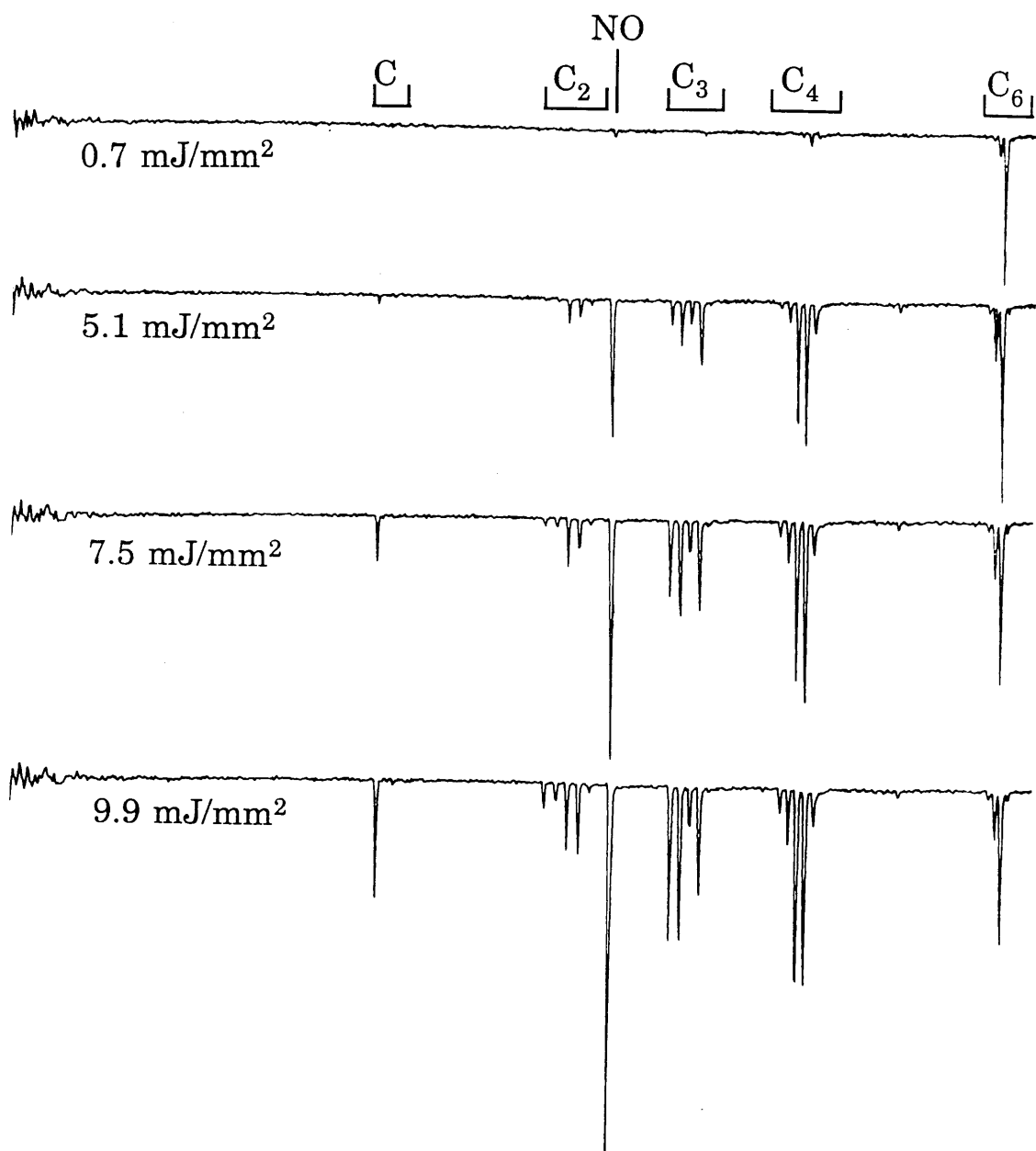


**Fig. 7.1:** TOF mass spectra of nitrobenzene vapour at various UV laser fluences.

ion signal has a strong dependence upon laser fluence. At laser fluences of greater than  $5.0 \text{ mJ/mm}^2$ , it is also apparent that the degree of fragmentation becomes greater and in particular the relative intensity of the carbon ion increases rapidly and becomes appreciable in magnitude with other fragment ion intensities. In fact, with the exception of the  $\text{C}_6\text{H}_5^+$  ion, the intensities of all  $\text{C}_n\text{H}_m^+$  fragment ions and the NO ion increase rapidly as the laser fluence is increased at this wavelength. This could possibly suggest that the dissociation processes occurring at low laser fluences create primarily neutral fragment species, via predissociation pathways, which are subsequently ionised or further fragmented as the laser fluence is increased. Alternatively, the increase may be due to an increase in the geometrical overlap between the laser beam and the sample molecules. In this case, the laser intensity in the wings of the pulse may be high enough to cause fragmentation whereas the intensity in the central part of the pulse is expected to be sufficiently high such that multiple photon fragmentation processes will proceed rapidly, thereby leading to an overall increase in the fragmentation.

The wavelength dependence of the carbon ion produced from nitrobenzene was investigated in the range 245-250 nm, (I.P.=9.88eV ( $\equiv 2$  photons @ 250.98nm) (Matyuk *et al*, 1979)), and is shown in Fig. 7.2. The shot-to-shot laser fluence profile was recorded simultaneously with the carbon ion signal and is also shown in Fig. 7.2. The sharp resonances labelled 1-4 unfortunately suffer a large amount of interference from the broad molecular background present in the spectrum. The sharp peaks have been identified as single and multiple photon resonances in atomic carbon, with transitions originating from

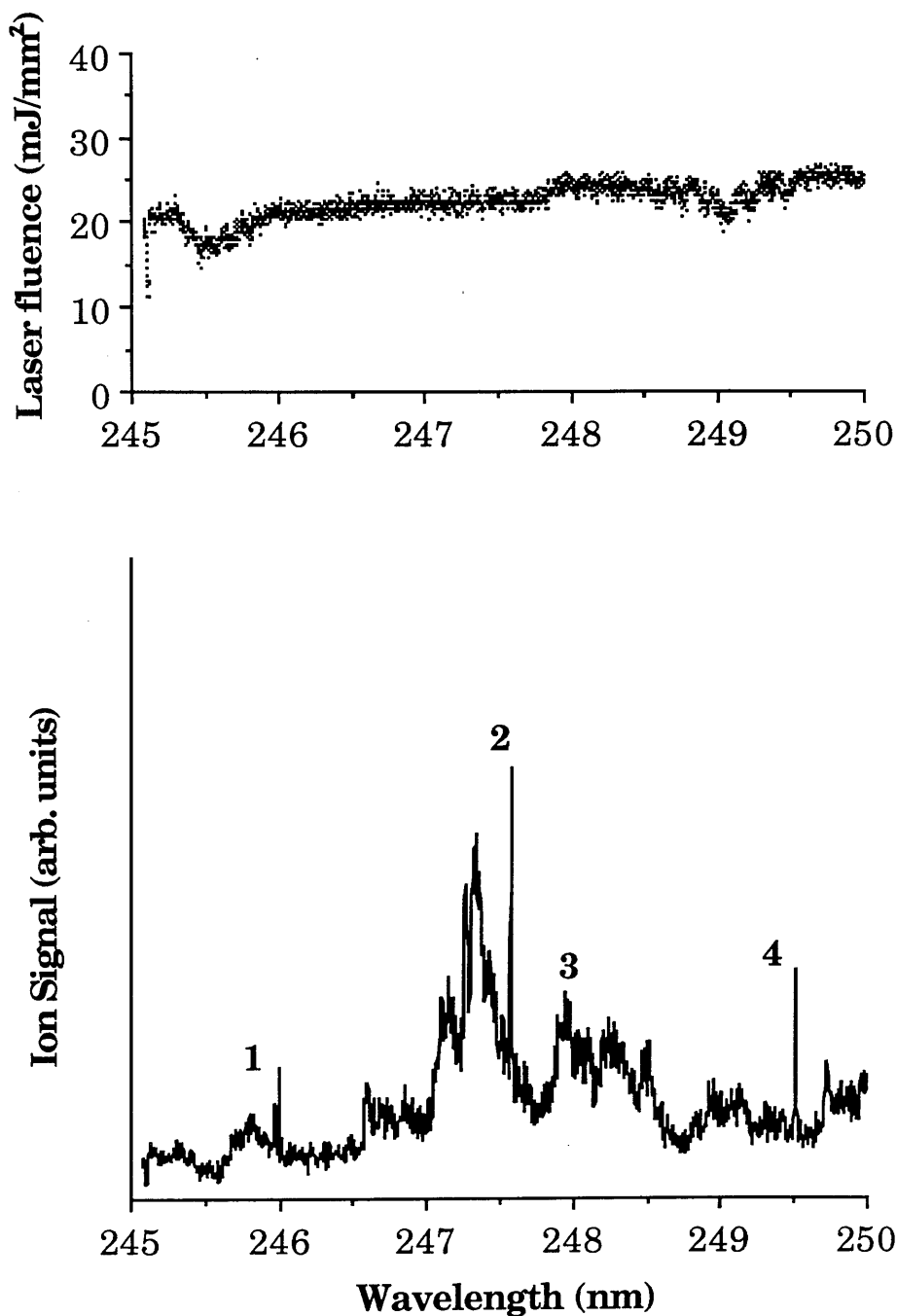


**Fig. 7.2:** Wavelength dependent ionisation spectrum of carbon ( $m/z=12$ ) produced from a nitrobenzene sample. The shot-to-shot laser fluence profile recorded simultaneously is also shown.

the  $^3\text{P}$  ground state and the  $^1\text{S}$  and  $^1\text{D}$  excited states.

In order to fully and more accurately determine the origin of the sharp peaks, the molecular sample was changed from nitrobenzene to nitrotoluene, which has a similar ionisation potential (9.69eV, (Matyuk *et al*, 1979)), and which was known to exhibit a much smoother molecular spectrum in this wavelength range as discussed in Chapter 5. Fig. 7.3 shows the spectrum of the carbon ion obtained from dissociation of p-nitrotoluene in the extended wavelength range 245-259nm. Also shown is the laser fluence profile which again was recorded simultaneously with the ionisation spectrum. The spectrum shown is the composite of three 5nm scans which have been normalised to the same detector and amplifier gains. This procedure was carried out due to the difficulty in obtaining a reasonable fluence profile over a 15nm range. The resonance labelled 1 is actually a multiplet corresponding to the  $2p\ ^3\text{P} \rightarrow 4p\ ^3\text{P}$  two-photon transition and will be discussed in detail later in the chapter.

The relatively wide atomic resonance at 247.93nm (peak 3) has been identified as a single photon resonant transition from the  $^1\text{S}$  state to the  $^1\text{P}^0$  state. Measurements made on this peak show the FWHM to be 0.2nm when the fluence of the laser pulse was  $24.8\text{ mJ/mm}^2$ , which corresponds to a flux of  $1 \times 10^8\text{ W/cm}^2$ . In order to explain the width of the peak, a simple power broadening model has been invoked (see Appendix 2). The Einstein A coefficient for the transition is  $1.8 \times 10^7\text{ s}^{-1}$  (Fuhr and Wiese, 1991). The Rabi flopping frequency for the transition is calculated to be 1,400 GHz. According to Appendix 2, when the laser is tuned to resonance and when the Rabi frequency is much greater than

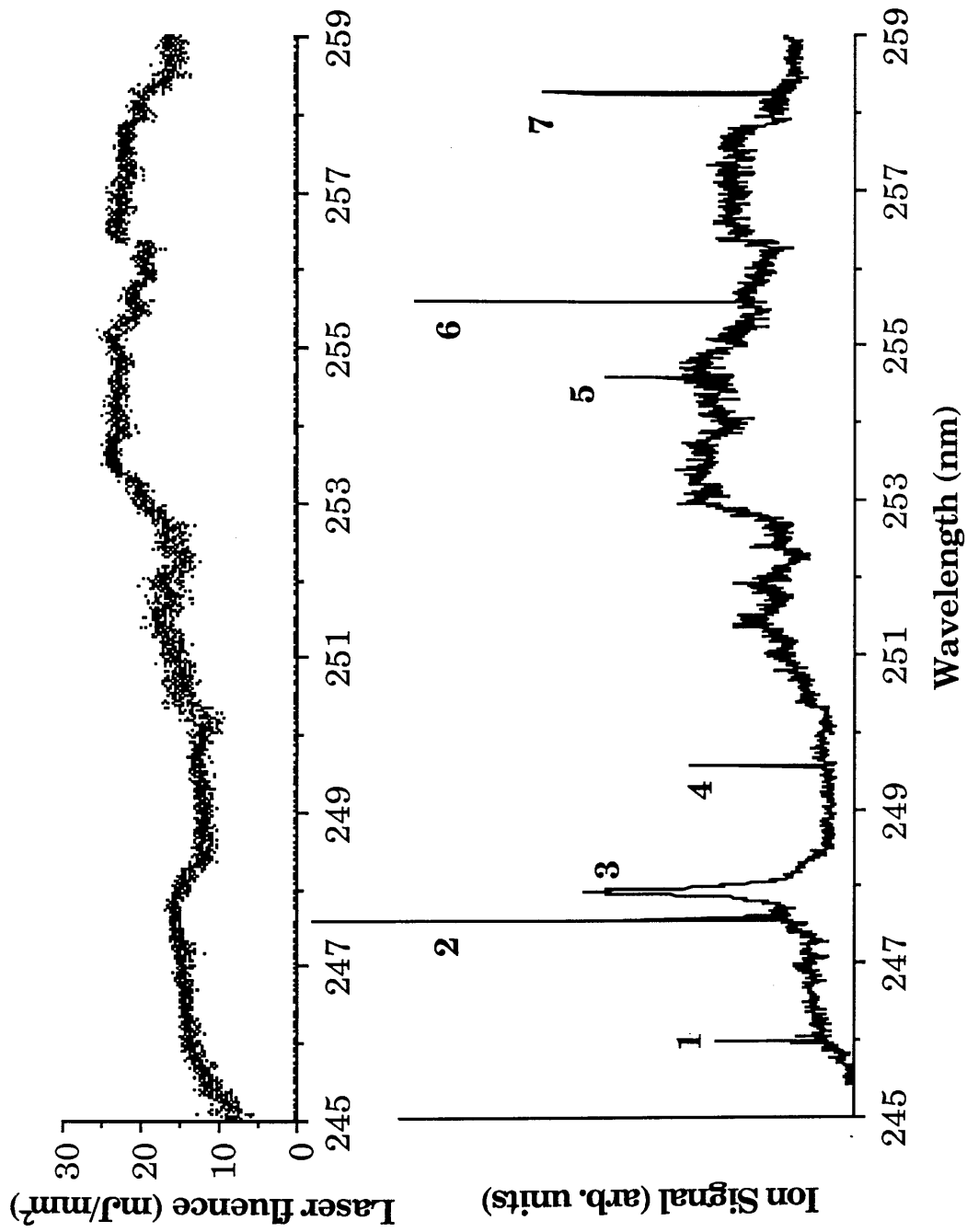


**Fig. 7.3:** Wavelength dependent ionisation spectrum of carbon ( $m/z=12$ ) produced from a p-nitrotoluene sample. The shot-to-shot laser fluence profile recorded simultaneously is also shown.

the natural width of the line, the transition width is simply given by twice the Rabi frequency, which in this case predicts a transition width of 0.56 nm. This, although larger than the measured width, is reasonable since the model used assumes that the laser flux is concentrated at the transition wavelength, whereas in reality, the intensity is distributed over the laser pulse bandwidth. The calculated value is therefore an upper estimate of the actual width, but compares favourably with the measured value of 0.2nm.

As can be seen from Table 7.1, many of the recorded transitions originate from the excited terms  $2p^2\ ^1S$  and  $2p^2\ ^1D$ . These states lie at energies of  $21648.4\text{cm}^{-1}$  and  $10193.7\text{cm}^{-1}$  respectively above the ground state and therefore cannot be populated at normal room temperature. Once populated, transitions originating from these states are likely to be observed during the length of the laser pulse ( $\sim 6\text{ns}$ ) since both are metastable with respect to the ground state, due to the  $\Delta S=0$  spin selection rule. Peaks 2, 4, 5, 6 and 7 (see Fig. 7.3) are singlet transitions which correspond to the two-photon resonances  $^1S \rightarrow ^1S$ ,  $^1S \rightarrow ^1D$ ,  $^1S \rightarrow ^1P$ ,  $^1D \rightarrow ^1P$  and  $^1D \rightarrow ^1D^0$  respectively. It follows that the UV dissociation process of the parent nitroaromatic molecule produces carbon not only in the atomic ground state, but also in excited states. A partial Grotrian diagram of carbon is shown in Fig. 7.4, where transitions giving rise to the observed sharp resonant structure are shown.

As already mentioned, the peak labelled 1 corresponds to the multiplet transition  $^3P \rightarrow ^3P$ . In total, only seven of the nine possible transitions of the  $^3P \rightarrow ^3P$  system are allowed, since the  $J=0 \leftrightarrow 1$  transitions are radiatively forbidden for equal frequency 2-photon excitation (Bonin and McIlrath, 1984). The multiplet is shown in



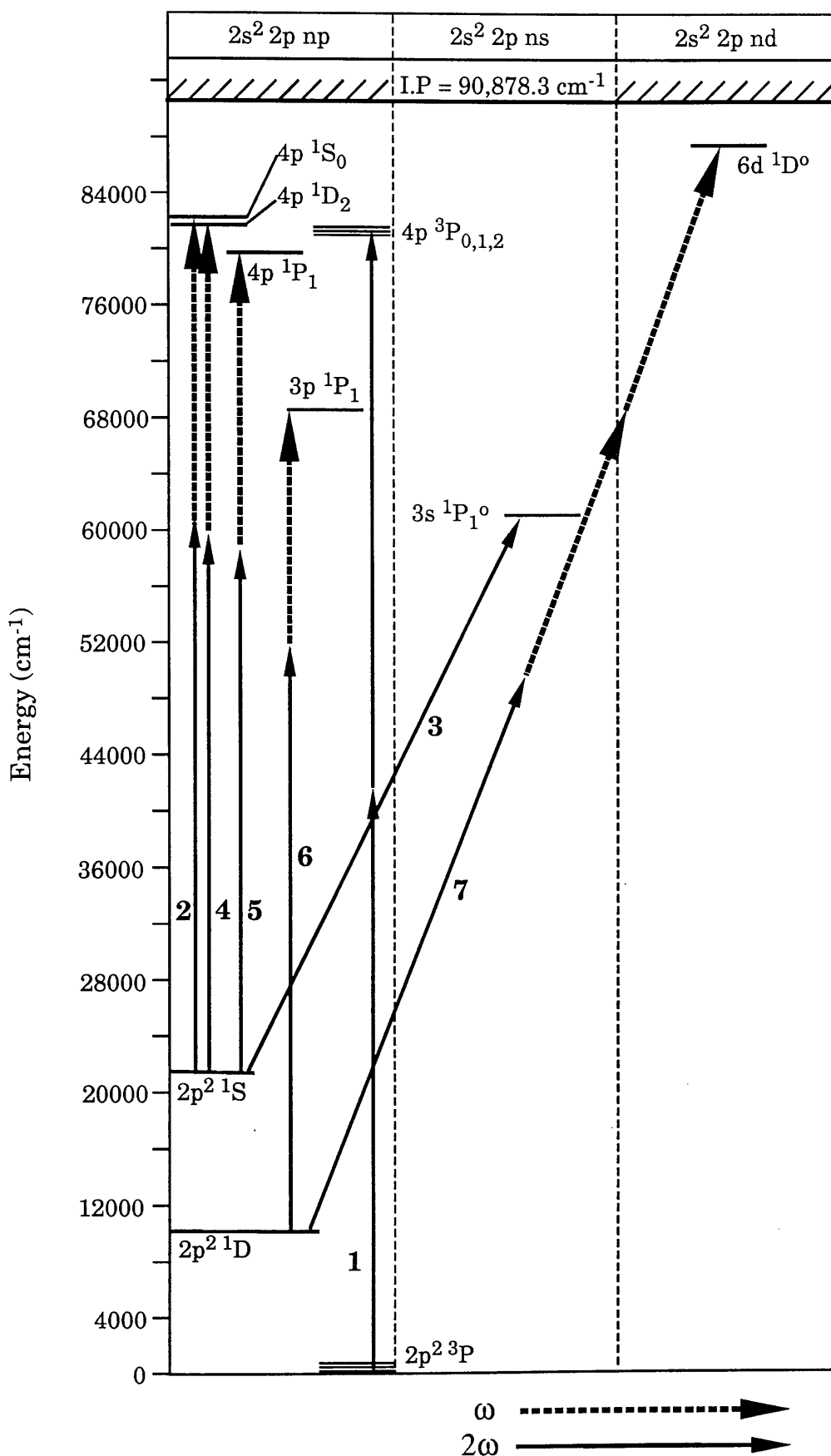


**Fig. 7.4:** Partial Grotrian diagram of atomic carbon showing relevant states.

much greater detail in Figs. 7.5a) and 7.5b). Fig. 7.5a) was recorded at a UV laser fluence of 24.8 mJ/mm<sup>2</sup>, and shows all allowed transitions. The positions of the 0→0 and 1→1 transitions are indicated, but unfortunately they are unresolved at this fluence, due to power broadening effects. However, the spectrum shown in Fig. 7.5b) was recorded at the lower UV fluence of 19.4mJ/mm<sup>2</sup>, and shows the 0→0 and 1→1 transitions partially resolved (splitting = 1.59 cm<sup>-1</sup>).

The width of the 246.0nm resonance is measured as 0.006nm, and is typical of the widths of other members of the multiplet. From the work by Wang *et al* (1991), an upper limit of 0.015nm is obtained for the bandwidth of the fundamental laser beam at the peak of the gain region of R-6G dye. It is reasonable to assume that for all dyes, the bandwidth of the laser beam will be close to this value, since the bandwidth is determined by the quality of the diffraction grating in the oscillator cavity of the laser. However, the measured width of the resonance is significantly smaller than this value, and is easily explained. If the dye laser output is assumed to have a Gaussian spectral profile,  $I(\nu)$ , given by,

$$I(\nu) = I_0 \exp \left[ \frac{-\beta^2(\nu - \nu_0)^2}{\nu_0^2} \right]$$

where  $\nu_0$  is the central frequency,  $I_0$  the maximum intensity and  $\beta$  a constant, then the bandwidth of the second harmonic pulse can be estimated since the efficiency of the SHG process is known to be proportional to the square of the fundamental intensity. The intensity profile,  $I(2\nu)$  of the second harmonic pulse is then seen to be proportional to,

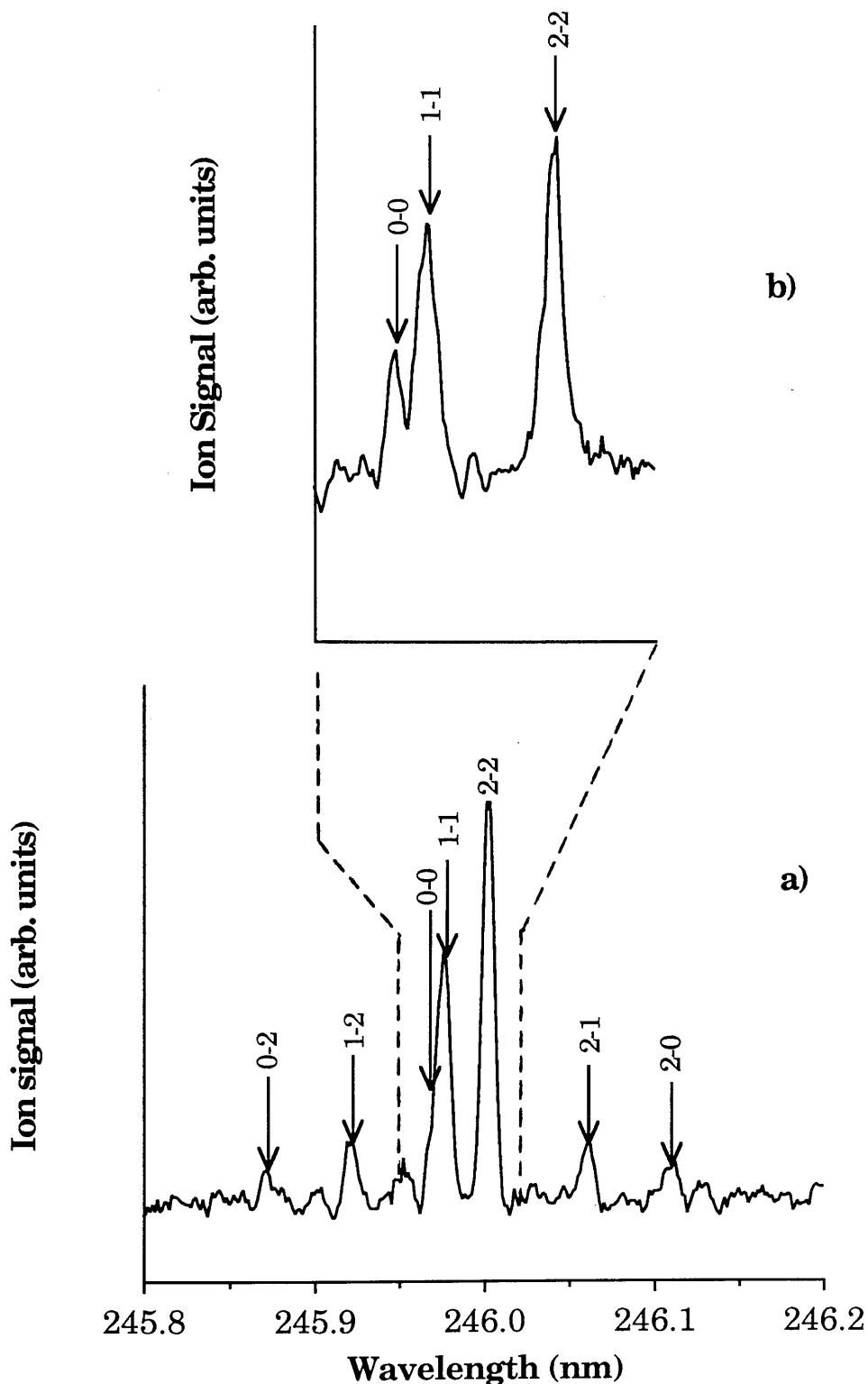


**Fig. 7.5a):** Ionisation spectrum recorded at a laser fluence of  $24.8 \text{ mJ/mm}^2$  showing the  $^3\text{P} \rightarrow ^3\text{P}$  multiplet in much greater detail. The  $0 \rightarrow 0$  and  $1 \rightarrow 1$  transitions are unresolved at this laser fluence.

**b):**  $^3\text{P} \rightarrow ^3\text{P}$  multiplet recorded at lower fluence,  $19.4 \text{ mJ/mm}^2$ , showing the  $0 \rightarrow 0$  and  $1 \rightarrow 1$  transitions partially resolved.

$$I(2\nu) \propto \exp\left[\frac{-2\beta^2(\nu-\nu_0)^2}{\nu_0^2}\right]$$

The linewidth of the two-photon resonance, one-photon ionisation transition is defined entirely by the excitation step, since the ionisation step is non-resonant and for two-photon excitation ( $2\nu + 2\nu$ ), the transition probability is proportional to the square of the  $2\nu$  intensity, which gives for the lineshape,  $S(\nu)$ ,

$$S(\nu) \propto \exp\left[\frac{-4\beta^2(\nu-\nu_0)^2}{\nu_0^2}\right]$$

which has width,  $\Delta$ , given by,

$$\Delta = \frac{1}{2}\Delta\nu_{\text{laser}}$$

Assuming the bandwidth of the dye laser to be 0.015nm, a linewidth of 0.0075nm is predicted, which compares favourably with the measured values of 0.006nm.

### **§7.5 Power dependence of carbon ion production.**

The physical processes occurring in the laser pulse were further investigated by monitoring the intensity of two carbon resonance lines as a function of UV laser fluence. Corresponding intensity dependences slightly off atomic resonance were also recorded since this represents a non-resonant dissociation background and must be subtracted to give the correct power dependence of the overall dissociation/ionisation process. The variations in the carbon ion signal at the resonant wavelength 247.51nm and when the laser wavelength was slightly detuned

from resonance (247.45nm) are shown in Fig. 7.6a). Similar graphs are shown in Fig. 7.7a) for the 249.49nm resonance, where the off-resonance wavelength was 249.20nm. In order to ascertain the overall nonlinear order of both the dissociation and resonance ionisation processes occurring at these wavelengths, log-log plots were drawn of ion intensity against laser fluence and are shown in Figs. 7.6b) and 7.7b). Both off-resonance power dependences give gradients of approximately 3, signifying that at least three photons of this wavelength are required to produce a single carbon ion, since some steps of the dissociation process may well be saturated.

A simple model was proposed in which the neutral carbon atoms formed by dissociation from parent molecules were assumed to have the same cubic power dependence as the carbon ions. With the laser wavelength tuned to each of the atomic resonances, and after the dissociation contribution from ionic carbon was subtracted, gradients of approximately 6 were obtained in both cases. It may be concluded therefore that, on-resonance, a further three photons participate in the overall process. This is to be expected since each of these resonant ionisation schemes involve a two photon resonance excitation followed by non-resonant one photon absorption into the ionisation continuum. Therefore, the production of carbon ions on resonance involves at least three photon absorption by the parent molecule to form carbon atoms via dissociation processes, followed by a three photon ionisation resonance ionisation process.

If it is further assumed that the appearance potentials for atomic carbon production from nitroaromatic molecules is similar to that of benzene, then a three photon process is not unreasonable. This assumption is based upon the fact that

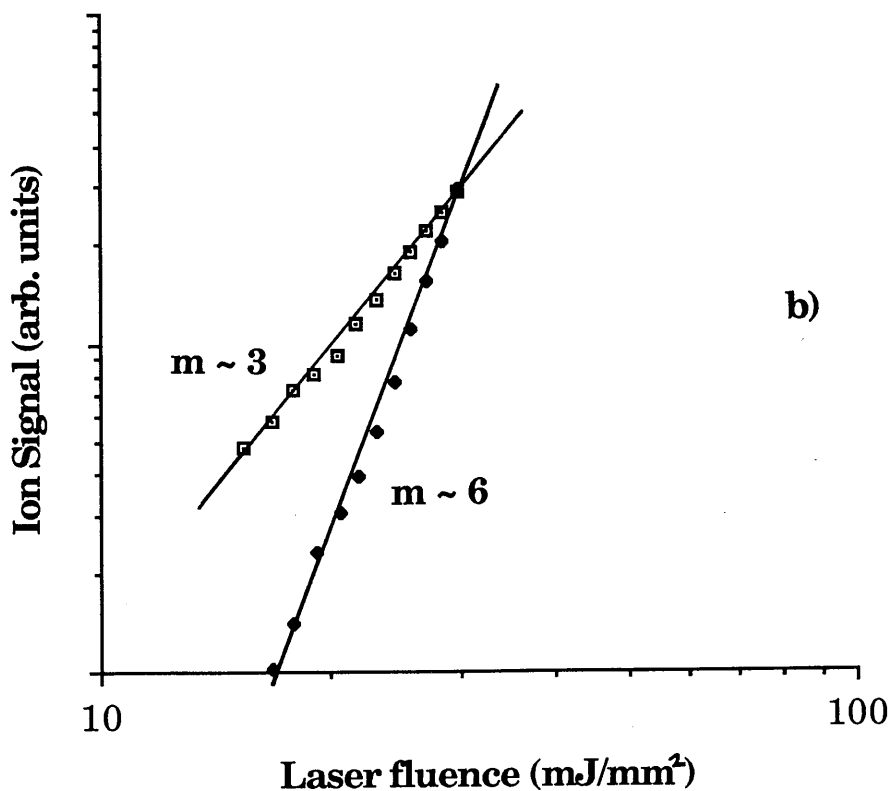
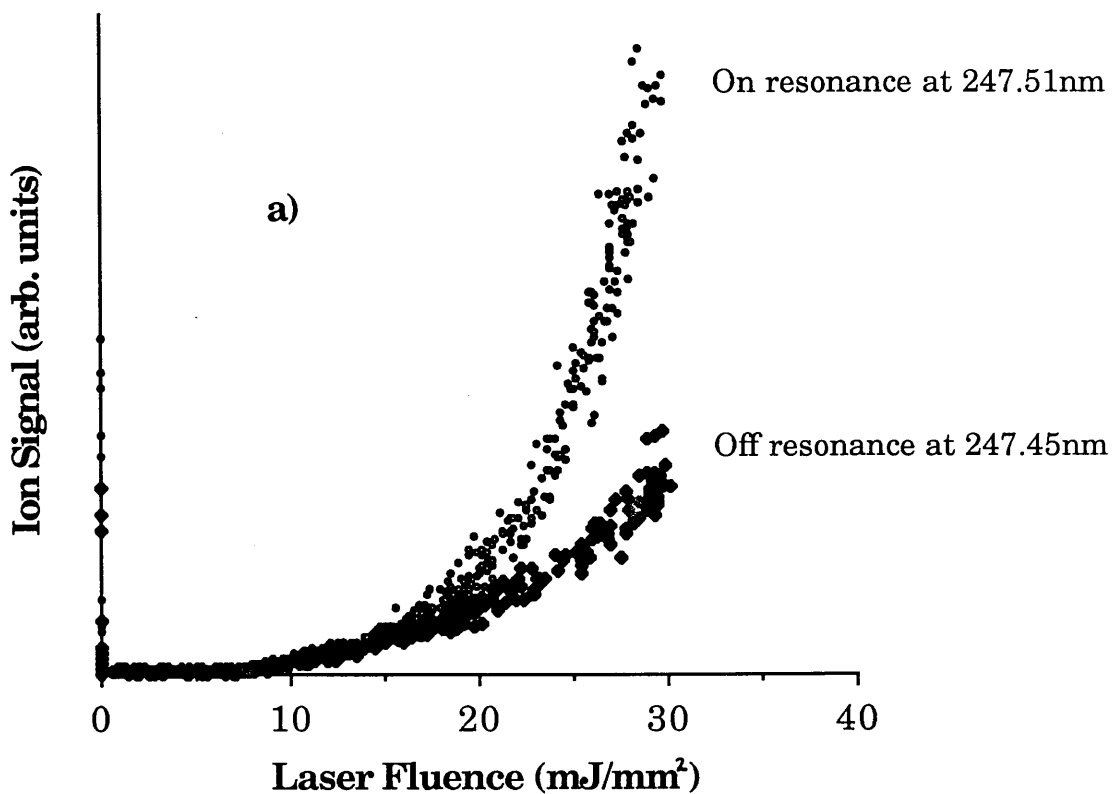


**Fig. 7.6a):** Carbon ion yield as a function of laser fluence on and off resonance.

**b):** Log-log graph showing third order dependence of carbon ion signal on laser fluence (off-resonance) and a sixth order power dependence on-resonance.

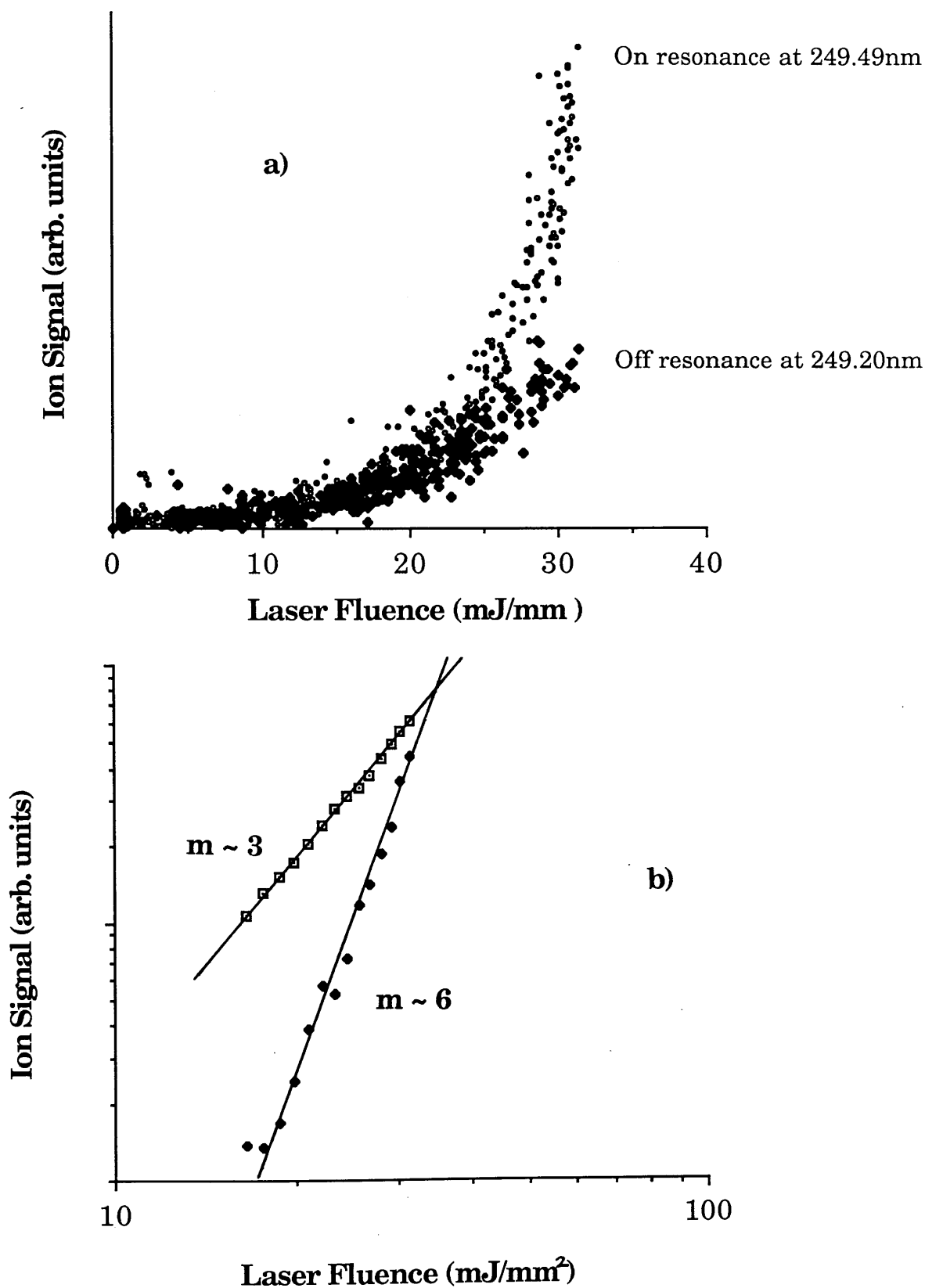


**Fig. 7.7a):** Carbon ion yield as a function of laser fluence on and off resonance.  
**b):** Log-log graph showing third order dependence of carbon ion signal on laser fluence (off-resonance) and a sixth order power dependence on-resonance.

nitroaromatics readily predissociate releasing  $\text{NO}_2$  and  $\text{C}_6\text{H}_5$  molecules. A diagram showing the appearance potentials of several fragment ions from benzene is shown in Fig. 7.8 (Zandee and Bernstein, 1979b). It is clear that about 15eV (which corresponds to 3 UV photons in our wavelength range) above the ground state of benzene, several  $\text{C}_n\text{H}_m^+$  type ions are formed, and that dissociative states to neutral carbon and hydrogen production are likely to abound in this region. In addition, the appearance potential for  $\text{C}^+$  ion production from benzene has been estimated to be 26eV above the ground state, which is approximately 11eV higher.

It is therefore concluded that there exist two possible mechanisms by which carbon ions are formed. Firstly, resonance enhanced ionisation may occur via a neutral atom pathway, requiring a further three photons to ionise the atom, or secondly, continued non-resonant up-pumping from ionic states is possible with subsequent fragmentation. In our wavelength range, the up-pumping mechanism would require six photons to produce  $\text{C}^+$  ions. According to Robin (1980), this up-pumping process often exhibits a power dependence which is considerably less than the number of photons energetically required to reach the appearance potentials. In particular, for  $\text{C}^+$  ion production from benzene, the power dependence measured was 3.5 (Zandee and Bernstein, 1979b), similar to the off-resonance power dependences observed above.

At both of these resonance wavelengths, an ionisation enhancement of  $\sim 4$  is observed at the maximum fluence levels available. Whetten *et al* (1983c) also observed an enhancement of  $\sim 4$  under optimised conditions whilst looking at the benzene



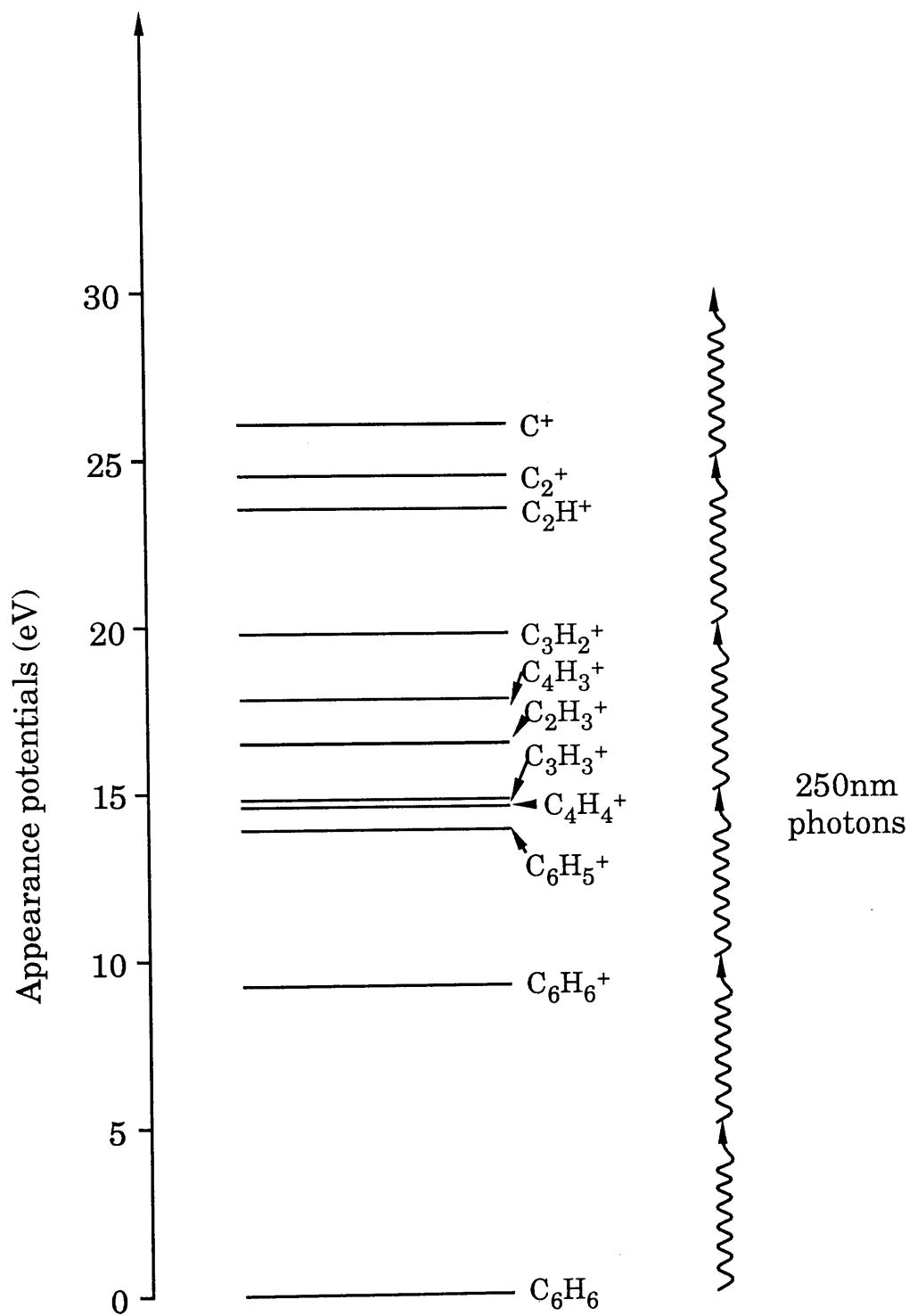


**Fig. 7.8:** Appearance potentials of selected fragment ions from benzene (Zandee and Bernstein, 1979).

molecule.

Once the cubic order of the dissociation of carbon ions from nitroaromatics was calculated, the ionisation spectrum shown in Fig. 7.3 was normalised by dividing, point by point, the ionisation signal by the cube of the laser fluence. The resulting normalised graph is shown in Fig. 7.9, where it is very clear that the dissociation background in p-nitrotoluene is structureless in this wavelength regime.

### **§7.6 Estimation of the number of neutral carbon atoms liberated per nitroaromatic molecule.**

Figs. 7.10a) and 7.10b) show respectively mass spectra recorded on and off atomic carbon resonance (247.51nm and 247.45nm respectively) at a laser fluence of 20mJ/mm<sup>2</sup> for a p-nitrotoluene sample. Clearly, all C<sub>n</sub> (n≠1) fragment ion intensities remain fairly constant at both wavelengths, whereas the carbon ion intensity increases dramatically on resonance. A simple model was invoked in order to estimate the number of neutral carbon atoms liberated per parent molecule in the laser interaction.

The total integrated ion signal was measured for both spectra, as were the intensities of the carbon ion signals. The enhancement of the carbon ion signal on resonance was measured to be ~5 relative to the off resonance signal intensity. In addition, the intensity of the on resonance carbon ion signal was measured to be approximately twice the total number of ions produced off-resonance. By simply assuming that each molecule which interacts with photons in the laser beam produces at least one ion, then this yields the result that *at least 2* neutral carbon atoms were liberated per parent molecule.

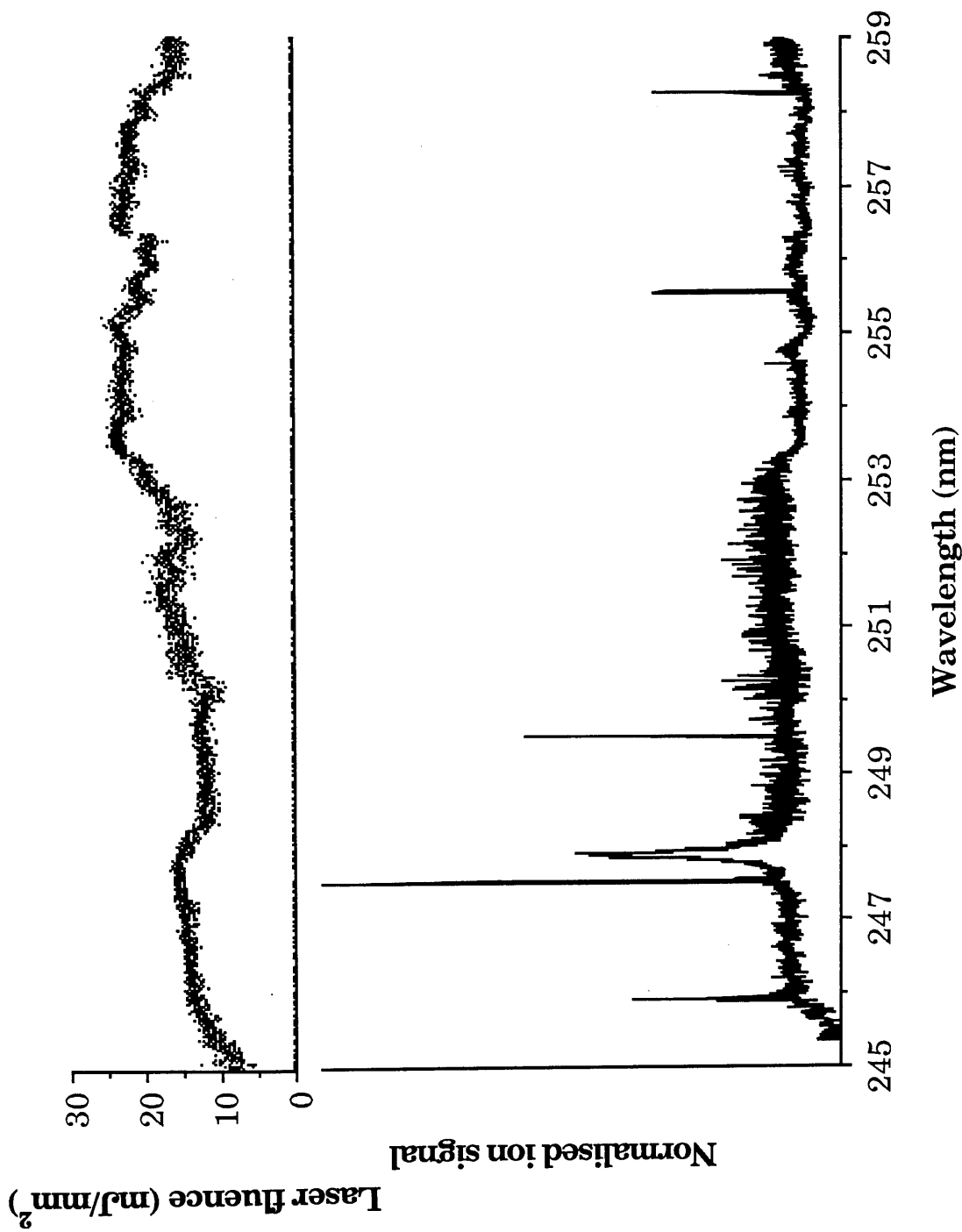


**Fig. 7.9:** Ionisation spectrum of carbon from p-nitrotoluene sample, normalised point-by-point to the laser fluence. The laser fluence which was recorded simultaneously is also shown.

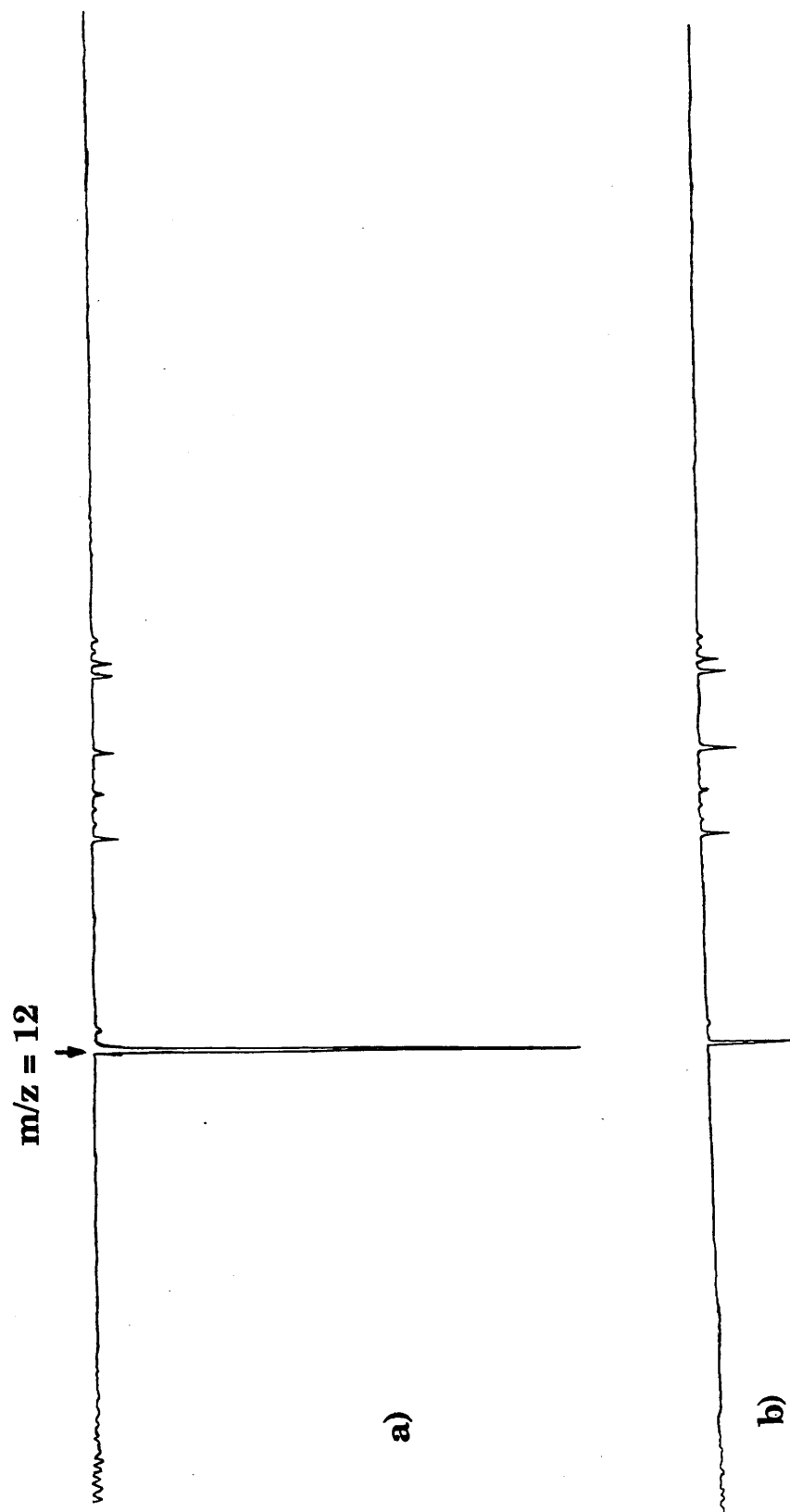


**Fig. 7.10:** a) TOF mass spectrum recorded at a laser fluence of  $20 \text{ mJ/mm}^2$  at the resonant wavelength 247.51 nm.  
b) TOF mass spectrum recorded at a laser fluence of  $20 \text{ mJ/mm}^2$  slightly detuned from resonance at 247.45 nm.

Finally, wavelength spectra were recorded for p-nitrotoluene over the range 245-260nm at very high laser fluences ( $>20 \text{ mJ/mm}^2$ ), as shown in Fig. 7.11. As is clear from this spectrum, the atomic resonances at 249.49nm, 254.60nm and 255.69nm are missing, which may be explained using the argument of Whetten *et al* (1983c). It was claimed that the dissociation pathways open to atomic carbon formation experience greater competition from non-resonant up-pumping of the molecule to ionisation/fragmentation. The shot-to-shot laser fluence profile which was recorded simultaneously is also shown in Fig. 7.11.

### **§7.7 RIMS of hydrogen atoms produced from nitroaromatic molecules.**

As mentioned in the introduction, the 243.13nm line in atomic hydrogen was observed whilst conducting studies of REMPI of some nitroaromatic molecules such as nitrobenzene and the isomers of nitrotoluene.

Unlike carbon, hydrogen atoms were only created in their ground state, which is most probably due to the fact that the lowest lying excited level has an energy of 10.17eV above the ground state. The dissociation process appeared to create only hydrogen in atomic form, since no ion component was observed off resonance, even at the highest possible laser fluences ( $\sim 30 \text{ mJ/mm}^2$ ). A TOF mass spectrum of nitrobenzene taken at a fluence of  $22.9 \text{ mJ/mm}^2$  and at 243.18nm is shown in Fig 7.12a), in which no peak corresponding to the hydrogen ion is visible. In comparison, the mass spectrum shown in Fig. 7.12b), which was recorded at the resonant wavelength 243.13nm and at the same fluence, shows a very large enhancement in the hydrogen ion

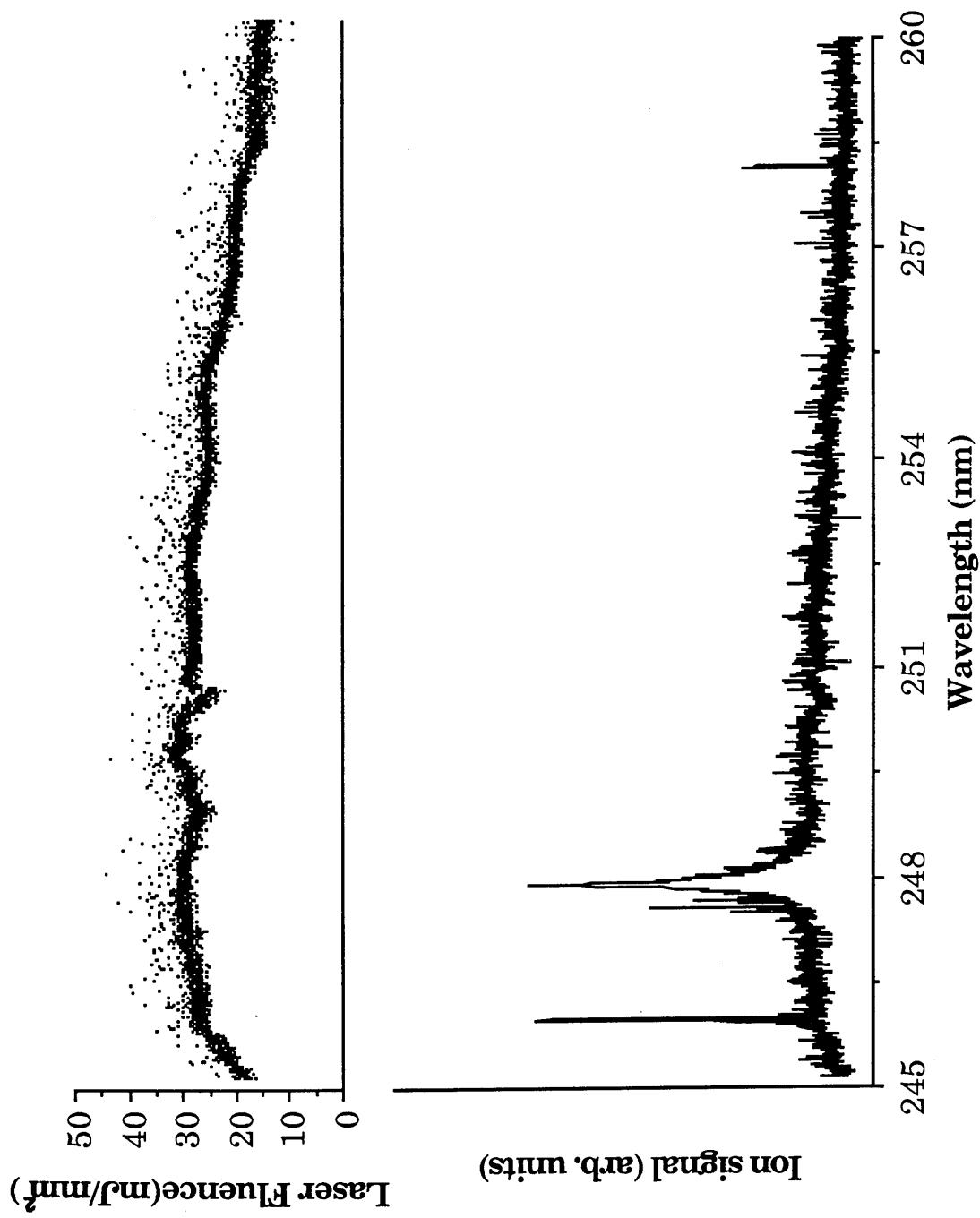


**Fig. 7.11:** Ionisation spectrum of carbon produced from a p-nitrotoluene sample, but recorded at a much higher fluence level. The laser fluence is also shown.

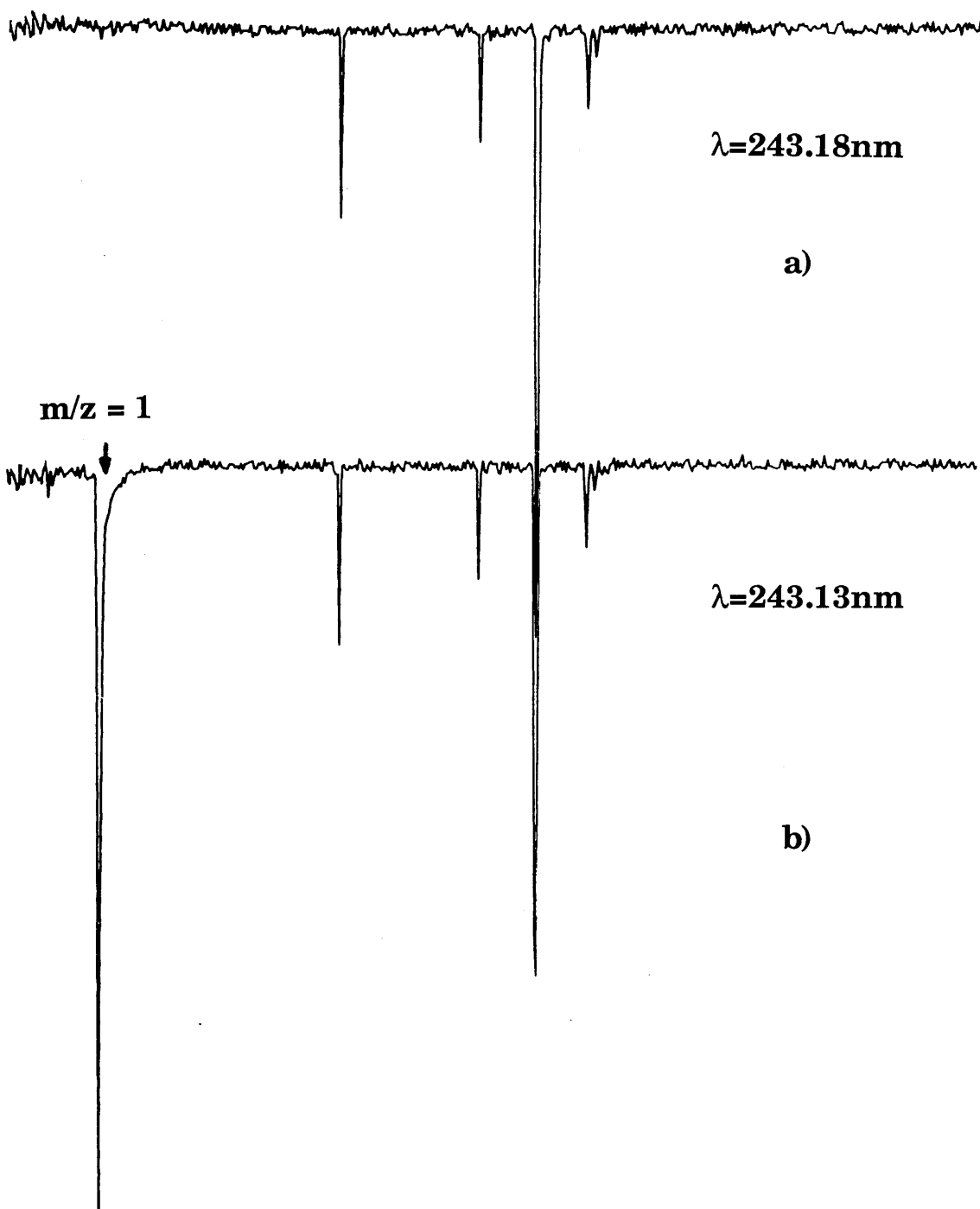


**Fig. 7.12:** a) TOF mass spectrum of nitrobenzene recorded at a laser fluence of  $22.9 \text{ mJ/mm}^2$  at wavelength  $243.18 \text{ nm}$ .

b) TOF mass spectrum recorded with the laser tuned to the  $1s \rightarrow 2s$  atomic hydrogen resonance. The laser fluence was  $22.9 \text{ mJ/mm}^2$ .

yield. It should be noted that the intensities of the other ions in both spectra remain fairly constant, which suggests that a substantial number of neutral hydrogen atoms are liberated in the dissociation process.

The RIS scheme involves the absorption of two UV photons, and proceeds through a short-lived virtual state to the 2s state. Subsequent absorption of another UV photon is sufficient to cause ionisation. Table 7.2 shows the energies of the states participating in the ionisation process. The ionisation scheme is shown in Fig. 7.13. The ionisation spectrum of the  $m/z=1$  peak is shown in Fig. 7.14, and was recorded at a laser fluence of  $15\text{mJ/mm}^2$ .

### **§7.8 Conclusions.**

In conclusion, the UV multiphoton dissociation of nitroaromatic molecules has been shown to be a source for efficient production of both carbon and hydrogen atoms. In total, 13 atomic carbon resonances have been observed in the wavelength range 245-260nm, which serve as an excellent means of laser wavelength calibration during REMPI experiments. Many laser spectroscopists use optogalvanic hollow cathode lamps in parallel with a laser ionisation experiment to calibrate wavelength scales, or a high quality Fabry-Perot etalon to obtain relative wavelength measurements. The results reported in this chapter could obviate the need to use such pieces of apparatus in ultraviolet REMPI studies of aromatic molecules. Many more carbon lines exist at shorter wavelengths, as do atomic oxygen and atomic nitrogen lines, so it seems feasible that this kind of wavelength calibration can also be carried out at shorter wavelengths.



State configuration	J-value	State energy (cm <sup>-1</sup> )
1s <sup>2</sup> S	1/2	0.000
2s <sup>2</sup> S	1/2	82,258.942
Ionisation limit	----	109,678.758

**Table 7.2:** Relevant energy levels of atomic hydrogen.

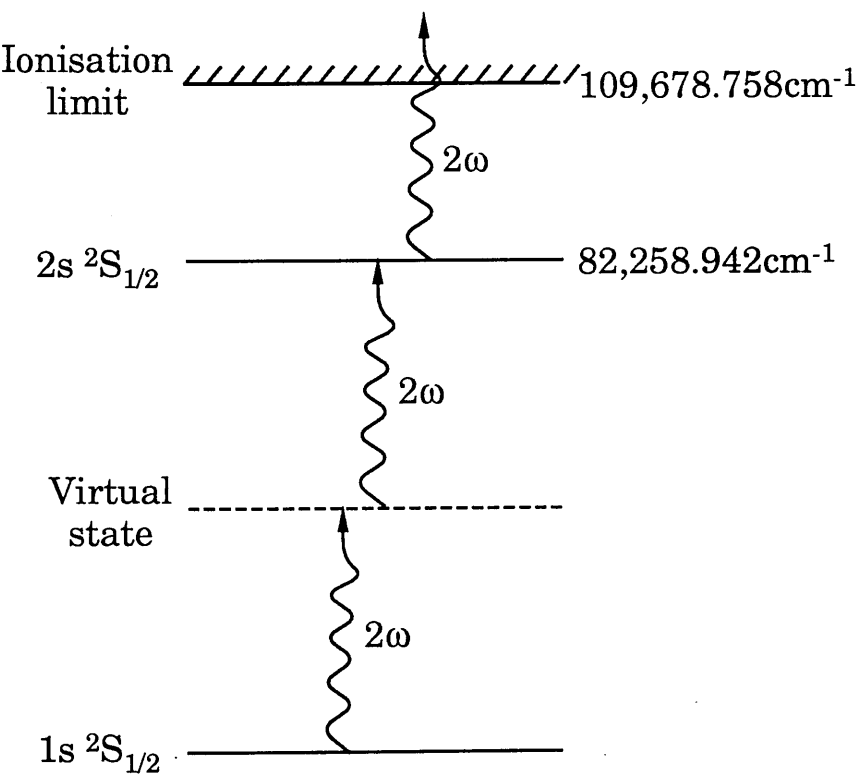


**Fig. 7.13:** Partial Grotrian diagram of atomic hydrogen showing relevant states and RIS scheme used.

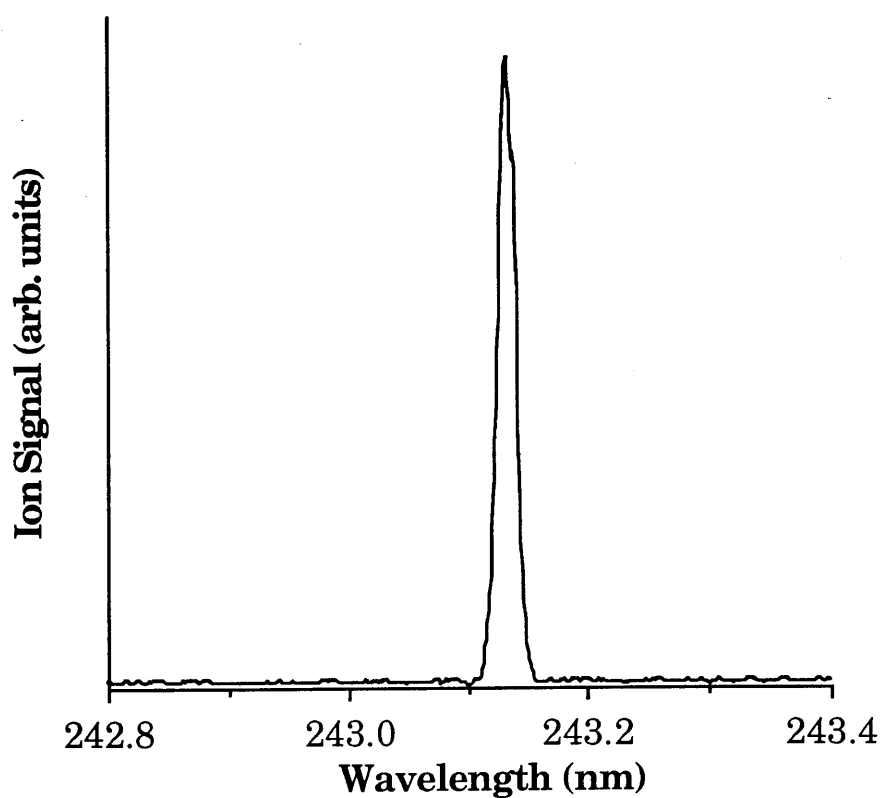


**Fig. 7.14:** Ionisation spectrum of hydrogen( $m/z=1$ ) produced from nitrobenzene showing strong resonance enhancement at 243.13nm

## **Chapter 8**

### **Conclusions and future experiments.**

A highly sensitive and selective procedure for the detection and identification of nitrobenzene and nitrotoluene molecules has been developed. The technique has been studied under vacuum conditions with time-of-flight mass spectrometric analysis.

Chapter 4 discussed preliminary R2PI experiments on the small aromatic molecules aniline and toluene in the quadrupole mass spectrometer system. The main conclusions to be drawn from this work is the strong similarity between the wavelength dependent behaviour of the molecular ions and the corresponding fragment ions. This fact would permit an enhancement in the overall detection sensitivity of these particular compounds if the total ionisation signal intensity from all ions produced in the laser interaction were monitored simultaneously, as opposed to mass selected detection. To this end, several experiments were conducted in a simple parallel plate ionisation chamber, in which ions were collected without charge amplification. Toluene, phenol and aniline were studied in the wavelength range 262-285nm. The characteristic spectra of toluene and phenol vapours were observed, whereas aniline showed no distinctively sharp resonant structure in this range at all. The possibility of discriminating between these particular compounds was investigated by recording the ionisation spectra of a mixture of the compounds. Resonance signals corresponding to both toluene and phenol were clearly observed in the spectra, even above the structureless background 'noise' corresponding to aniline ionisation. Experiments have shown that the REMPI approach is an

important analytical tool for detecting and identifying aromatic type compounds.

The results discussed in Chapter 5 could serve, on a laser induced molecular fragmentation basis alone, to distinguish between nitrobenzene and nitrotoluene. In both cases, no parent ion was observed in the mass spectrum as a result of rapid predissociation of the molecules in intense ultraviolet radiation fields. For nitrobenzene, a strong  $m/z=77$  ion signal, corresponding to the  $C_6H_5^+$  ion (Parent -  $NO_2$ ), was observed, whereas the highest  $m/z$  value observed in the mass spectra of any of the nitrotoluene isomers was 51, corresponding to the  $C_4H_3^+$  ion. No ion corresponding to the parent molecule minus  $NO_2$  was observed for any of the nitrotoluene isomers.

In addition, the wavelength dependent production of fragment ions from nitrobenzene showed resonant structure at several points in the wavelength range 245-250nm, which was thought to arise from the spectral characteristics of some intermediate molecular or ionic species, possibly  $C_6H_5$  or  $C_6H_5^+$ . This was in contrast to nitrotoluene isomers, where no wavelength dependent structure was observed in the spectra of any of the fragment ions.

Consequently, the presence of nitrobenzene could be detected in a nitrotoluene/nitrobenzene mixture by observing both a  $m/z=77$  ion in the mass spectrum of the mixture and the characteristic wavelength dependence of this ion in the range 245-250nm. It would be much more difficult to confirm the presence of nitrotoluene in such a mixture since no wavelength dependent structure exists in the range 245-250nm, and all

fragment ions observed in the mass spectrum of nitrotoluene isomers were also observed in the mass spectrum of nitrobenzene. In both compounds, strong ion signals at  $m/z=30$  were observed, which correspond to the  $\text{NO}^+$  ion. The dominance of the  $\text{NO}^+$  ion clearly identifies  $\text{NO}_2$ -containing compounds and also means detection sensitivity is enhanced.

The work of Chapter 6 helped elucidate the dissociation mechanisms which prevail in the interaction of UV laser light with nitroaromatic molecules. The results strongly suggest that the  $\text{NO}_2$  group is readily predissociated from the parent molecule, which then itself undergoes a single-photon predissociation process to form NO and O. The NO molecules undergo two-photon ionisation to form  $\text{NO}^+$  ions, which dominated the mass spectra of the nitroaromatic molecules at certain wavelengths.

The resonant structure is also very important in identifying the states participating in the resonant ionisation of NO. Chapter 6 also shows that the states in which the NO molecules are formed in the predissociation of  $\text{NO}_2$  is dependent on the irradiating wavelength. In addition, the oxygen atoms which are liberated in the same process are prepared in either the  $^3\text{P}$  ground state or the  $^1\text{D}$  excited state. The wavelength dependent ionisation signature of the  $\text{NO}^+$  ion in the range 233-239nm distinguishes between NO molecules originating from NO gas and from  $\text{NO}_2$  and nitroaromatic species due to the different rotational line intensities at wavelengths below  $\sim 235\text{nm}$ . Ionisation spectra in the range 245-250nm could be used to completely distinguish between  $\text{NO}^+$  ions produced from  $\text{NO}_2$  and nitroaromatic molecules.

Chapter 7 discussed the ionisation spectra of carbon and

hydrogen ions which had been produced from samples of nitrobenzene and nitrotoluene. The transitions were identified as resonances in atomic carbon and hydrogen. In carbon, the  $2p^2\ ^1S$  and  $2p^2\ ^1D$  excited states were populated in the dissociation process. As a bonus, the large number of such resonances in the wavelength range studied permits accurate wavelength calibration to be made during REMPI experiments on aromatic species.

In addition to carbon and hydrogen atoms, there also exist several atomic resonances of oxygen and nitrogen in the deep UV region. In particular, a triplet-triplet transition originating from the  $^3P$  ground state of oxygen occurs at 225.7nm and both absorption and ionisation cross-sections have been measured experimentally (Bamford *et al*, 1986, 1987, 1988; Dixit *et al*, 1988) and calculated theoretically (Saxon and Eichler, 1986; Saxon *et al*, 1989). One particularly interesting experiment, which could possibly confirm the actual dissociation mechanisms in nitroaromatic species, is to look for the above resonance in atomic oxygen. If observed it would suggest that oxygen is being liberated in the predissociation from  $NO_2$  molecules which are themselves liberated from the parent nitroaromatics by single photon predissociation. In the case of nitrobenzene, the only other possibility is that the  $C_6H_5O$  species which is liberated in mechanism (5.4) dissociates either spontaneously or by absorption of photons from the beam to produce these oxygen atoms.

It is also planned to investigate the wavelength dependent ionisation/fragmentation patterns of nitroaromatics in the wavelength range 220-245nm. The absorption spectrum of pure

NO gas shown in Fig. 6.10 shows that the absorption intensity is much greater at 226nm relative to the absorption at 236nm, and therefore by tuning the laser wavelength to this value, the detection sensitivity could be greatly enhanced. Preliminary investigations are currently underway at Glasgow and show very large  $\text{NO}^+$  ion signals at 226nm from samples of NO and  $\text{NO}_2$  gases. If the detection sensitivity is optimised at 226nm for nitroaromatic molecules, some effort will be directed at obtaining a fixed frequency laser source at this wavelength, in order to eliminate the necessity of dye lasers. Several possibilities exist including Raman shifting the fifth harmonic output of a Nd:YAG laser in a suitable medium or by using the quadrupled output of a Titanium doped Sapphire laser ( $\text{Ti: Al}_2\text{O}_3$ ).

In addition, other nitro-containing compounds are of immediate interest to the group at Glasgow, and will be studied in the deep UV region. In particular, nitroaromatic species which have more than one  $\text{NO}_2$  group per molecule will be of immediate interest. The possibility of enhancing detection sensitivity exists by monitoring the  $\text{NO}^+$  ion if more than one  $\text{NO}_2$  group is released per parent molecule. It is also hoped that an ion mobility spectrometer will be purchased soon and it will be used in parallel with the current TOF system in order to observe mobility spectra and TOF mass spectra simultaneously. This would permit studies to be carried out at atmospheric pressure which is desirable in terms of environmental monitoring and more importantly, no need to employ high vacuum equipment.

## Appendix 1

### Second Harmonic Generation.

The technique of Second Harmonic Generation was used extensively during the course of experiments described in this thesis in order to produce tunable laser light in the range 232-300nm.

When a high intensity laser beam of frequency  $\omega$  passes through a nonlinear optical medium, several multiple frequency components ( $2\omega$ ,  $3\omega$ , etc.) are observed in the transmitted beam. (Miloni and Eberly, 1988) In a non-linear optical medium, the polarisation,  $P$ , induced by a passing electromagnetic wave is given by,

$$P = \epsilon_0(\chi_1 E + \chi_2 E^2 + \chi_3 E^3 + \dots) \quad \text{-(A1.1)}$$

where  $\chi_i$  is the  $i$ 'th order nonlinear susceptibility of the medium, and depends upon both the crystal properties and direction of propagation in the crystal.

If the electromagnetic wave is written in the form,

$$E = E_0 \sin \omega t \quad \text{-(A1.2)}$$

then the induced polarisation in the medium may be written as,



$$P = \epsilon_0 \chi_1 E_0 \sin \omega t + \epsilon_0 \chi_2 E_0^2 (1 - \cos 2\omega t) + \epsilon_0 \chi_3 E_0^3 (3 \sin \omega t - \sin 3\omega t) + \dots \quad \text{-(A1.3)}$$

It is clear from (A1.3) that the induced polarisation contains terms which oscillate at twice and three times the driving frequency  $\omega$ . This observation forms the basis of nonlinear optical techniques.

A polarisation wave is generated in the crystal which propagates with wavelength  $\lambda_1 = c/2\nu n_1$  where  $n_1$  is the refractive index of the medium at the fundamental frequency  $\omega$ . This polarisation wave induces the generation of light in the crystal of frequency  $2\omega$ , which propagates with wavelength  $\lambda_2 = c/2\nu n_2$ . Of course, due to dispersion in the crystal,  $n_1 \neq n_2$ , and consequently the waves propagate with different velocities and eventually become out of phase.

For a crystal of length  $l$ , the intensity of the second harmonic beam,  $I(2\omega)$ , as it leaves the crystal is given by,

$$I(2\omega) \propto I^2(\omega) \frac{\sin^2\left(\frac{2\pi\Delta n l}{\lambda}\right)}{\left(\frac{2\pi\Delta n l}{\lambda}\right)^2} \quad \text{-(A1.4)}$$

where  $\Delta n = n_{2\omega} - n_{\omega}$  and  $\lambda_0$  is the vacuum wavelength of the fundamental radiation (Levenson and Kano, 1982). Clearly, the intensity of the second harmonic beam is maximised if the argument of the  $\sin^2$  term is  $\pi/2$ , which occurs when  $l = \lambda/4\Delta n$ . This value of  $l$  is called the coherence length. For most crystals, the coherence length predicted by this condition for optimised conversion is generally less than  $10\mu\text{m}$ .

However, if the value of  $\Delta n$  is decreased, then the coherence

length is increased and the technique becomes much easier to implement practically. This can be done by using a suitable birefringent optical medium. In these crystals, waves of different polarisations generally have different propagation velocities. If the fundamental radiation propagates as an ordinary wave, which therefore has a refractive index independent of propagation direction, then the second harmonic beam will propagate in the crystal as an extraordinary wave, which has a refractive index dependent upon direction. The variation of the refractive indices of both ordinary and extraordinary waves as a function of angle from the optical axis are shown in Fig. A1.1. It can be seen that if the fundamental beam propagates at a certain angle to the optic axis, then the refractive indices of the fundamental and second harmonic beams are the same (where the ellipse and circle intersect), and the coherence length is maximised. This is known as phase matching. The technique is implemented experimentally by rotating the doubling crystal relative to the incoming fundamental beam as the laser wavelength is varied.

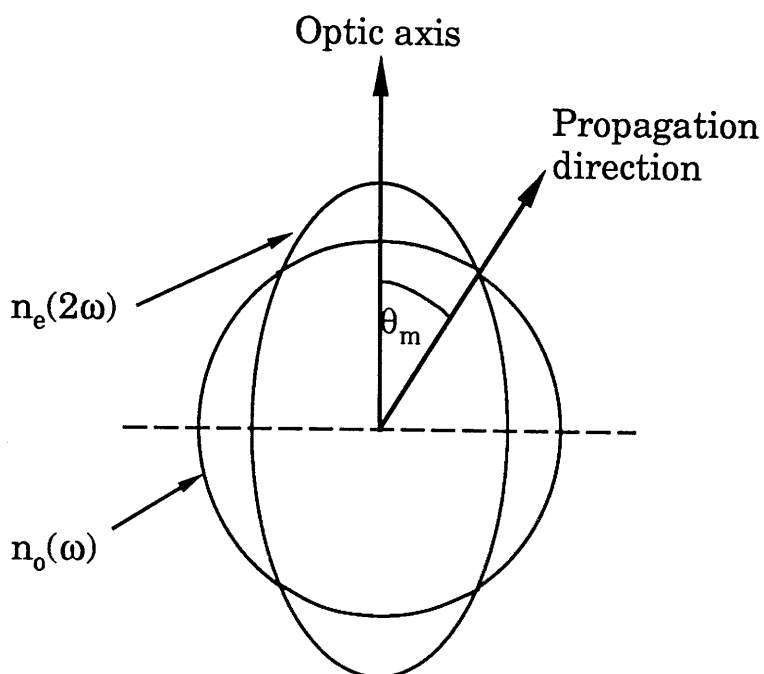


**Fig. A1.1:** Index ellipsoids for ordinary and extraordinary rays showing the condition for phase matching.

## Appendix 2

### Interaction of a 2-level system with strong laser fields: Power broadening.

The treatment given in Chapter 2 is valid only in the regime of low laser intensities, in which it is reasonable to assume that the ground state population  $|a(t)|^2$  changes very little during the interaction time. However, when the laser intensity is very high, this approximation is no longer valid, since the ground state population is significantly altered by the radiation field.

In the RWA, as discussed in Chapter 2, the population amplitudes of the ground and excited states change according to equations (2.14) and (2.15),

$$\dot{a}(t) = \frac{i\chi_{ab}}{\hbar} b(t)e^{-i(\omega_{ba}-\omega)t} \quad -(2.14)$$

$$\dot{b}(t) = \frac{i\chi_{ab}}{\hbar} a(t)e^{+i(\omega_{ba}-\omega)t} \quad -(2.15)$$

In the regime of high radiation intensities, a trial solution of an oscillatory nature must be assumed, since it envisaged the population cycling will occur under the influence of high fields (Dembroder, 1982). The trial solution is written as,

$$a(t) = e^{i\mu t} \quad -(A2.1)$$

where  $\mu$  is dependent upon the radiation frequency and the parameters of the 2-level system. By substitution of equation

(A2.1) in (2.15), we obtain for  $b(t)$ ,

$$b(t) = \frac{\hbar\mu}{\chi_{ab}} e^{i(\omega_{ba}-\omega+\mu)t} \quad \text{-(A2.2)}$$

Substitution of equation (A2.4) into (A2.2) yields,

$$2\mu_{\pm} = -(\omega_{ba}-\omega) \pm \left[ (\omega_{ab}-\omega)^2 - \frac{4\chi_{ab}^2}{\hbar^2} \right]^{\frac{1}{2}} \quad \text{-(A2.3)}$$

The general solutions for the state probability amplitudes are therefore given by,

$$a(t) = C_1 e^{i\mu_+ t} + C_2 e^{i\mu_- t} \quad \text{-(A2.4)}$$

$$b(t) = \frac{\hbar}{\chi_{ab}} e^{i(\omega_{ba}-\omega)t} [\mu_+ C_1 e^{i\mu_+ t} + \mu_- C_2 e^{i\mu_- t}] \quad \text{-(A2.5)}$$

In addition, if it is assumed that all atoms/molecules occupy their ground states at the instant the laser field is 'switched on', the coefficients  $C_1$  and  $C_2$  may be evaluated. In doing so, the expression for  $b(t)$  can finally be written as,

$$b(t) = \frac{2i\chi_{ab}}{\hbar\mu} e^{i\frac{1}{2}(\omega_{ba}-\omega)t} \sin\left(\frac{1}{2}\mu t\right) \quad \text{-(A2.6)}$$

where

$$\mu = \mu_+ - \mu_- \quad \text{-(A2.7)}$$

The probability of finding the system in state **b** at time  $t$  after the laser is switched on is given by,

$$|b(t)|^2 = \frac{4\chi_{ab}^2}{\hbar^2\mu^2} \sin^2\left(\frac{1}{2}\mu t\right) \quad \text{-(A2.8)}$$

where 
$$\mu = \left[ (\omega_{ba} - \omega)^2 + \frac{4\chi_{ab}^2}{\hbar^2} \right]^{\frac{1}{2}} \quad \text{-(A2.9)}$$

The term  $\mu$  is called the Rabi flopping frequency and describes the oscillatory nature of the population densities in strong field interactions. It is dependent on the degree of detuning from the transition frequency, and on resonance it has the value,

$$\mu = \frac{2\chi_{ab}}{\hbar} = \frac{2e}{\hbar^2} \underline{E}_0 \cdot \underline{R}_{ab} \quad \text{-(A2.10)}$$

The predicted width of the transition on resonance is then just twice the Rabi frequency. From equation (A2.10), it is clear that the width of the transition line is increased when the radiation field intensity is increased. This effect is known as power broadening.

In order to evaluate the width of the single photon transition at 247.31nm in carbon, it is necessary to evaluate the transition dipole matrix element,  $\underline{R}_{ik}$ , where the subscripts  $i$  and  $k$  refer to the initial and final states respectively. This may be evaluated from a knowledge of the oscillator strength of the transition or alternatively from the Einstein coefficient  $A_{ki}$ , which are readily available in the published literature. The theoretical expression for the quantity  $A_{ki}$  is given by,

$$A_{ki} = \frac{16\pi^3 e^2}{3\epsilon_0 \hbar g_k \lambda_{ik}^3} S_{ik} \quad \text{-(A2.11)}$$

where 
$$S_{ik} = \sum_{m=1}^{g_i} \sum_{n=1}^{g_k} |\underline{R}_{imkn}|^2 \quad \text{-(A2.12)}$$

$S_{ik}$  is called the transition line strength, and takes into account the degeneracy of the initial and final states. In equation (A2.12),  $g_i$  and  $g_k$  are the statistical weights of the initial and final states, and  $\nu_{ik}$  is the transition frequency. The double sum extends over all magnetic substates in the transition  $i \rightarrow k$ . It is possible that some of the  $R_{i_m k_n}$  in the sum may vanish because of selection rules.

For the situation where none of the dipole matrix elements vanish, the double sum is simply equal to  $|R_{ik}|^2$  and the matrix element  $R_{ik}$  may be expressed in terms of the Einstein coefficient  $A_{ik}$  by,

$$R_{ik}^2 = \frac{3\epsilon_0 h \lambda_{ik}^3 g_k A_{ki}}{16\pi^3 e^2} \quad \text{-(A2.13)}$$

From equations (A2.11), (A2.12) and (A2.13) the Rabi frequency,  $\mu$ , can be written as,

$$\mu(s^{-1}) = \left[ \frac{3\lambda^3 I g_k A_{ki}}{2\pi c h} \right]^{\frac{1}{2}} \quad \text{-(A2.14)}$$

## References.

Ambartsumyan R V and Letokhov V S(1972)

*Selective two-step photoionisation of atoms and photodissociation of molecules by laser radiation.*

Appl. Opt., 11, 354

Ambartsumyan R V, Apatin A M, Letokhov V S, Makarov A A, Mishin V I, Puretskii A A and Furzikov N P(1976)

*Selective two-step ionization of rubidium by laser radiation.*

Sov. Phys. JETP 43(5), 866

Antonov V S and Letokhov V S(1981)

*Laser Multiphoton and Multistep Photoionization of Molecules and Mass Spectrometry.*

Appl. Phys., 24, 89

Antonov V S, Letokhov V S and Shibano A N(1984)

*Laser resonance photoionization spectroscopy of molecules.*

Sov. Phys.Usp., 27(2), 81

Apel E C and Nogar N S, (1986)

*Multiphoton photoionisation mass spectra of nitrobenzene and 2,4,6-trinitrotoluene.*

Int. J. Mass Spectrom. and Ion Pro., 70, 243

Apel E C, Anderson J E, Estler R C, Nogar N S and Miller C M (1987)

*Use of two-photon excitation in resonance ionization mass spectrometry.*

Applied Optics Vol. 26 No. 6, 1045



Bamford D J, Dyer M J and Bischel W K(1987)

*Single frequency laser measurements of two-photon cross sections and Doppler-free spectra for atomic oxygen.*

Phys. Rev. A 36 No. 7, 3497

Bamford D J, Jusinski L E and Bischel W K(1986)

*Absolute two-photon absorption and three-photon ionization cross sections for atomic oxygen.*

Phys. Rev. A, Vol 34, No. 1, 185

Bamford D J, Saxon R P, Jusinski L E, Buck J D and Bischel W K(1988)

*Two-photon excitation of atomic oxygen at 200.6, 192.5, and 194.2 nm: Absolute cross sections and collisional ionization rate constants.*

Phys. Rev. A 37 No. 9, 3259

Bekov G I and Letokhov V S(1983)

*Laser Atomic Photoionization Spectral Analysis of Element Traces.*

Appl. Phys. B, 30, 161

Bekov G I, Letokhov V S and Mishin V I(1978)

*Ionization of high-lying states of the sodium atom by a pulsed electric field.*

Sov. Phys. JETP 46(1), 81

Bernstein R B(1978)

*Systematics of multiphoton Ionization-Fragmentation of polyatomic molecules*

J. Phys. Chem., 86, 1178

- Bigio L and Grant E R(1985)  
*Optical selection in double-resonant two-photon photodissociation: Near threshold state-to-state fragmentation dynamics of  $\text{NO}_2 + 2h\nu \rightarrow \text{NO}(X^2\Pi_{1/2}, v=0, J, \Lambda) + \text{O}(^1\text{D})$*   
 J. Chem. Phys., 89, 5855
- Boesl U, Neusser H J and Schlag E W(1979)  
*Visible and UV multiphoton ionization and fragmentation of polyatomic molecules.*  
 J. Chem. Phys., 72(8), 4327
- Boesl U, Neusser H J and Schlag E W(1981a)  
*Multi-photon ionization in the mass spectrometry of polyatomic molecules: cross-sections.*  
 Chem. Phys., 55, 193
- Boesl U, Neusser H J and Schlag E W(1981b)  
*Isotope selective soft multiphoton ionization and fragmentation of polyatomic molecules.*  
 J. Am. Chem. Soc., Vol. 103 No. 17, 5058
- Bonin K D and McIlrath T J(1984)  
*Two-photon electric dipole selection rules.*  
 J. Opt. Soc. Am. B1, 52
- Brand J C D, Williams D R and Cook T J(1966)  
*Vibrational analysis of the first ultraviolet band system of aniline.*  
 J. Mol. Spec., 20, 359
- Bray R G, Hochstrasser R M and Wessel J E(1974)  
*Continuously tunable two-photon excitation of individual rotational levels of the  $A^2\Sigma$  state of nitric oxide.*  
 Chem. Phys. Lett., 27(2), 167

- Brophy J H and Rettner C T(1979)  
*Laser two-photon ionisation of aniline in a molecular beam and the bulk gas phase.*  
Chem. Phys. Lett., Vol. 67 No. 2, 351
- Brown P(1970)  
*Kinetic studies in mass spectrometry-IX: Competing [M-NO<sub>2</sub>] and [M-NO] reactions in substituted nitrobenzenes. Approximate activation energies from ionization and appearance potentials.*  
Org. Mass Spectrom., 4, 533
- Busch G E and Wilson K R(1972)  
*Triatomic photofragment spectra: I. Energy partitioning in NO<sub>2</sub> photodissociation.*  
J. Chem. Phys., 56, 3626
- Cameron A E and Eggers D F(1948)  
*An Ion "Velocitron".*  
Rev. Sci. Instrum., 19, 605
- Chernoff D A and Rice S A(1979)  
*Single vibronic level fluorescence from aniline.*  
J. Chem. Phys., 70(5), 2511
- Clark CW, Fassett J D, Lucatorto T B, Moore L J(1984)  
*Enhancement of the isotopic abundance sensitivity of mass spectrometry by Doppler-free resonance ionization.*  
Proceedings RIS 84, 107
- Cohen M J and Karasek F W(1970)  
*Plasma chromatography-A new dimension for gas chromatography and mass spectrometry.*  
F. of Chromat. Science, Vol. 8, 330

- Corney A(1977)  
*Atomic and laser spectroscopy.*  
Oxford University Press, Oxford
- Das P, Ondrey G, van Veen N and Bersohn R(1983)  
*Two-photon laser induced fluorescence of carbon atoms.*  
J. Chem. Phys., 79(2), 724
- Demtroder W(1982)  
*Laser spectroscopy: Basic concepts and instrumentation.*  
Springer Verlag, Chemical Physics 5
- Dietz T G, Duncan M A and Smalley R E(1982)  
*Time evolution studies of triplet toluene by two-colour photoionisation.*  
J. Chem. Phys., 76(3), 1227
- Dietz T G, Duncan M A, Liverman M G and Smalley R E (1980a)  
*Efficient multiphoton ionisation of jet-cooled aniline.*  
Chem. Phys. Lett., Vol. 70 No. 2, 246
- Dietz T G, Duncan M A, Liverman M G and Smalley R E(1980b)  
*Resonance enhanced two-photon ionization studies in a supersonic molecular beam: Bromobenzene and iodobenzene.*  
J. Chem. Phys., 73(10), 4816
- Dixit S N, Levin D A and McKoy B V(1988)  
*Resonant enhanced multiphoton ionization studies in atomic oxygen.*  
Phys. Rev. A 37 No. 11, 4220

Drysdale S L T, Ledingham K W D, Raine C, Smith K M, Smyth M H C, Stewart D T, Towrie M and Houston C M(1986)

*Detection of toluene in a proportional counter gas by resonant two photon ionisation spectroscopy.*

Nuc. Inst. Meth. in Phys. Res., A252, 521

Esherick P and Anderson R J M(1980)

*Multiphoton ionization of molecules in selectively excited rovibrational states.*

Chem. Phys. Lett., 70, No. 3, 621

Esherick P and Owyong A(1983)

*Ionization-detected stimulated Raman spectroscopy.*

Chem. Phys. Lett., 103, No. 3, 235

Feigerle C S and Miller J C(1989)

*Multiphoton ionization of vibrationally hot nitric oxide produced in a pulsed supersonic glow discharge.*

J. Chem. Phys., 90(6), 2900

Fisanick G J, Eichelberger IV T S, Heath B A and Robin M B(1980)

*Multiphoton ionization mass spectroscopy of acetaldehyde.*

J. Chem. Phys. 72(10), 5571

Frueholz R, Wessel J and Wheatley E(1980)

*Resonance enhanced two-photon photoionisation spectroscopy applied to detection of naphthalene vapor.*

Anal. Chem., 52, 281

Fuhr J R and Wiese W L(1991)

*Atomic transition probabilities in CRC Handbook of Chemistry and Physics.*

72nd edition, Editor D R Lide, CRC Press Boca Raton, 10

- Goldstein N, Greenblatt G D and Wiesenfeld(1983)  
*Observation by laser ionization spectroscopy of vibrationally excited nitric oxide following  $O(^1D_2) + N_2O \rightarrow 2NO$ .*  
Chem. Phys. Lett., Vol. 96 No. 4, 410
- Goodman L and Rava R P(1981)  
*Two-photon spectra of substituted benzenes.*  
J. Chem. Phys., 74(9), 4826
- Hager J W and Wallace S C(1988)  
*Two-laser photoionization supersonic jet mass spectrometry of aromatic molecules.*  
Anal. Chem., Vol. 60 No. 1, 5
- Harris D C and Bertolucci M D(1978)  
*Symmetry and spectroscopy.*  
Oxford University Press, Inc.l, USA
- Herzberg G(1950)  
*Molecular Spectra and Molecular Structure: Spectra of diatomic molecules.*  
D. Van Nostrand Company, Inc
- Hodges R V, Lee L C and Moseley J T(1981)  
*Multiphoton ionization of Xe and several small molecules at 193 and 248nm.*  
Int. J. of Mass Spectrom. and Ion Proc., 39, 133
- Hollas J M(1987)  
*Modern Spectroscopy.*  
John Wiley and Sons Ltd., Great Britain

Houston C M, Drysdale S L T, Jennings R, Land A P, Ledingham K W D, Singhal R P, Smyth M H C, Stewart D T and Towrie M(1988)

*Two and three photon ionisation transitions in caesium vapour.*

J. Phys. D: Appl. Phys., 21

Hurst G S and Payne M G(1988a)

*Elemental Analysis using Resonance Ionization Spectroscopy.*

Spectrochim. Acta., 43B, 715

Hurst G S and Payne M G(1988b)

*Principles and Applications of Resonance Ionization Spectroscopy.*

Adam Hilger, Bristol, England.

Hurst G S, Nayfeh M H and Young J P(1977)

*A demonstration of one-atom detection.*

Appl. Phys. Lett., 30, 5, 229

Hurst G S, Payne M G, Kramer S D and Chen C H(1980)

Physics Today, September 1980

Hurst G S, Payne M G, Kramer S D and Young J P(1979)

*Resonance ionization spectroscopy and one-atom detection.*

Rev. of Mod. Phys., Vol. 54 No. 4, 767

Jacobs D C, Madix R J and Zare R N(1986)

*Reduction of 1+1 resonance enhanced MPI spectra to population distributions: Application to the NO  $A^2\Sigma^+$  -  $X^2\Pi$  system.*

J. Chem. Phys., 85(10), 5469

Johnson P M(1975)

*Multiphoton ionization spectroscopy: A new state of benzene.*

J. Chem. Phys., Vol. 62 No. 11, 4562

Johnson P M(1980)

*Molecular multiphoton ionisation spectroscopy.*

Appl. Optics 19, No. 23, 3920

Karasek F W(1947)

*Plasma chromatography.*

Anal. Chem., Vol. 46 No. 8, 710A

King G W(1964)

*Spectroscopy and molecular structure.*

Holt, Rinehart and Winston, Inc., USA

Kobayashi T and Nagakura S(1972)

*Photoelectron spectra of nitro-compounds.*

Chem. Lett., 903

Kolaitis L and Lubman D M(1986a)

*Detection of nonvolatile species by laser desorption atmospheric pressure mass spectrometry.*

Anal. Chem., Vol. 58 No. 11, 2137

Kolaitis L and Lubman D M(1986b)

*Atmospheric pressure ionization mass spectrometry with laser-produced ions.*

Anal. Chem., Vol. 58 No. 9, 1993

Kosanetzky J, Vormann H, Dunnwald H, Rohbrech W and Urban W(1980)

*IR laser induced UV fluorescence in nitric oxide.*

Chem. Phys. Lett., Vol. 71 No. 1, 60



Lahmani F, Lardeux C, Solgadi D, Zehnacker A, Dimicoli I, Boivineau M, Mons M and Piuzzi F(1985)

*Two-color, two-photon excitation of the NO ( $A^2\Sigma^+$ ) state.*  
J. Chem. Phys., 89, 5646

Lawson G and Todd J F J(1972)

*Radiofrequency quadrupole mass spectrometers.*  
Chemistry in Britain Vol. 8 No. 9, 373

Ledingham K W D, Cahill J W, Drysdale S L T, Raine C, Smith K M, Smyth M H C, Stewart D T, Towrie M and Houston C M(1986)

*An application of resonant ionisation spectroscopy to accelerator based high energy physics.*  
Inst. Phys. Conf. Ser. No. 84: Sec. 8, 289

Ledingham K W D, Raine C, Smith K M, Campbell A M, Towrie M Trager C and Houston C M(1984)

*Laser induced ionisation in proportional counters seeded with low ionisation potential vapours.*  
Nuc. Inst. Meth. in Phys. Res., 225, 319

Ledingham K W D, Raine C, Smith K M, Smyth M H C, Stewart D T, Towrie M and Houston C M(1985)

*Wavelength dependence of laser induced ionisation in proportional counters.*  
Nucl. Inst. and Meth. in Phys. Res., A241, 441

Letokhov V S(1979)

*Laser Isotope Separation.*  
Nature, 277, 605

Letokhov V S(1983)

*Laser-induced chemistry.*  
Nature, 305, 103

Letokhov V S(1985)

*Laser photoionization spectroscopy of single atoms and molecules.*

Optica A. Vol. 32 Nos. 9/10, 1191

Letokhov V S(1987)

*Laser Photoionisation Spectroscopy.*

Academic Press Inc.,

Letokhov V S(1988)

*Detecting individual atoms and molecules with lasers.*

Scientific American Sept., 44

Leutwyler S and Even U(1981)

*Isotopically selective two-photon ionisation of aniline in supersonic beams.*

Chem. Phys. Lett., Vol. 81 No. 3, 578

Levenson M D and Kano S S(1982)

*Introduction to nonlinear laser spectroscopy.*

Academic Press, Inc. London Ltd.

Li L and Lubman D M(1988)

*Resonant two-photon ionization spectroscopic analysis of indole and catechol derivatives using pulsed laser desorption with entrainment into supersonic jet expansions.*

Anal. Chem., Vol. 60 No. 23, 2591

Lichtin D A, Bernstein R B and Newton K R(1981)

*Experimental appraisal of the maximal-entropy theory of multiphoton ionisation-fragmentation: The alternative pathway test.*

J. Chem. Phys., 75(12), 5728

Loudon R(1973)

*The quantum theory of light.*  
Oxford University Press, Inc.

Lubman D M and Kronick M N(1982)

*Plasma chromatography with laser-produced ions.*  
Anal. Chem., Vol. 54 No. 9, 1546

Lubman D M and Kronick M N(1983a)

*Multiwavelength-selective ionization of organic compounds in an ion mobility spectrometer.*  
Anal. Chem., Vol. 55 No. 6, 867

Lubman D M and Kronick M N(1983b)

*Resonance-enhanced two-photon ionization spectroscopy in plasma chromatography.*  
Anal. Chem., Vol. 55 No. 9, 1486

Lubman D M(1981)

*Comparison of multiphoton fragmentation patterns for the azulene and naphthalene isomers. A test of the maximal-entropy theory.*  
J. Phys. Chem., 85, 3752

Lubman D M(1988a)

*Analytical multiphoton ionization mass spectrometry. Part I. Theory and instrumentation.*  
Mass. Spectrom. Rev., 7, 535

Lubman D M(1988b)

*Analytical multiphoton ionization mass spectrometry. Part II. Applications.*  
Mass. Spectrom. Rev., 7, 559

- Lubman D M, Naaman R and Zare R N,(1980)  
*Multiphoton ionisation of azulene and naphthalene.*  
J. Chem. Phys., 72(5), 3034
- Lubman D M, Tembreull R and Sin C H(1985)  
*Isotopically selective resonant two-photon ionization in supersonic beams.*  
Anal. Chem., Vol. 57 No. 6, 1084
- Marshall A, Clark A, Ledingham K W D and Singhal R P(1991)  
*Resonant Two-photon Ionisation for Detection of Aromatic Molecules.*  
Meas. Sci. Tech. 2, 1078
- Matyuk V M, Potapov V K and Prokhoda A L(1979)  
*Photoexcitation and Photoionisation of Nitro-derivatives of benzene and toluene.*  
Russ. J. Phys. Chem., 53, 538
- McFarlane J, Polanyi J C and Shapter J G(1991)  
*Photodissociation dynamics of NO<sub>2</sub> at 248nm.*  
J. Photochem. Photobiol. A: Chem., 58, 139
- McKendrick C B, Fotakis C and Donovan R J(1982)  
*Laser photodissociation of NO<sub>2</sub> at 248nm and production of NO(A <sup>2</sup>Σ<sup>+</sup> → X <sup>2</sup>Π) fluorescence.*  
J. Photochemistry, 20, 175
- McLean C J, Marsh J H, Cahill J W, Drysdale S L T, Jennings R, McCombes P T, Land A P, Ledingham K W D, Singhal R P, Smyth M H C, Stewart D T and Towrie M (1988)  
*Application of resonant ionisation mass spectroscopy to depth profiling in III-V semiconductor devices.*  
Inst. Phys. Conf. Ser. No. 94: Sec. 4, 193

- Melikechi N and Allen L(1985)  
*Two-photon electric dipole selection rules and non-degenerate real intermediate states.*  
J. Opt. Soc. Am. B3, 41
- Mikami N, Hiraya A, Fujiwara I and Ito M(1980)  
*The fluorescence excitation spectrum of aniline in a supersonic free jet: Double minimum potential for the inversion vibration in the excited state.*  
Chem. Phys. Lett., Vol. 74 No. 3, 531
- Miloni P W and Eberly J H(1988)  
*Lasers.*  
Wiley-Interscience, John-Wiley and Sons, Inc.
- Moore C E(1971)  
*Atomic energy levels.*  
NSRDS-NBS 35, US government printing office,  
Washington DC
- Morrison R J S and Grant E R(1982)  
*Dynamics of the two-photon photodissociation of NO<sub>2</sub>: A molecular beam multiphoton ionization study of NO photofragment internal energy distributions.*  
J. Chem. Phys., 77(12), 5994
- Morrison R J S, Rockney B H and Grant E R(1981)  
*Multiphoton ionization of NO<sub>2</sub>: Spectroscopy and dynamics.*  
J. Chem. Phys., 75(6), 2643
- Murakami J, Ito M and Kaya K(1981)  
*The multiphoton ionization spectrum of toluene in a supersonic free jet: Internal rotation of the methyl group.*  
Chem. Phys. Lett., 80(1), 203

- Nakayama T, Kitamura M Y and Watanabe K(1959)  
J. Chem. Phys., 30, 1180
- Palmer M H, Moyes W, Spiers M and Ridyard J N A(1979)  
*The electronic structure of substituted benzenes; Ab initio calculations and photoelectron spectra for nitrobenzene, the nitrotoluenes, dinitrotoluenes and fluorobenzenes.*  
J. Mol. Struct., 55, 243
- Parker D H(1983)  
*Laser ionization spectroscopy and mass spectrometry.*  
Ultrasensitive Laser Spectroscopy, Klinger D S, Academic Press
- Philis J G and Goodman L(1989)  
*Two-photon ( $A^1B_2 \leftarrow X^1A_1$ ) supersonic jet spectrum of aniline.*  
Spectrochimica Acta. Vol. 45A No. 5, 561
- Pratt S T, Dehmer J L and Dehmer P M(1985)  
*Photoelectron angular distributions from resonant multiphoton ionization of atomic carbon.*  
J. Chem. Phys., 82(2), 676
- Price D and Milnes G J(1990b)  
*The renaissance of time-of-flight mass spectrometry.*  
Int. J. Mass Spectrom. Ion Proc., 99, 1
- Price D(1990a)  
*The resurgence in time-of-flight mass spectrometry.*  
Trends in Anal. Chem., 9(1), 21
- Rabalais J W(1972)  
*Phototelectron Spectroscopic Investigation of the Electronic Structure of Nitromethane and Nitrobenzene.*  
J. Chem. Phys., 57(2), 960

- Rebentrost F, Kompa K L and Ben-Shaul A(1981)  
*A statistical model for the fragmentation of benzene by multiphotoionization.*  
Chem. Phys. Lett., 77(2), 394
- Rettner C T and Brophy J H(1981)  
*Resonance enhanced laser ionisation mass spectrometry of four aromatic molecules.*  
Chem. Phys., 56, 53
- Robin M B(1980)  
*Multiphoton fragmentation and ionization.*  
Applied Optics, 19, 3941
- Rossi M and Eckstrom D J(1985)  
*Quantitative aspects of benzene photoionization at 248nm.*  
Chem. Phys. Lett., 120 No.2, 118
- Saxon R P and Eichler J(1986)  
*Theoretical calculation of two-photon absorption cross sections in atomic oxygen.*  
Phys. Rev. A 34 No. 1, 199
- Saxon R P, Nesbet R K and Noble C J(1989)  
*Photoionisation of excited atomic oxygen: Theory and calculations.*  
Phys. Rev. A 39 No. 3, 1156
- Schlag E W and Neusser H J(1983)  
*Multiphoton mass spectrometry.*  
Acc. Chem. Res., 16, 355
- Silberstein J and Levine R D(1980)  
*Fragmentation patterns in multiphoton ionisation: A statistical interpretation.*  
Chem. Phys. Lett., Vol. 74 No. 1, 6

Silberstein J and Levine R D(1981)

*Statistical fragmentation patterns in multiphoton ionisation: A comparison with experiment.*

J. Chem. Phys., 75(12), 5735

Sin C H, Tembreull R and Lubman D M(1984)

*Resonant two-photon ionization spectroscopy in supersonic beams for discrimination of disubstituted benzenes in mass spectrometry.*

Anal. Chem., Vol. 56 No. 14, 2776

Singhal R P, Land A P, Ledingham K W D and Towrie M(1988)

*Population rate equation solution of a general resonant ionisation scheme.*

Proceedings RIS 88, 69

Singhal R P, Land A P, Ledingham K W D and Towrie M(1989)

*Population Rate Equations Modelling of a Resonant Ionisation Process.*

J. of Anal. Atomic Spectrom., 4, 599

Sirkin E R, Asscher M and Haas Y(1982)

*Multiphoton ionization and two-photon excitation spectroscopy of nitric oxide.*

Chem. Phys. Lett., Vol. 86 No. 3, 265

Slanger T G, Bischel W K and Dyer M J(1983)

*Nascent NO vibrational distribution from 2485Å NO<sub>2</sub> photodissociation.*

J. Chem. Phys., 79(5), 2230

Smalley R E, Wharton L and Levy D H(1977)

*Molecular optical spectroscopy with supersonic beams and jets.*

Acc. Chem. Res., Vol 10, 139



St. Louis R H and Hill Jr HH(1990)

*Ion mobility spectrometry in analytical chemistry.*

Crit. Rev. in Anal. Chem., 21 Issue 5, 321

Steinfeld J I(1974)

*Molecules and radiation: An introduction to modern molecular spectroscopy.*

Harper's Chemistry Series, Harper and Row, New York

Tembreull R and Lubman D M(1986)

*Pulsed laser desorption with resonant two-photon ionization detection in supersonic beam mass spectrometry.*

Anal. Chem., Vol 58 No 7, 1299

Tembreull R, Sin C H, Li P, Pang H M and Lubman D M(1985)

*Applicability of Resonant Two-Photon Ionization in Supersonic Beam Mass Spectrometry to Halogenated Aromatic Hydrocarbons.*

Anal. Chem., 57 No.7, 1186

Thonnard N, Parks J E, Willis R D, Moore L J and Arlinghaus H F(1989)

*Resonance ionisation of neutral atoms with applications to surface science, noble gas detection and biomedical analysis.*

Surface and interface analysis, 14

Towrie M, Cahill J W, Ledingham K W D, Raine C, Smith K M, Smyth M H C, Stewart D T and Houston C M(1986)

*Detection of phenol in proportional-counter gas by two-photon ionisation spectroscopy.*

J. Phys. B: At. Mol. Phys., 19, 1989

Uselman W M and Lee E K C(1976)

*A study of nitrogen dioxide ( $2\ ^2B_2$ ) photodecomposition to  $O(^1D)$  and  $NO(^2\Pi)$  in its second predissociation region 2500-2139Å.*

J. Chem. Phys., 65(5), 1948

Wang L, Borthwick I S, Jennings R, McCombes P T, Ledingham K W D, Singhal R P and McLean C J(1991)

*Observations and Analysis of Resonant Laser Ablation of GaAs.*

Appl. Phys. B 53, 34

Weast R C(1972)

*Handbook of Chemistry and Physics, 53rd Edition, 1972-1973.*

CRC Press

Whetten R L, Fu K J and Grant E R(1983a)

*Ultraviolet two-photon spectroscopy of benzene: A new gerade Rydberg series and evidence for the  $1\ ^1E_{2g}$  valence state.*

J. Chem. Phys., 79(6), 2626

Whetten R L, Fu K J and Grant E R(1983b)

*Photodissociation dynamics of  $Fe(CO)_5$ : Excited state lifetimes and energy disposal.*

J. Chem. Phys., 79(10), 4899

Whetten R L, Fu K J, Tapper R S and Grant E R(1983c)

*Highly efficient production of neutral carbon atoms in the ultraviolet multiphoton fragmentation of aromatic molecules.*

The J. of Phys. Chem., Vol. 87, No. 9, 1484

- Wiley W C and McLaren I H(1955)  
*Time-of-flight mass spectrometer with improved resolution.*  
Rev. Scien. Inst., 26, No. 12, 1150
- Winkler I C, Stachnik R, Steinfeld J I and Miller S(1986)  
*Evaluation of 2-photon ionization spectroscopy as a probe of NO ground state population distributions.*  
Spectrochimica Acta, Vol 42A No. 2/3, 339
- Wolff M M and Stephens W E(1953)  
*A pulsed mass spectrometer with time dispersion.*  
Rev. Sci. Instrum., 24, 616
- Zacharias H, Geilhaupt M, Meier K and Welge K H(1980)  
*Laser photofragment spectroscopy of the NO<sub>2</sub> dissociation at 337nm: A nonstatistical decay process.*  
J. Chem. Phys., 74(1), 218
- Zakheim D S and Johnson P M(1980)  
*Rate equation modelling of molecular multiphoton ionization dynamics.*  
Chem. Phys., 46, 263
- Zandee L and Bernstein R B(1979a)  
*Laser ionization mass spectrometry: Extensive fragmentation via resonance-enhanced multiphoton ionization of a molecular benzene beam.*  
J. Chem. Phys., 70(5), 2574
- Zandee L and Bernstein R B(1979b)  
*Resonance-enhanced multiphoton ionization and fragmentation of molecular beams: NO, I<sub>2</sub>, benzene and butadiene.*  
J. Chem. Phys., 71(3), 1359

- Zandee L, Bernstein R B and Lichtin D A(1978)  
*Vibronic/mass spectroscopy via multiphoton ionisation of a molecular beam: the I<sub>2</sub> molecule.*  
J. Chem. Phys., 69(7), 5059
- Zhu J, Lustig D, Sofer I and Lubman D M(1990)  
*Selective Laser-Induced Resonant Two-Photon Ionization and Fragmentation of Substituted Nitrobenzenes at Atmospheric Pressure.*  
Anal. Chem., 62, 2225
- Zoller P and Lambropoulos P(1980)  
*Laser temporal coherence effects in two-photon resonant three photon ionization.*  
J. Phys. B 13, 69

